A STUDY OF CRITICAL PHENOMENA
IN KRYPTON

Thesis by

Esin Cetegen Güları

In Partial Fulfillment of the Requirements
For the Degree of
Doctor of Philosophy

California Institute of Technology
Pasadena, California
1973

(submitted April 30, 1973)

ACKNOWLEDGEMENT

I wish to express my thanks to my research advisor, Professor C. J. Pings, for his helpful guidance and support during the course of this investigation.

Special thanks go to Dr. S. Y. Wu and H. H. Reamer for the valuable discussions in acquainting me with the instrumentation.

I am thankful to Dr. J. M. H. Levelt Sengers for the helpful suggestions for the analysis of the data.

During my graduate studies I have received financial support from the California Institute of Technology, the Air Force Office of Scientific Research, the National Science Foundation and the Procter and Gamble Company in the form of Graduate Teaching and Research Assistantships. These supports are hereby gratefully acknowledged.

I also wish to thank my parents for their endless care, encouragement and financial sacrifices and Erdoğan for keeping the competition high in the family.

ABSTRACT

A detailed experimental study of equilibrium critical phenomena in krypton was made. Using the method of angle of minimum deviation the refractive index was measured along the coexistence curve, along 16 isotherms above and along 11 isotherms below the critical temperature. The range of the temperature measurements in terms of t the reduced temperature difference from T_c was $-6.8\times10^{-2}\leqq t \leqq -5.7\times10^{-5}$ and $3.8\times10^{-5}\leqq t \leqq 4.8\ 10^{-2}$. The measurements were planned so that the region very near the critical point was covered in most detail. The refractive index was related to the density through the Lorentz-Lorenz relation.

After proper weight assignment, the data were analyzed in terms of the asymptotic power laws. The following values of the critical parameters, exponents and coefficients were determined: $T_c=209.286\pm0.010$°K, $P_c=54.213\pm0.003$ atm., $LL_c=0.070588\pm0.000006$, $\beta=0.3571\pm0.0008$, $B=1.840\pm0.001$ $\gamma=1.182\pm0.008$, $\Gamma=0.0835\pm0.0011$; $\gamma'_G=1.15\pm0.01$, $\Gamma'_G=0.021\pm0.001$, $\gamma'_L=1.13\pm0.01$, $\Gamma'_L=0.025\pm0.001$; $\delta=4.25\pm0.25$. The law of the rectilinear diameter was obeyed with its slope= 0.0918 ± 0.0004.

The reduced chemical potential differences and the reduced density differences were calculated. The chemical potential was observed to show antisymmetry for $-2\times10^{-3}\leqq t<4.8\times10^{-2}$ and $-0.3<\Delta LL<0.3$. The data in this

range were analyzed using Widom's equation of state and the closed-form(29) of h(x). The proposed equation was found to fit the experimental data very well.

The predictions of the linear model(32) were also checked and were observed to be consistent with the experimental results.

TABLE OF CONTENTS

(Continued)

LIST OF FIGURES

Figure Page

LIST OF TABLES

KEY NOMENCLATURE

D - angle of minimum deviation

D_c - angle of minimum deviation at the critical state

n - refractive index

n_c - critical refractive index

LL - $(n^2-1)/(n^2+2)$

LL_c - critical LL

ΔLL - $(LL-LL_c)/LL_c$

T - temperature

T_c - critical temperature

t - $(T-T_c)/T_c$

P - pressure

P_c - critical pressure

ρ - density

ρ_c - critical density

$\Delta\rho$ - $(\rho-\rho_c)/\rho_c$

μ - chemical potential

$\Delta\mu$ - reduced chemical potential difference

K_T - isothermal compressibility

C_v - specific heat at constant volume

F - Helmholtz free energy

β, B - critical exponent and coefficient related to the shape of the coexistence curve

δ, Δ - critical exponent and coefficient related to the shape of the critical isotherm

γ, Γ - critical exponent and coefficient related to the behaviour of K_T on the critical isochore

γ'_G, Γ'_G - critical exponent and coefficient related to the behaviour of K_T along the gas side of the coexistence curve

γ'_L, Γ'_L - critical exponent and coefficient related to K_T along the liquid side of the coexistence curve

x - $t/|\Delta\rho|^{1/\beta}$

x_o - $B^{-1/\beta}$

E_1, E_2 - constants of the scaled equation of state

r, θ - variables in the parametric representation of scaling

a, b^2 - parameters in the parametric representation of scaling

I. INTRODUCTION

During the last decade, the discrepancies between the predictions of the classical equations of state and the experimental data, together with the recognition that widely different systems behaved similarly near their critical points, have led to many theoretical and experimental investigations of the critical phenomena. A serious limitation in both testing the predictions of the new theories and comparing the behaviour of different systems has been the accuracy of the available thermodynamic data. In a fluid system, the conventional method(3) of obtaining PVT data yields results that are not accurate enough for critical state analysis. An alternate method of determining the volume or the density is to measure the refractive index which can be related to the density through the Lorentz-Lorenz relation, the validity of which is discussed in section I-1. This method is extremely valuable in the study of the critical phenomena because the refractive index can be measured much more precisely than the density near the critical state.

In this study, very careful and accurate measurements of refractive index, temperature and pressure of krypton were made along the two-phase boundary and along constant temperature curves both above and below the critical temperature. Then the data were analyzed in terms of the asymptotic power laws describing the approach to the critical point. The critical phenomena in general and particularly the power laws and the related critical exponents and coefficients are reviewed in section I-2.

A recent formulation of the static scaling hypothesis in the critical region, based on the assumption of homogeneous functions, has led to the propositions of two equations of state, (see section I-3). The data were also analyzed in view of the scaling hypothesis to test its validity and to determine the parameters appearing in the proposed equations of state.

1. The Lorentz-Lorenz Relation and its Validity

The instantaneous electric field acting of a molecule of a dielectric is affected by the fields of the surrounding molecules if the distances between neighboring molecules are comparable with molecular dimensions. This is true for dense gases and liquids. The simplest theory that takes electrostatic interactions into account is that of Lorentz in which the local field $\bar{E}^*$ is given by,

$$\bar{E}^* = \bar{E} + (4\pi/3)\ \bar{P} \tag{1}$$

where $\bar{E}$ is the external field and $\bar{P}$ is the polarization. The derivation of Eq. (1) and the underlying assumptions are summarized in Appendix A. When $\bar{P}$ is related to the dielectric constant ε, the resulting relationship is known as the Claussius-Mossotti equation.

$$\text{CM relation:} \qquad \frac{\varepsilon-1}{\varepsilon+2} = \frac{4\pi\alpha_m}{3M}\rho = \text{constant}\times\rho \tag{2}$$

where α_m is the molecular polarizability, M is the molecular weight and ρ is the density .

If ε in Eq. (2) is replaced with n^2, the Lorentz-Lorenz relation, which is used to relate the refractive index n to the density, is obtained.

$$\text{LL relation:} \qquad \frac{n^2-1}{n^2+2} = \frac{4\pi\alpha_m}{3M}\rho = \text{constant}\times\rho \tag{3}$$

The Lorentz local field formula has been derived for a lattice of dipoles with cubic symmetry and each having the same moment vector. Therefore the relationship in Eq. (3) is an approximation because the real materials do not necessarily comply with these assumptions. In fact, density and temperature dependent corrections to the right hand sides of Eqs. (2) and (3) are expected theoretically$^{(4)}$. Also, it is possible that the refractive index is not analytic at the critical point. However, Larsen, Mountain and Zwanzig$^{(5)}$ have shown that at least the real part of the refractive index behaves analytically through the critical point. Moreover, the experimental results suggest that for non-polar gases CM and LL relations are very good approximations and are valid over wide ranges of temperature and density within experimental error. For example, the maximum deviation in LL value of argon is quoted$^{(6)}$ to be 1.5% throughout the three states of matter. Amey and Cole$^{(7)}$ report that the changes in CM values between liquid and gaseous phases of the simple molecules Ar, Kr and CH_4 are less than 0.7%. Further, in Ref. (8) LL values for different states of matter of CF_4, N_2, O_2 and H_2 are calculated and shown not to deviate more than a few percent.

Unfortunately, data for Kr are scarce. Recent PVT measurements by Theeuwes and Bearman$^{(44)}$ were used to test the linearity between $(n^2-1)/(n^2+2)$ and ρ in Appendix D. This comparison indicates that LL relation is valid over the whole range of the data taken in this study within .6%.

2. Critical Phenomena(9-11)

The equation of state of a fluid is a functional relationship of the form $f(P,\rho,T)=0$, which relates pressure density and temperature. In a three-dimensional space, this function defines a surface whose coordinates are P, ρ and T and each point on this surface is an equilibrium state of the system. The critical state is represented by a point on this surface where the densities of the gas and the liquid phases become identical. The coordinates of this point are (P_c,ρ_c,T_c) where P_c, ρ_c and T_c are the critical pressure, the critical density and the critical temperature respectively. An order parameter is associated with each critical point. This is a quantity which is non-zero below T_c and vanishes above T_c. The order parameter for a gas-liquid critical point is the density difference between the coexisting phases, $(\rho_L-\rho_G)$.

One of the characteristics of a system approaching its critical point is the increase of microscopic fluctuations. For example, in a system of pure fluid at a temperature slightly below T_c, the energy and density differences between the coexisting phases are very small, and it is possible to find regions at densities slightly different from the equilibrium density in each homogeneous phase. These regions exist for measurable periods of time since the driving force to restore these fluctuations back to their equilibrium values are small. Another way to express this phenomenon is to assign a correlation length ξ that is characteristic of the range of these fluctuations and consider ξ becoming very large in the vicinity of the critical point. The existence of these fluctuations is best illustrated by the phenomenon called the "critical opalescence" which occurs when the correlation length is on the same order of magnitude of the wavelength of the incident light.

In thermodynamical terms, the critical phenomena are second-order phase transitions in which the first derivatives of the energy or the thermodynamic potentials remain continuous or piecewise-continuous while higher-order derivatives vanish or become very large. In fluids, the isothermal compressibility K_T,

$$K_T = \frac{1}{V}\left[\left(\frac{\partial^2 F}{\partial V^2}\right)_T\right]^{-1} \tag{4}$$

where V is volume and F is the Helmholtz free energy, and the specific heat at constant volume C_v,

$$C_v = -T \left(\frac{\partial^2 F}{\partial T^2}\right)_V \tag{5}$$

are two such quantities which exhibit anamolous behaviour. Consequently, a problem of great interest and importance in the study of the critical phenomena is the determination of the asymptotic laws describing the behaviour of quantities like K_T and C_v as the critical point is approached.

These asymptotic laws are basically simple power laws involving exponents and coefficients. To define a critical-point exponent describing the behaviour of general function f(t),

where $$t \equiv \frac{T-T_c}{T_c} \qquad (6)$$

is the reduced temperature difference from the critical temperature, it is assumed that this function f(t) is positive and continuous for small positive values of t, and that the limit,

$$\lambda \equiv \lim_{t \to 0} \frac{\ln f(t)}{\ln t} \qquad (7)$$

exists. Then this limit λ is called the critical-point exponent associated with f(t). Alternately, it can also be expressed as,

$$f(t) \simeq t^{\lambda} \qquad (8)$$

It must be pointed out that the definition in Eq. (7) does not distinguish between

$$f(t) = At^{x} \qquad (x=\lambda) \qquad (9)$$

and $$f(t) = At^{x}(1+Bt^{y}+\ldots.) \ , \qquad (y>0) \qquad (10)$$

with A and B constant coefficients. Thus, it takes into account that a typical thermodynamic function is not as simple as in Eq. (9) and that correction terms as in Eq. (10) can be expected. But sufficiently near the critical point the leading term dominates and the asymptotic laws are in the form of Eq. (9).

Some of these asymptotic laws that are of interest in this study in Fisher's notation(12) are:

Coexistence curve: $\Delta\rho \simeq B(-t)^{\beta}$ (11)

Critical Isotherm: $|P(T_c,\rho)-P(T_c,\rho_c)| \simeq \Delta\{\Delta\rho|\Delta\rho|^{\delta-1}\}$ (12)

Isothermal compressibility:

on the critical isochore, $K_T \simeq \Gamma t^{-\gamma}$, $T>T_c$ (13)

along the coexistence curve, $\rho^2 K_T \simeq \Gamma'(-t)^{-\gamma'}$, $T<T_c$ (14)

Specific heat at constant volume:

on the critical isochore, $C_v \simeq (A^+/\alpha)t^{-\alpha}$, $T>T_c$ (15)

$C_v \simeq (A^-_{II}/\alpha')(-t)^{-\alpha'}$, $T<T_c$ (16)

along the coexistence curve, $C_v \simeq (A^-_I/\alpha')(-t)^{-\alpha'}$, $T<T_c$ (17)

All properties above are reduced by the critical parameters, thus the temperature is measured in units T_c, the density in units ρ_c, the pressure in units P_c and $\Delta\rho=(\rho-\rho_c)/\rho_c$.

The critical-point exponents are not completely independent of each other. The requirements of thermodynamic stability lead to some inequalities among these exponents. One such relation, which is known as the Rushbrooke inequality(13), is

$$\alpha' + 2\beta + \gamma' \geqq 2 \quad (19)$$

Another inequality, which is due to Griffiths(14), is

$$\alpha' + \beta(\delta+1) \geqq 2 \quad (20)$$

These inequalities are useful for checking experimental results. They also suggest the functional form of the free energy and other thermodynamic potentials in the vicinity of the critical point.

A survey of the theoretical attempts explaining the critical phenomena show that they can be classified into two groups, namely the classical theories and model systems. The basic assumption in all the classical theories (van der Waal's theory(15), Weiss' molecular-field theory(16), Landau's thory(17), etc.) is that the free energy is analytic at the critical point and hence it can be expanded in Taylor series in density and temperature. Another approximation that is obvious in Weiss' molecular-field theory and inherent in all the other classical theories is the neglect of local fluctuations in replacing them by effectively constant "mean-field" values. Under these assumptions the classical values of the critical-point exponents are $\beta=1/2$, $\gamma=1$, $\delta=3$ and $\alpha=0$. These values contradict with experimental results. The discrepancy is most pronounced in the value of β because for a variety of systems $\beta\simeq 1/3$ is a well known fact.

The wrong predictions of the classical theories have led to studies of quantum-mechanical model systems incorporating more realistic interparticle interactions. These techniques can be illustrated by applying them to a model Hamiltonian for a spin system in the form,

$$H^{(D)} = -J \sum_{<ij>} s_i^{(D)} \cdot s_j^{(D)} \tag{21}$$

where $s_i^{(D)}$ are D-dimensional unit vectors and $-J$ is the energy of neighboring pair <ij> of parallel spins situated on sites i and j of the lattice.

This model Hamiltonian reduces to the Ising model if the spins are one-dimensional 'sticks' that can have two discrete orientations of +1 (up) and -1 (down). The Ising model has been solved for a one-dimensional lattice by Ising(18) and for a two-dimensional lattice by Onsager(19). When the spins in Eq. (21) are two-dimensional unit vectors, the resulting model is called the planar Heisenberg model, and for the case of three-dimensional spins, the model Hamiltonian describes the classical Heisenberg model.

Although the Ising model started as a crude model of ferromagnetism, it has been extended into other systems such as the lattice-gas model for a one-component fluid. The lattice-gas model treats identical point particles occupying discrete sites of a lattice and interacting with pair potentials. The solutions of this model for two-dimensional and three-dimensional lattices are obtained through approximation techniques involving series expansions and the results depend on the dimensionality of the system. The values of the critical-point exponents obtained from the lattice-gas model for two-dimensional lattices(20-23) are:

$\beta=1/8$, $\gamma=\gamma'=1\frac{3}{4}$, and $\alpha=\alpha'=0$.

The predictions of three-dimensional lattices(9,21-25) are: $\beta=5/16$, $\gamma=\gamma'=1\frac{1}{4}$, $\alpha=1/8$ and $\alpha'=1/16$.

The experimental data strongly indicate that $\beta\simeq 1/3$ and $\gamma\simeq 1.2$. Therefore the three-dimensional models predict the most realistic values of the critical-point exponents.

3. Scaled Equations of State

The values of the critical exponents obtained from both experimental and theoretical work satisfy the inequalities in Eqs. (19) and (20) and moreover in some cases, these inequalities are satisfied as equalities. So far there has been no proof of the inequalities to be equalities but a recent development called the static scaling law leads to such a result.

The first formulation of the scaling hypothesis for a fluid system is due to Widom$^{(26)}$. In all the classical theories, the chemical potential μ in the immediate neighborhood of the critical point is given as a function of density and temperature by,

$$\mu(\rho,T)-\mu(\rho_c,T) = (\rho-\rho_c)[T-\tau(\rho)]\Phi \qquad (22)$$

where Φ is a constant and $T=\tau(\rho)$ is the equation of the coexistence curve. Further, the coexistence curve is parabolic, that is,

$$T_c-\tau(\rho) = a|\rho-\rho_c|^d \qquad (23)$$

where a is a constant and $d=2$.

Eq. (22) assures that $\mu(\rho,T)$ reduces to $\mu(\rho_c,T)$ both when $\rho=\rho_c$ on the critical isochore and $T=\tau(\rho)$ on the coexistence curve. These are necessary aspects of any correct equation of state but the constancy of Φ is a feature of the classical theories only and it is possible to show$^{(26)}$ that this constancy of Φ leads to the incorrect classical results for the critical exponents. Thus, in formulating a more general equation of state, Widom proposes that the same form as in Eq. (22) can be retained but that Φ must not be assumed constant.

In the study of critical phenomena, it is convenient to measure the temperature by,

$$\chi = T-T_c \tag{24}$$

and the density by,

$$y = T_c-\tau(\rho) = a|\rho-\rho_c|^d \tag{25}$$

Under the transformations in Eqs. (24) and (25) and if Φ is let to be a function of χ and y, the equation of state in Eq. (22) can be written as,

$$\mu(\rho,T)-\mu(\rho_c,T) = (\rho-\rho_c)(\chi+y)\Phi(\chi,y) \tag{26}$$

where y is an even function of $\rho-\rho_c$ and $\mu(\rho,T)-\mu(\rho_c,T)$ is an odd function of $\rho-\rho_c$.

In this χ,y plane, the critical point is at the origin. The two-phase region is defined by $\chi+y<0$ and the coexistence curve becomes a straight line $\chi+y=0$. The critical isochore coincides with the χ-axis and the critical isotherm lies on the positive y-axis.

The main assumption behind the scaling hypothesis is that Φ is a homogeneous function of its variables, such that if the degree of homogeneity is $\gamma-1$, then

$$\begin{aligned}\Phi(\chi,y) &= y^{\gamma-1}\Phi(\chi/y,1)\\ &= \chi^{\gamma-1}\Phi(1,y/\chi) \quad \text{if } \chi>0\end{aligned} \tag{27}$$

$$= (-\chi)^{\gamma-1}\Phi(1,y/-\chi) \quad \text{if } \chi<0$$

This assumption leads to several relations among the critical exponents (see Appendix B). These relations are not independent of one another and in fact the knowledge of any two exponents is enough to determine the remaining ones. Some of these relations are:

$$\alpha' + 2\beta + \gamma' = 2 \tag{28}$$

$$\alpha + \beta(\delta+1) = 2 \tag{29}$$

$$\gamma(\delta+1) = (2-\alpha)(\delta-1) \tag{30}$$

$$\gamma = \beta(\delta-1) \tag{31}$$

$$\gamma = \gamma' \tag{32}$$

$$\alpha = \alpha' \tag{33}$$

Griffiths(27) has shown that Widom's proposed equation of state incorporating the homogeneous function assumption can be expressed as,

$$\Delta\mu = \Delta\rho|\Delta\rho|^{\delta-1}h(x) \tag{34}$$

where $\Delta\mu=\mu(\rho,T)-\mu(\rho_c,T)$, $\Delta\rho=(\rho-\rho_c)/\rho_c$, $t=(T-T_c)/T_c$ and

$$x = \frac{t}{|\Delta\rho|^{1/\beta}} \tag{35}$$

The properties imposed on h(x) by its formulation and thermodynamics are that it is a real positive function of x in the range $-x_o<x<\infty$ and it vanishes at the phase boundary $x=-x_o$ with a finite slope, with $x_o=B^{-1/\beta}$ where B is the coefficient appearing in Eq. (11). Further, the condition that

$$\beta\delta h(x) \geq xh'(x) \tag{36}$$

must be satisfied for the isothermal compressibility to be positive.

The application of experimental data to the proposed equation of state in Eq. (34) was first accomplished by M. Vicentini-Missoni, J. M. H. Levelt Sengers and M. S. Green(29). In this process, the main problem is the form of h(x). To find a simple functional expression for h(x) is very hard. Making use of the asymptotic laws, it is possible to expand h(x) in series form for limiting values of x. For example, about x=0, h(x) can be expressed as,

$$h(x) = \sum_{j=0}^{\infty} h_j x^j = h_o + h_1 x + h_2 x^2 + \ldots \tag{37}$$

so that, on the critical isotherm, $h(x)=h_o$ and

$$|\Delta\mu| = h_o |\Delta\rho|^{\delta} \tag{38}$$

Therefore Δ in Eq. (12) is given by,

$$\Delta = h_o \tag{39}$$

For large x, h(x) can be written as,

$$h(x) = \sum_{n=1}^{\infty} \eta_n x^{\beta(\delta+1-2n)} \tag{40}$$

Hence, assuring that on the critical isochore,

$$\left(\frac{\partial\mu}{\partial\rho}\right)_{\rho=\rho_c} = \frac{1}{K_T} = \eta_1 t^{\beta(\delta-1)} = \eta_1 t^{\gamma} \tag{41}$$

with $\quad 1/\eta_1 = \Gamma$ (42)

In Ref. (29), the suggested form of h(x) is,

$$h(x) = \frac{x+x_o}{x_o}\,\phi(x) \tag{43}$$

where $$\phi(x) = E_1 \left[1 + E_2 \left(\frac{x+x_o}{x_o} \right)^{2\beta} \right]^{(\gamma-1)/2\beta}$$

with E_1 and E_2 constants.

This form of h(x) has six adjustable parameters to be determined from the available chemical potential and density data. However, three of these, namely T_c, β and x_o can be fixed independently from the coexistence curve analysis leaving δ, E_1 and E_2 to be determined. Also, combining the relations in Eqs. (38-42) with the proposed form of h(x) in Eq. (43), expressions for the critical coefficients can be obtained and they are:

$$\Delta = E_1 \left(1+E_2 \right)^{(\gamma-1)/2\beta} \tag{44}$$

$$\Gamma^{-1} = x_o^{-\gamma} \, E_1 (E_2)^{(\gamma-1)/2\beta} \tag{45}$$

$$(\Gamma')^{-1} = \frac{1}{\beta} \, x_o^{-\gamma} \, E_1 \tag{46}$$

The parametric representation of the scaled equation of state has been formulated by P. Schofield$^{(30)}$. In this formulation, if r is a measure of the distance of a point from the critical point and θ measures the distance along a contour of constant r, the proposed transformations are:

$$\mu(r,\theta) = a \, r^{\beta\delta} \theta (1-\theta^2) \tag{47}$$

and $$t(r,\theta) = r \, (1-b^2\theta^2) \tag{48}$$

where a and b are disposable parameters with $a>0$, $b>1$.

Also, the choice of

$$P(r,\theta) = r^{\beta(\delta+1)} p(\theta) \tag{49}$$

which leads to "scaling law" behaviour implies that

$$\Delta\rho(r,\theta) = r^{\beta} m(\theta) \tag{50}$$

Thus, $\theta=0$ represents the critical isochore, $\theta=\pm 1$ the two branches of the coexistence curve and $\theta=\pm b^{-1}$ coincides with the critical isotherm.

Ho and Litster(31) have found that $m(\theta)$ is very nearly linear in θ for $CrBr_3$ under the transformation of the parametric representation. This result has led to the development of a model equation of state(32) called the "linear model". In this model, $\mu(\theta)$ and $t(\theta)$ are given by

$$\mu(\theta) = a\,\theta(1-\theta^2) \tag{51}$$

$$t(\theta) = (1-b^2\theta^2) \tag{52}$$

and

$$m(\theta) = g\,\theta \tag{53}$$

with g a constant.

The parameter a is determined by requiring that the tangent to $m(\theta)$ at $\theta=0$ to pass through $m(1)$ at $\theta=1$. This results in

$$a = B(b^2-1)^{\beta}/\Gamma \tag{54}$$

where B and Γ are the critical coefficients.

Another condition implied by the linearity of $m(\theta)$ is that $m(b^{-1})$ must lie on the straight line between $m(0)$ and $m(1)$. This requirement leads to

$$\frac{\Gamma\,B^{\delta-1}}{D^{\delta}} = \frac{b^{(\delta-3)}}{(b^2-1)^{\gamma-1}} \tag{55}$$

where D is related to the coefficient Δ such that $D=(1/\Delta)^{1/\delta}$.

Also, requiring the isothermal compressibilities on the critical isochore and along the coexistence curve to be consistent with linear $m(\theta)$ results in

$$\Gamma/\Gamma' = \frac{2}{(b^2-1)^{\gamma-1}} [1-b^2(1-2\beta)]^{-1} \quad (56)$$

In the linear model, b^2 is chosen such that

$$b^2 = (\delta-3)/[(\delta-1)(1-2\beta)] \quad (57)$$

which is obtained from considering the right-hand sides of Eqs. (55) and (56) as functions of b^2 and determining the value of b^2 at which these functions have their minima.

Thus, with this choice of b^2, the entire equation of state is defined by two of the critical exponents and the critical coefficients can be related to the exponents.

II. APPARATUS

1. The Cell, Cryostat and Spectrometer Assembly

The cell, cryostat and spectrometer assembly is shown in Fig. 1. Basically, it was the same apparatus as the one described in Refs. (33-35) with the modifications mentioned in Ref. (36). The sample was contained in a prism-shaped stainless steel cell, shown in Fig. 2. The cell was equipped with sapphire windows and surrounded by a radiation shield and was located at the center of rotation of a spectrometer. The apex angle of the cell had been measured(36) and was 44° 16.14±0.31'. A sodium light of 5893 Å wavelength illuminated the sample through an adjustable slit on a collimating telescope arrangement.

The angle of minimum deviation was directly measured on the spectrometer, as described in Appendix B of Ref. (36). The reproducibility of these measurements was ±0.10'. The refractive index n was calculated from the angle of minimum deviation by employing the formula,

$$n = \sin \frac{1}{2}(A + D)/\sin \frac{1}{2} A \qquad (58)$$

where A is the apex angle of the cell and D is the angle of minimum deviation. Since the space around the cell was evacuated to a vacuum lower than 10^{-4} mm. Hg, the calculated refractive index was the true refractive index. Any errors due to the windows of the cell and cryostat not being parallel were minimized by taking the zero reading of the spectrometer for the evacuated cell. A small front-aluminized flat mirror mounted on the cell was used to check the positioning of the cell. The details of the mounting and use of this mirror are described in Appendix A of Ref. (36). Corrections in alignment could be made by adjusting the leveling screws shown in Fig. 1.

An addition to the cell, cryostat and spectrometer assembly was the installing of a shut-off valve and a plunger of adjustable volume close to the cell on the inlet sample line. The shut-off valve was extremely useful during the measurements of the coexisting phases because it improved the stability of the system by eliminating most of the volume at room temperature. The plunger was very convenient for the fine adjustments in the loading of the cell. Also, all the sample lines at room temperature were insulated with fiber-glass wool, thus minimizing the small changes in the volume due to changes in the room temperature.

2. Temperature Measurement and Control

The measurements made in this study covered a temperature range from 194°K to 220°K. The temperature measuring and controlling circuits shown in Fig. 3 were essentially the same as those described by Teague(35) and Wu(36).

Liquid nitrogen was used for cooling. It was injected into the annular space in between the two vacuum jackets of the cryostat. A copper-constantan thermocouple mounted on the inner shield was used to measure the shield temperature which was set approximately one degree colder than the aimed operating temperature in the cell. The shield temperature was regulated by means of the shield heater and control unit. The temperature sensing element for the cell was a miniature platinum resistance thermometer, number 4 of the set mentioned in Refs. (37) and (38). It has an ice point resistance of 100.04718Ω and has been calibrated(38) against an NBS certified strain-free platinum resistance thermometer. It was surrounded by an aliminum radiation shield and was embedded in the block of the cell as shown in Fig. 2. The regulation of the cell temperature was attained by means of the cell heater and control unit.

One of the improvements made involved the cooling system. Previously, the frequency of the cycling of liquid nitrogen was adjusted by guessing at the setting of a plastic-glass rod. This rod was essentially a crude temperature sensing circuit breaker, which turned the heater in the liquid nitrogen cylinder on and off, thus causing the coolant to be injected into the jacket. The improvement was to replace the plastic-glass rod by a timer and circuit breaker unit. This unit gave a better control in setting the rate of cooling because both the duration of cycles and the time interval between cycles could be adjusted separately. Hence, a wider range with better control was achieved for the rate of cooling. Another addition which was not an improvement but a great convenience for saving time was the use of a commercial timer which would turn on the cooling system **several** hours before the control circuits had to be connected.

The temperature measuring and controlling circuit, shown in Fig. 3, utilized the potential drop across the standard resistor of the thermometer circuit as an emf input to the potentiometer's standard resistor. This idea was originally suggested by Daneman and Mergner(39). The superiority of this method was that the ratio of the currents in the thermometer and potentiometer circuits, not each current separately, had to be stable during the measurements. This was accomplished by introducing a current of one milliampere in the thermometer circuit and then by balancing the potential drop across the standard resistor STD Ω_1 against the standard resistor STD Ω_2 through a 300 mfd capacitor. The idea of using capacitors to compare voltages and to isolate electrical circuits was due to Dauphinee(40). A Leeds and Northrup 2284C high sensitivity galvanometer served as the null meter in the balancing procedure. During the experiment, any changes or drifts in both circuits could be compensated for by adjusting the resistance of the Mueller G-2 bridge, so that R_t/STD Ω_1 was kept equal to R_w/STD Ω_2. The replacement of a set of adjustable resistors with sliding contacts by the variable branch of a Leeds and Northrup Mueller G-2 bridge refined the balancing process. The Mueller bridge was highly accurate with very clean contacts and resistance increments as small as 0.0001Ω could be dialed on it directly.

The components of both the shield and the cell temperature controlling circuits were the identical type of commercial equipment from Leeds and Northrup, namely, #9835B DC amplifiers, Speedomax G recorders and series 60 C.A.T. control units.

Previously, the changes in the room temperature were completely neglected. During this study, it was noticed that these changes caused slight variations in the resistance of the standard resistor STD Ω_1 in Fig. 3. This affected the temperature setting for the cell and it was observed that if no corrections were made, there could be as much as 0.002°K temperature difference for the same Wenner setting with 1.0°K change in the room temperature. STD Ω_1 was a Leeds and Northrup manganin standard resistor of 1000.04Ω. From its certificate, within the interval 15°C to 35°C, the change of its resistance with temperature was given by the equation,

$$R_t = R_{25}[\ 1+a(t-25)+b(t-25)^2\ ] \tag{59}$$

where R_t is the resistance at t°C, R_{25} is the resistance at 25°C, a and b are constants with a=0.000007 and b=-0.0000005. The room temperature correction of the temperature setting was made as follows: The room temperature around STD Ω_1 was measured and corresponding R_t was calculated. Then the dial setting on the Wenner potentiometer for this R_t was determined. A change of one degree in the room temperature corresponded roughly to a correction of one digit in the Wenner setting. Since the drift in the room temperature was usually less than a degree, the correction could not be directly dialled. But it was observed that the control point of the Speedomax G recorder did not change when its zero setting was adjusted. This observation was extremely useful because the zero setting of the recorder was used as a vernier-type fine adjustment for the Wenner setting.

Consequently, after all the refinements made in both the cell and cryostat assembly and the temperature measuring and controlling circuits, the temperature of the cell could be controlled within ±0.0002°K. The comparison of the temperature control records in Figs. 4 and 5 illustrates the magnitude of the improvement achieved after the above mentioned refinements. The reproducibility of the temperature was better than ±0.001°K and the absolute accuracy was ±0.010°K. This latter figure included all errors due to the thermometer calibration and measuring method.

The Wenner potentiometer dial setting E_w with the room temperature correction was used to calculate the temperature of the sample. The resistance of the thermometer R_{th} could be computed by,

$$R_{th} = (R_t/R_{25})\ (1000.04/1.01926\times10^{-6})\ E_w \qquad (60)$$

where 1000.04 is the resistance of STD Ω_1 in ohms and 1.01926×10^{-6} is the potential drop across STD Ω_2 in volts. The temperature corresponding to R_{th} was then determined from the calibration table of the thermometer.

3. Pressure Measurement and Control

The pressure measurements made in this study covered a range from 27 to 76 atmospheres. The pressure measuring system, shown in Fig. 6, with the exception of the automatic pressure control unit was essentially the same as that described by Wu(36).

The pressures were measured with a Hart pressure balance manufactured by High Pressure Equipment Company, Erie, Pennsylvania. The operation of the Hart balance was based on the use of a piston placed in a very closely fitting cylinder, pressuring a hydraulic oil system. The upward force exerted by the oil was counterbalanced by known weights. The piston had to be rotated in the cylinder in order to reduce the frictional forces. The accuracy of the pressure measurements on the Hart balance was claimed to be 1:10000 and the reproducibility to be 1: 20000 by the manufacturing company.

A pressure transducer, model P3D supplied by Pace Engineering Company, North Hollywood, was used to separate the sample from the hydraulic oil. The operation and the design of similar pressure transducers have been described by Reamer and Sage(41) and Honeywell and Pings(42). The basic principle was the existence of an inductance difference due to a difference in pressure across a metal diaphragm. The diaphragm was made of stainless steel and was welded to the surface of a backing plate which was slightly concave to permit movement of the diaphragm. The change in the ratio of the inductances of the two coils placed on both sides of the diaphragm was converted into a DC signal by a model CD10 miniature carrier-demodulator supplied by Pace Engineering Company. This DC output was then displayed on a microammeter. The sensitivity of the microammeter was adjusted to 0.01 psi per division.

A Texas Instruments model 141 precision pressure gage connected directly to the sample line was used to obtain the aimed pressure while loading the cell and to set the pressure of the Hart balance close to the sample pressure so that the pressure difference across the diaphragm was in the range of the microammeter. Fine adjustment of the pressure could be made through a plunger installed on the sample line.

Previously, the pressure was controlled manually by a valve with adjustable volume. During this investigation an automatic pressure control unit was installed. The components and the operation of this unit are described in detail in Appendix C. Basically, its operation depended on the variable supply of radiant heat to a portion of the sample line. This was accomplished by converting the signal from the Pace carrier-demodulator into a light signal by the use of a galvanometer. The deflection of the galvanometer was sensed by a resistance type CdS light cell, which was connected to a commercial light dimmer. The light dimmer regulated the intensity of the light from a pair of heat lamps shining on a portion of the sample line. The light dimmer could be set such that the heat lamps operated at a medium intensity when the pressure was controlling, thus allowing some range on both sides to restore controlling in case of a small drop or small increase in pressure. This unit could control the pressure within ±0.001 atm. Consequently, the accuracy and the reproducibility of the pressure measurements in this study were equal to those of the Hart balance.

The following formula was used to calculate the pressure:

$$P(\text{psia})=P_a+(.998885)[\ W+\text{grams}\times 7.0897\times 10^{-3}+0.095+0.3513-0.01079\times G-0.0276\times h\ ] \qquad (61)$$

where P_a is the atmospheric pressure, W is the value obtained from the calibration table of the Hart balance equal to the pressure produced by the weights hanging on it, 0.998885 is the local gravity correction factor, 0.095 is the correction for the elevation difference between the balance and the diaphragm, h is the piston height in cm., G is the oil gauge reading when h=1.0 cm. with the correction for the oil head equal to -(h-30)(0.0108).

4. Sample

The krypton sample used in this investigation was the "Research Grade Krypton" supplied by the Matheson Gas Company. Each sample cylinder came with a batch analysis showing the amount of each impurity. The impurities were: xenon less than 25 ppm, nitrogen less than 25 ppm, oxygen less than 4 ppm, argon less than 4 ppm, hydrogen less than 5 ppm, and hydrocarbons as methane less than 10 ppm. The dew point of the sample was -110°F. A check of the purities of two different sample cylinders was made by repeating the same measurements with a sample from a nearly empty cylinder and another sample from a full cylinder. The measurements were reproducible within the experimental uncertainties.

Before the introduction of the sample into the cell, all the sample lines and the cell were evacuated and then they were purged with sample to a pressure slightly above the atmospheric pressure and reevacuated. This procedure was repeated two times before the actual loading of the cell. When the equipment was not being used, the pressure inside the cell was kept above the atmospheric pressure in order to avoid any leaks into the system.

III. EXPERIMENT

1. Experimental Procedure

The experimental procedure during a run consisted of several steps as follows: The inner and the outer jackets of the cryostat were evacuated continuously and kept at a vacuum below 10^{-3} mm Hg all the time. On the day of a run, the positioning of the cell was checked and any required adjustments were made. The shield was cooled with liquid nitrogen and the shield temperature was controlled at approximately one degree below the cell temperature. The cell temperature was set and controlled at an aimed value. In the meantime , the cell and the sample lines were evacuated and the vacuum reading of the cell was checked. Then the cell was loaded to the operating pressure and the cell temperature control, disturbed during the loading, was restored.The Hart balance was attached and any necessary fine pressure corrections were made either by adjusting the small weights of the balance or by changing the loading of the system slightly. To guarantee that the sample was in equilibrium the following criteria were satisfied before making any measurements. First, the temperature and the pressure were kept on perfect control for about an hour and secondly, the image had to be sharp and distinct. In the case of two phase data, a third condition was that the relative amounts of the phases in the cell did not change.

2. Data

The data consisted of three sets of measurements namely, the coexisting gas and liquid states along the phase boundary and the single phase states along isotherms above and below the critical temperature.

Coexisting gas and liquid data: This set of measurements consisted of 35 states spread over a temperature range of 195.002°K to 209.274°K and a pressure range of 35.905 to 54.198 atm. In Table I, temperatures, pressures and angles of minimum deviation are listed for these 35 states. 15 of these 35 states were within 0.283°K of the critical temperature with the last state being 12 millidegrees K below T_c.

Single phase isotherms above T_c: This set of data was taken along 16 isotherms. It covered a temperature range of 219.301°K to 209.294°K and a pressure range of 75.745 to 53.672 atm. The pressure and the angle of minimum deviation of each state along every isotherm are reported in Table II. The temperature of the isotherm closest to the phase boundary was 8 millidegrees K above T_c. The measurements along each isotherm were made on at least two, sometimes three or four, days as indicated by the number of the runs in Table II. The data taken on different days were compared by repeating the two end states for each day and obtaining reproducible measurements. Such repeated states on each isotherm are indexed with the same number of stars in Table II.

Single phase isotherms below T_c: This set of data, taken along 11 isotherms below the critical temperature, covered a temperature range of 199.302°K to 209.274°K and a pressure range of 27.797 to 70.987 atm. The pressures and the angles of minimum deviation along these isotherms are tabulated in Table III. The temperature of the isotherm closest to the critical point was 12 millidegrees K below T_c. Each isotherm was scanned on two, sometimes three, days and measurements on different days along the same isotherm were checked by repeating some of the states as indicated with stars in Table III.

IV. RESULTS AND ANALYSES

1. Refractive Index and Isothermal Compressibility

The refractive index was calculated from the measured angle of minimum deviation D using the formula,

$$n = \frac{\sin\frac{1}{2}(A+D)}{\sin\frac{1}{2}A} \tag{62}$$

where A is the apex angle of the cell and A=44° 16.14'±.31'. The experimental uncertainties in measuring D and A, σ_D and σ_A, were ±0.10' and ±0.31' respectively. The error in the refractive index σ_n was computed from these experimental uncertainties by propagation of error. The formula used in this computation was

$$\sigma_n = \frac{\sin\frac{1}{2}D}{2\sin^2\frac{1}{2}A}\sigma_A + \frac{\cos\frac{1}{2}(A+D)}{2\sin\frac{1}{2}A}\sigma_D \tag{63}$$

The refractive indices and their errors for the coexisting gas and liquid data are reported in Table IV. The experimental uncertainties in D for states within one degree of the critical temperature were doubled because very small density and temperature gradients caused broadening of the image. The refractive indices along the phase boundary are plotted versus temperature in Figs. 7 and 8. Fig. 8 has an expanded temperature scale showing the states close to the critical point.

The refractive indices along the 16 isotherms above

T_c are plotted versus pressure in Figs. 9 and 10 in the order of decreasing temperature difference from the critical temperature. Similar plots for the 11 isotherms below T_c are shown in Figs. 10 and 11 in the order of increasing temperature difference from T_c.

The refractive index can be related to the density through the Lorentz-Lorenz law. The validity of the LL-relationship within the temperature and pressure range of this study is illustrated in Appendix D. The LL-function which is directly proportional to density ρ is given by,

$$LL = \frac{n^2-1}{n^2+2} = \frac{\rho}{A} \tag{64}$$

where A is a constant.

From the definition of the isothermal compressibility K_T

$$K_T = \frac{1}{\rho}(\partial\rho/\partial P)_T \tag{65}$$

and from the simple relationship in Eq. (64),

$$K_T = \frac{1}{LL}(\partial LL/\partial P)_T \tag{66}$$

But, $(\partial LL/\partial P)_T = dLL/dn \times \partial n/\partial D \times (\partial D/\partial P)_T$

$$= \frac{6n}{(n^2+2)^2} \times \frac{n}{2}\cot\frac{1}{2}(A+D) \times (\partial D/\partial P)_T \tag{67}$$

Therefore,

$$K_T = \frac{3n^2}{(n^2-1)(n^2+2)} \cot\frac{1}{2}(A+D)(\partial D/\partial P)_T \tag{68}$$

Consequently, it was necessary to determine the first derivative $(\partial D/\partial P)_T$ in order to be able to compute the isothermal compressibility. These first derivatives were determined by the numerical spline fit(45). This technique described in Appendix E is very similar to the "draftsman's" spline and essentially assigns sections of cubics to every interval between adjacent data points requiring continuity at the junctions.

The first derivatives calculated with this method and the isothermal compressibilities computed from Eq. (68) together with the refractive indices and the pressures along the isotherms above T_c are tabulated in Table V and in Figs. 12,13 and 14, the isothermal compressibilities on these isotherms are plotted versus pressure.

The spline fit was highly accurate in all intervals with the exception of the two end sections which were affected by the choice of the two end conditions (See Appendix E). This inaccuracy was not important in the case of the isotherms above T_c because the range of interest was confined to the vicinity of the critical density. However, the situation reversed for the isotherms below T_c because the range of importance was along the phase boundary or at the end points of the isotherms. Therefore the numerical method of determining the first derivative had to be modified. Also, an additional graphical technique was used to check the predictions of the numerical technique. The graphical method of estimating the first derivatives was to draw large graphs of D versus P with both scales being sensitive to experimental uncertainties, then to determine the normal at each data point using a front-aluminized flat mirror and to calculate the slope of the tangent from the slope of the normal. The modified numerical technique as described in Appendix E involved the use of the same graphs to create more intervals within the last interval on each isotherm and extrapolating for the value of the slope at the phase boundary.

The isothermal compressibilities from the values of the first derivative determined by the modified numerical spline fit, together with the graphical and the numerical values of the first derivative, the refractive indices and the pressures along the 11 isotherms below T_c are reported in Table VI. In Figs. 15,16 and 17 plots of K_T versus P are shown on these isotherms.

2. The Coexistence Curve and the Rectilinear Diameter

The density along the coexistence curve in its most general form can be written as,

$$\rho^{\pm} = \rho_c(1+B_1^{\pm}|t|^{\beta_1^{\pm}}+B_2^{\pm}|t|^{\beta_2^{\pm}}+\dots) \qquad (69)$$

where ρ is the density and $t=(T-T_c)/T_c$ with

$$\beta_1^{+}<\beta_2^{+}<\dots \quad , \quad \beta_1^{-}<\beta_2^{-}<\dots$$

and the plus sign refers to the liquid and the minus to the gas densities.

The theoretical models such as the lattice gas theories do not distinguish between the two branches of the coexistence curve because they assume a built-in symmetry, $\rho^{+}+\rho^{-}=2\rho_c$. But this symmetry is absent in real gases. Therefore it is worthwhile to consider the most general form in the analysis of the experimental data. However, the results of the existing experimental studies suggest very strongly that $\beta_1^{+}=\beta_1^{-}$, $B_1^{+}=-B_1^{-}$ and most probably $\beta_2^{+}=\beta_2^{-}\simeq 1$ and $B_2^{+}\simeq B_2^{-}$. Recently, these relationships were demonstrated for CO_2, N_2O and $CClF_3$ by J. M. H. Levelt Sengers, J. Straub and M. Vicentini-Missoni(46). If these symmetry features were present in real fluids, then from Eq. (69),

$$(\rho_L-\rho_G)/2\rho_c = B_1|t|^{\beta_1}+\dots \qquad (70)$$

and

$$(\rho_L+\rho_G)/2\rho_c = B_2|t|+\dots \qquad (71)$$

with Eq. (70) describing the top of the coexistence curve and Eq. (71) expressing the law of the rectilinear diameter. If the density is replaced by LL and only the leading terms are considered, the above relationships become

$$(LL_L-LL_G)/LL_c = 2B_1|t|^{\beta_1} \tag{72}$$

and

$$LL_L+LL_G = 2LL_c+2B_2|t| \tag{73}$$

Before attempting to fit the coexistence data to Eqs. (72) and (73), careful weight assignments were necessary. The two independent sources of error were in the refractive index σ_n and in the temperature σ_T. Since the errors in n reported in Table IV did not vary too much, $\sigma_n=1\times10^{-4}$ and $\sigma_T=0.001°K$ were used. The standard error in LL was calculated using propagation of error to be,

$$\sigma_{LL}= \frac{6n}{(n^2+2)^2}\sigma_n \tag{74}$$

Therefore,

$$\begin{aligned}\mathrm{Var}_n[LL_L-LL_G] &= \mathrm{Var}_n[LL_L+LL_G] \\ &= 6^2\left[\frac{n_L^2}{(n_L^2+2)^4}+\frac{n_G^2}{(n_G^2+2)^4}\right]\sigma_n^2 \end{aligned}\tag{75}$$

where the subscript n indicates the contribution to the variance of the quantity in brackets due to error in n. Since LL_L and LL_G changed with temperature approximately as $B_1|t|^{\beta_1}$,

$$\sigma_T[LL_L] = \sigma_T[LL_G] = \tfrac{1}{2}(LL_L-LL_G)(\beta_1\sigma_t/|t|) \tag{76}$$

Thus, from Eqs. (75) and (76),

$$\mathrm{Var}[LL_L+LL_G] = 6^2\left[\frac{n_L^2}{(n_L^2+2)^4} + \frac{n_G^2}{(n_G^2+2)^4}\right]\sigma_n^2 + \frac{1}{4}(LL_L-LL_G)^2(\beta_1^2\sigma_t^2/t^2) \qquad (77)$$

The contribution of the error in temperature to the variances of LL_L and LL_G was partially cancelled when the sum was formed but not when the difference was formed. Hence, $\mathrm{Var}_t[LL_L+LL_G]$ was set equal to one-half of $\mathrm{Var}_t[LL_L-LL_G]$. Therefore,

$$\mathrm{Var}[(LL_L-LL_G)/LL_c] = (1/LL_c)^2\left\{6^2\left[\frac{n_L^2}{(n_L^2+2)^4} + \frac{n_G^2}{(n_G^2+2)^4}\right]\sigma_n^2 + \frac{1}{2}(LL_L-LL_G)^2(\beta_1^2\sigma_t^2/t^2)\right\} \qquad (78)$$

The weights used in the fitting procedure were equal to the inverses of the variances.

Two slightly different least squares fitting routines were used interchangeably. When the parameters in the fitted equation were roughly known, method of Ref. (47) was used. In this case, all the error was attributed to the dependent variable and the weights were directly calculated. When no knowledge of the parameters existed, the routine of Ref. (48) was employed. Since the parameter corresponding to the slope of the fit appears in the calculation of the weights, an initial guess at the value of this parameter was made and then an iteration involving the recalculation of weights was performed. The standard deviation of the fit was equal to the square root of the variance of the fit s^2. For the case of a straight line fit to N data points,

$$s^2 = \frac{\frac{1}{N-2}\,\Sigma[w_i(y_{expt.}-y_{calc.})^2]}{\frac{1}{N}\,\Sigma w_i} \tag{79}$$

where w_i is the weighting factor for each data point.

The fit to Eq. (73) was performed for several critical temperatures ranging from 209.280°K to 209.288°K. The results of the fit are presented in Table VII and the difference between the experimental and the calculated values of LL_L+LL_G is shown in Fig. 18 for T_c=209.286°K. The values of T_c and the corresponding values of $2LL_c$ computed from both least squares fitting routines are tabulated in Table VIII. The best value of the intercept $2LL_c$ was observed to be independent of the choice of T_c within this range. The optimum values of $2LL_c$ and the slope with their respective standard deviations are also given in Table VII.

Recently a curved diameter of the form $|t|^{1-\alpha}$ was found in model calculations(49) and was suggested in the generalized parametric representation(50) of the scaling hypothesis. The results of the fit to the curved diameter are shown in Fig. 19. The present data did not favor a curved diameter.

The best value of LL_c determined from the fit of the rectilinear diameter was used to reduce the difference LL_L-LL_G. The reduced difference was then fitted to the following equation,

$$\ln [(LL_L-LL_G)/LL_c] = \ln 2B_1 + \beta_1 \ln|t| \qquad (80)$$

obtained taking the logarithm of both sides of Eq. (72). The fit was performed for several values of T_c and the value of T_c corresponding to the minimum standard deviation of the fit was chosen as the best value of T_c namely, 209.286°K. The values of $(LL_L-LL_G)/LL_c$, the estimated errors and the residuals of the fits are listed in Table IX and also the optimum values of T_c, B_1 and β_1 are given with their respective standard deviations. In Fig. 20, $\ln [(LL_L-LL_G)/LL_c]$ is plotted versus $\ln|t|$ with the slope of the fitted straight line equal to β_1. The residuals are shown in Fig. 21.

To make sure that the optimum values thus determined were independent of the range, both fits were repeated for decreasing values of $|t|_{max}$. The results are summarized in Tables X and XI for the rectilinear diameter and the coexistence curve fits respectively. There was no variation in LL_c exceeding its error and no appreciable change was observed in β_1 outside its error for $|t|_{max}$ from 6.8 to 0.4 %. Consequently, the expression $(LL_L-LL_G)/LL_c=2B_1|t|^{\beta_1}$ was valid within error over $-0.068<t<0$.

The simple exponent relationship in Eq. (72) and its linear form in $\ln|t|$ in Eq. (80) contain only the leading term of the general expression. To find out if the higher-order terms in (T_c-T) were significant, the results of the fits to the following equations

$$\ln[LL_L-LL_G] = A_o+\beta\ln(T_c-T) \tag{81}$$

and
$$\ln[LL_L-LL_G] = A_o+\beta\ln(T_c-T)+A_1(T_c-T)+A_2(T_c-T)^2 \tag{82}$$

were compared. An unweighted linear least squares fitting of Eq. (81) predicted $A_o=-3.247\pm0.003$ and $\beta=0.352\pm0.001$ with the minimum in the standard deviation of the fit $\sigma_{fit}=0.0165$ occuring at $T_c=209.282°K$. An unweighted non-linear least squares fitting routine$^{(51)}$ was used to determine the five parameters, namely T_c, β, A_o, A_1 and A_2, in Eq. (82). The results were $T_c=209.282\pm0.001°K$, $\beta=0.3524\pm0.0026$, $A_o=-3.239\pm0.004$, $A_1=-0.0067\pm0.0006$ and $A_2=0.00057\pm0.00008$ with $\sigma_{fit}=0.0184$. The standard deviations of both fits were comparable. For $(T_c-T)<1$, the contributions of the linear and quadratic terms were insignificant and for $(T_c-T)>1$, due to the difference in their signs, their contributions mostly cancelled each other.

To test the symmetry features of the coexistence curve, the leading term,

$$LL-LL_c = B_1^{\pm}|t|^{\beta_1^{\pm}} \tag{83}$$

in Eq. (69) was studied on both branches of the phase boundary. In Tables XII and XIII values of $\ln|B_1^+|$, β_1^+, $\ln|B_1^-|$ and β_1^-, their standard deviations and the standard deviations of the fits are tabulated as functions of $|t|_{max}$ for the optimum value of LL_c. There were systematic differences in the values of the exponent and the coefficient on the gas and the liquid sides. For $|t|_{max}<0.3\%$, the coefficients $|B_1^+|$, $|B_1^-|$ and the exponents β_1^+, β_1^- became equal within error. The approach of the exponent to equal values with decreasing $|t|_{max}$ is illustrated in Fig. 22.

In summary of the analysis of the coexistence data, following values of the critical parameters were obtained: $T_c=209.286\pm0.010$°K, $2LL_c=0.141175\pm0.000012$, slope of the rectilinear diameter, $a=0.0918\pm0.0004$, $B_1=1.840\pm0.001$ and $\beta_1=0.3571\pm0.0008$.

3. Determination of the Critical Pressure

The vapor pressure data, listed in Table I, were analyzed using the following classical equation.

$$\ln P = A/T + B \ln T + C\, T + D \qquad (84)$$

where A, B, C and D are adjustable parameters.
The results of a non-linear least squares analysis(51) for the values of the four parameters were: $A=-197.82\pm0.64$, $B=0.002623\pm0.000014$, $C=0.023816\pm0.000015$ and $D=-0.05979\pm 0.00029$ with $\sigma_{fit}=9.2\times10^{-4}$. From this fit, P_c corresponding to $T_c=209.286°K$ was 54.237 ± 0.049 atm.

Experimentally, P_c was known to be between 54.198 atm. and 54.2285 atm. If a linear relationship between ΔP and ΔT was assumed on the critical isochore, $P_c=54.313$ atm. was obtained. This assumption was tested by computing $(\Delta P/\Delta T)$ along the critical isochore in the range of the measurements of this study. As shown in Table XXI, $(\Delta P/\Delta T)$ was very nearly constant. An arithmetic mean of $(\Delta P/\Delta T)$ obtained from the first twelve intervals was 1.550. The values of P_c computed using this ratio and the value of $P(LL_c)$ on the isotherm for which $(T-T_c)= 0.008°K$ and $P(LL_c)$ on the isotherm for which $(T-T_c)= 0.052°K$ were 54.216 atm. and 54.213 atm. respectively.

Therefore the best value of P_c was chosen to be 54.213 ± 0.03 atm.

4. Determination of γ on the Critical Isochore

The critical isochore is defined by LL_c, the value of the LL-function at the critical point. In the present analysis, LL_c was determined from the rectilinear diameter fit . For the best value of T_c, 209.286°K, LL_c was 0.070588 which corresponded to the critical refractive index n_c = 1.10808 and the critical angle of minimum deviation D_c = 305.10 minutes of arc.

The behaviour of the isothermal compressibility K_T on the critical isochore is described by Eq. (13) or its logarithmic form,

$$\ln K_T = \ln \Gamma - \gamma \ln t \qquad (85)$$

The values of the first derivative $(\partial D/\partial P)_T$ were calculated from the spline fit and interpolated for $(\partial D/\partial P)_T$ at D_c on each isotherm. Then the corresponding K_T's were computed using Eq. (68) and fitted to Eq. (85).

In assigning errors to K_T, the main source of error was in the determination of $(\partial D/\partial P)_T$ whose accuracy diminished as the critical point was approached. In this analysis, to obtain an estimate of this accuracy, the data points around D_c on each isotherm were moved within the experimental uncertainties of D and P and the numerical spline fit was repeated to obtain $(\partial D/\partial P)_T$ at D_c for these distorted data. The errors were then based on the fractional difference x between the two values of $(\partial D/\partial P)_T$ at

D_c. Hence, the error assigned to ln K_T was

$$\sigma^2_{\ln K_T} = x^2 + \frac{1.44\ \sigma^2_T}{(T-T_c)^2} \tag{86}$$

The fit to Eq. (85) was performed for various values of T_c. The results for T_c=209.286°K, which corresponded to the minimum of the standard deviation of the fit, are presented in Table XIV and shown in Fig. 23. The values of the critical parameters determined from this fit were: γ=1.182±0.008 and Γ=0.00154±0.00002 atm^{-1} or Γ=0.0835 with minimum σ_{fit}=0.0647 occuring at T_c=209.286°K.

To ensure that these values did not depend on the range of the data, the fit was repeated for decreasing values of t_{max}. The results , which are summarized in Table XV, indicated no variations in the values of γ and Γ within their respective errors.

5. Locus of Maximum Isothermal Compressibility

It can be shown that the locus of the inflection points $(\partial^2 P/\partial\rho^2)_T=0$ coincides with the locus of

$$\rho(\partial^2\mu/\partial\rho^2)_T + (\partial\mu/\partial\rho)_T = 0 \qquad (87)$$

However, $(\partial\mu/\partial\rho)_T$ is always positive, so that this locus lies in a region where $(\partial^2\mu/\partial\rho^2)_T$ is negative.

Using the scaling hypothesis, Widom(26) has shown that this locus is restricted to $\rho<\rho_c$ and near the critical point is defined by,

$$\rho-\rho_c = -b(T-T_c)^{2\beta} \qquad (88)$$

where b is a constant. He has also pointed out that the compressibility along $(\partial^2 P/\partial\rho^2) = 0$ is asymptotically the same as the compressibility along the critical isochore. In a more recent paper, J. M. H. Levelt Sengers(52) has indicated that the locus of maximum isothermal compressibility is similar to the one described by Eq. (88). Hence, the compressibilities along the three loci, $(\partial^2 P/\partial\rho^2)_T= 0$, $[\partial(1/K_T)/\partial\rho]_T= 0$ and $\rho=\rho_c$, have the same exponent γ.

The maximum isothermal compressibility on each isotherm was determined by an inverse interpolation method(53) which used interpolated values of K_T at equal intervals obtained from the spline fit of pressure versus angle. The values of $(K_T)_{max}$ from the 7-point formula of Ref. (53) and the values of pressure, angle, refractive index and

LL-function at which the maximum occured on each isotherm are listed in Table XVI. The locus of $(K_T)_{max}$ is shown in Fig. 24 with the dashed curve obtained from the fit to Eq. (88) and the solid line representing the rectilinear diameter. The substantial scatter of the points was due to the steepness of the isotherms which made it extremely hard to determine the angle at which $(K_T)_{max}$ occurred.

The fit to

$$\ln [(LL/LL_c)^2 (K_T)_{max}] = \ln \Gamma - \gamma \ln t \tag{89}$$

was performed for various values of T_c. The minimum in the standard deviation of the fit corresponded to T_c=209.286°K with γ=1.23±0.01, Γ=0.00117 atm^{-1} and σ_{fit}=0.0597. The fit is shown in Fig. 25. This value of γ was considerably higher than the value on the critical isochore.

6. Determination of γ_G' and γ_L' Along the Coexistence Curve

The behaviour of the isothermal compressibility along the phase boundary is governed by the power law in Eq. (14). Substituting LL/LL_c instead of the reduced density and considering the two branches separately, one obtains

$$(LL_L/LL_c)^2 K_T = \Gamma_L' \, (-t)^{-\gamma_L'} \tag{90}$$

and

$$(LL_G/LL_c)^2 K_T = \Gamma_G' \, (-t)^{-\gamma_G'} \tag{91}$$

To determine the above critical exponents and coefficients, the data were fitted to the following logarithmic forms,

$$\ln[(LL_L/LL_c)^2 K_T] = \ln \Gamma_L' - \gamma_L' \ln|t| \tag{92}$$

and

$$\ln[(LL_G/LL_c)^2 K_T] = \ln \Gamma_G' - \gamma_G' \ln|t| \tag{93}$$

The isothermal compressibilities on the phase boundary were determined by a modified spline fit described in Appendix E. The standard error assigned to $\ln[(LL/LL_c)^2 K_T]$ was

$$\sigma_{\ln[(LL/LL_c)^2 K_T]} = \left[x^2 + \sigma_n^2 \left(\frac{6n}{n^2+2} \right)^2 \left(\frac{2}{LL} \right)^2 \right]^{1/2} \tag{94}$$

where x was the fractional error in K_T.

The results of fitting the data to Eqs. (92) and (94) are presented in Table XVII. $\ln[(LL/LL_c)^2 K_T]$ on the gaseous and liquid branches of the coexistence curve are plotted versus $\ln|t|$ in Figs. 26 and 27. The values of the critical parameters obtained from this analysis were:

For T_c=209.286°K

$\gamma'_G = 1.15\pm0.01$, $\Gamma'_G = 0.021\pm0.001$ with σ_{fit}=0.074

$\gamma'_L = 1.12\pm0.01$, $\Gamma'_L = 0.0260\pm0.0005$ with σ_{fit}=0.019

The phase boundary is symmetric around the rectilinear diameter $\bar{\rho} = (\rho_L+\rho_G)/2$. Since $\bar{\rho} \neq \rho_c$, if the variable $\bar{\rho}$ rather than ρ_c is chosen as the reducing parameter, equations (92) and (93) become

$$\ln[(LL_L/\ \overline{LL})^2 K_T] = \ln \Gamma'_L - \gamma'_L \ln|t| \qquad (95)$$

and

$$\ln[(LL_G/\ \overline{LL})^2 K_T] = \ln \Gamma'_G - \gamma'_G \ln|t| \qquad (96)$$

The results of fitting the data to Eqs. (95) and (96) are shown in Figs. 28 and 29 for the gaseous and liquid branches respectively and are tabulated in Table XVIII. The values of the exponents and the coefficients thus determined were:

For T_c=209.286°K

$\gamma'_G = 1.16\pm0.01$, $\Gamma'_G = 0.0195\pm0.0011$ with σ_{fit}=0.074

$\gamma'_L = 1.14\pm0.01$, $\Gamma'_L = 0.0238\pm0.0005$ with σ_{fit}=0.020

The variations in the values of γ'_G and γ'_L obtained from the two methods of analysis were within their respective errors. In fact, the results indicated that γ'_G and γ'_L were indistinguishable.

7. Shape of the Critical Isotherm

The shape of the critical isotherm is defined by the power law in Eq. (12). This relationship is valid strictly at $T=T_c$. However, it is very hard to obtain precise data at the critical temperature and the value of δ cannot be easily determined. In fact, most δ values quoted in literature are calculated from treating Griffith's inequality as an equality or from scaling laws.

In this study, it was possible to approach the critical point 0.008°K from above and 0.012°K from below T_c along constant temperature curves. In this section, an attempt will be made to determine at least a limiting value of δ from the data on the seven isotherms close to T_c. Four of these were above and three were below T_c. Along the isotherms above T_c, the pressures at the critical density interpolated from the spline fit and along those below T_c, the vapor pressures were used as P_c. Then each isotherm was treated as though it was the critical isotherm and the values of δ on high-density and low-density sides were determined from a weighted linear least squares fit to the following logarithmic form.

$$\ln|P-P_c| = \ln \Delta + \delta \ln|(LL-LL_c)/LL_c| \qquad (97)$$

Both the dependent and the independent variables were assigned errors with

$$\sigma_{\ln|P-P_c|} = \sigma_P / |P-P_c| \tag{98}$$

and $$\sigma_{\ln|(LL-LL_c)/LL_c|} = (\sigma_n/|LL-LL_c|)(6n/(n^2+2)^2) \tag{99}$$

The weight at each point was calculated from the formula,

$$w_i = \{\sigma^2_{\ln|P-P_c|} + \delta^2\sigma^2_{\ln|(LL-LL_c)/LL_c|}\}^{-1} \tag{100}$$

Values of $|P-P_c|$ and $|LL-LL_c|$ on each isotherm are listed in Table XIX and the fits to Eq. (97) along two isotherms, for which $(T-T_c)=0.008°K$ and $(T-T_c)=-0.012°K$ respectively, are shown in Figs. 30 and 31. The values of δ obtained as described above are presented in Table XX and in Fig. 32, δ is plotted versus $(T-T_c)$. This analysis suggested $\delta=4.25\pm0.25$. This value compared very favorably with $\delta \geqq 4.22\pm0.02$ calculated from Eqs. (19) and (20) (Rushbrooke and Griffiths inequalities) using $\gamma'=1.15\pm0.01$ and $\beta=0.3571\pm0.0008$.

8. Evaluation of $\Delta\mu$

The difference in chemical potential can be evaluated by graphical integration from the following thermodynamic relationship,

$$\mu(\rho,t) - \mu(\rho_c,t) = \int_{P(\rho_c,t)}^{P(\rho,t)} \frac{1}{\rho}\, dP \qquad (101)$$

If ρ is replaced by LL and the μ is reduced by P_c/LL_c, the reduced difference in chemical potential is given by,

$$\Delta\mu = \frac{LL_c}{P_c} \int_{P(LL_c,t)}^{P(LL,t)} \frac{1}{LL}\, dP \qquad (102)$$

LL_c=0.070588 was obtained from the rectilinear diameter analysis. P_c was determined to be 54.213 atm. $P(LL_c)$ on each isotherm was computed by interpolation from the spline fit of LL versus P. The integral in Eq. (102) was performed integrating the spline fit of 1/LL versus P between adjacent data points on each isotherm. Each integral was checked by reversing the independent and the dependent variables in the spline fit and evaluating,

$$\mu - \mu_c = \left[\frac{P(LL)}{LL} - \frac{P(LL_c)}{LL_c}\right] - \int_{LL_c}^{LL} P\, d\left(\frac{1}{LL}\right) \qquad (103)$$

For the isotherms above T_c, the absolute values of $\Delta\mu$ calculated in this manner, when plotted versus absolute values of ΔLL, were anisymmetric around LL_c as illustrated in Figs. 33, 34, 35 and 36. Also P, LL, ΔLL and $\Delta\mu$ at single phase states above T_c are listed in Table XXII.

For $T<T_c$, $\Delta\mu=\mu(LL,t)-\mu(LL_{coex},t)$ and since the coexistence curve is antisymmetric around $\overline{LL}=(LL_L+LL_G)/2$, the variable $\overline{LL}$ rather than LL_c was used in calculation of ΔLL. In Figs. 37, 38, and 39, $|\Delta\mu|$ and $|\Delta LL|$ along isotherms below T_c are shown. These plots indicated that the range of antisymmetry for $T<T_c$ was much smaller than the range for $T>T_c$. In fact the former was confined to $-0.2\%\leq t<-5.7\times10^{-5}$ and $-30\%<\Delta LL<30\%$. The values of $\Delta\mu$, ΔLL, LL and P for the antisymmetric range of the isotherms below T_c are tabulated in Table XXIII.

As a result of this investigation the antisymmetric range of $\Delta\mu$ for krypton was found to extend over $-0.2\%\leq t<4.8\%$ and $-30\%<\Delta LL<30\%$.

9. The Analysis of the $\Delta\mu$, ΔLL, t Data

If $\Delta\rho$ is replaced by ΔLL and the scaling relationship among the critical exponents in Eq. (31) is used, the scaled equation of state in Eq. (34) can be expressed as

$$\Delta\mu = \Delta LL \; |\Delta LL|^{\gamma/\beta} \; h(x) \tag{104}$$

with $x = t/|\Delta LL|^{1/\beta}$

Hence, $h(x)$ can be calculated using the $\Delta\mu$, ΔLL data from Eq. (104) and these values can be fitted to the proposed form of $h(x)$ in Eq. (43) which contains six parameters E_1, E_2, γ, β, T_c and x_o.

In this study, the values of T_c, β and x_o were known from the analysis of the coexistence curve. Therefore, $T_c = 209.286°K$, $\beta = 0.357$ and $x_o = 1/B^{1/\beta} = 0.18122$ were fixed. Then, an unweighted non-linear least squares fit(51) was performed to determine γ, E_1 and E_2. The results were: $\gamma = 1.167 \pm 0.005$, $E_1 = 2.13 \pm 0.02$ and $E_2 = 0.259 \pm 0.005$.

Fixing T_c, β and x_o made a weighted linear least squares fit(48) possible in which γ could be varied parametrically to determine the corresponding E_1 and E_2. When Eqs. (43) and (104) were combined, the following convenient form for the linear fit was obtained.

$$\left(\frac{x_o}{x+x_o}\,\frac{\Delta\mu}{\Delta LL|\Delta LL|^{\gamma/\beta}}\right)^{2\beta/(\gamma-1)} = E_1^{\,2\beta/(\gamma-1)}\left[1+E_2\left(\frac{x+x_o}{x_o}\right)^{2\beta}\right] \tag{105}$$

Setting

$$X = \left(\frac{x+x_o}{x_o}\right)^{2\beta}$$

and
$$Y = \left[\frac{x_o}{x+x_o}\,\frac{\Delta\mu}{\Delta LL|\Delta LL|^{\gamma/\beta}}\right]^{2\beta/(\gamma-1)}$$

X and Y were calculated from the $\Delta\mu,\Delta LL$ data for a given value of γ. The errors σ_Y and σ_X assigned to Y and X were respectively,

$$\sigma_Y^2 = \frac{\left(\frac{\sigma_{\Delta\mu}}{\Delta\mu}\right)^2 + \left(\frac{\sigma_t}{t}\right)^2\left(\frac{x}{x+x_o}\right)^2 + \left(\frac{\sigma_{\Delta LL}}{\Delta LL}\right)^2\left(1+\frac{\gamma}{\beta}-\frac{x}{\beta(x+x_o)}\right)^2}{\left(\frac{\gamma-1}{2\beta Y(X)}\right)^2} \tag{106}$$

$$\sigma_X^2 = \frac{\left[\left(\frac{\sigma_t}{t}\right)^2 + \frac{1}{\beta^2}\left(\frac{\sigma_{\Delta LL}}{\Delta LL}\right)^2\right] X^2}{\left(\frac{x+x_o}{2\beta x}\right)^2} \tag{107}$$

where $\sigma_t=0.001/T_c$, $\sigma_{\Delta LL}=\sigma_{LL}/LL_c$ and $\sigma_{\Delta\mu}=2\sigma_P/P_c\simeq 1.0\times 10^{-4}$. A weighted linear least squares fit to Eq. (105) was performed for various values of γ. The minimum in the standard deviation of the fit occured for $\gamma=1.18$ with $E_1=2.21\pm0.01$ and $E_2=0.264\pm0.004$. To illustrate the quality of this fit, $\ln h(x)$ and $\ln[(x+x_o)/x_o]$ calculated from the $\Delta\mu$, ΔLL data are plotted in Figs. 40 and 41 with the solid line obtained using the above values of γ, E_1 and E_2. The relative deviations $[h(x)_{exp't}-h(x)_{fitted}]/h(x)_{exp't}$, shown in Fig. 42, were scattered randomly.

To ensure that the determined parameters were independent of the range of the data, the fit to Eq. (105) was repeated by successively decreasing the range of t and observing the variations in the values of γ, E_1 and E_2. The results are summarized in Table XXIV and no appreciable changes were noted.

Also, using the values of γ, E_1 and E_2 obtained from the weighted fit, values of Δ, Γ and Γ' were calculated from Eqs. (44), (45) and (46). These were: $\Delta=2.34$, $\Gamma=0.084$ and $\Gamma'=0.021$.

A further test of the fit was made by comparing the isothermal compressibilities calculated from the differentiation of the data and listed in Tables V and VI with those calculated from

$$K_T = \frac{1}{\rho^2 (\frac{\partial\mu}{\partial\rho})_T} = \frac{LL_c}{LL^2 P_c (\frac{\partial\Delta\mu}{\partial LL})_T} \tag{108}$$

where $$(\frac{\partial\Delta\mu}{\partial LL})_T = \frac{1}{LL_c}\left[\frac{\delta\Delta\mu}{\Delta LL} - \frac{x}{x+x_o}\,\frac{1}{\beta|\Delta LL|}\,\Delta\mu\left(1+\frac{1+\gamma G}{1+G}\right)\right]$$

and $$G = E_2\left(\frac{x+x_o}{x_o}\right)^{2\beta}$$

These comparisons are shown in Figs. 43, 44 and 45 along three isotherms for which $T-T_c=-0.160$°K, $T-T_c=0.164$°K and $T-T_c=1.024$°K respectively. The agreement between the experimental and the calculated K_T was very good.

10. Predictions of the Linear Model(32)

An interesting feature of the linear model is that the critical coefficients are determined by the critical exponents. If the disposable parameter b^2 in Eq. (48) is chosen according to Eq. (57), then

$$\Gamma/\Gamma' = \frac{\gamma}{\beta}\left[\frac{\gamma(1-2\beta)}{2\beta(\gamma-1)}\right]^{\gamma-1} \tag{109}$$

$$\Gamma B^{\delta-1}D^{-\delta} = \left[\frac{\gamma-2\beta}{(1-2\beta)}\right]^{(\gamma-2\beta)/2\beta}\left[\frac{1-2\beta}{2\beta}\,\frac{\gamma}{\gamma-1}\right]^{\gamma-1} \tag{110}$$

where $D=(1/\Delta)^{1/\delta}$.

In this study, from direct application of the data to the power laws in Eqs. (11), (12), (13) and (14) the following values of exponents and coefficients were found. $\beta=0.357$, $B=1.84$, $\gamma=1.18$, $\Gamma=0.0835$, $\Gamma'=0.0217$ and $\delta=4.25$. From the analysis of the $\Delta\mu$, ΔLL data and Eq. (44), $\Delta=2.34$ and $\delta=1+\gamma/\beta=4.30$ were obtained. Thus, the predictions of the linear model in Eqs. (109) and (110) could be tested using these values. The comparison of the experimental coefficients with the predictions of the linear model are summarized below:

$$b^2 = \frac{\delta-3}{(\delta-1)(1-2\beta)} = 1.38$$

$$a = B(b^2-1)^{\beta}/\Gamma = 15.6$$

Γ/Γ'	model	3.93
	expt.	3.8±0.5

$\frac{\Gamma B^{\delta-1}}{D^{\delta}}$	model	1.78
	expt.	1.4±0.2

The above comparison showed that the predictions of the linear model were in good agreement with the experimental results within the experimental uncertainties.

V. CONCLUSIONS

Making use of the method of angle of minimum deviation, refractive indices, pressures and temperatures of krypton at states near its critical point were measured. The data included 35 states along the two-phase boundary and measurements along 16 isotherms above and along 11 isotherms below the critical temperature.

The refractive index was related to the density through the Lorentz-Lorenz formula whose validity for the range of the data was substantiated in Appendix D.

The P, T, ρ data thus obtained were applied to the asymptotic power laws to determine the critical exponents and coefficients which govern the approach to the critical point. From the coexistence curve and the rectilinear diameter analyses, the following values of the critical parameters were obtained: $T_c = 209.286 \pm 0.010$°K, $LL_c = 0.070588 \pm 0.000006$ or $n_c = 1.10808 \pm 0.00010$, $\beta = 0.3571 \pm 0.0008$ and $B = 1.840 \pm 0.001$ with a straight rectilinear diameter whose slope was 0.0918 ± 0.0004. The critical pressure was determined from the vapor pressures and the pressures along the critical isochore and was 54.213 ± 0.003 atm. Values of $\gamma = 1.182 \pm 0.008$ and $\Gamma = 0.0835 \pm 0.0011$ were obtained from the isothermal compressibilities on the critical isochore. The locus of maximum isothermal compressibility $(K_T)_{max}$ was established and the behaviour of K_T along this locus predicted $\gamma=1.23\pm0.01$ which did not agree with γ on the critical isochore. The discrepancy was most likely due to the inaccuracy in locating the maxima. From analyzing K_T along the two branches of the coexistence curve separately and taking the averages of the results predicted by reducing with LL_c and $\overline{LL}$, the following values of the critical exponents and coefficients were found: $\gamma'_G=1.15\pm0.01$, $\Gamma'_G=0.021\pm0.001$ and $\gamma'_L=1.13\pm0.01$, $\Gamma'_L=0.025\pm0.01$. These values indicated that γ'_G and γ'_L were not distinguishable and suggested $\gamma'<\gamma$ rather than $\gamma'=\gamma$. A limiting value for δ was obtained from treating seven isotherms close to the critical temperature as though each one was the critical isotherm and then interpolating for the best value of δ which was $\delta=4.25\pm0.25$. This value was in good agreement with the limit $\delta\geqq4.22\pm0.02$ set by the Rushbrooke and Griffiths inequalities for $\gamma'=1.15\pm0.01$ and $\beta=0.3571\pm0.0008$.

The reduced chemical potential differences and the reduced density differences were calculated from the ρ,P data along single phase isotherms. $\Delta\mu$ was observed to be antisymmetric with respect to LL_c for $-0.2\%\leqq t<4.8\%$ and $-30\%<\Delta\rho<30\%$. The data in the antisymmetric range were fit to the proposed equation of state$^{(26,27)}$ using the form of $h(x)$ suggested in Ref. (29). After fixing T_c, β and x_o the results of a three-parameter non-linear fit were: $\gamma=1.167\pm0.005$, $E_1=2.13\pm0.02$, $E_2=0.259\pm0.005$; the results of a weighted linear fit were: $\gamma=1.18\pm0.01$, $E_1=2.21\pm0.01$, $E_2=0.264\pm0.004$. Using the latter values of γ, E_1 and E_2, the critical coefficients Δ, Γ and Γ' were determined to be $\Delta=2.34$, $\Gamma=0.084$ and $\Gamma'=0.021$. The values of γ, Γ, Γ' obtained from the scaled equation of state were in very good agreement with those determined from the isothermal compressibilities. Moreover, the values of coefficients compared very favorably with those quoted for other fluids and obtained from similar analyses as illustrated in Table XXIV.

The predictions of the linear model(32) derived from the parametric representation of the scaling hypothesis were also tested. The linear model predicted $\Gamma/\Gamma'=3.93$ and $\Gamma B^{\delta-1}/D^{\delta}=1.78$ but $\Gamma/\Gamma'=3.8\pm0.5$ and $\Gamma B^{\delta-1}/D^{\delta}=1.4\pm0.2$ were determined using the results from the direct application of the data to the power laws. Hence, the predictions of the linear model were consistent with the experimental results within error limits.

The values of the critical exponents obtained in this study support the recognition that widely different systems behave similarly near their critical points. In Table XXV β, γ, and δ values for several substances obtained by different techniques are tabulated. In spite of the diversity in the natures of these systems and in the methods of analysis, there seems to be evidence for universal behaviour.

REFERENCES

1. H. A. Lorentz, The Theory of Electrons, (B. G. Teubner, Germany, 1909)
2. W. F. Brown, Encyclopedia of Physics, Vol. XVII, edited by S. Flugge, (Springer-Verlag, Berlin, Germany, 1956)
3. J. A. Beattie, Proc. Acad. Arts & Sci. **30**, 422(1952)
4. J. G. Kirkwood, J. Chem. Phys. **4**, 592(1936); J. Yvon, C. R. Acad. Sci.,Paris **202**, 35(1936); L. Jansen and P. Mazur, Physica, Haag **21**, 193(1955)
5. S. Y. Larsen, R. D. Mountain and R. Zwanzig, J. Chem. Phys. **42**, 2187(1965)
6. R. K. Teague and C. J. Pings, J. Chem. Phys. **48**, 4973(1968)
7. R. L. Amey and R. H. Cole, J. Chem. Phys. **40**, 146(1964)
8. C. M. Knobler, C. P. Abbiss and C. J. Pings, J. Chem. Phys. **41**, 2200(1964)
9. M. E. Fisher, Rep. Prog. Phys. **30**, 615(1967)
10. H. E. Stanley, Introduction to Phase Transitions and Critical Phenomena (Oxford University Press, New York, 1971)
11. J. S. Rowlinson, Liquids and Liquid Mixtures (Plenum Press, New York, 1969) Chap. 3.
12. M. E. Fisher, Critical Phenomena, Proc. of a Conference, Washington, D. C. ,1965, [edited by M. S. Green and J. V. Sengers, NBS Miscell. Publ. No 273 (U. S. Government Printing Office, Washington, D. C., 1966)], p. 21.

13. G. S. Rushbrooke, J. Chem. Phys. 39, 842(1963)

14. R. B. Griffiths, Phys. Rev. Letters 14, 623(1965)

15. J. D. van der Waals, Z. Physik. Chem. 13, 657(1894)

16. C. Kittel, Solid State Physics, (New York; John Wiley, 1956)

17. L. D. Landau and E. M. Lifshitz, Statistical Physics (Oxford: Pergamon Press, 1958)

18. E. Ising, Z. Phys. 31, 253(1925)

19. L. Onsager, Phys. Rev. 65, 117(1944)

20. C. Domb, Adv. Phys. 9,149(1960)

21. G. A. Baker, Phys. Rev. 129, 99(1963)

22. J. W. Essam and M. E. Fisher, J. Chem. Phys. 38, 802(1963)

24. M. F. Sykes, J. W. Essam and D. S. Gaunt, J. Math. Phys. 6, 283(1965)

23. M. F. Sykes and M. E. Fisher, Physica 28, 919(1962)

25. M. A. Moore. D. Jasnow and M. Wortis, Phys. Rev. Letters 22, 940(1969)

26. B. Widom, J. Chem. Phys. 43, 3898(1965)

27. R. B. Griffiths, Phys. Rev. 158, 176(1967)

28. R. B. Griffiths and J. C. Wheeler, Phys. Rev. A2, 1047(1970)

29. M. Vicentini-Missoni, J. M. H. Levelt Sengers, and M. S. Green, J. Res. Nat. Bur. Std. 73A, 563(1969)

30. P. Schofield, Phys. Rev. Letters 22, 606(1969)

31. John T. Ho and J. D. Litster, Phys. Rev. Letters 22, 603(1969)

32. P. Schofield, J. D. Litster and John T. Ho, Phys. Rev. Letters <u>23</u>, 1098(1969)

33. B. L. Smith, Rev. Sci. Instr. <u>34</u>, 19(1963)

34. C. P. Abbiss, C. M. Knobler, R. K. Teague and C. J. Pings, J. Chem. Phys. <u>42</u>, 4145(1965)

35. R. K. Teague, doctoral thesis, California Institute of Technology, Pasadena, California, 1968.

36. S. Y. Wu, doctoral thesis, California Institute of Technology, Pasadena, California, 1972.

37. C. M. Knobler, W. I. Honeywell and C. J. Pings, Rev. Sci. Instr. <u>34</u>, 1437(1963)

38. W. I. Honeywell, doctoral thesis, California Institute of Technology, Pasadena, California, 1964.

39. H. L. Daneman and G. C. Mergner, Rev. Sci. Instr. <u>39</u>, 1498(1968)

40. T. M. Dauphinee, Can. J. Phys. <u>31</u>, 577(1953)

41. H. H. Reamer and B. H. Sage, Rev. Sci. Instr. <u>39</u>, 709(1958)

42. W. I. Honeywell and C. J. Pings, Rev. Sci. Instr. <u>36</u>, 754(1965)

43. RCA Transistor, Thyristor and Diode Manual, Radio Corporation of America, 1969, pp. 162-165.

44. F. Theeuwes and R. J. Bearman, J. Chem. Thermodynamics <u>2</u>, 171(1970)

45. J. L. Walsh, J. H. Ahlberg and E. N. Nilson, J. Math & Mech. <u>11</u>, 225(1962)

46. J. M. H. Levelt Sengers, J. Straub and M. Vicentini-Missoni, J. Chem. Phys. <u>54</u>, 5034(1971)

47. P. R. Bevington, Data Reduction and Error Analysis, (McGraw-Hill Company, New York, 1969) pp. 104-105.

48. J. H. Williamson, Can. J. Phys. 46, 1845(1968)

49. B. Widom and J. Rowlinson, J. Chem. Phys. 52, 1670(1970)

50. M. S. Green, M. J. Cooper and J. M. H. Levelt Sengers, Phys. Rev. Letters 26, 492(1971)

51. D. W. Marquardt, J. Soc. Industrial & Appl. Math. 11, 431(1963)

52. J. M. H. Levelt Sengers, Ind. Eng. Chem. Fundam. 9, 470(1970)

53. H. E. Salzer, Math. Tables & Other Aids to Computation 5, 213(1951)

54. H. A. Kierstead, Phys. Rev. A7, 242(1973)

55. L. A. Weber, Phys. Rev. A2, 2379(1970)

56. J. M. H. Levelt Sengers and S. C. Greer, Int. J. Heat Mass Transfer 15, 1865(1972)

57. M. A. Weinberger and W. G. Schneider, Can. J. Chem. 30, 422(1952)

58. P. R. Roach and D. H. Douglas, Phys. Rev. Letters 17, 1083(1966)

59. H. M. Roder, D. B. Diller, L. A. Weber and R. D. Godwin, Cryogenics 3, 16(1963)

60. J. H. Lunacek and D. S. Conell, Phys. Rev. Letters 17, 841(1971)

61. J. Zollweg, G. Hawkins, I. W. Smith, M. Giglio and G. B. Benedek, J. Phys. Suppl. 33, 135(1972)

62. V. G. Puglielli and N. C. Ford, Phys. Rev. Letters 25, 143(1970)

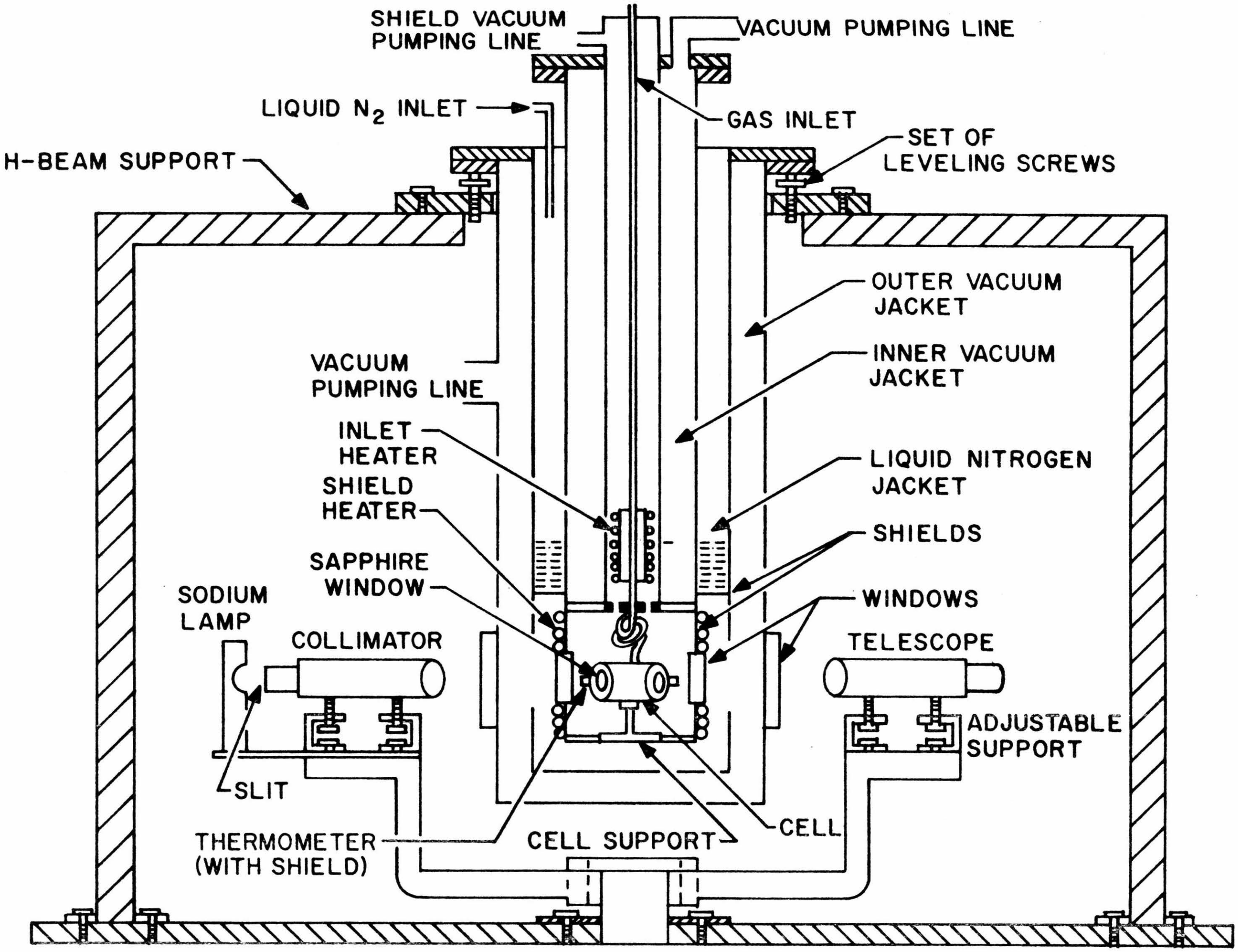

Figure 1. Cell, Cryostat and Spectrometer Assembly

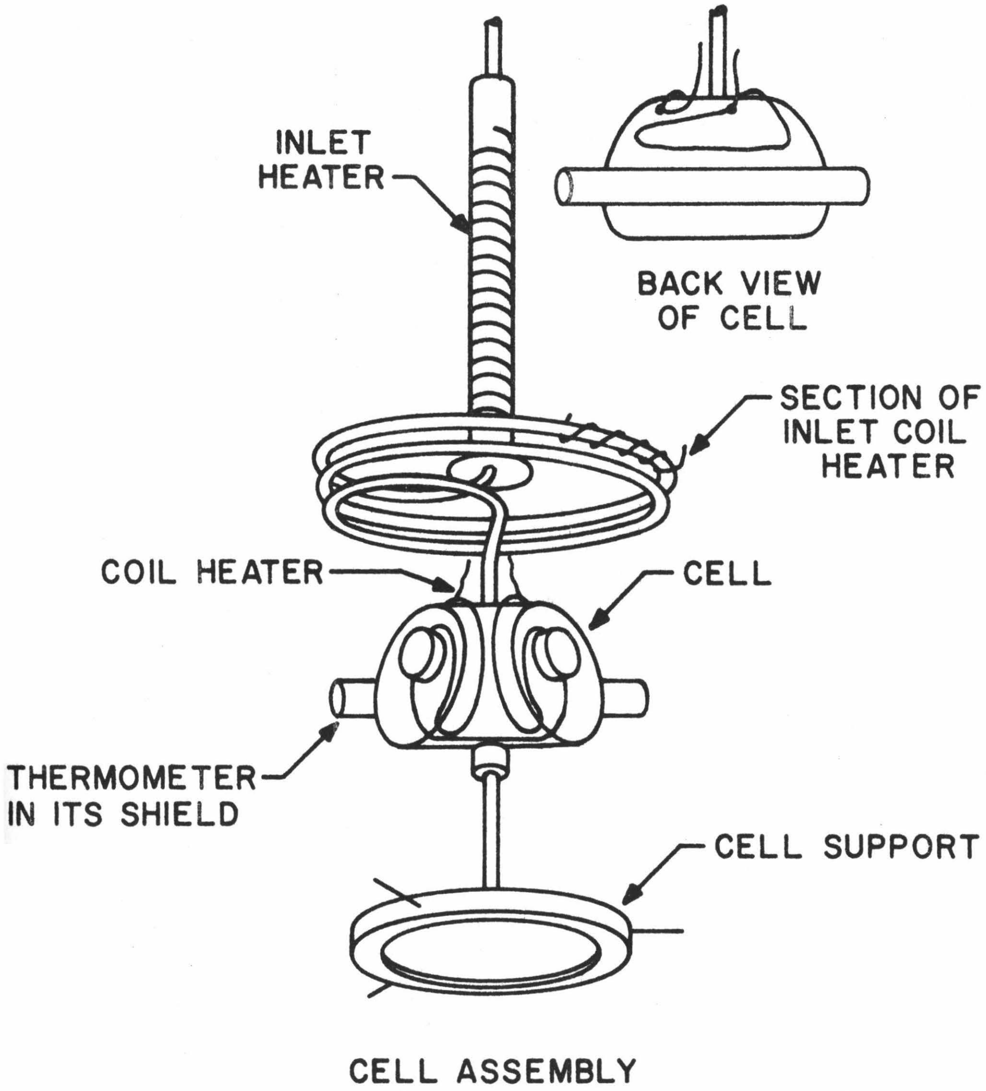

Figure 2. The Cell

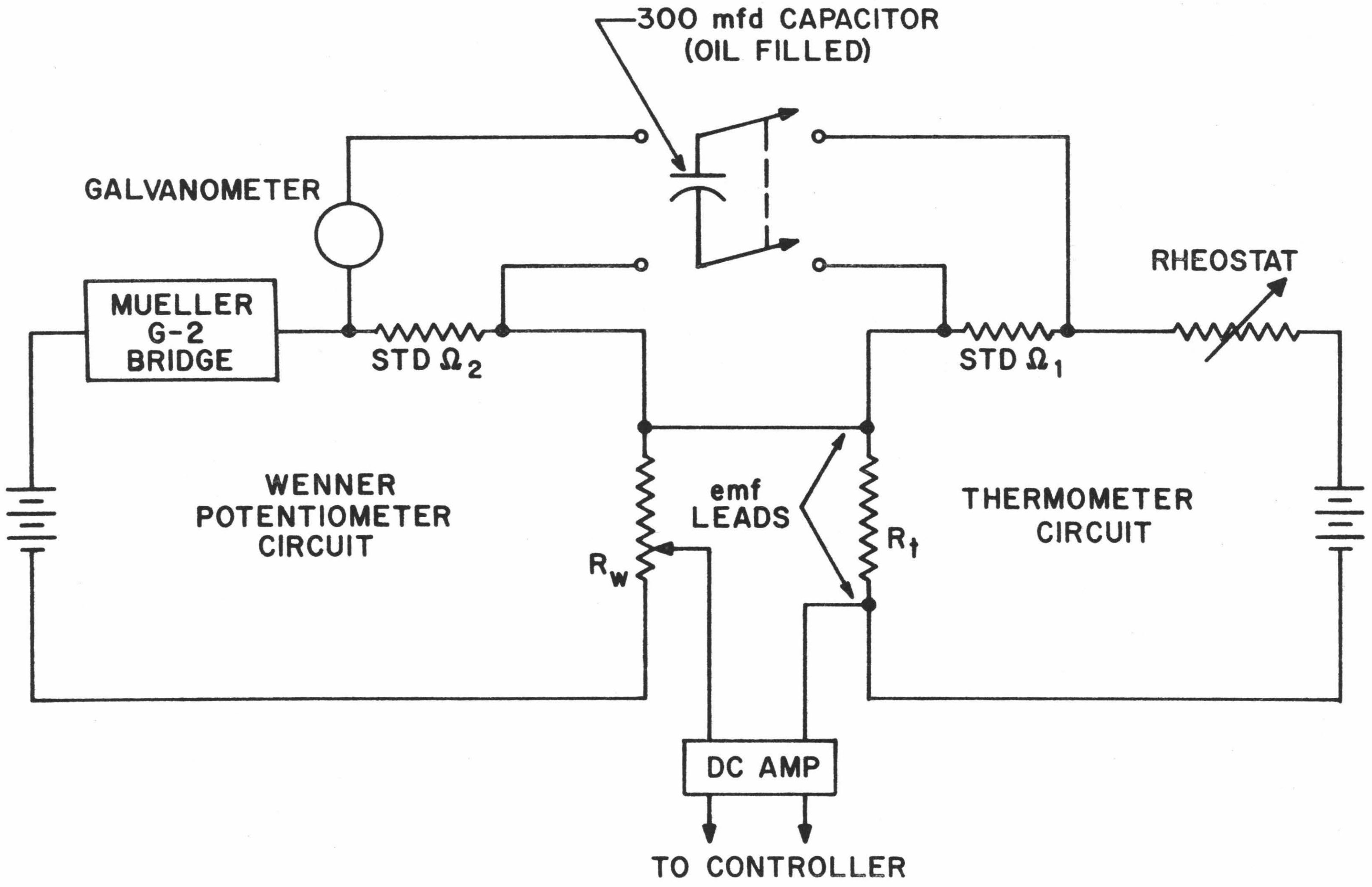

Figure 3. Temperature Measurement and Control Circuit

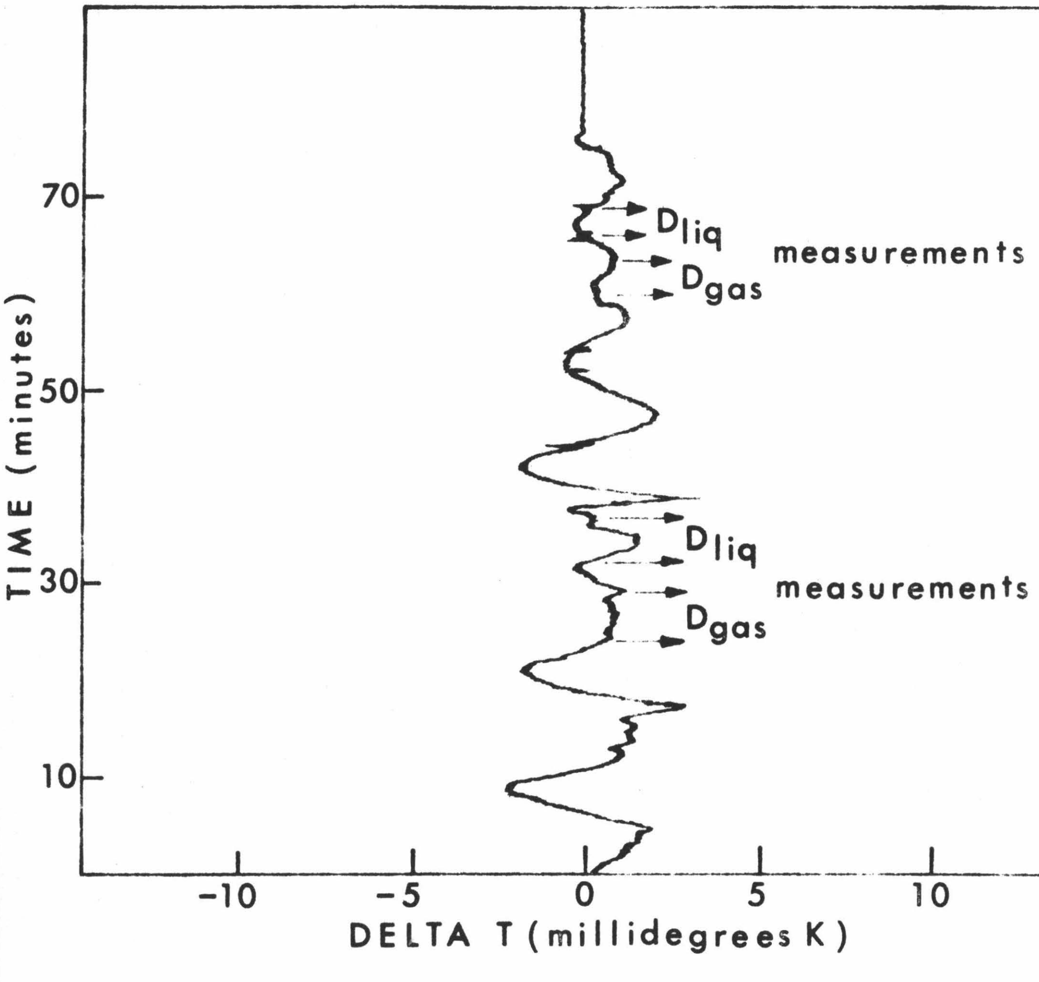

Figure 4. Temperature Control Record at the start of the study

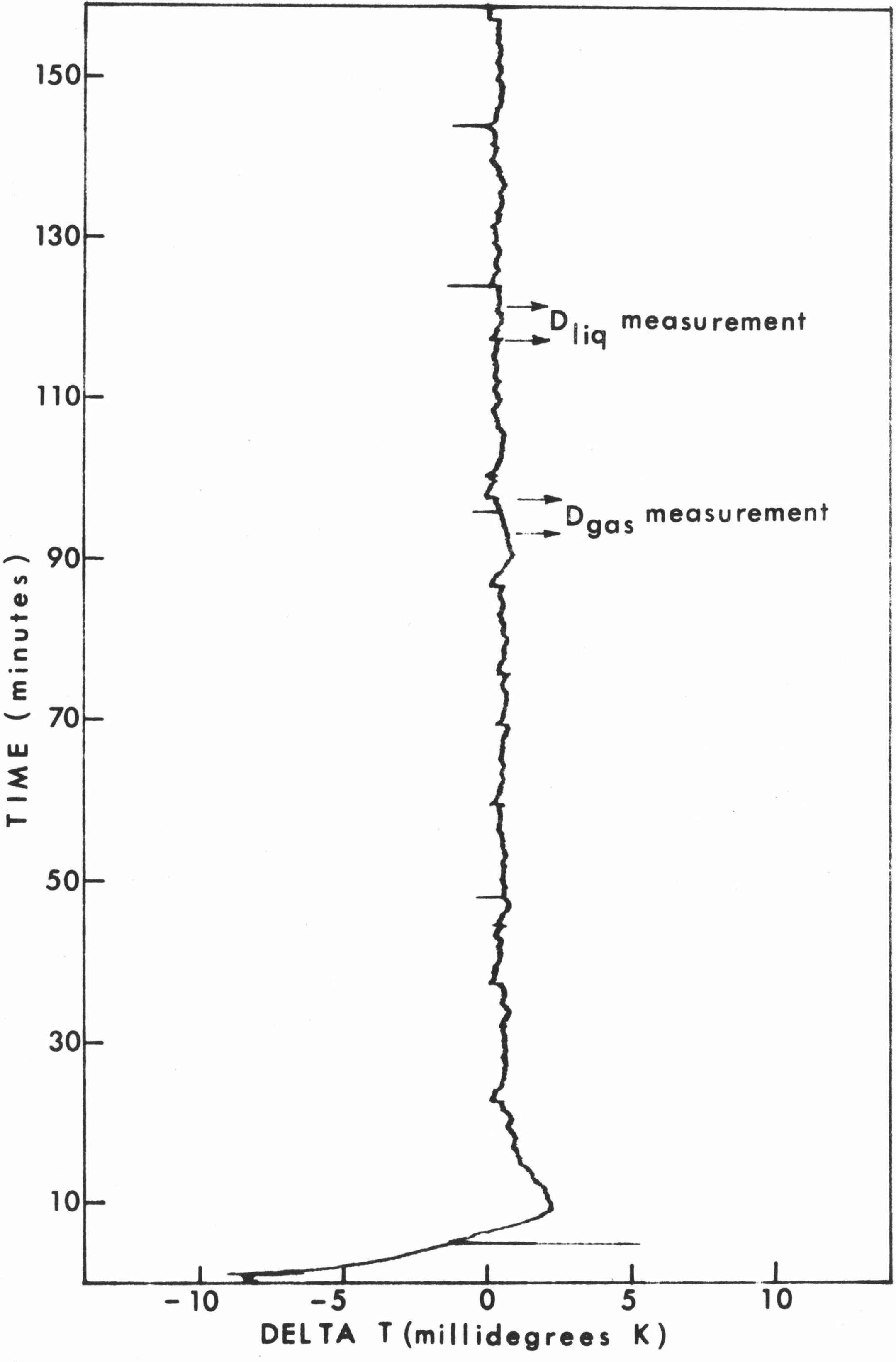

Figure 5. Improved Temperature Control Record

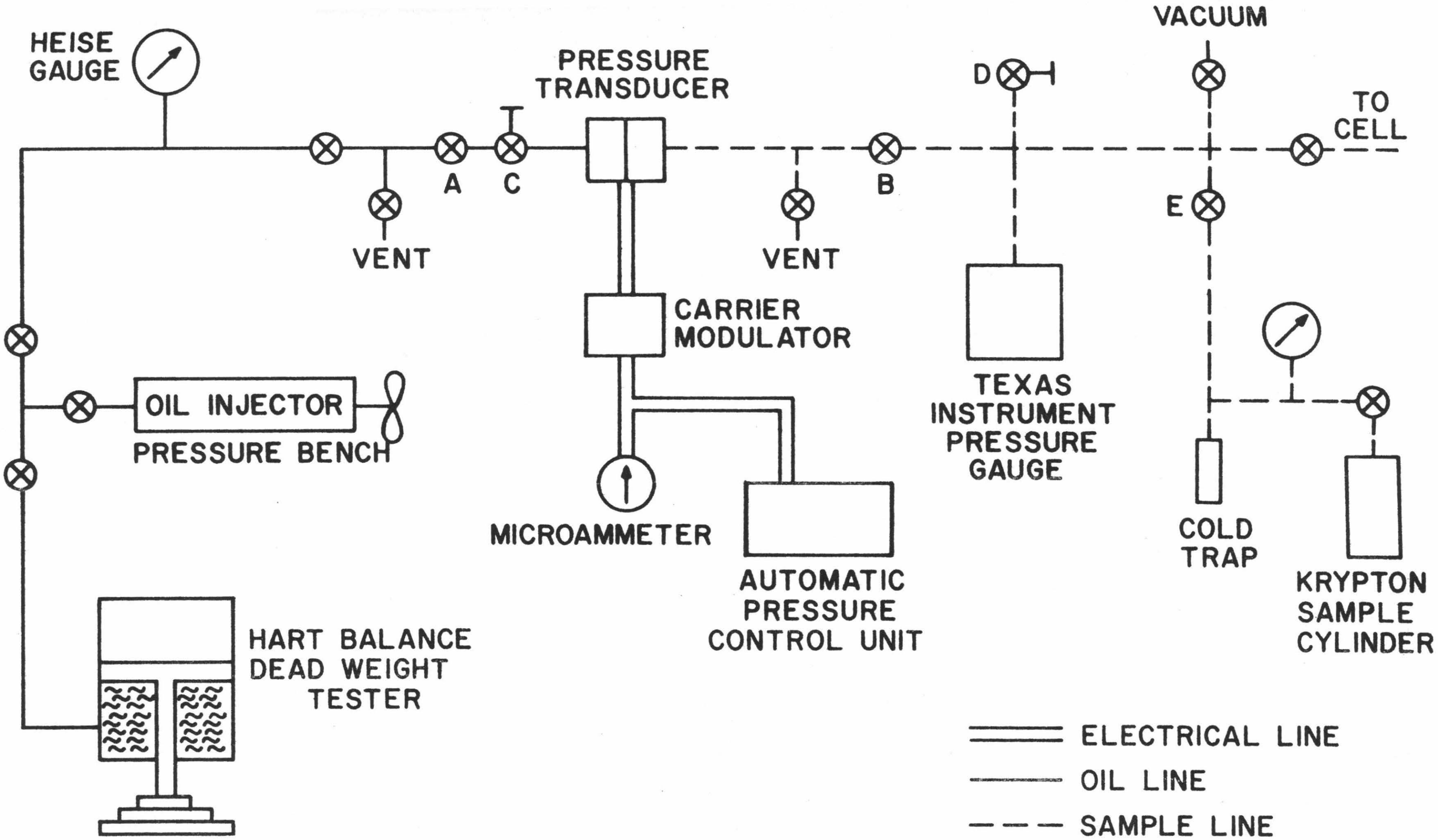

Figure 6. Pressure Measurement and Control Chart

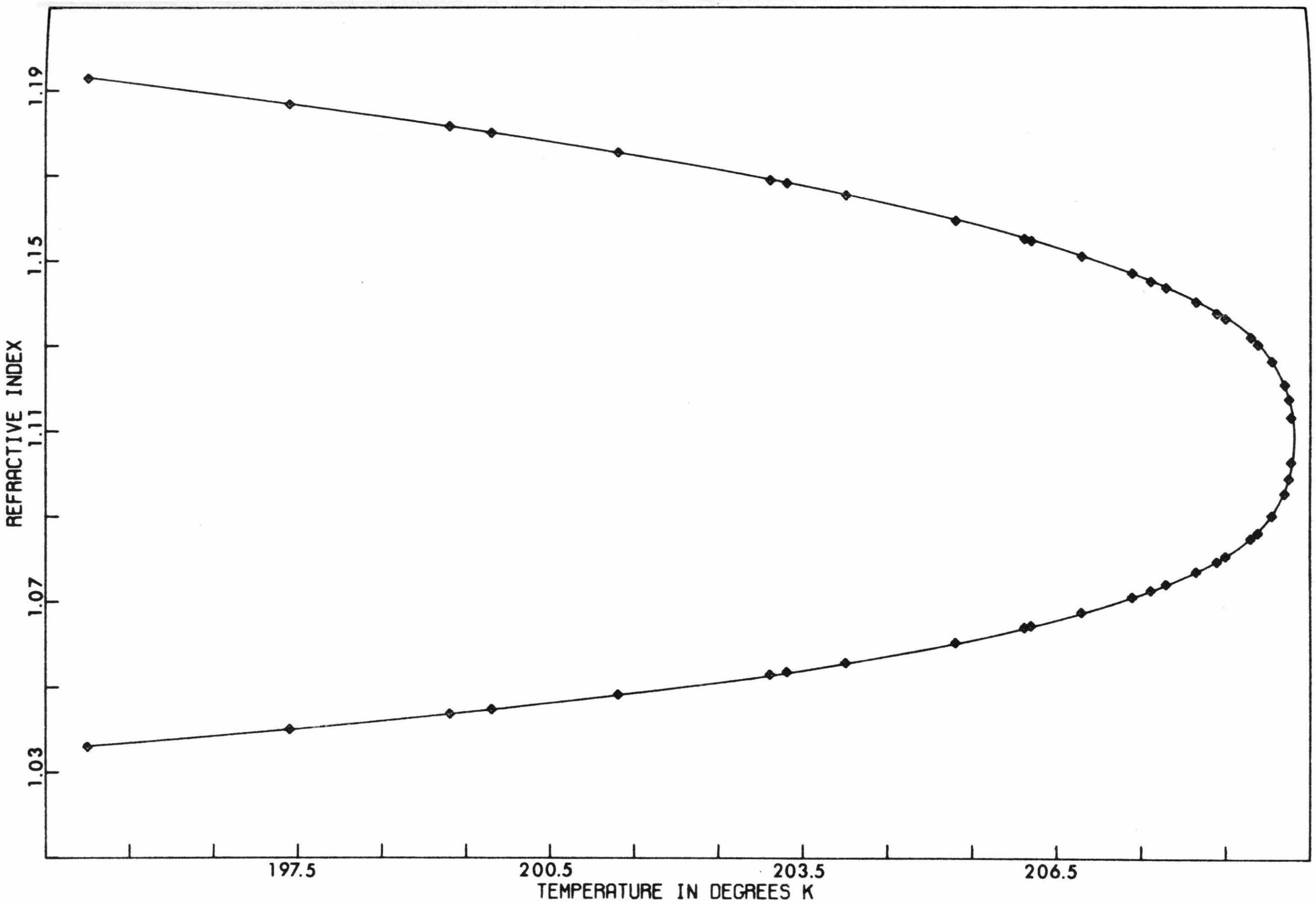

Figure 7. Coexistence Curve of Krypton

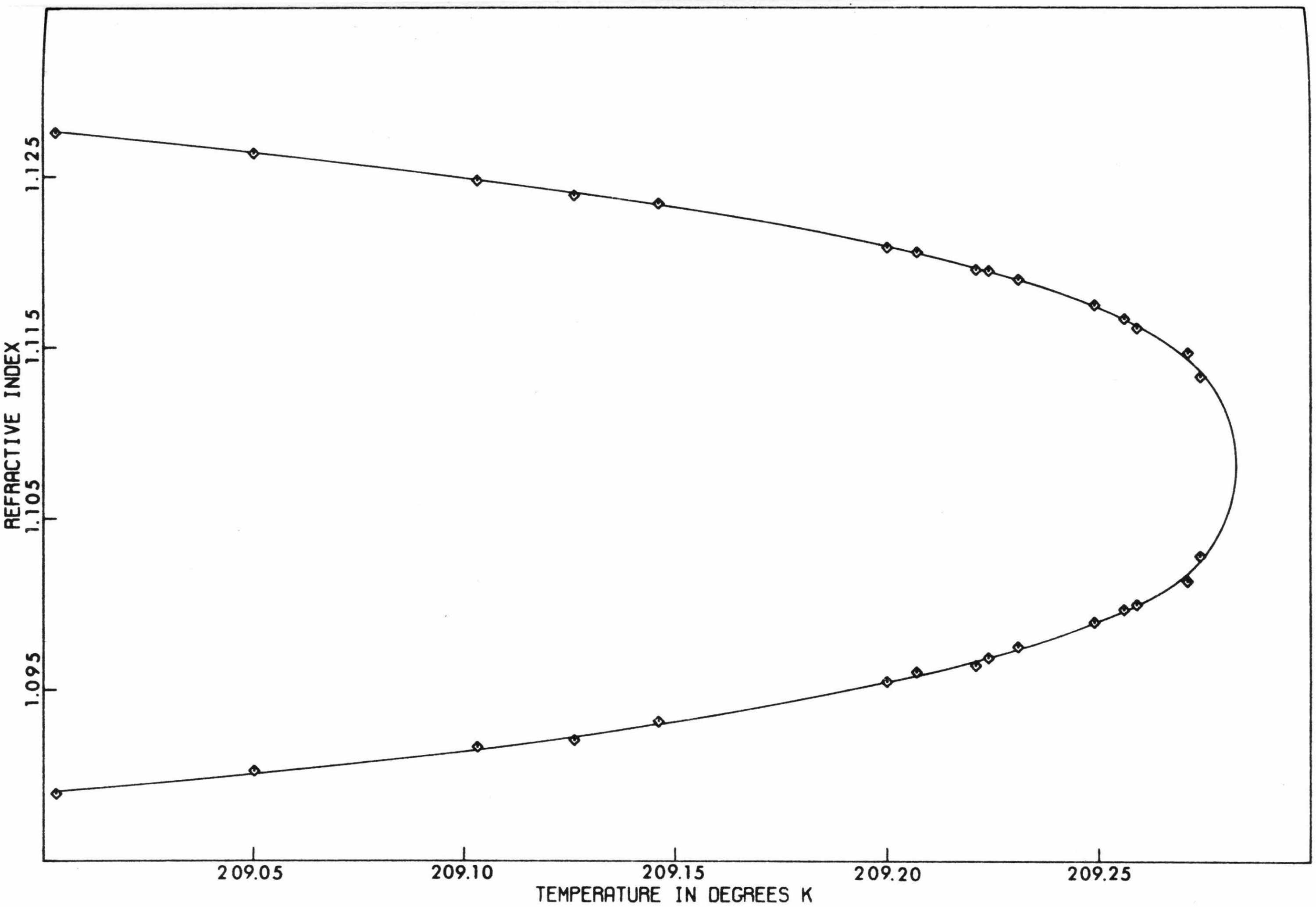

Figure 8. Coexistence Curve of Krypton close to the Critical Point

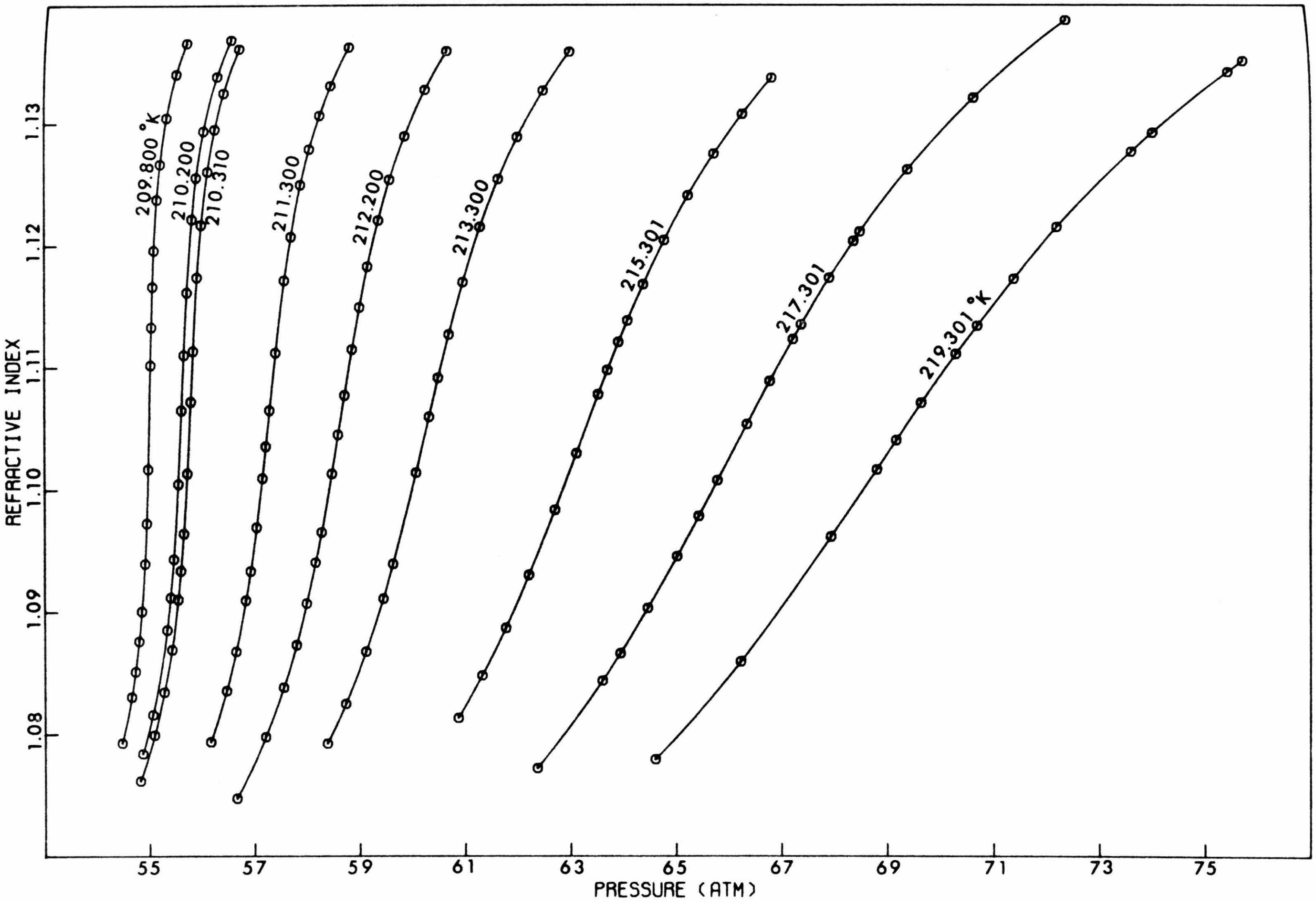

Figure 9. Single Phase Isotherms above T_C

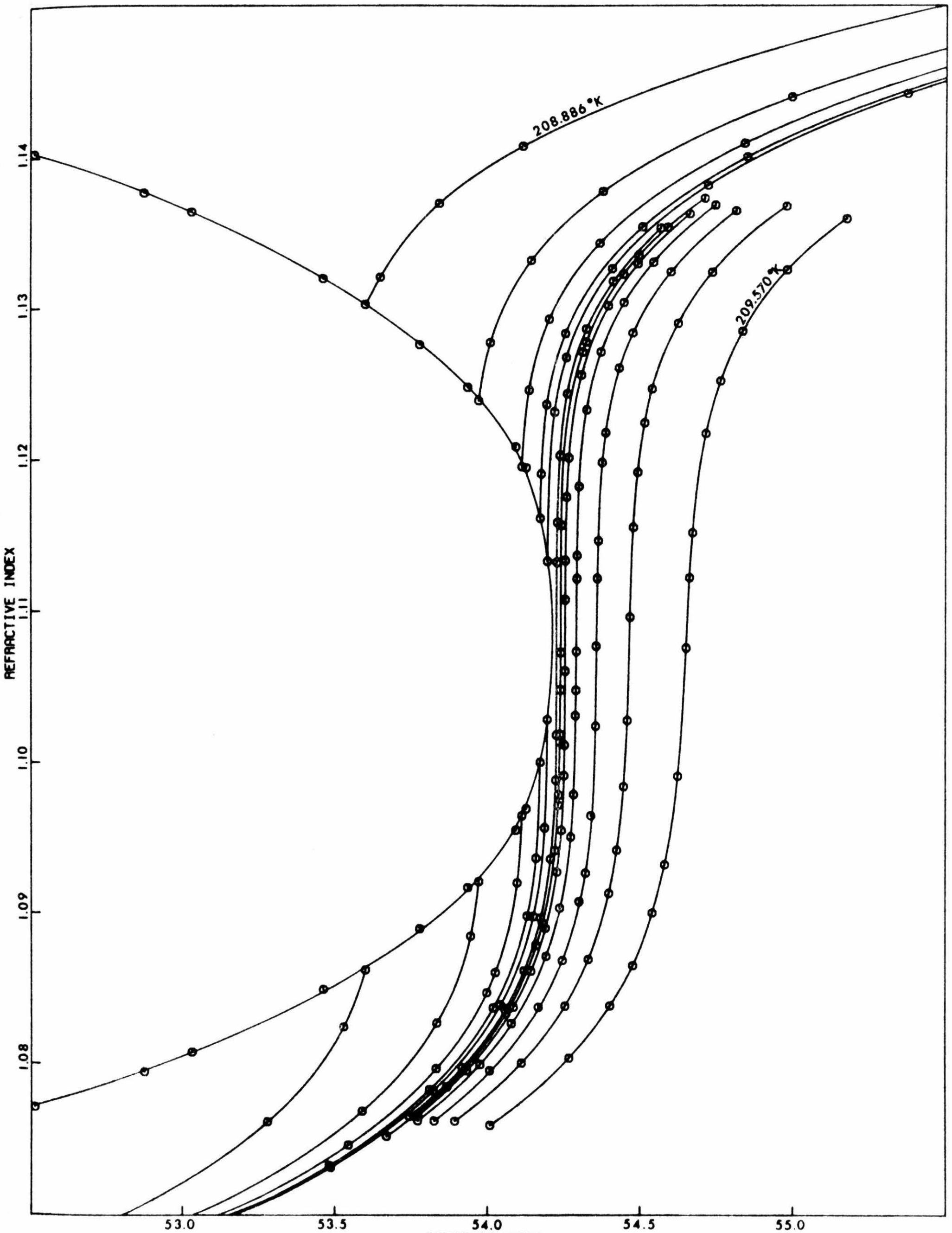

Figure 10. Isotherms close to T_c. Temperatures from left to right are 208.886, 209.126, 209.221, 209.259, 209.274, 209.294, 209.302, 209.315, 209.338, 209.380, 209.450, and 209.570°K.

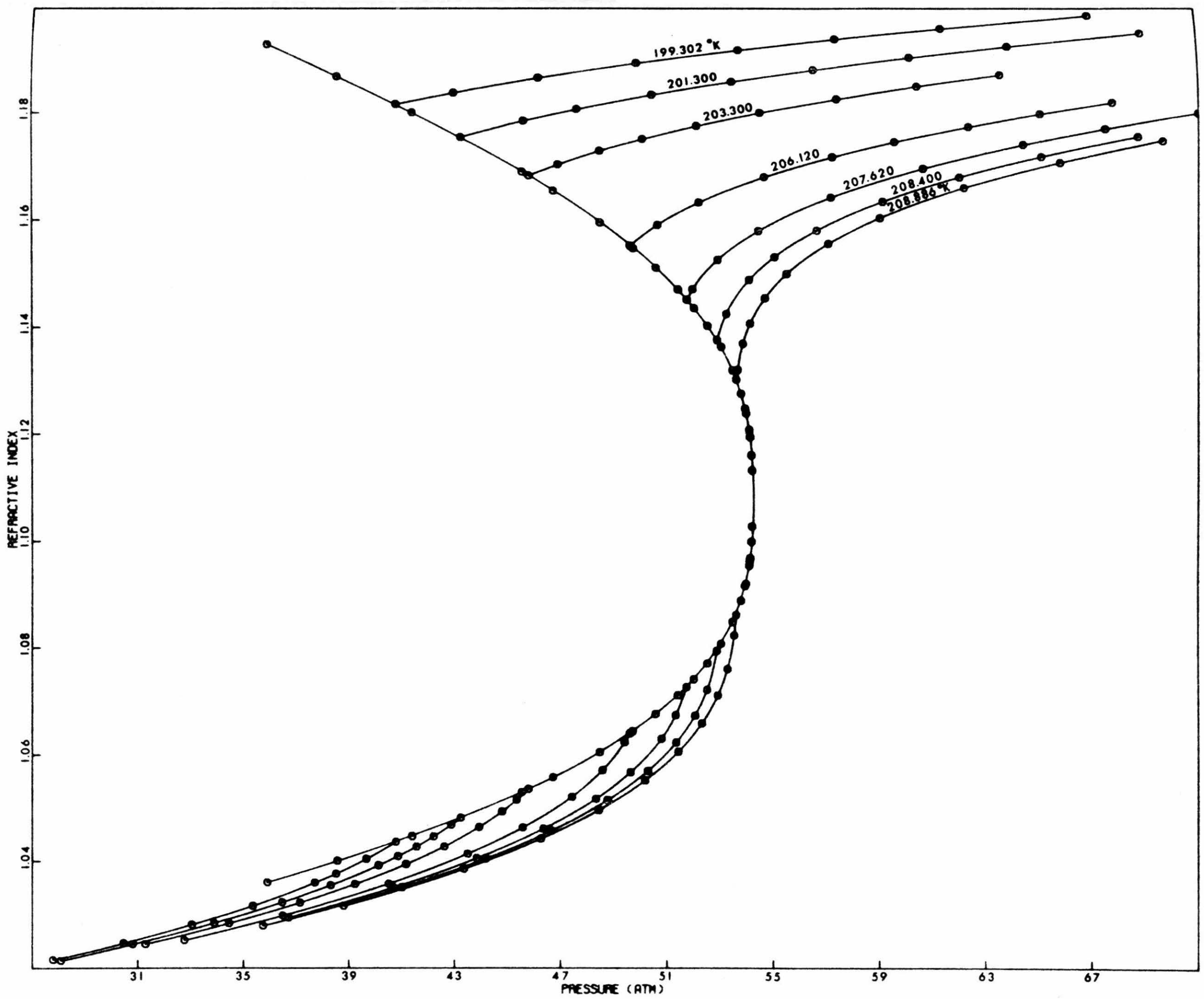

Figure 11. Single Phase Isotherms below T_c

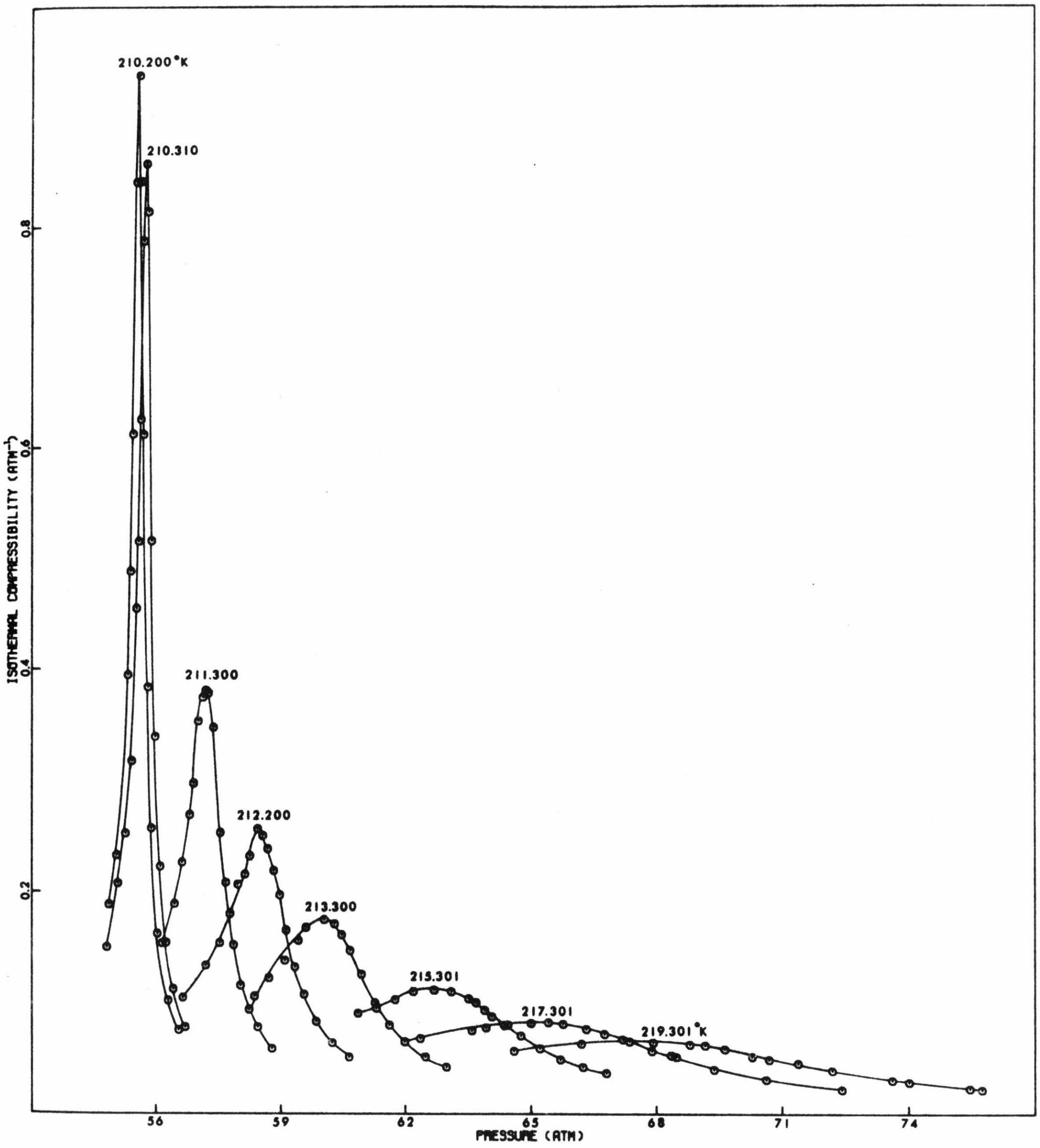

Figure 12. Isothermal Compressibility along 210.200°K to 219.301°K Isotherms

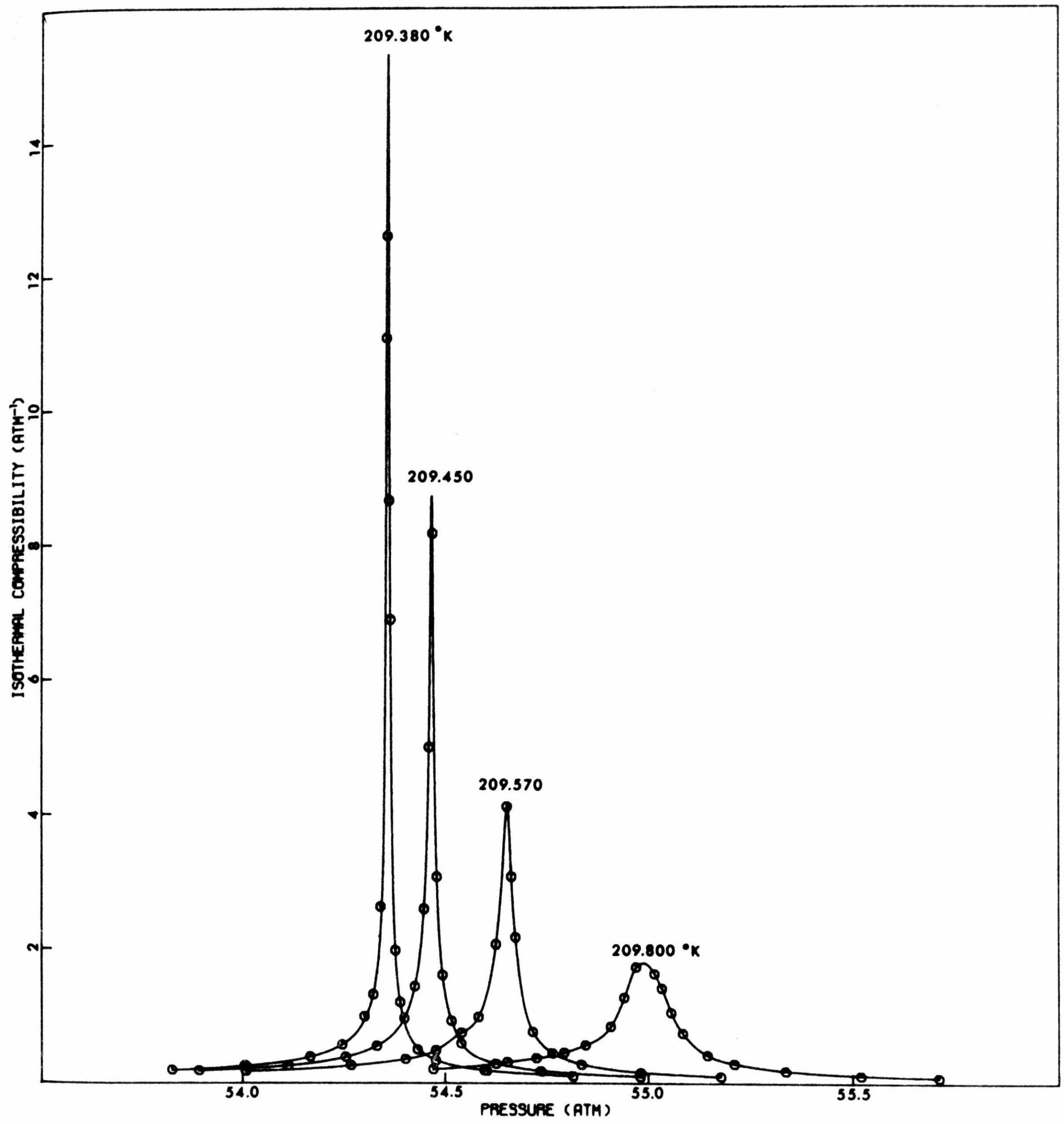

Figure 13. Isothermal Compressibility along 209.380°K to 209.800°K Isotherms

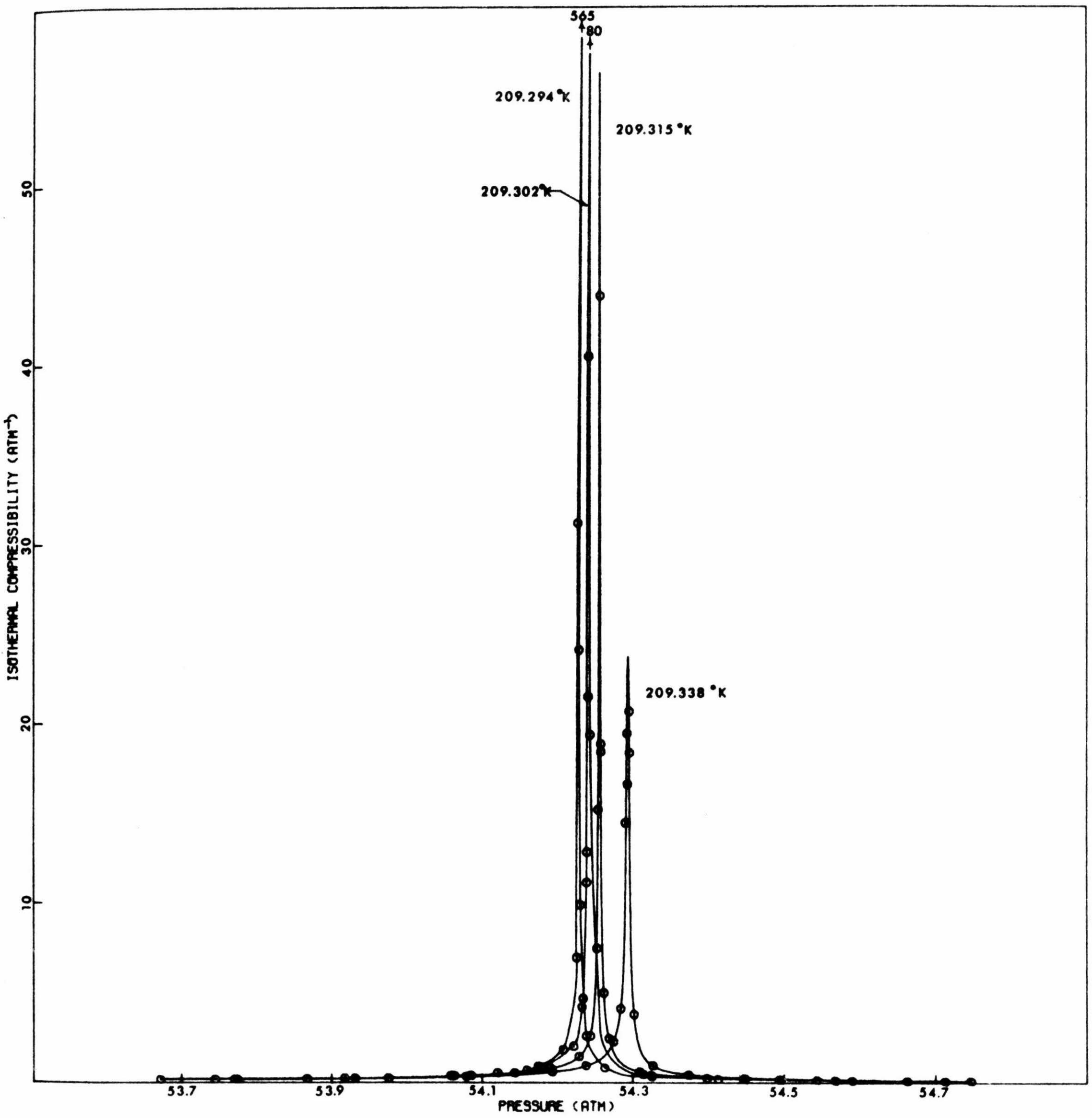

Figure 14. Isothermal Compressibility along 209.294°K to 209.338°K Isotherms

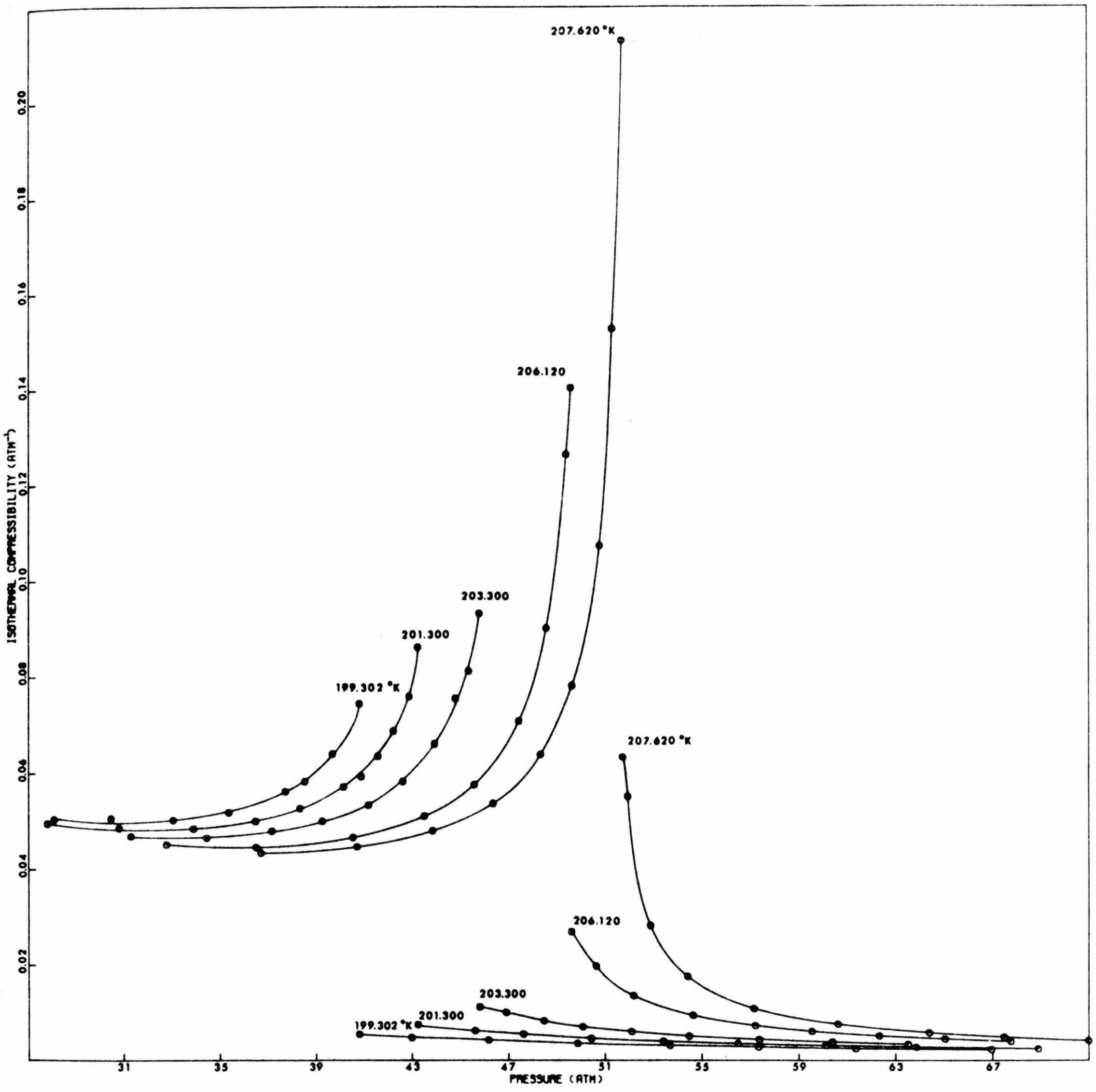

Figure 15. Isothermal Compressibility along 199.302°K to 207.620°K Isotherms

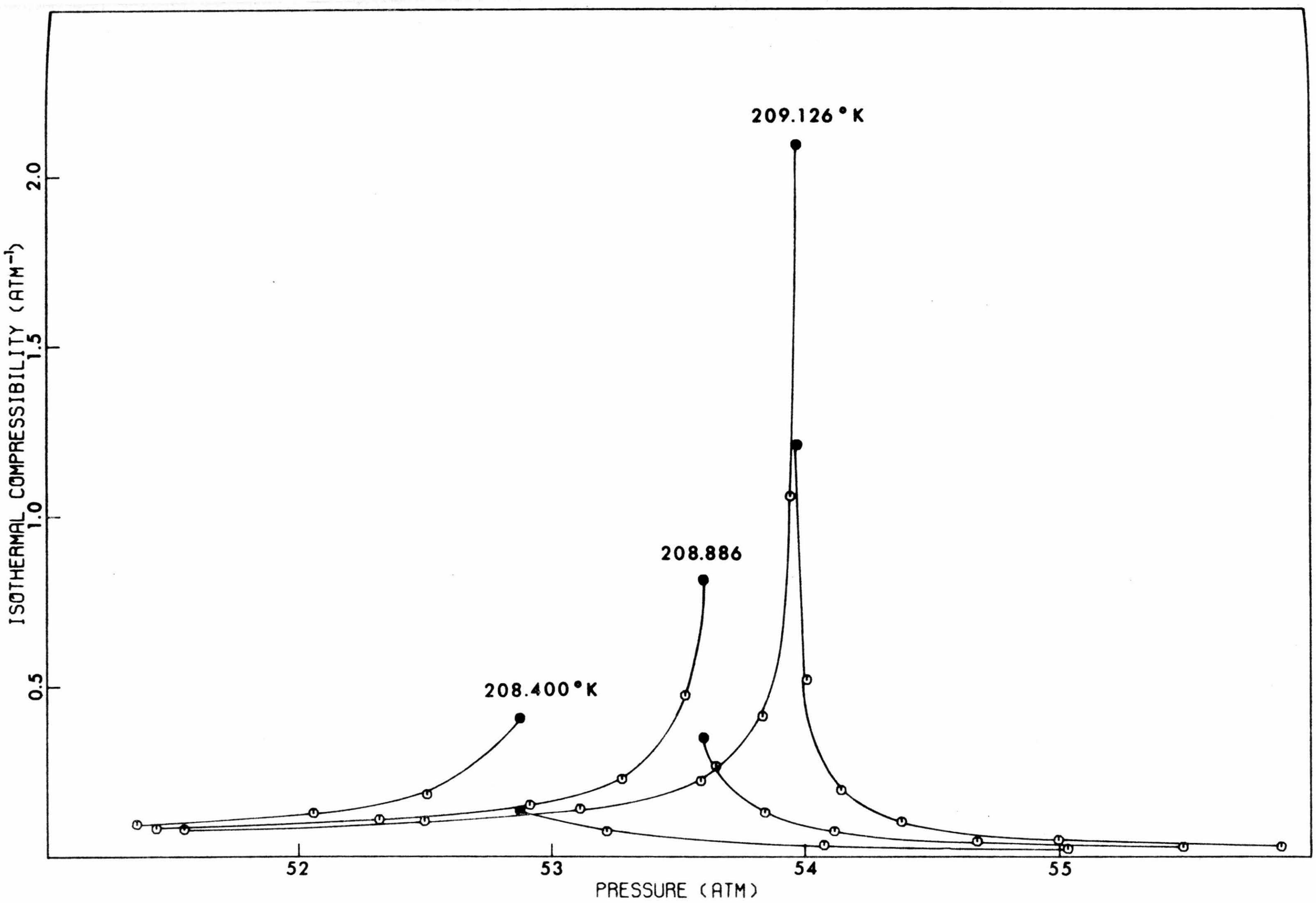

Figure 16. Isothermal Compressibility along 208.400°K to 209.126°K Isotherms. Closed symbols indicate values on the phase boundary.

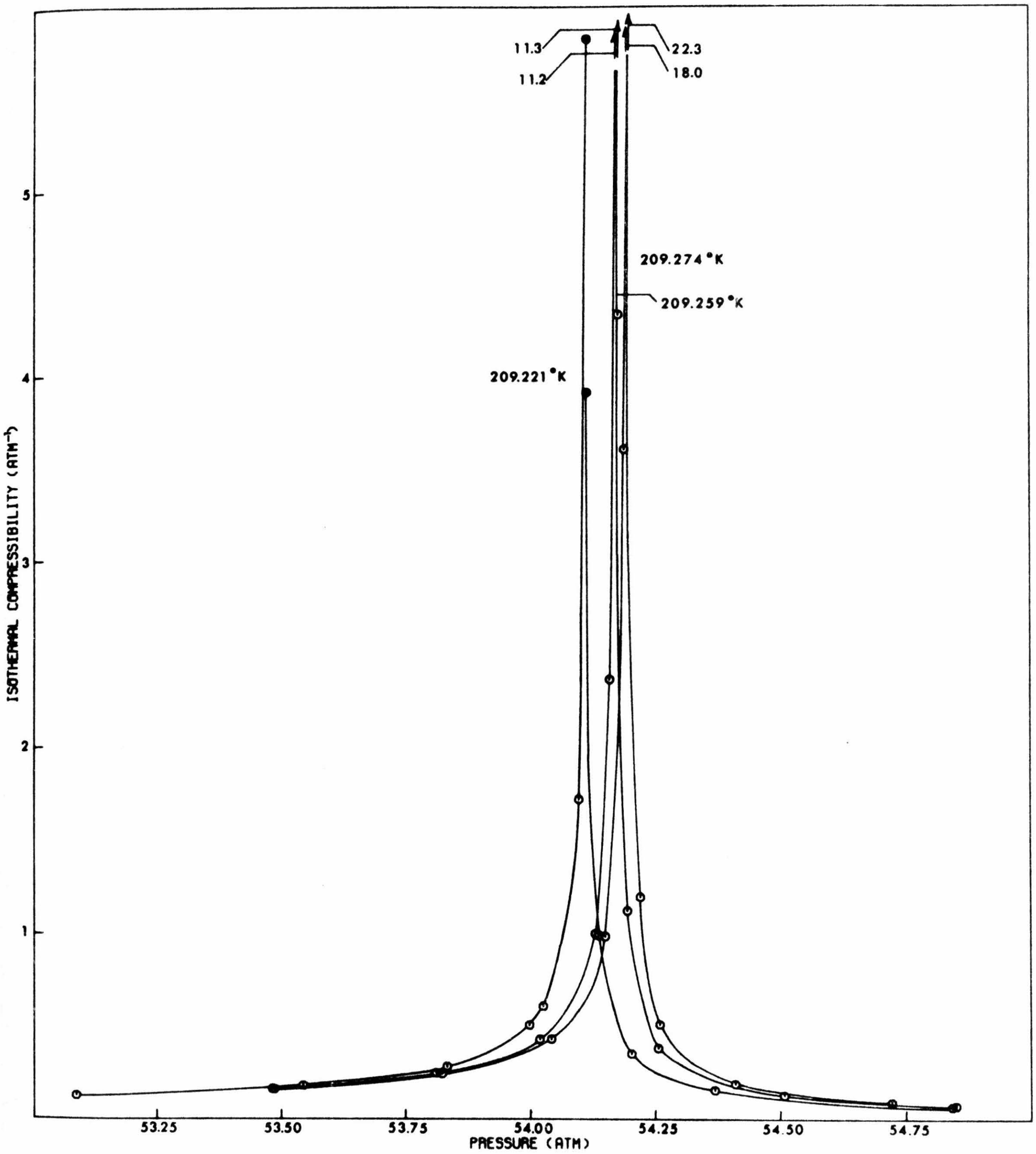

Figure 17. Isothermal Compressibility along 209.221°K to 209.274°K Isotherms. Closed symbols indicate values on the phase boundary.

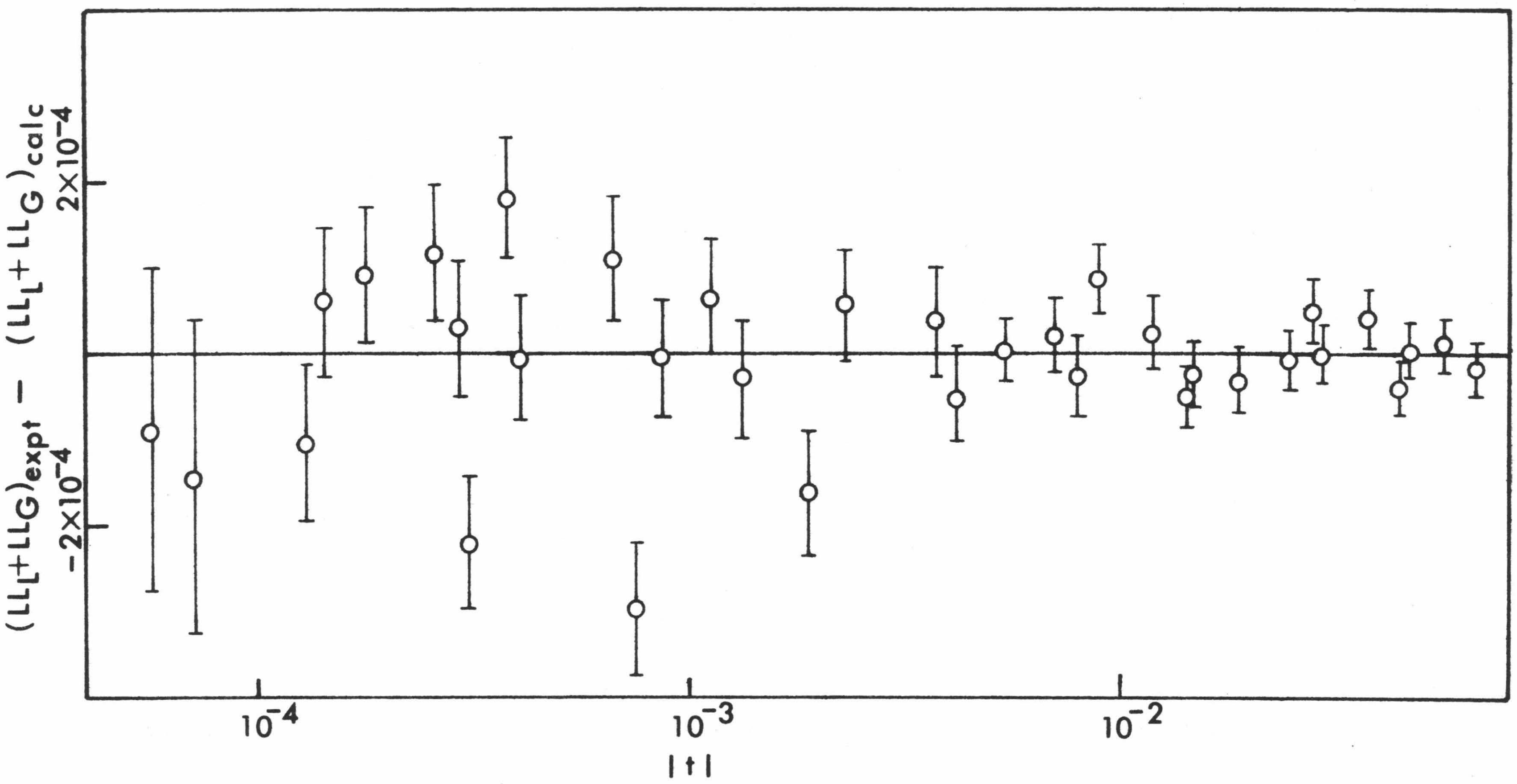

Figure 18. Residuals of the Rectilinear Diameter Fit

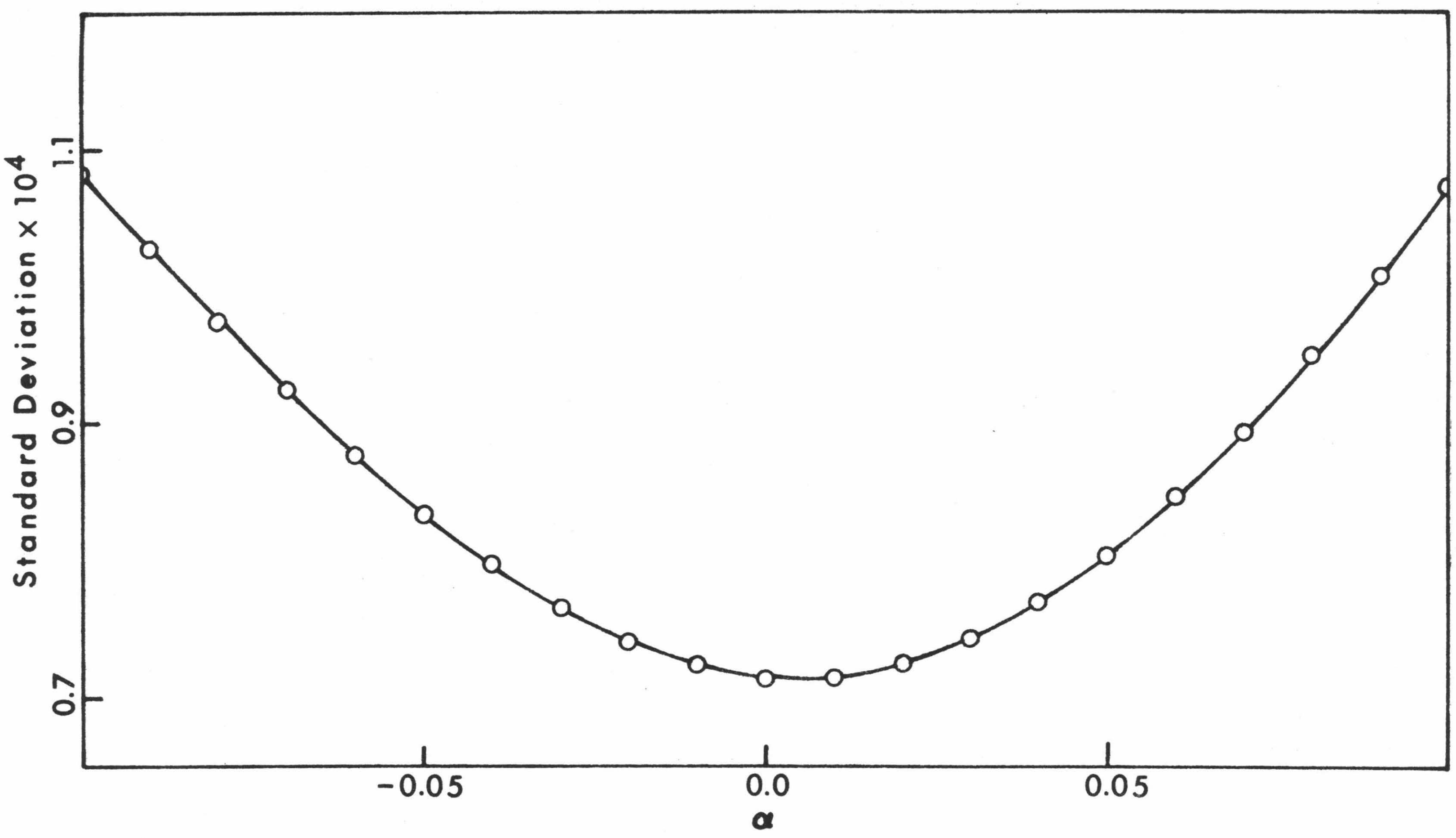

Figure 19. Standard Deviation of the Fit for the Curved Diameter

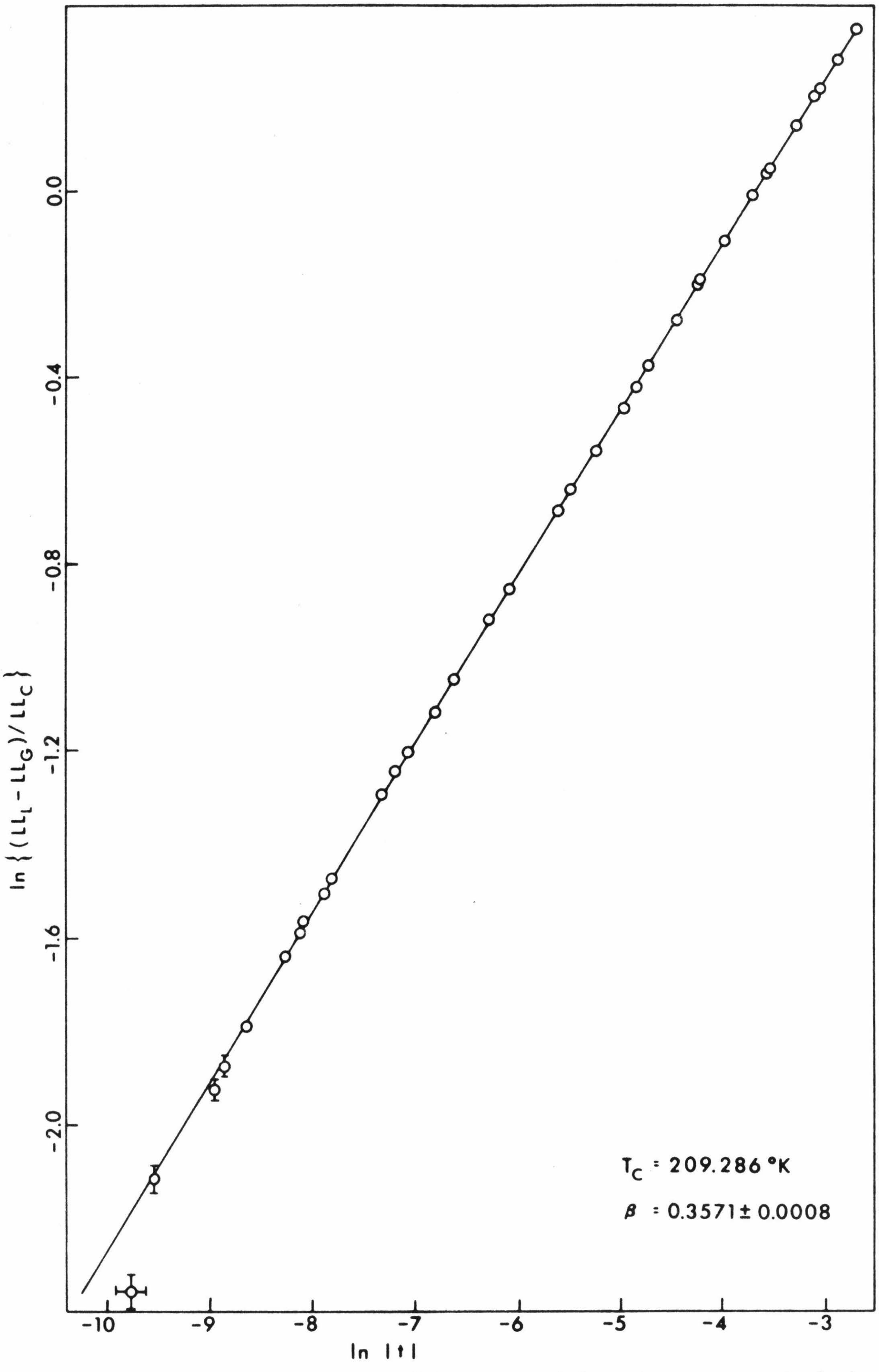

Figure 20. Plot of $\ln[(LL_L-LL_G)/LL_c]$ versus $\ln|t|$

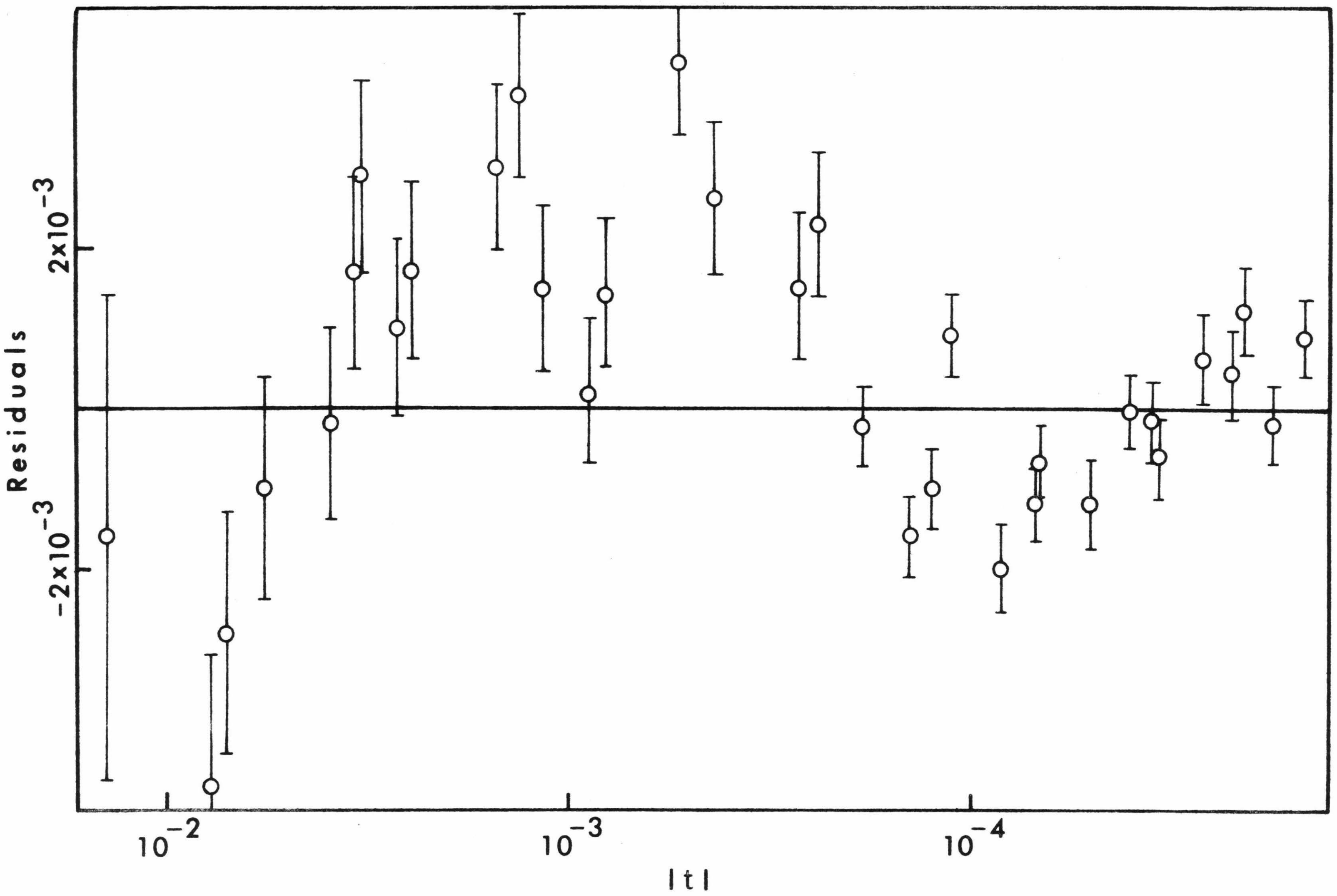

Figure 21. Plot of $\{\ln[(LL_L-LL_G)/LL_c]\}_{expt}-\{\ln[(LL_L-LL_G)/LL_c]\}_{calc}$ versus $|t|$

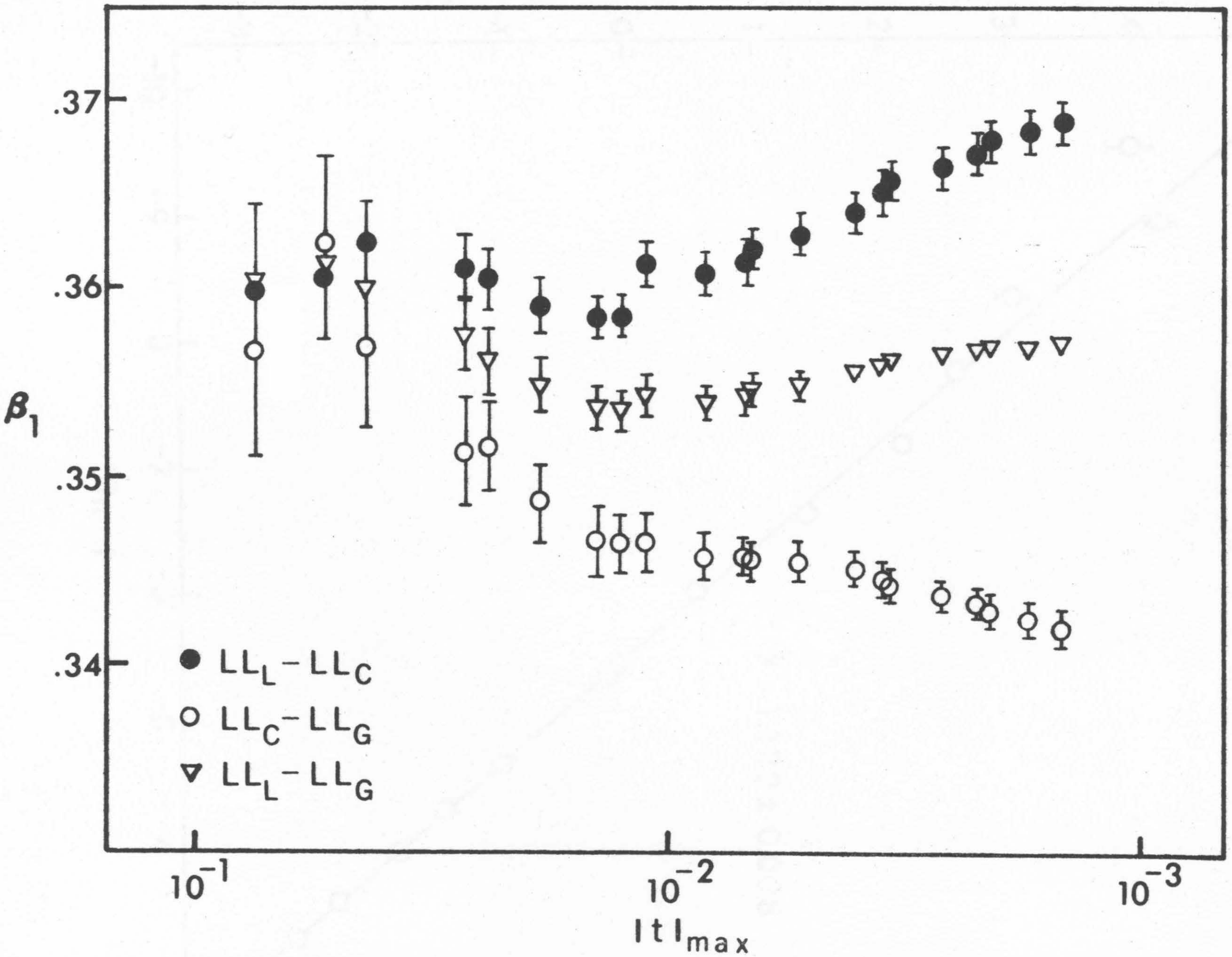

Figure 22. Values of $\beta_1^{\pm}$ as function of the Reduced Temperature Range $|t|_{max}$

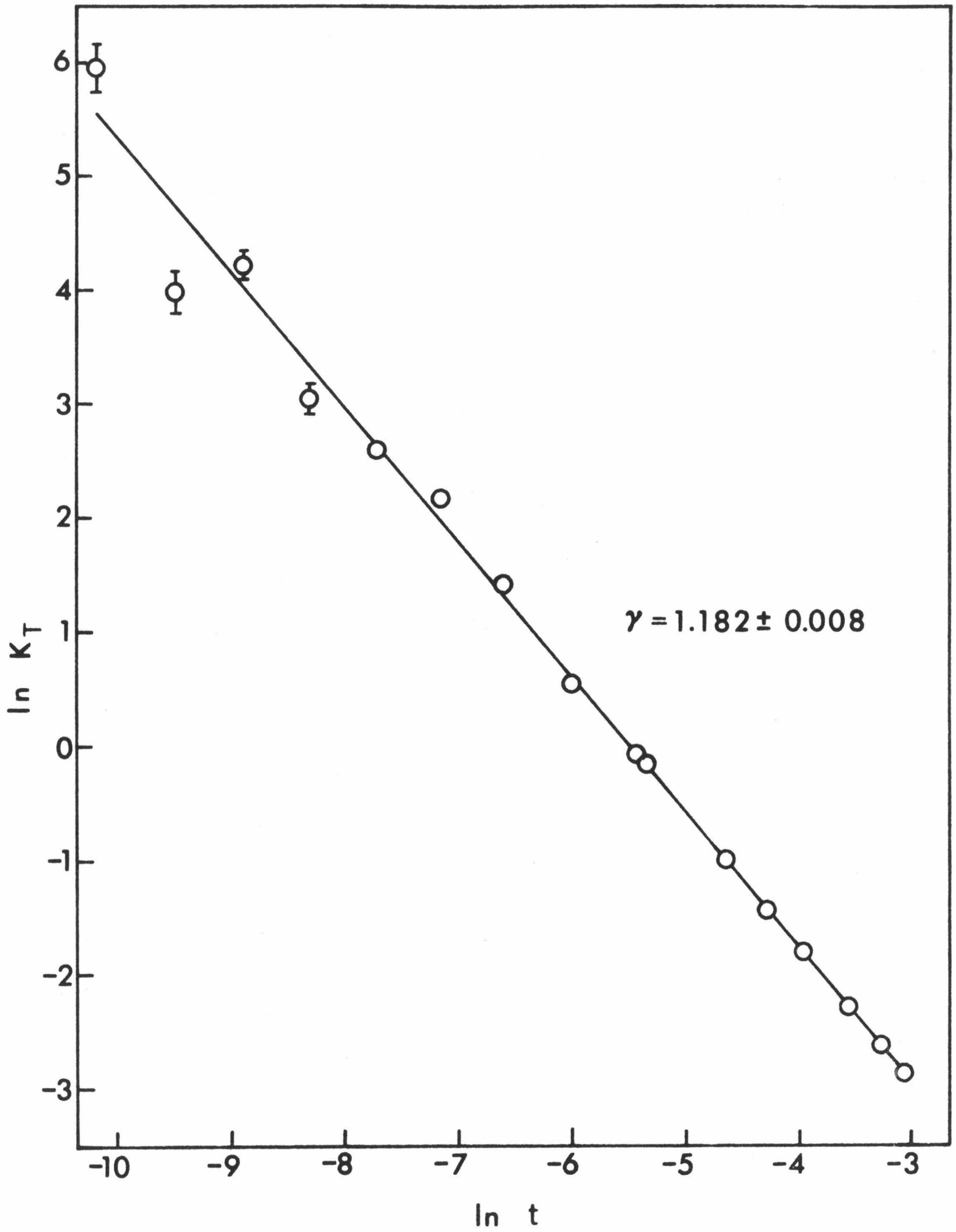

Figure 23. Plot of ln K_T versus ln t on the Critical Isochore

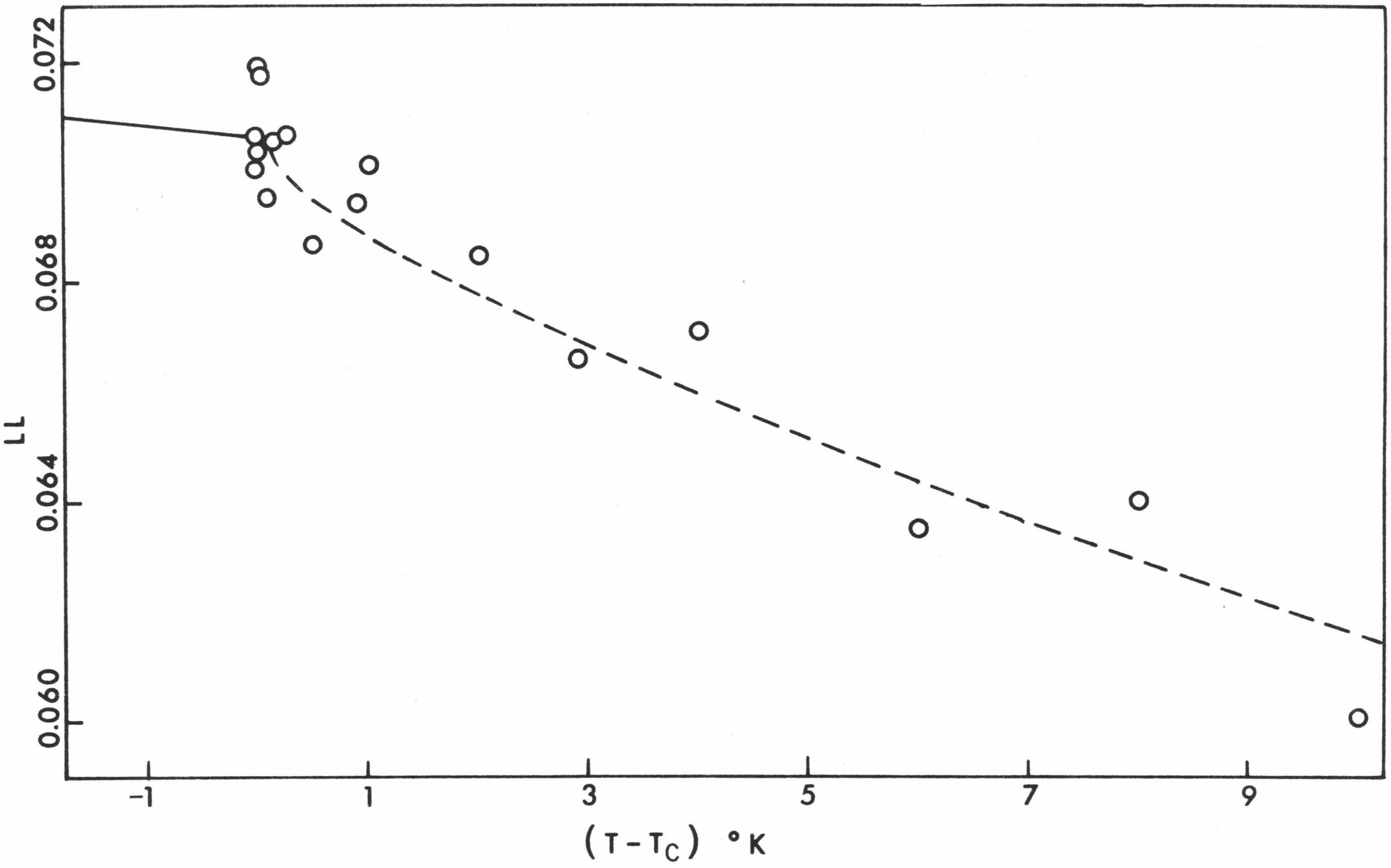

Figure 24. The Locus of Maximum Isothermal Compressibility in the LL-T Plane

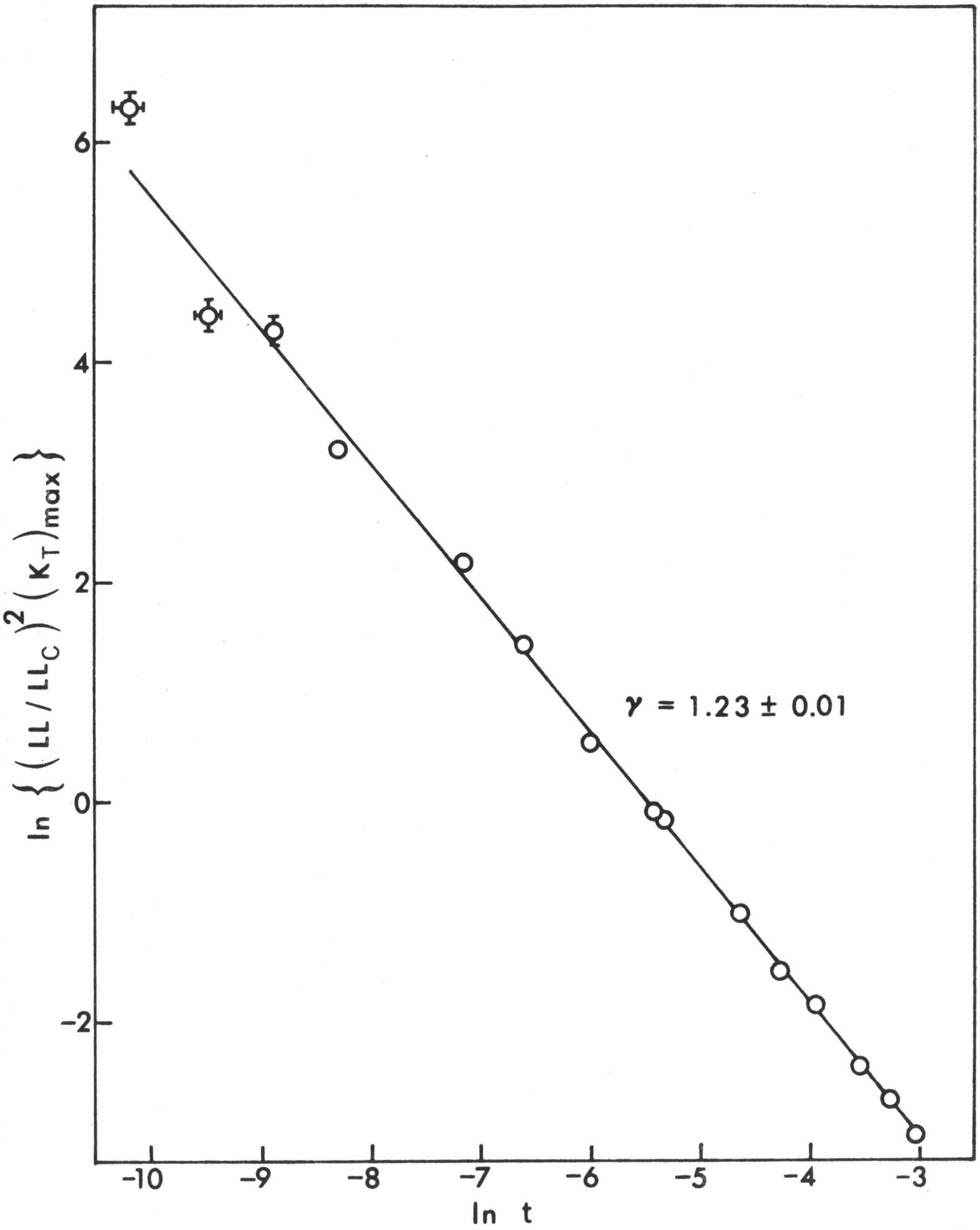

Figure 25. Plot of $\ln[(LL/LL_c)^2K_T]$ versus ln t on the Locus of $(K_T)_{max}$

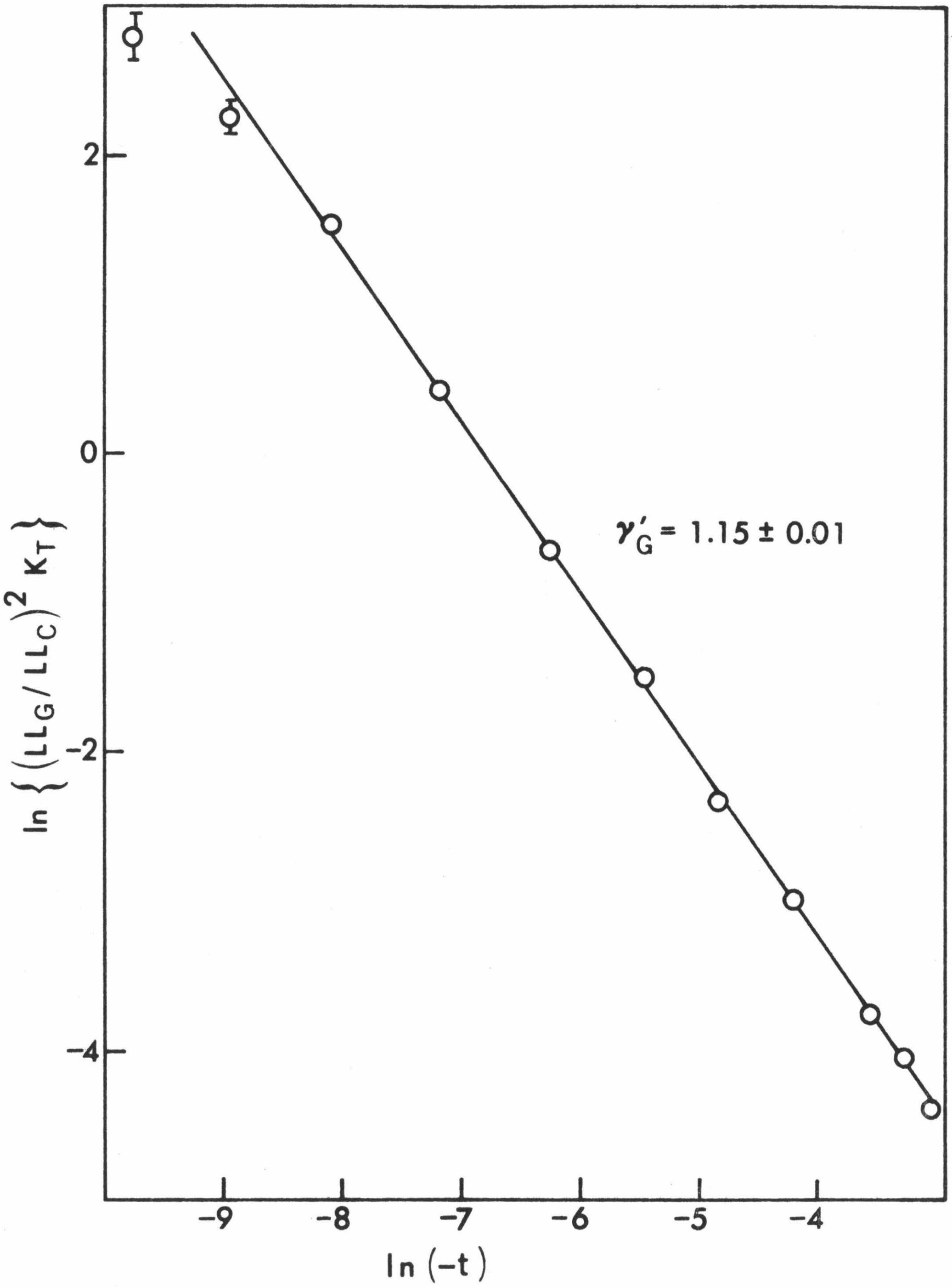

Figure 26. Plot of $\ln[(LL/LL_c)^2 K_T]$ versus $\ln|t|$ along the Gas side of the Coexistence Curve

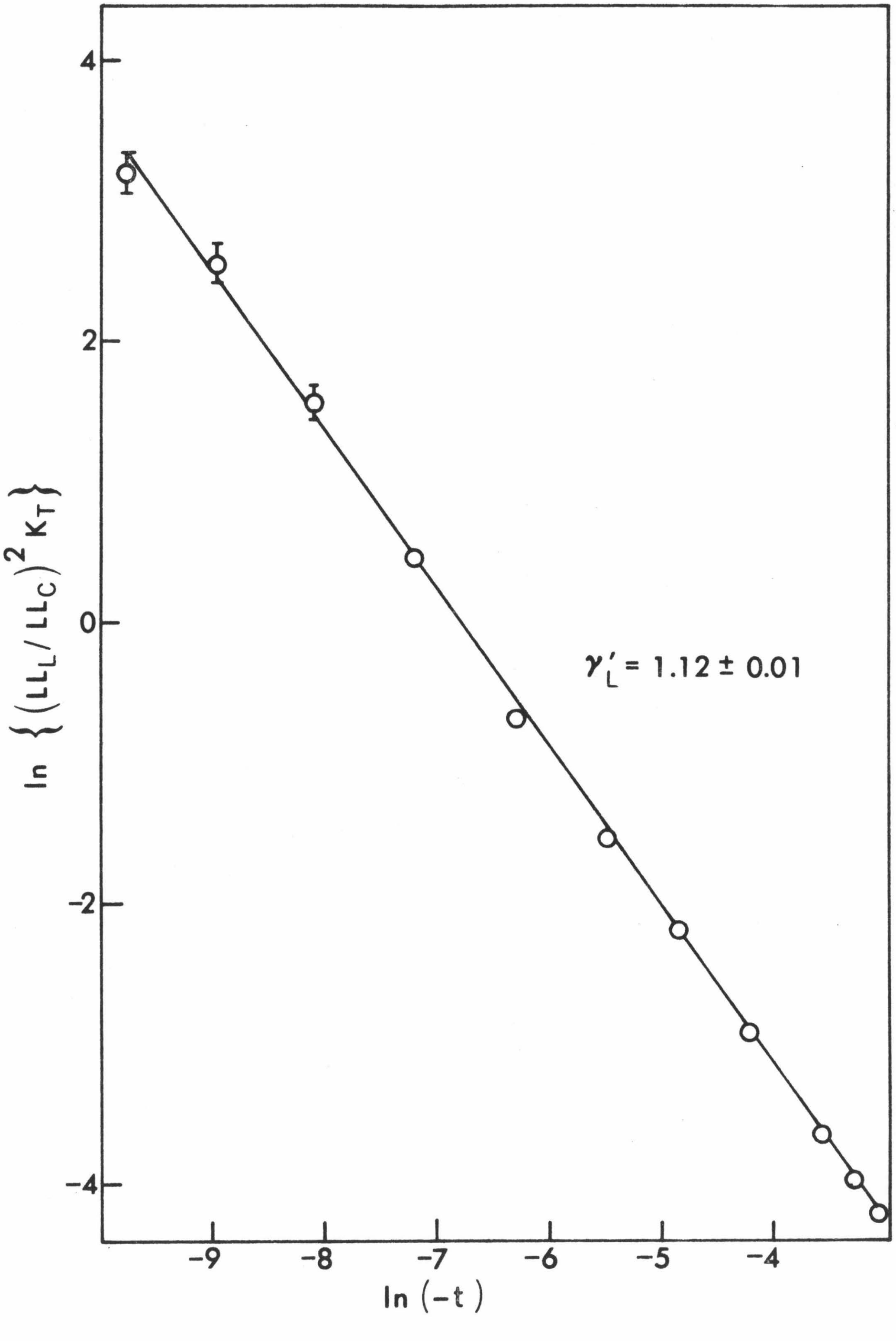

Figure 27. Plot of $\ln[(LL/LL_C)^2 K_T]$ versus $\ln|t|$ along the Liquid side of the Coexistence Curve

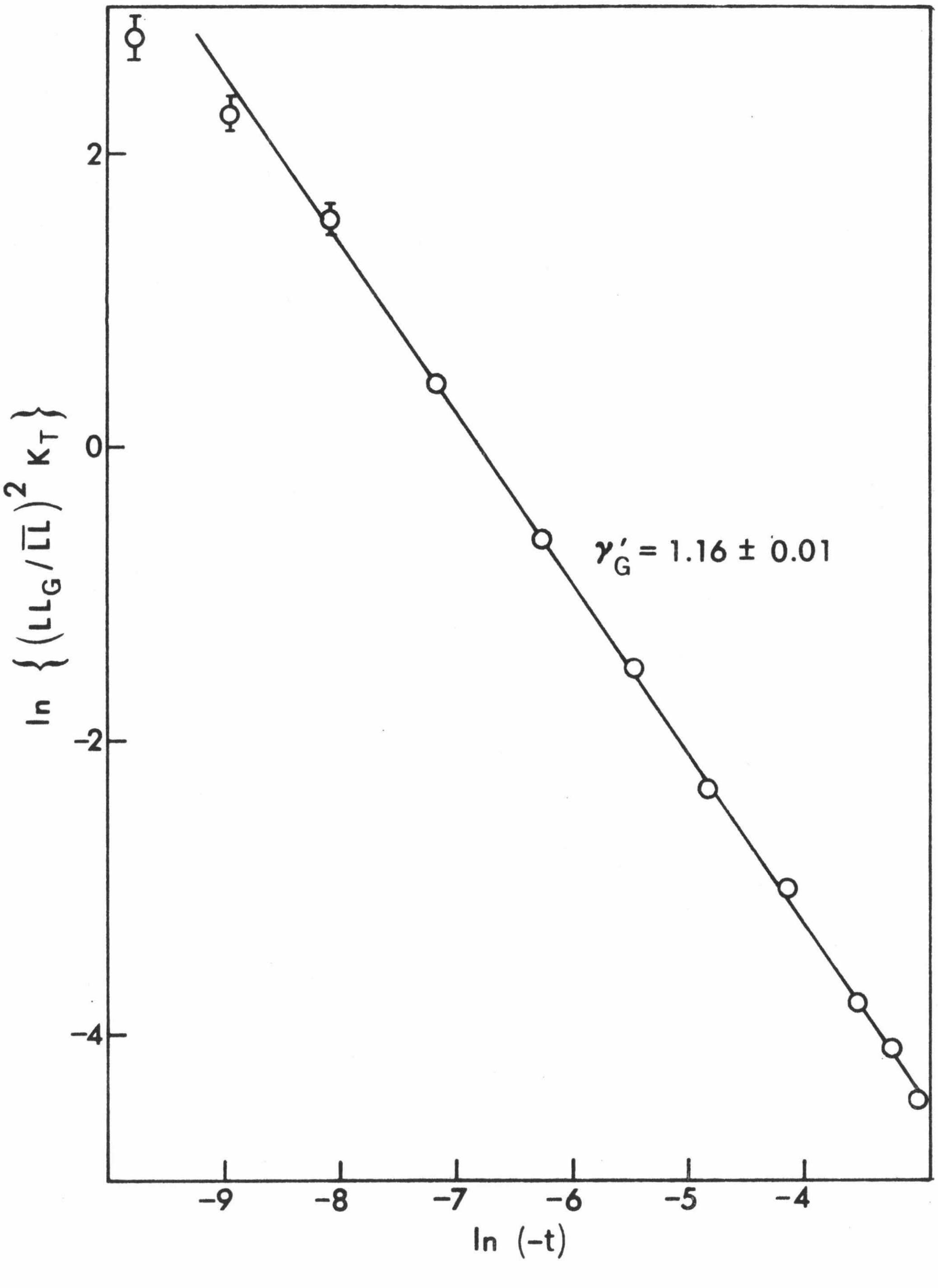

Figure 28. Plot of $\ln[(LL/\overline{LL})^2 K_T]$ versus $\ln|t|$ along the Gas side of the Coexistence Curve

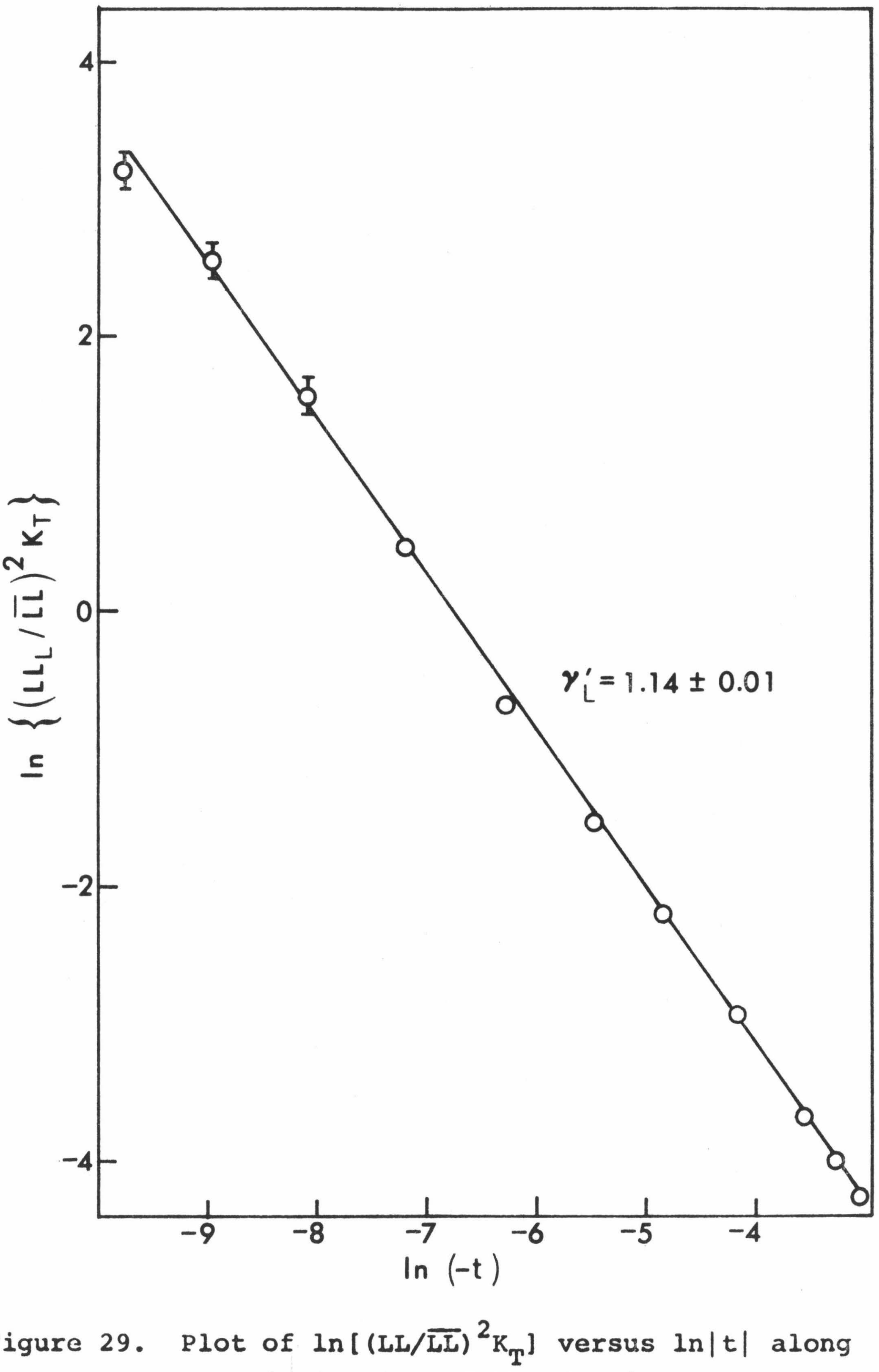

Figure 29. Plot of $\ln[(LL/\overline{LL})^2 K_T]$ versus $\ln|t|$ along the Liquid side of the Coexistence Curve

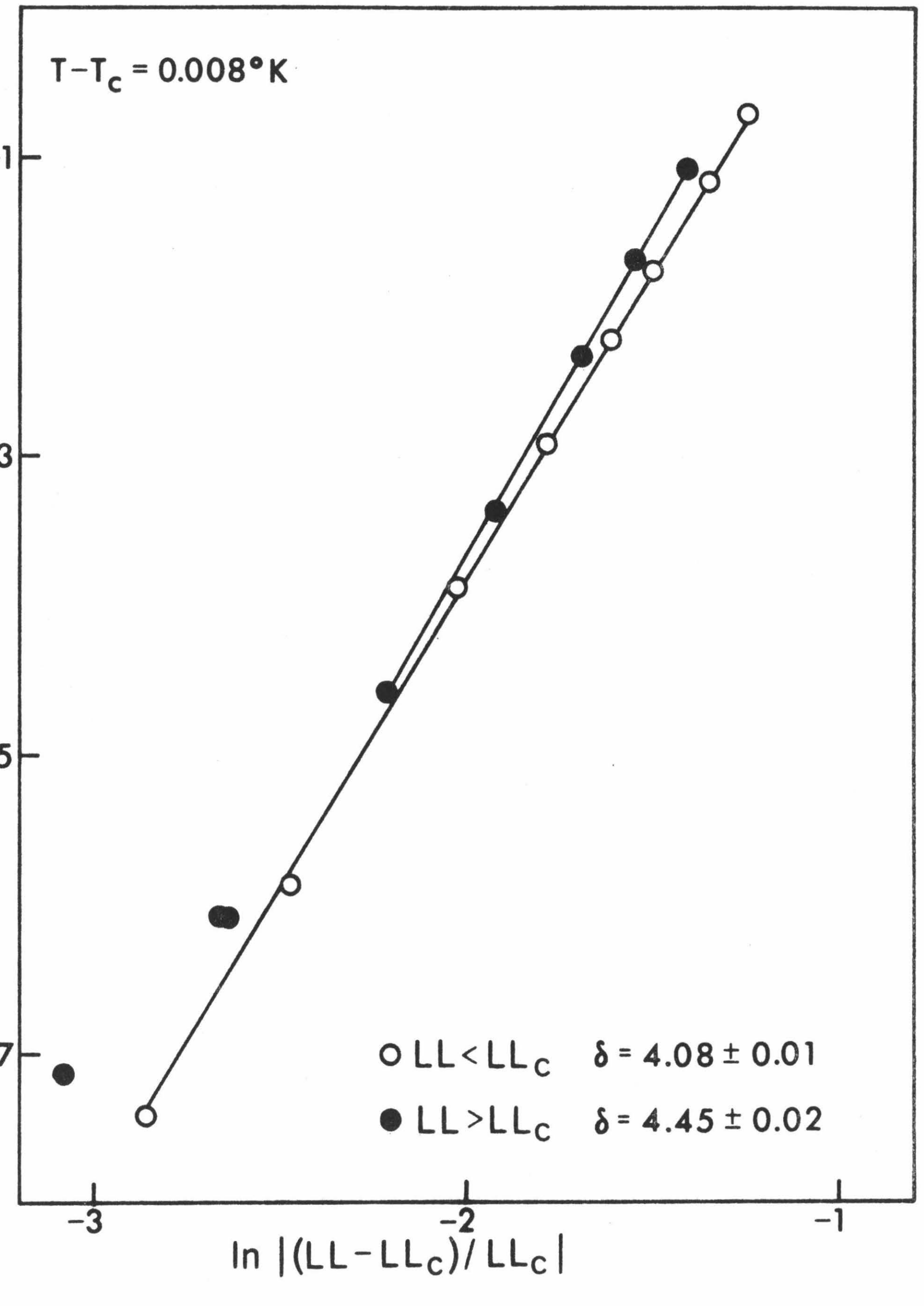

Figure 30. Plot of $\ln|P-P_c|$ versus $\ln|(LL-LL_c)/LL_c|$ for $T-T_c= 0.008°K$

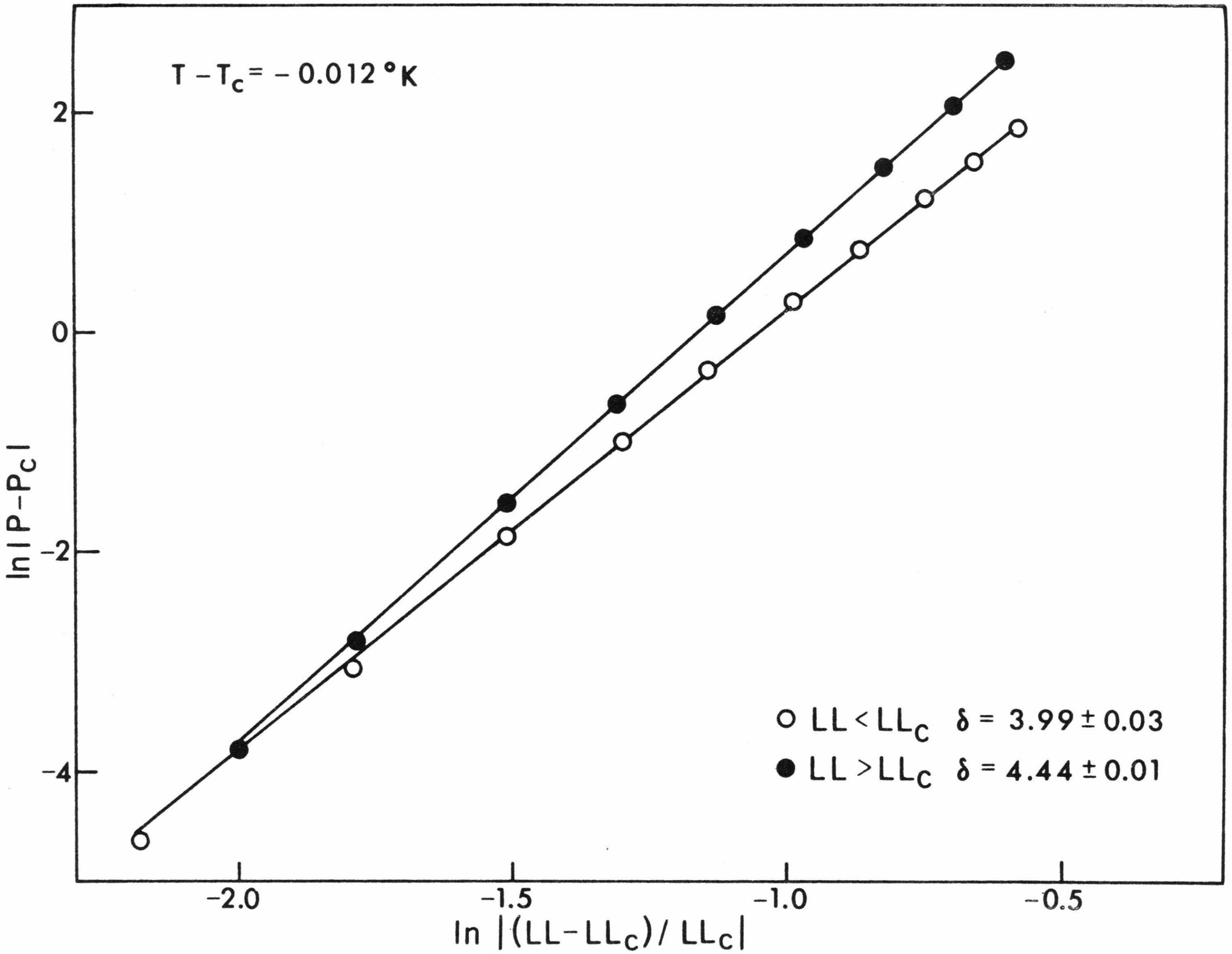

Figure 31. Plot of $\ln|P-P_c|$ versus $\ln|(LL-LL_c)/LL_c|$ for $T-T_c = -0.012°K$

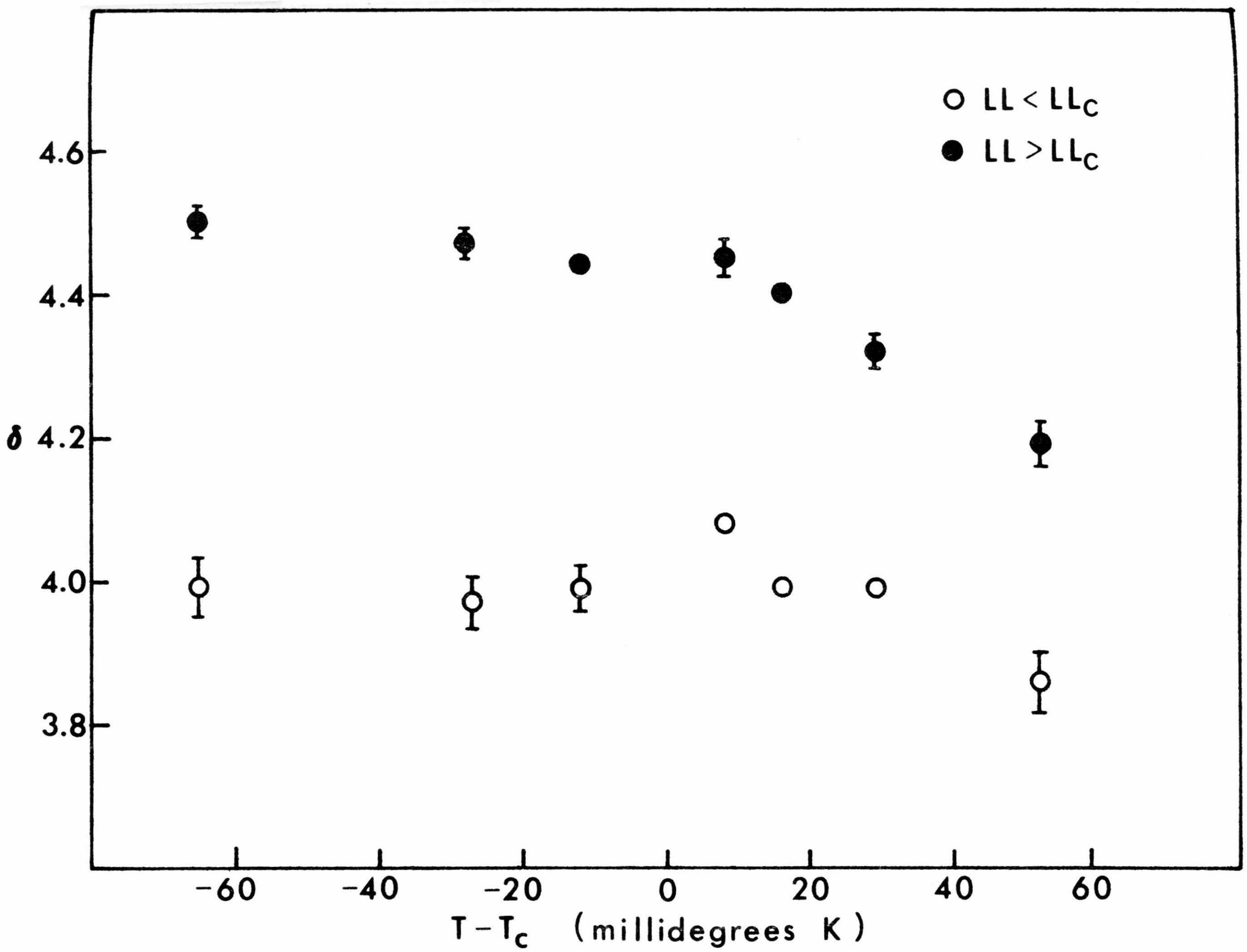

Figure 32. Values of δ as function of $(T-T_c)$

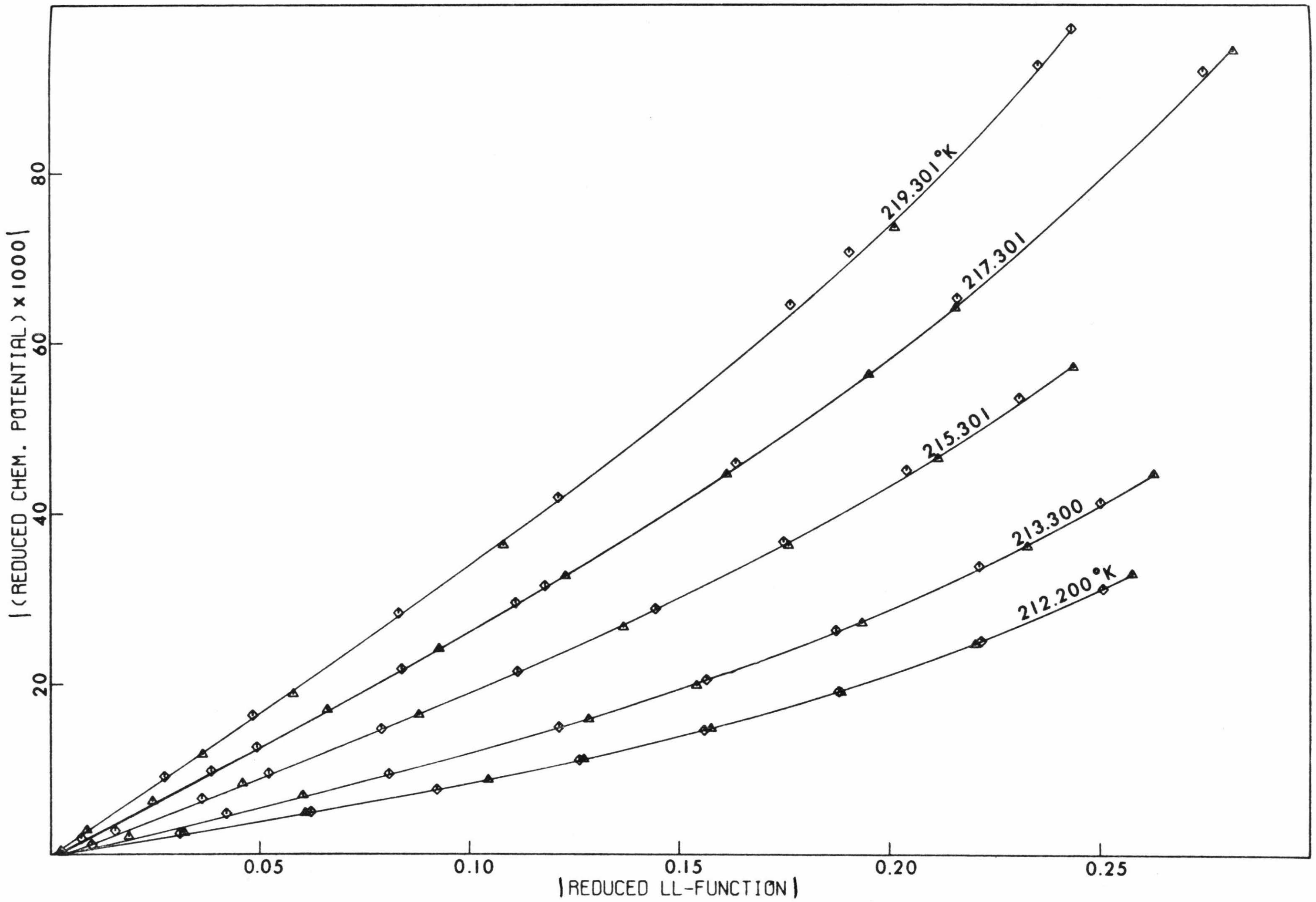

Figure 33. Plot of |Δμ| versus |ΔLL| on 212.200°K to 219.301°K Isotherms.
△-LL<LL$_c$, ◇-LL>LL$_c$.

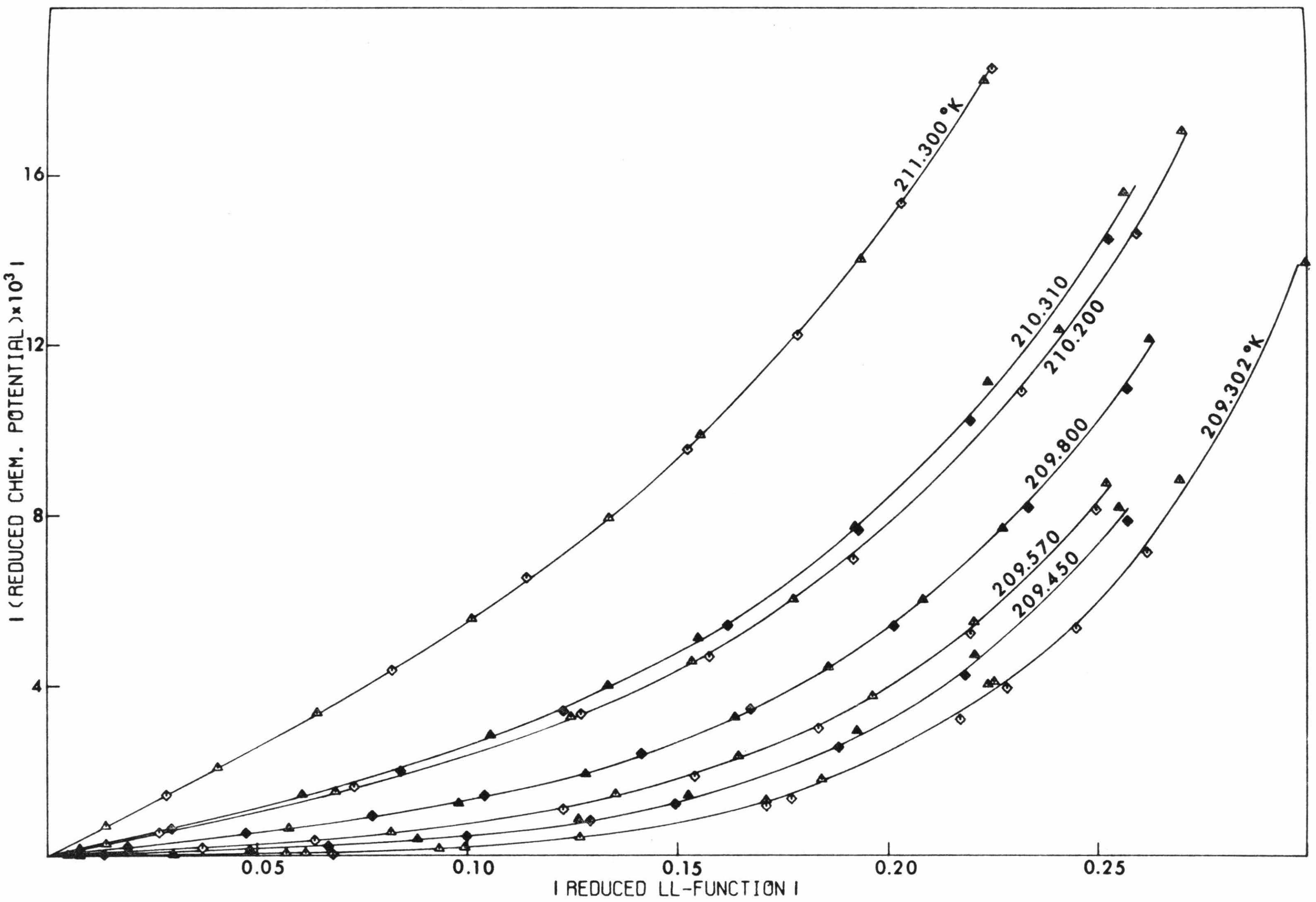

Figure 34. Plot of |Δμ| versus |ΔLL| on 209.302°K and 209.450°K to 211.300°K Isotherms. △-LL<LL$_c$, ◇-LL>LL$_c$.

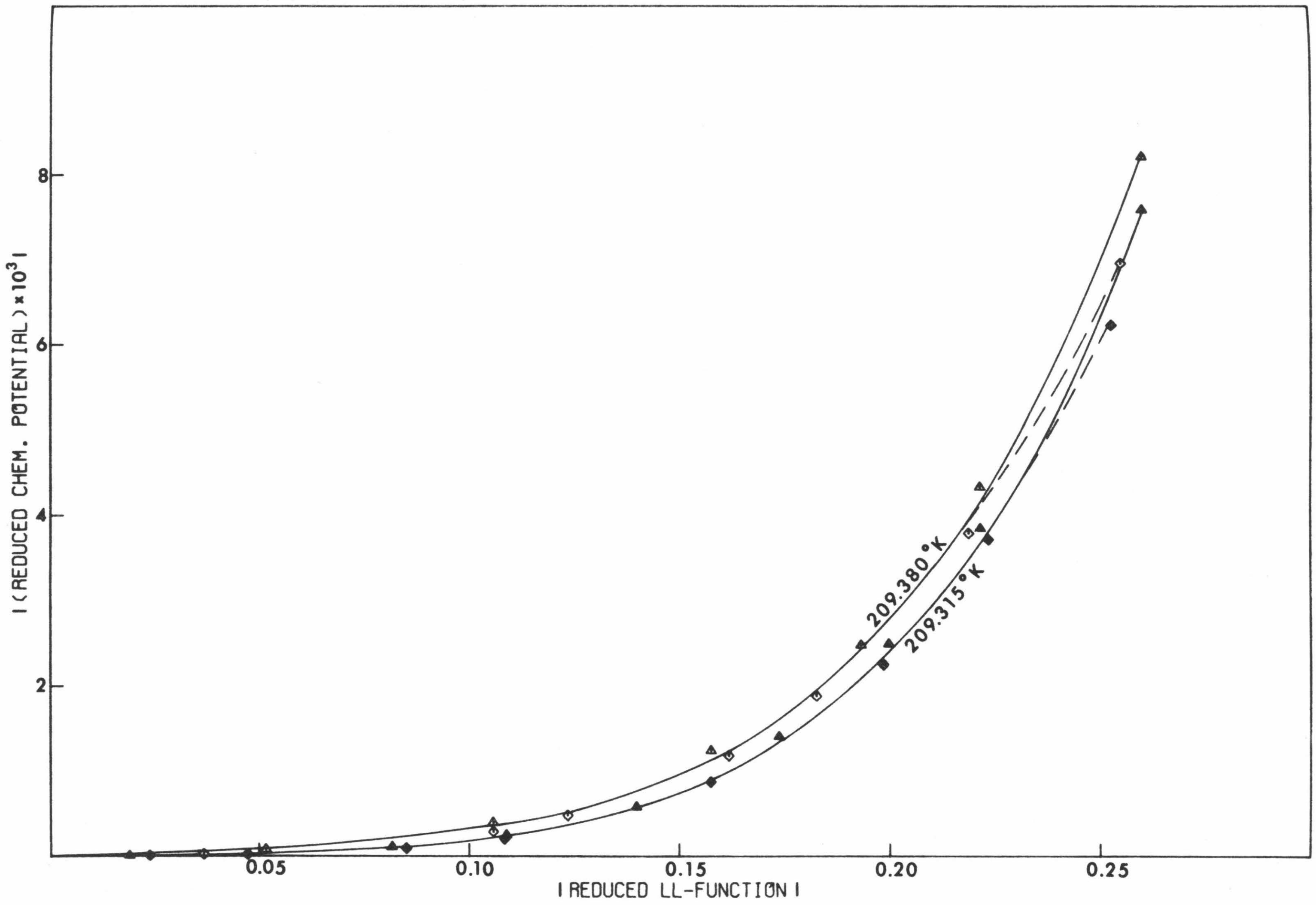

Figure 35. Plot of $|\Delta\mu|$ versus $|\Delta LL|$ on 209.315°K and 209.380°K Isotherms. $\triangle$-$LL<LL_c$, $\diamond$-$LL>LL_c$.

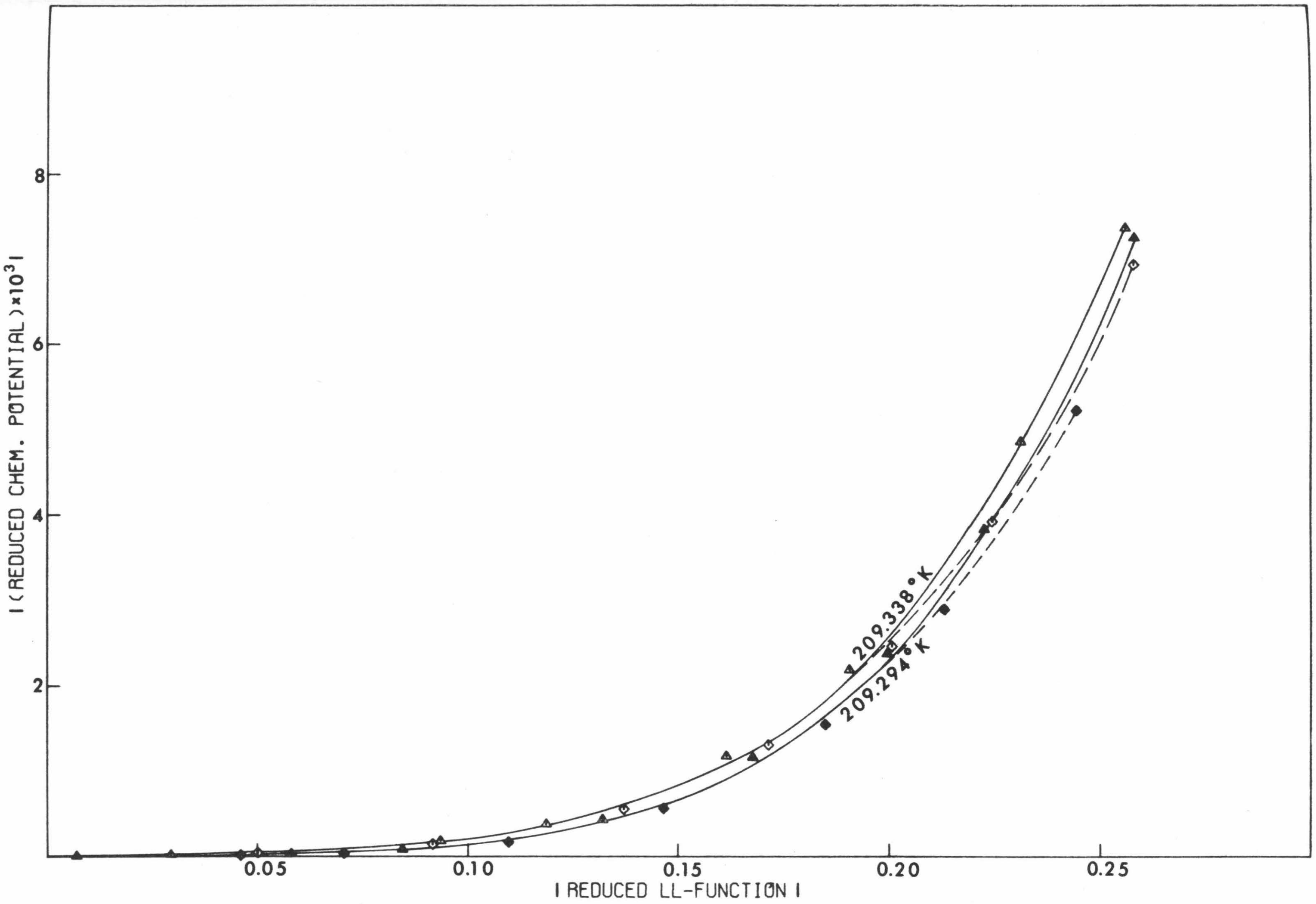

Figure 36. Plot of $|\Delta\mu|$ versus $|\Delta LL|$ on 209.294°K and 209.338°K Isotherms.
△-$LL<LL_c$, ◇-$LL>LL_c$.

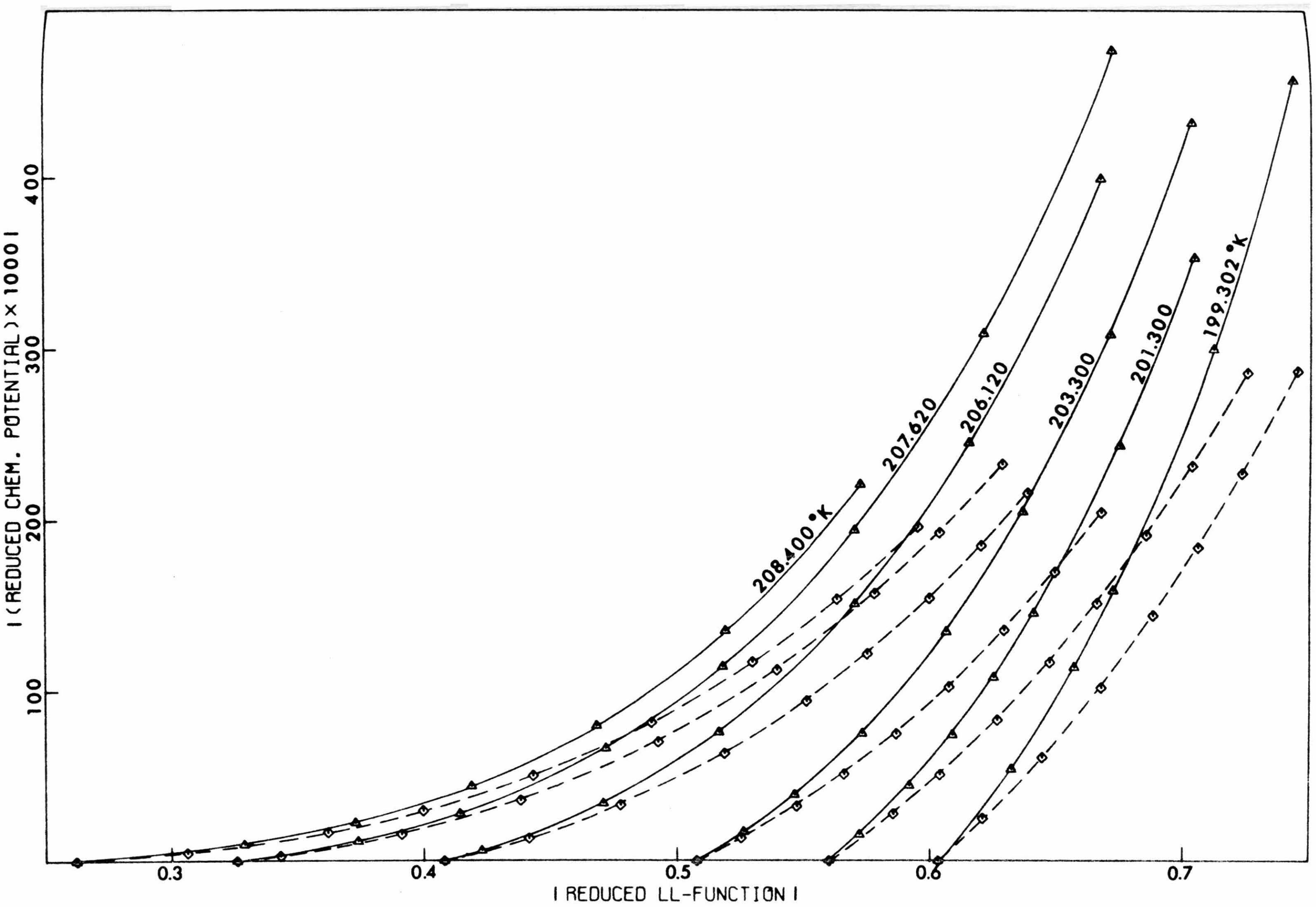

Figure 37. Plot of $|\Delta\mu|$ versus $|\Delta LL|$ on 199.302°K to 208.400°K Isotherms.
△ $-LL<LL_c$, ◇ $-LL>LL_c$.

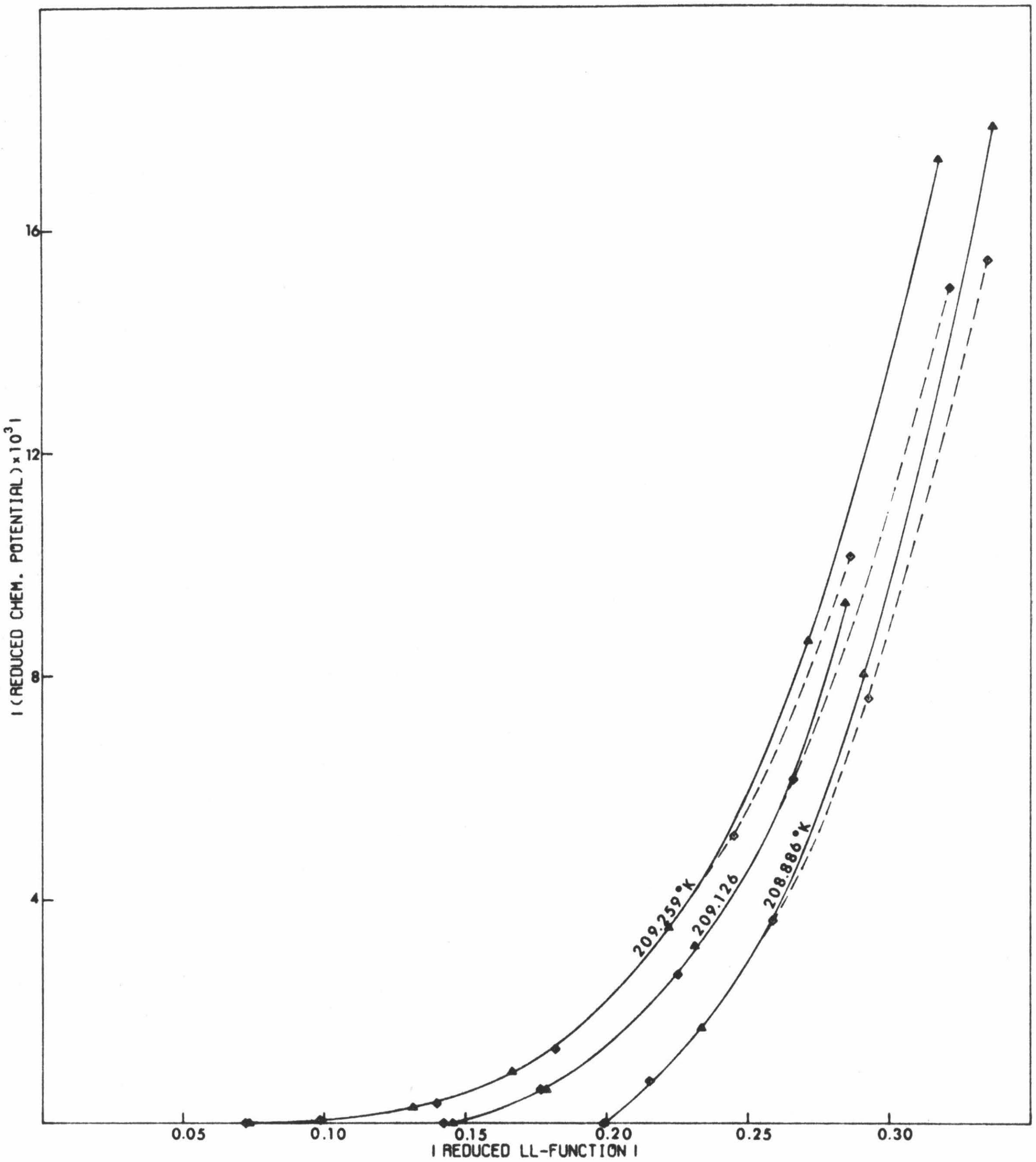

Figure 38. Plot of $|\Delta\mu|$ versus $|\Delta LL|$ on 208.886°K, 209.126°K and 209.259°K Isotherms. △ $-LL<LL_c$, ◇ $-LL>LL_c$.

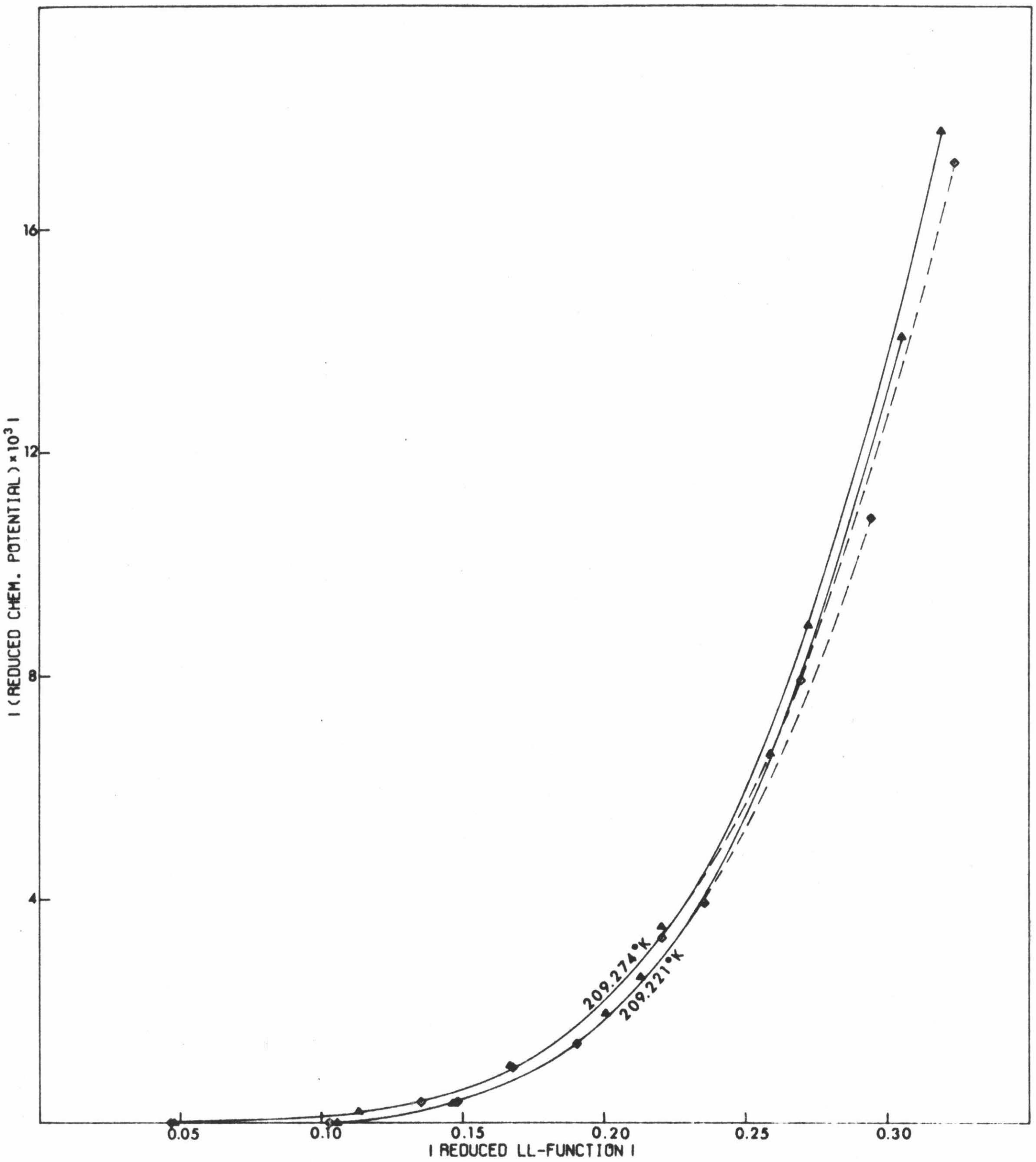

Figure 39. Plot of |Δμ| versus |ΔLL| on 209.221°K and 209.274°K Isotherms.
△-LL<LL_c, ◇-LL>LL_c.

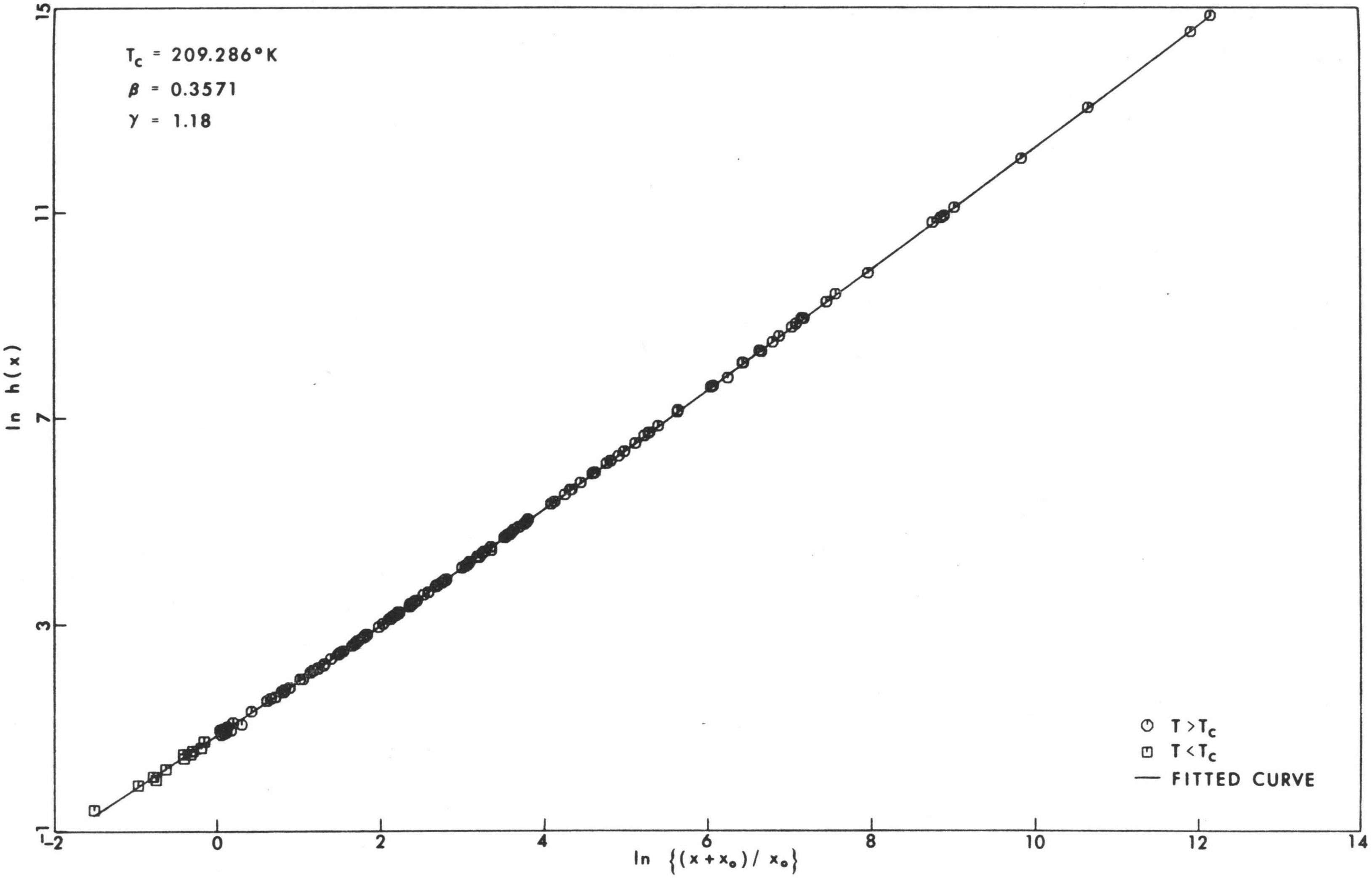

Figure 40. Plot I of ln h(x) versus ln$[(x+x_o)/x_o]$.
Solid line represents the fitted curve.

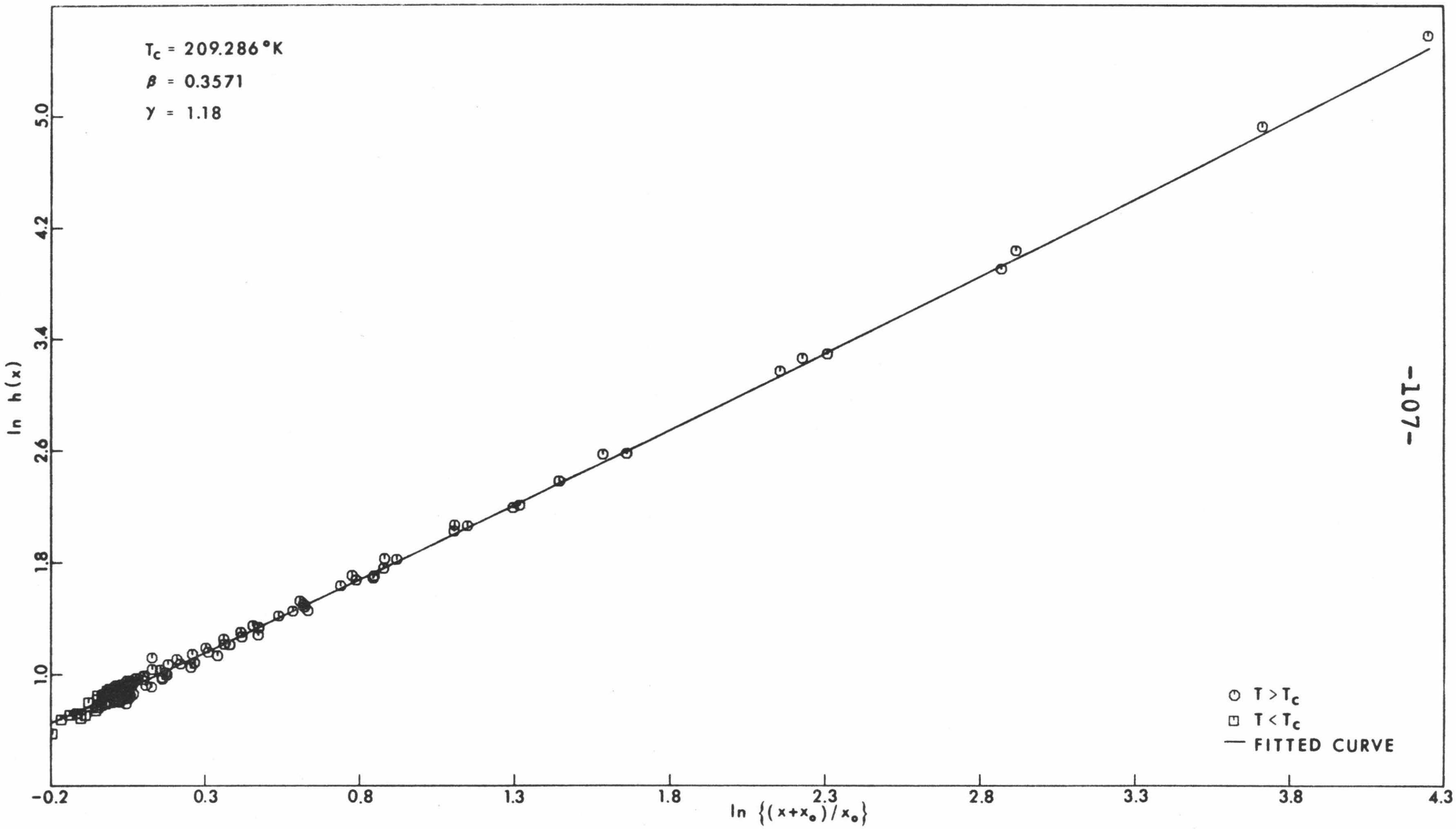

Figure 41. Plot II of ln h(x) versus $\ln[(x+x_o)/x_o]$.
Solid line represents the fitted curve.

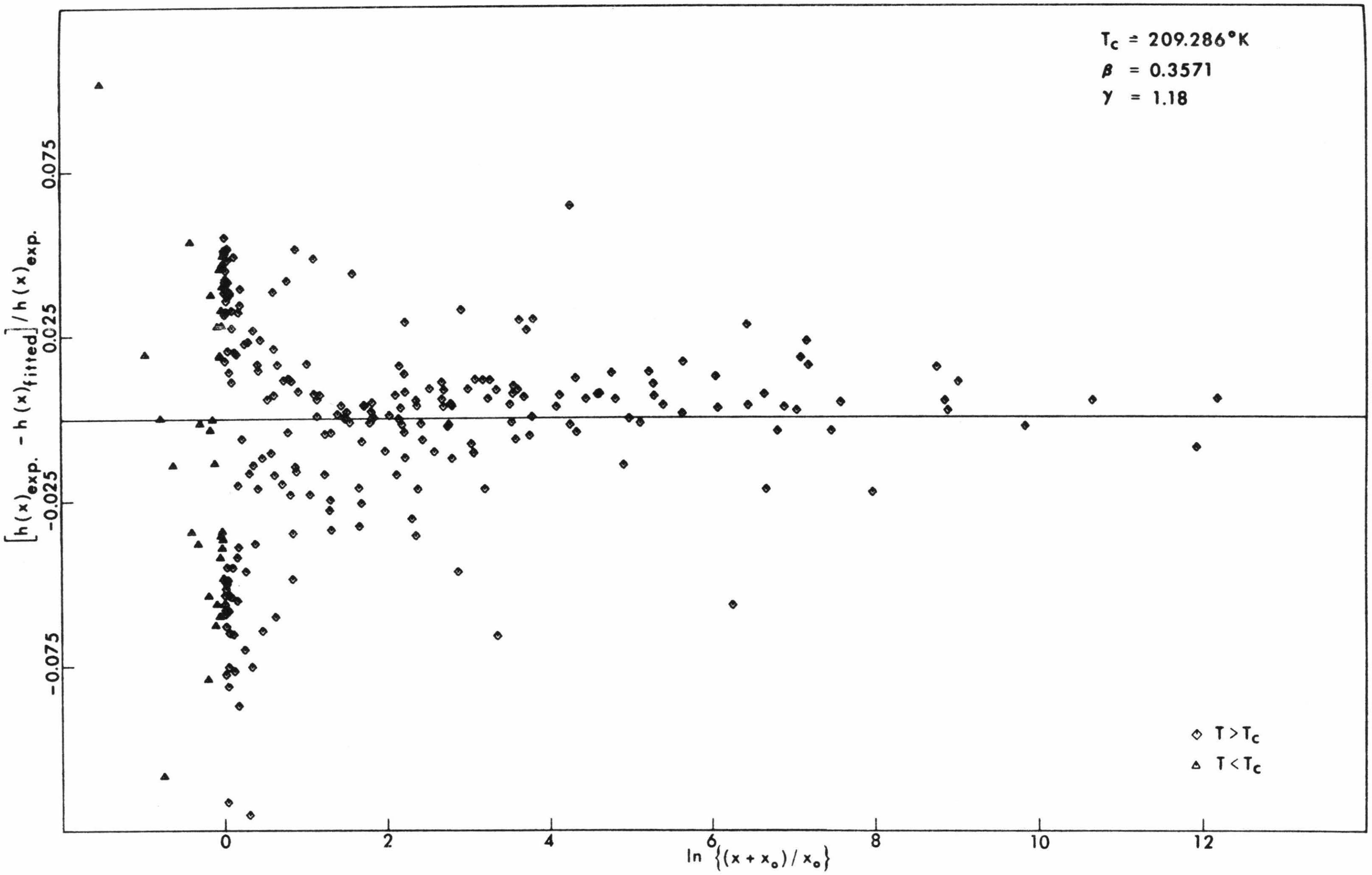

Figure 42. Plot of Relative Deviation $[h(x)_{exp't} - h(x)_{fitted}]/h(x)_{exp't}$ versus $\ln[(x+x_o)/x_o]$

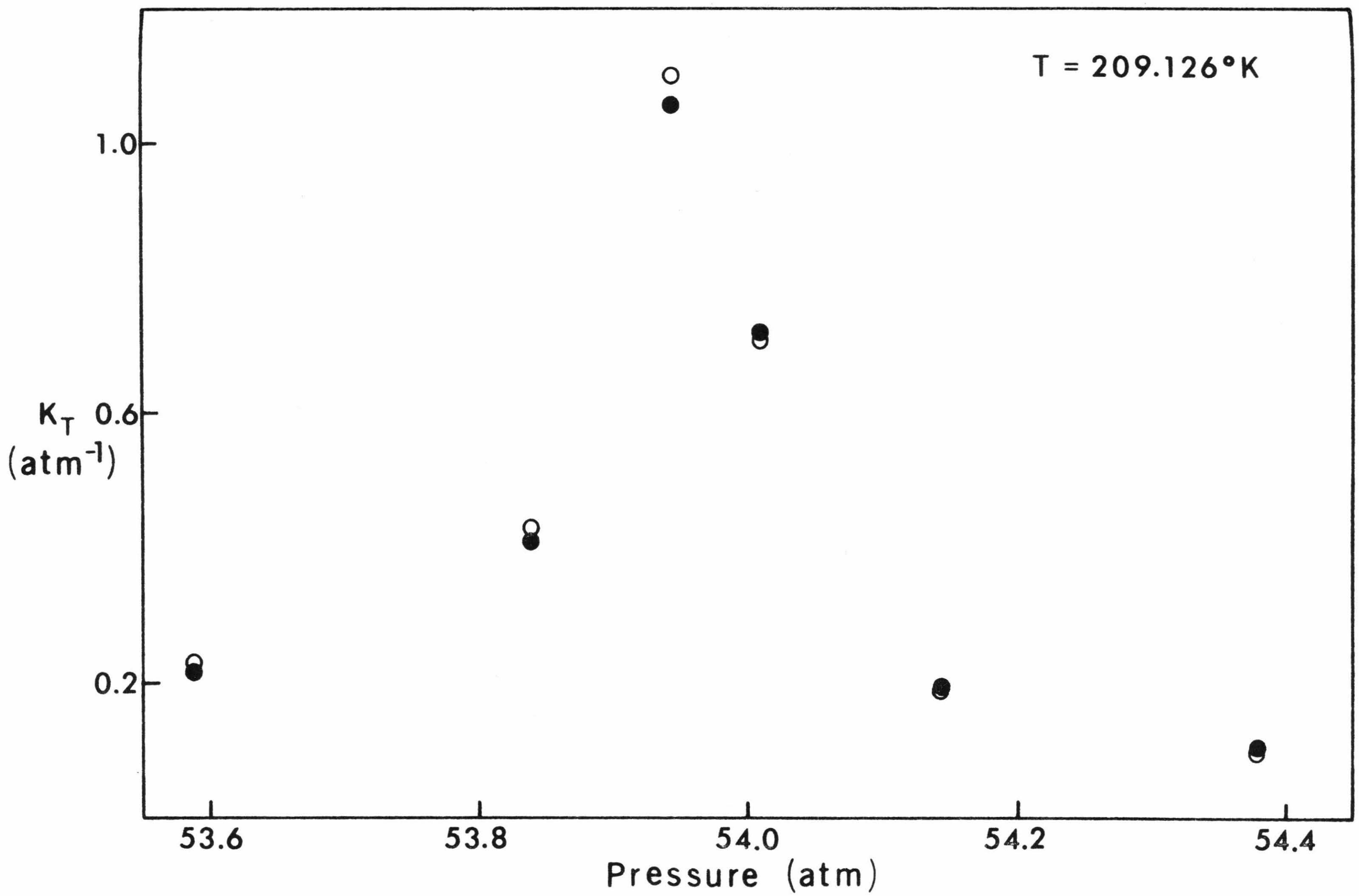

Figure 43. Comparison of Experimental and Calculated K_T along 209.126°K Isotherm. ●-experimental, ○-calculated.

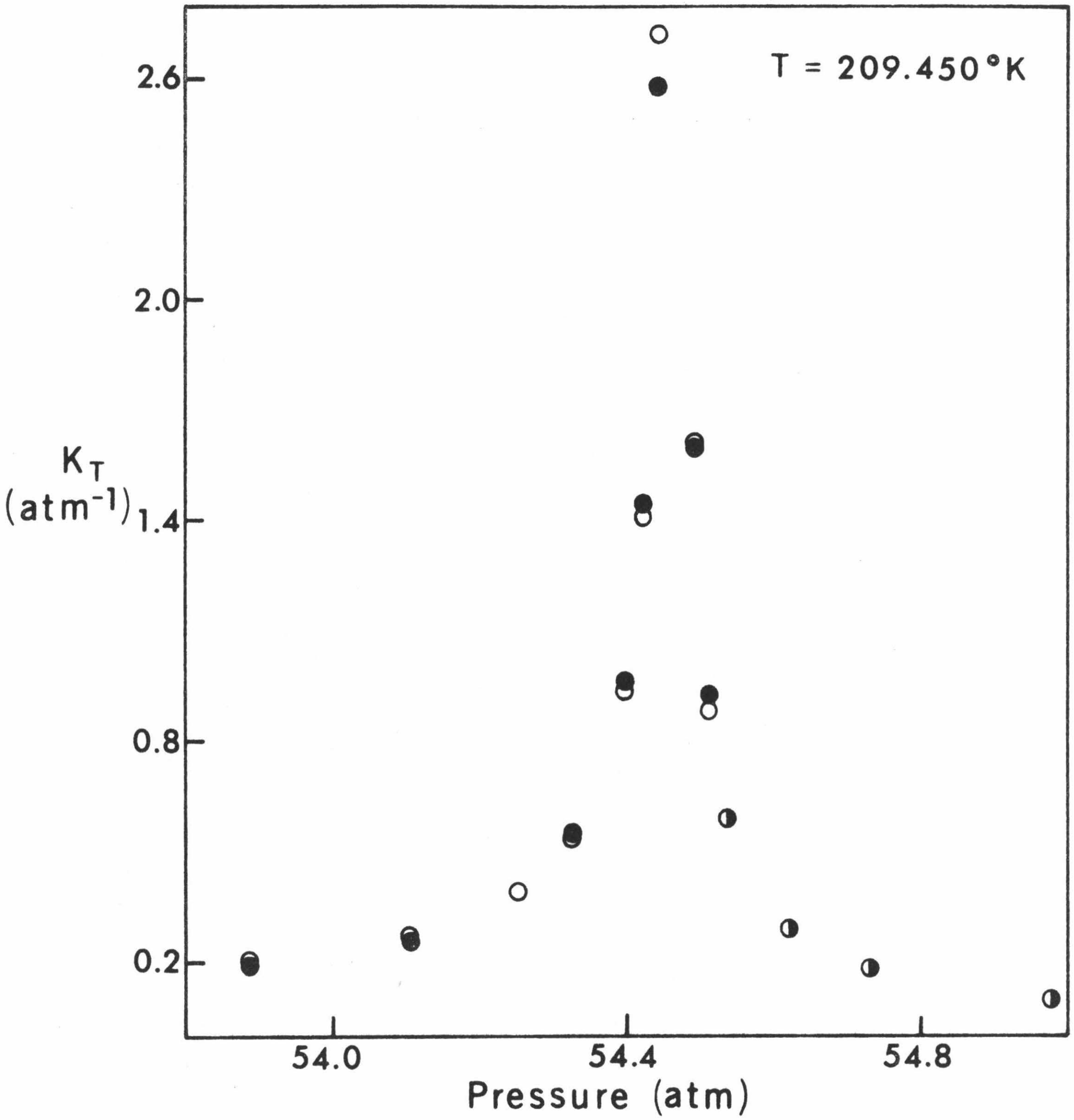

Figure 44. Comparison of Experimental and Calculated K_T along 209.450°K Isotherm. ●-experimental, ○-calculated.

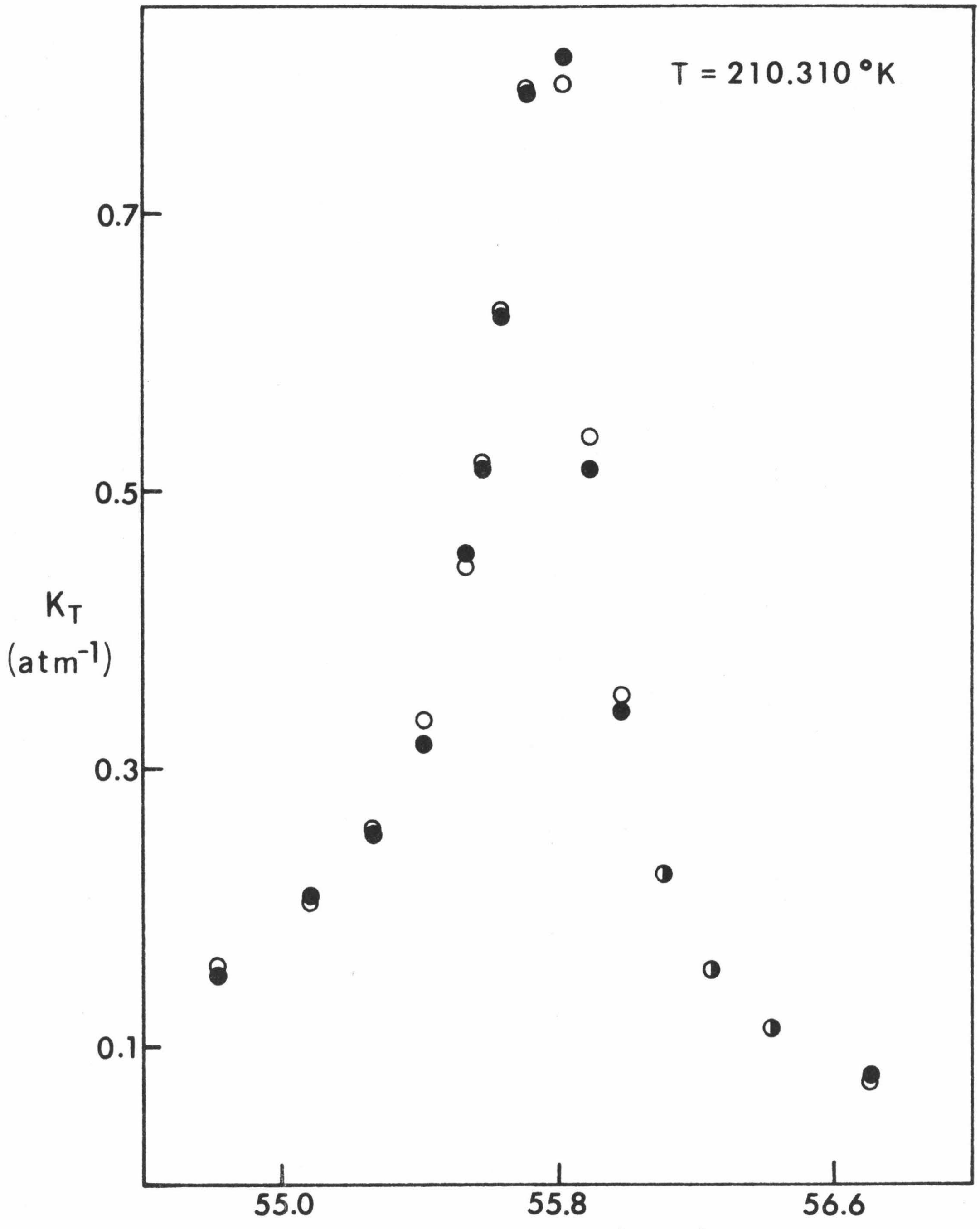

Figure 45. Comparison of Experimental and Calculated K_T along 210.310°K Isotherm.
● -experimental, ○ -calculated.

TABLE I

EXPERIMENTAL VALUES OF ANGLE OF MINIMUM DEVIATION OF KRYPTON FOR THE COEXISTING GAS-LIQUID STATES

Temperature (°K)	Pressure (atm)	Angle of Minimum Deviation (minutes of arc)	
		Gas	Liquid
195.002	35.905	101.03	548.92
197.400	38.566	112.54	531.32
199.302	40.792	122.60	516.29
199.800	41.405	125.56	511.81
201.300	43.209	135.34	498.45
203.099	45.538	148.93	479.82
203.300	45.796	150.65	477.79
204.001	46.715	156.71	469.57
205.299	48.477	170.08	452.49
206.120	49.600	180.07	440.21
206.201	49.715	181.19	438.75
206.800	50.572	190.19	428.33
207.401	51.407	200.26	416.79
207.620	51.734	204.64	411.23
207.800	52.008	208.71	406.82
208.154	52.513	217.12	397.24
208.400	52.875	223.77	389.58
208.502	53.031	227.46	385.97
208.799	53.462	239.19	373.32
208.886	53.601	242.82	368.42
209.003	53.779	250.57	360.82
209.050	-	254.32	357.29
209.103	53.936	258.33	352.77
209.126	53.972	259.46	350.26
209.146	-	262.55	348.91
209.200	54.094	269.19	341.50
209.207	-	270.78	340.72
209.221	54.114	271.90	337.75
209.224	54.128	273.18	337.56
209.231	-	274.99	336.10
209.249	-	279.07	331.85
209.256	-	281.16	329.54
209.259	54.174	281.99	327.96
209.271	-	285.87	323.84
209.274	54.198	290.04	319.87

TABLE II

EXPERIMENTAL VALUES OF ANGLE OF MINIMUM DEVIATION OF KRYPTON ALONG ISOTHERMS ABOVE THE CRITICAL TEMPERATURE

	Angle D (minutes of arc)	Pressure (atm)
219.301°K : Run I		
	*242.21	66.220
	293.68	69.165
	331.40	71.386
	361.12	73.613
	379.89	75.453
Run II		
	*242.35	66.218
	271.16	67.931
	302.36	69.634
	313.73	70.288
	343.50	72.199
	**365.83	74.010
Run III		
	219.28	64.599
	*242.16	66.221
	286.89	68.799
	320.37	70.694
	**365.58	74.012
	382.49	75.745
217.301°K : Run I		
	*244.14	63.091
	284.35	65.778
	320.69	67.365
	357.00	69.372
	**392.54	72.428
Run II		
	237.65	63.592
	*244.02	63.931
	266.54	65.009
	307.46	66.769
	342.50	68.478
	**392.50	72.428

---

*Same number of stars indicate repeated states on each isotherm.

TABLE II (continued)

	Angle D (minutes of arc)	Pressure (atm)
217.301°K : Run III		
	217.27	62.361
	*244.00	63.933
	275.97	65.422
	317.25	67.207
	340.27	68.357
	**392.45	72.430
Run IV		
	*244.11	63.933
	254.53	64.452
	297.44	66.335
	331.63	67.896
	373.78	70.624
	**392.53	72.430
215.301°K : Run I		
	*229.03	60.866
	262.21	62.196
	290.67	63.099
	310.01	63.690
	321.58	64.067
	350.90	65.219
	**378.61	66.820
Run II		
	*228.90	60.864
	249.94	61.759
	304.34	63.514
	330.09	64.369
	340.42	64.768
	369.99	66.257
	**378.41	66.817
Run III		
	*228.96	60.862
	238.90	61.311
	277.47	62.691
	316.56	63.898
	360.64	65.714
	**378.54	66.816

TABLE II (continued)

	Angle D (minutes of arc)	Pressure (atm)
213.300°K : Run I		
	*223.09	58.375
	232.28	58.721
	256.77	59.432
	286.17	60.056
	318.40	60.681
	354.79	61.624
	364.64	61.990
	**384.87	62.990
Run II		
	*222.93	58.366
	264.81	59.616
	308.27	60.478
	343.57	61.277
	**384.86	62.980
Run III		
	*223.00	58.371
	244.49	59.103
	299.20	60.304
	330.69	60.949
	375.55	62.482
	**384.81	62.985
212.200°K : Run I		
	*224.59	57.206
	272.29	58.262
	314.90	58.841
	354.62	59.565
	375.71	60.243
	**385.02	60.653
Run II		
	210.26	56.657
	*224.57	57.202
	265.15	58.146
	304.17	58.695
	345.11	59.347
	**385.00	60.654
Run III		
	*224.56	57.205
	246.02	57.786
	285.98	58.455
	324.78	58.985
	364.86	59.856
	**384.97	60.654

TABLE II (continued)

	Angle D (minutes of arc)	Pressure (atm)
212.200°K : Run IV		
	*224.65	57.203
	236.13	57.542
	255.67	57.977
	295.05	58.574
	334.32	59.138
	**385.03	60.652
211.300°K : Run I		
	*223.79	56.156
	256.35	56.822
	284.90	57.136
	331.10	57.558
	353.46	57.873
	**385.96	58.794
Run II		
	*223.41	56.157
	235.31	56.456
	273.35	57.026
	314.12	57.390
	361.79	58.043
	**385.90	58.795
Run III		
	*223.57	56.164
	244.48	56.637
	292.31	57.202
	341.29	57.687
	369.71	58.244
	**386.00	58.804
Run IV		
	*223.58	56.164
	263.14	56.913
	300.70	57.274
	376.72	58.454
	**386.03	58.802
210.310°K : Run I		
	214.33	54.820
	*224.92	55.087
	256.54	55.537
	286.01	55.714
	314.50	55.824
	344.05	55.986

TABLE II (continued)

	Angle D (minutes of arc)	Pressure (atm)
210.310°K : Run I		
	**374.82	56.421
	385.58	56.710
Run II		
	*225.02	55.090
	244.92	55.420
	271.95	55.645
	302.67	55.780
	331.76	55.901
	366.45	56.254
	**375.00	56.423
Run III		
	*225.25	55.091
	235.05	55.274
	263.22	55.589
	356.51	56.111
	**375.10	56.424
210.200°K : Run I		
	*220.56	54.860
	257.00	55.392
	283.53	55.539
	328.25	55.708
	355.11	55.894
	**387.59	56.546
Run II		
	*220.49	54.860
	229.79	55.055
	265.97	55.453
	313.57	55.647
	366.06	56.040
	**387.57	56.548
Run III		
	*220.71	54.866
	249.49	55.326
	300.68	55.602
	345.40	55.810
	378.93	56.300
	**387.72	56.552

TABLE II (continued)

	Angle D (minutes of arc)	Pressure (atm)
209.800°K : Run I		
	*222.95	54.461
	253.80	54.846
	287.00	54.970
	320.10	55.033
	349.97	55.144
	**386.86	55.701
Run II		
	*223.16	54.471
	233.94	54.653
	264.88	54.908
	311.20	55.015
	358.25	55.210
	**386.99	55.709
Run III		
	*223.05	54.469
	239.87	54.724
	274.33	54.941
	329.61	55.056
	369.15	55.336
	**386.94	55.704
Run IV		
	*222.94	54.467
	246.89	54.793
	338.10	55.084
	379.48	55.520
	**386.87	55.703
209.570°K : Run I		
	213.70	54.008
	*225.71	54.258
	253.55	54.541
	**375.03	54.978
Run II		
	*226.27	54.268
	236.08	54.403
	262.65	54.582
	279.38	54.625
	316.82	54.663
	344.05	54.716
	363.39	54.836
	**375.00	54.982

TABLE II (continued)

	Angle D (minutes of arc)	Pressure (atm)
209.570°K : Run III		
	*226.24	54.269
	243.62	54.478
	303.58	54.652
	325.28	54.673
	354.01	54.764
	**374.96	54.983
	384.66	55.177
209.450°K : Run I		
	*225.35	54.112
	236.03	54.255
	265.41	54.426
	289.90	54.461
	326.31	54.480
	352.54	54.540
	**374.59	54.736
Run II		
	214.50	54.115
	*225.50	54.110
	257.26	54.400
	277.40	54.4487
	346.11	54.516
	**374.54	54.737
	387.08	54.980
Run III		
	*225.65	54.115
	244.79	54.332
	309.40	54.4697
	336.75	54.494
	364.93	54.625
	**375.06	54.744
209.380°K : Run I		
	214.53	53.826
	*223.54	54.0056
	244.58	54.2464
	261.04	54.3232
	288.80	54.3568
	323.76	54.3661
	344.20	54.3894
	363.09	54.4775
	**374.40	54.5973
	386.23	54.8146

TABLE II (continued)

	Angle D (minutes of arc)	Pressure (atm)
209.380°K : Run II		
	*223.91	54.0074
	235.81	54.1669
	255.68	54.3018
	271.89	54.3411
	303.93	54.3583
	316.68	54.3624
	338.54	54.3780
	356.43	54.4328
	**374.66	54.6016
209.338°K : Run I		
	*214.56	53.7721
	225.08	53.9761
	245.38	54.1929
	267.86	54.2750
	275.88	54.2845
	295.55	54.2927
	316.58	54.2957
	333.97	54.3020
	359.47	54.3741
	376.49	54.5443
	**387.30	54.7465
Run II		
	*214.61	53.7744
	232.76	54.0790
	254.48	54.2381
	290.77	54.2907
	302.87	54.2935
	320.94	54.2961
	348.51	54.3269
	368.84	54.4486
	**387.26	54.7474
209.315°K : Run I		
	*215.46	53.7715
	223.91	53.9316
	242.53	54.1432
	261.22	54.2288
	269.08	54.2442
	279.42	54.2528
	299.13	54.2565
	331.95	54.2622
	355.07	54.3097
	376.17	54.4942
	**385.61	54.6628

TABLE II (continued)

	Angle D (minutes of arc)	Pressure (atm)
209.315°K : Run II		
	*215.49	53.7710
	235.77	54.0854
	250.63	54.1912
	285.19	54.2546
	312.58	54.2573
	319.97	54.2581
	339.39	54.2688
	368.18	54.3981
	**385.51	54.6631
209.302°K : Run I		
	*211.86	53.6718
	235.07	54.0633
	247.41	54.1597
	265.30	54.2217
	275.78	54.2345
	287.20	54.2397
	302.67	54.2422
	361.33	54.3250
	377.80	54.4958
	**388.78	54.7128
Run II		
	*211.64	53.6694
	220.86	53.8674
	234.60	54.0608
	251.52	54.1815
	273.88	54.2330
	285.75	54.2392
	295.63	54.2414
	326.64	54.2439
	359.43	54.3141
	374.21	54.4466
	383.11	54.5905
	**388.57	54.7113
209.294°K : Run I		
	*215.33	53.7446
	235.44	54.0587
	252.52	54.1746
	287.11	54.2279
	327.72	54.2308
	351.52	54.2629
	372.84	54.4129
	**382.90	54.5675

TABLE II (continued)

	Angle D (minutes of arc)	Pressure (atm)
209.294°K : Run II		
	*215.35	53.7447
	224.43	53.9179
	242.59	54.1207
	263.67	54.2079
	278.53	54.2257
	287.06	54.2279
	319.65	54.2293
	327.12	54.2308
	339.81	54.2388
	363.78	54.3253
	**382.91	54.5681

TABLE III

EXPERIMENTAL VALUES OF ANGLE OF MINIMUM DEVIATION OF KRYPTON ALONG ISOTHERMS BELOW THE CRITICAL TEMPERATURE

	Angle D (minutes of arc)	Pressure (atm)
199.302°K : Run I		
	*60.60	27.798
	78.97	33.048
	100.97	37.708
	122.73 516.43	[coexisting states] 40.793
	538.45	49.845
	551.72	57.342
	**565.34	66.958
Run II		
	*60.48	27.796
	69.26	30.469
	88.79	35.361
	105.79	38.522
	113.56	39.671
	122.46 516.15	[coexisting states] 40.790
	522.33	42.976
	530.39	46.159
	545.56	53.678
	557.70	61.361
	**565.20	66.956
201.300°K : Run I		
	60.05	28.086
	68.74	30.812
	79.82	33.893
	90.66	36.472
	99.67	38.315
	110.17	40.128
	115.08	40.872
	120.15	41.573

---

* Same number of stars indicate repeated states on each isotherm.

TABLE III (continued)

	Angle D (minutes of arc)		Pressure (atm)
201.300°K : Run I			
	125.46		42.219
	131.58		42.878
	135.33 498.46	[coexisting states]	43.237
Run II			
	135.34 498.45	[coexisting states]	43.241
	507.08		45.603
	513.39		47.602
	521.12		50.413
	528.19		53.412
	534.61		56.501
	541.29		60.135
	547.46		63.846
	554.93		68.890
203.300°K : Run I			
	68.70		31.296
	79.62		34.451
	90.45		37.146
	100.28		39.240
	110.83		41.175
	120.18		42.619
	130.47		43.939
	138.71		44.801
	144.93		45.352
	150.54 477.76	[coexisting states]	45.795
Run II			
	150.54 477.81	[coexisting states]	45.796
	483.65		46.895
	491.00		48.457
	497.31		50.063
	504.28		52.093
	511.31		54.475
	518.67		57.368
	525.49		60.398
	531.75		63.531

TABLE III (continued)

	Angle D (minutes of arc)		Pressure (atm)
206.120°K : Run I			
	70.80		32.768
	83.71		36.499
	100.52		40.519
	116.33		43.507
	130.20		45.581
	146.58		47.435
	160.65		48.582
	175.48		49.409
	180.11 440.17	[coexisting states]	49.600
Run II			
	180.02 440.25	[coexisting states]	49.600
	451.26		50.628
	463.23		52.179
	476.82		54.633
	487.54		57.206
	495.55		59.544
	503.71		62.337
	510.61		65.037
	516.61		67.755
207.620°K : Run I			
	82.61		36.700
	98.50		40.694
	114.07		43.857
	129.61		46.365
	145.45		48.336
	159.57		49.638
	177.35		50.798
	189.78		51.330
	204.71 411.25	[coexisting states]	51.736
Run II			
	204.57 411.21	[coexisting states]	51.733
	416.82		51.949
	432.52		52.888
	447.99		54.421

TABLE III (continued)

	Angle D (minutes of arc)	Pressure (atm)
207.620°K : Run II		
	465.85	57.157
	481.28	60.624
	494.05	64.396
	502.61	67.489
	510.87	70.987
208.400°K : Run I		
	78.41	35.749
	98.57	41.027
	113.71	44.179
	128.55	46.661
	144.77	48.771
	160.29	50.288
	175.46	51.357
	189.61	52.058
	223.43 389.40	[coexisting states] 52.871
Run II		
	203.21	52.508
	224.10 389.75	[coexisting states] 52.879
	403.74	53.218
	421.81	54.076
	434.13	55.034
	448.36	56.629
	463.69	59.112
	476.77	62.000
	487.77	65.083
	498.37	68.719
208.886°K : Run I		
	88.79	38.808
	108.34	43.363
	124.30	46.267
	139.46	48.448
	155.26	50.189
	170.26	51.435
	185.49	52.319
	200.27	52.914
	*214.20	53.273

TABLE III (continued)

	Angle D (minutes of arc)		Pressure (atm)
208.886°K : Run II			
	*214.43		53.282
	232.08		53.529
	242.60 368.49	[coexisting states]	53.600
	243.03 368.35	[coexisting states]	53.602
	373.58		53.650
	387.62		53.843
	**398.52		54.118
Run III			
	**398.47		54.115
	412.10		54.676
	425.01		55.490
	441.22		57.070
	454.94		59.012
	471.03		62.181
	484.61		65.798
	496.11		69.653
209.126°K : Run I			
	99.14		41.475
	118.31		45.387
	140.16		48.689
	154.58		50.303
	169.21		51.546
	184.62		52.498
	198.94		53.112
	216.31		53.590
	*232.37		53.830
Run II			
	*233.23		53.839
	249.11		53.945
	259.46 350.26	[coexisting states]	53.972
	361.20		54.010
	376.78		54.144
	**389.77		54.379

TABLE III (continued)

	Angle D (minutes of arc)	Pressure (atm)
209.126°K : Run III		
	**390.06	54.381
	407.72	54.997
	422.42	55.881
	434.58	56.951
	450.81	59.021
	468.32	62.292
	483.16	66.136
	493.46	69.509
209.221°K : Run I		
	118.11	45.379
	134.31	47.960
	150.03	49.890
	165.14	51.298
	180.70	52.359
	195.91	53.087
	210.01	53.544
	224.27	53.833
	238.46	53.998
Run II		
	242.28	54.026
	259.17	54.098
	271.90 337.75 [coexisting states]	54.114
	352.17	54.137
	*365.30	54.200
Run III		
	*365.80	54.205
	380.08	54.369
	398.97	54.842
	419.97	55.923
	441.52	57.982
	462.09	61.248
	477.26	64.754
	489.93	68.575
209.259°K : Run I		
	121.09	45.940
	136.40	48.280
	155.40	50.474
	174.29	52.003

TABLE III (continued)

	Angle D (minutes of arc)		Pressure (atm)
209.259°K : Run I			
	190.07		52.877
	206.21		53.482
	220.33		53.811
	*235.56		54.019
Run II			
	*235.74		54.019
	252.91		54.1308
	263.83		54.1600
	281.99 327.96	[coexisting states]	54.1736
	336.33		54.1768
	**348.31		54.1916
Run III			
	**350.70		54.1984
	362.92		54.2563
	383.17		54.508
	396.41		54.850
	412.47		55.562
	432.59		57.118
	454.53		60.046
	467.49		62.571
209.274°K : Run I			
	131.76		47.642
	145.23		49.395
	158.43		50.789
	174.71		52.041
	189.44		52.862
	205.84		53.486
	220.13		53.823
	*235.93		54.0411
Run II			
	*236.43		54.0440
	252.84		54.1507
	269.53		54.1887
	290.04 319.87	[coexisting states]	54.1985
	348.07		54.2208

TABLE III (continued)

	Angle D (minutes of arc)	Pressure (atm)
209.274°K : Run III		
	358.39	54.2593
	375.26	54.4102
	391.03	54.722
	408.32	55.374
	426.36	56.574
	445.81	58.743
	465.11	62.095
	481.04	66.075

TABLE IV

REFRACTIVE INDEX OF KRYPTON FOR COEXISTING GAS-LIQUID STATES

Temperature (°K)	Pressure (atm)	GAS STATE		LIQUID STATE	
		Refractive Index	Error	Refractive Index	Error
195.002	35.905	1.03602	± 0.00004	1.19288	± 0.00004
197.400	38.566	1.04010	0.00004	1.18681	0.00004
199.302	40.792	1.04368	0.00004	1.18162	0.00004
199.800	41.405	1.04473	0.00004	1.18007	0.00004
201.300	43.239	1.04820	0.00004	1.17545	0.00004
203.099	45.538	1.05301	0.00004	1.16899	0.00004
203.300	45.796	1.05362	0.00004	1.16829	0.00004
204.001	46.715	1.05577	0.00004	1.16544	0.00004
205.299	48.477	1.06050	0.00004	1.15951	0.00004
206.120	49.600	1.06404	0.00004	1.15525	0.00004
206.201	49.715	1.06443	0.00004	1.15474	0.00004
206.800	50.572	1.06761	0.00004	1.15112	0.00004
207.401	51.407	1.07117	0.00004	1.14710	0.00004
207.620	51.734	1.07272	0.00004	1.14517	0.00004
207.800	52.008	1.07416	0.00004	1.14363	0.00004
208.154	52.513	1.07712	0.00004	1.14029	0.00004
208.400	52.875	1.07947	0.00007	1.13762	0.00007
208.502	53.031	1.08077	0.00007	1.13636	0.00007
208.799	53.462	1.08490	0.00007	1.13195	0.00007
208.886	53.601	1.08618	0.00007	1.13024	0.00007
209.003	53.779	1.08891	0.00007	1.12758	0.00007
209.050	-	1.09023	0.00007	1.12635	0.00007
209.103	53.936	1.09164	0.00007	1.12477	0.00007
209.126	53.972	1.09204	0.00007	1.12389	0.00007
209.146	-	1.09313	0.00007	1.12342	0.00007
209.200	54.094	1.09546	0.00007	1.12083	0.00007
209.207	-	1.09602	± 0.00007	1.12055	± 0.00007

TABLE IV (continued)

Temperature	Pressure	GAS STATE		LIQUID STATE	
(°K)	(atm)	Refractive Index	Error	Refractive Index	Error
209.221	54.114	1.09642	± 0.00007	1.11951	± 0.00007
209.224	54.128	1.09687	0.00007	1.11945	0.00007
209.231	-	1.09750	0.00007	1.11894	0.00007
209.249	-	1.09894	0.00007	1.11745	0.00007
209.256	-	1.09967	0.00007	1.11664	0.00007
209.259	54.174	1.09996	0.00007	1.11609	0.00007
209.271	-	1.10132	0.00018	1.11464	0.00018
209.274	54.198	1.10279	± 0.00018	1.11325	± 0.00018

TABLE V

REFRACTIVE INDEX AND ISOTHERMAL COMPRESSIBILITY OF KRYPTON ALONG ISOTHERMS ABOVE THE CRITICAL TEMPERATURE

Pressure (atm)	Angle D (minute of arc)	Refractive Index	Derivative $(dD/dP)_T$ (min./atm)	Isothermal Compressibility (atm^{-1})
219.301°K Isotherm:				
64.599	219.28	1.07789	12.66	0.05643
66.221	242.16	1.08595	15.62	0.06287
67.931	271.16	1.09616	17.88	0.06408
68.799	286.89	1.10168	18.42	0.06227
69.165	293.68	1.10407	18.65	0.06153
69.634	302.36	1.10711	18.14	0.05808
70.288	313.73	1.11110	16.66	0.05132
70.694	320.37	1.11343	16.16	0.04872
71.386	331.40	1.11729	15.64	0.04550
72.199	343.50	1.12153	13.89	0.03894
73.613	361.12	1.12769	11.42	0.03039
74.012	365.58	1.12924	10.90	0.02863
75.453	379.89	1.13424	9.058	0.02285
75.745	382.49	1.13515	8.753	0.02192
217.301°K Isotherm:				
62.361	217.27	1.07718	15.06	0.06779
63.592	237.65	1.08436	18.25	0.07490
63.931	244.02	1.08661	19.35	0.07732
64.452	254.53	1.09031	20.89	0.07989
65.009	266.54	1.09453	22.29	0.08131
65.422	275.97	1.09785	23.31	0.08203
65.778	284.35	1.10079	23.63	0.08060
66.335	297.44	1.10539	23.33	0.07597
66.769	307.46	1.10890	22.76	0.07160
67.207	317.25	1.11233	21.94	0.06681
67.365	320.69	1.11354	21.59	0.06499
67.896	331.63	1.11737	19.40	0.05641
68.357	340.27	1.12040	18.53	0.05245
68.478	342.50	1.12118	18.19	0.05113
69.372	357.00	1.12625	14.83	0.03991
70.624	373.78	1.13211	12.01	0.03082
72.428	392.50	1.13864	8.983	0.02189

TABLE V (continued)

Pressure (atm)	Angle D (minute of arc)	Refractive Index	Derivative $(dD/dP)_T$ (min./atm)	Isothermal Compressibility (atm^{-1})
215.301°K Isotherm:				
60.862	228.96	1.08130	21.18	0.09034
61.311	238.90	1.08480	23.22	0.09480
61.759	249.94	1.08869	26.31	0.1025
62.196	262.21	1.09301	29.63	0.1099
62.691	277.47	1.09837	31.80	0.1112
63.099	290.67	1.10301	32.90	0.1097
63.514	304.34	1.10781	32.50	0.1033
63.690	310.01	1.10980	32.04	0.09993
63.898	316.56	1.11209	30.53	0.09318
64.067	321.58	1.11385	29.08	0.08732
64.369	330.09	1.11683	27.16	0.07936
64.768	340.42	1.12045	24.78	0.07012
65.219	350.90	1.12411	21.39	0.05865
65.714	360.64	1.12752	18.32	0.04880
66.257	369.99	1.13078	16.20	0.04201
66.816	378.54	1.13377	14.46	0.03660
213.300°K Isotherm:				
58.371	223.00	1.07920	24.13	0.1057
58.721	232.28	1.08247	29.07	0.1222
59.103	244.49	1.08677	34.62	0.1380
59.432	256.77	1.09109	41.13	0.1559
59.616	264.81	1.09392	45.65	0.1676
60.056	286.17	1.10143	51.53	0.1746
60.304	299.20	1.10600	52.76	0.1707
60.478	308.27	1.10919	51.27	0.1609
60.681	318.40	1.11274	48.40	0.1468
60.949	330.69	1.11704	43.01	0.1254
61.277	343.57	1.12155	35.61	0.09978
61.624	354.79	1.12547	29.42	0.07973
61.990	364.64	1.12892	24.61	0.06481
62.482	375.55	1.13273	20.06	0.05122
62.985	384.81	1.13596	16.95	0.04218
212.200°K Isotherm:				
56.657	210.26	1.07470	22.47	0.1046
57.202	224.57	1.07975	30.71	0.1336
57.542	236.13	1.08383	37.24	0.1539
57.786	246.02	1.08731	45.45	0.1800
57.977	255.67	1.09071	54.19	0.2063
58.146	265.15	1.09404	58.71	0.2153
58.262	272.29	1.09655	64.94	0.2317

TABLE V (continued)

Pressure (atm)	Angle D (minute of arc)	Refractive Index	Derivative $(dD/dP)_T$ (min./atm)	Isothermal Compressibility (atm^{-1})
212.200°K Isotherm continued:				
58.455	285.98	1.10136	75.50	0.2560
58.574	295.05	1.10455	76.11	0.2499
58.695	304.17	1.10775	74.85	0.2381
58.841	314.90	1.11151	71.25	0.2186
58.985	324.78	1.11497	66.26	0.1969
59.138	334.32	1.11831	57.31	0.1652
59.347	345.11	1.12209	47.42	0.1323
59.565	354.62	1.12541	39.60	0.1074
59.856	364.86	1.12899	31.54	0.08300
60.243	375.71	1.13278	25.01	0.06382
60.654	385.00	1.13602	20.51	0.05101
211.300°K Isotherm:				
56.157	223.41	1.07934	35.13	0.1537
56.456	235.31	1.08354	45.55	0.1889
56.637	244.48	1.08677	56.75	0.2263
56.822	256.35	1.09095	70.77	0.2687
56.913	263.14	1.09333	80.33	0.2969
57.026	273.35	1.09692	99.24	0.3526
57.136	284.90	1.10098	109.9	0.3742
57.202	292.31	1.10359	114.7	0.3803
57.274	300.70	1.10653	117.4	0.3778
57.390	314.12	1.11124	112.8	0.3469
57.558	331.10	1.11719	86.71	0.2525
57.687	341.29	1.12075	73.73	0.2081
57.873	353.46	1.12501	55.83	0.1519
58.043	361.79	1.12792	43.52	0.1155
58.244	369.71	1.13069	36.14	0.09379
58.454	376.72	1.13313	30.67	0.07805
58.795	385.90	1.13634	23.64	0.05865
210.310°K Isotherm:				
54.820	214.33	1.07614	32.90	0.1501
55.090	225.02	1.07991	47.78	0.2074
55.274	235.05	1.08345	60.69	0.2520
55.420	244.92	1.08692	79.61	0.3168
55.537	256.54	1.09101	119.7	0.4541
55.589	263.22	1.09336	139.3	0.5146
55.645	271.95	1.09643	174.9	0.6250
55.714	286.01	1.10137	232.1	0.7871
55.780	302.67	1.10722	268.0	0.8570
55.824	314.50	1.11137	264.7	0.8135

TABLE V (continued)

Pressure (atm)	Angle D (minute of arc)	Refractive Index	Derivative $(dD/dP)_T$ (min./atm)	Isothermal Compressibility (atm^{-1})
210.310°K Isotherm continued:				
55.901	331.76	1.11742	177.2	0.5150
55.986	344.05	1.12172	121.0	0.3385
56.111	356.51	1.12607	82.50	0.2224
56.254	366.45	1.12955	58.84	0.1541
56.423	375.00	1.13253	43.92	0.1123
56.710	385.58	1.13623	31.41	0.07799
210.200°K Isotherm:				
54.866	220.71	1.07839	42.56	0.1885
55.055	229.79	1.08159	54.71	0.2325
55.326	249.49	1.08853	100.9	0.3942
55.392	257.00	1.09117	128.8	0.4876
55.453	265.97	1.09433	167.3	0.6116
55.539	283.53	1.10050	245.6	0.8403
55.602	300.68	1.10652	291.2	0.9374
55.647	313.57	1.11104	272.9	0.8412
55.708	328.25	1.11619	208.0	0.6112
55.810	345.40	1.12219	137.5	0.3831
55.894	355.11	1.12559	94.81	0.2567
56.040	366.06	1.12941	61.80	0.1621
56.300	378.93	1.13391	40.28	0.1019
56.552	387.72	1.13697	30.49	0.07528
209.800°K Isotherm:				
54.471	223.16	1.07925	47.04	0.2060
54.653	233.94	1.08305	75.26	0.3140
54.724	239.87	1.08514	91.79	0.3732
54.793	246.89	1.08762	115.0	0.4537
54.846	253.80	1.09005	147.2	0.5649
54.908	264.88	1.09395	228.7	0.8394
54.941	274.33	1.09727	357.8	1.267
54.970	287.00	1.10172	508.9	1.719
55.015	311.20	1.11021	521.2	1.619
55.033	320.10	1.11333	465.5	1.404
55.056	329.61	1.11666	356.9	1.044
55.084	338.10	1.11964	259.9	0.7407
55.144	349.97	1.12379	150.9	0.4148
55.210	358.25	1.12668	107.4	0.2881
55.336	369.15	1.13049	69.90	0.1817
55.520	379.48	1.13410	45.97	0.1161
55.709	386.99	1.13672	34.71	0.08587

TABLE V (continued)

Pressure (atm)	Angle D (minute of arc)	Refractive Index	Derivative $(dD/dP)_T$ (min./atm)	Isothermal Compressibility (atm^{-1})
209.570°K Isotherm:				
54.008	213.70	1.07592	39.05	0.1787
54.268	226.27	1.08035	61.20	0.2642
54.403	236.08	1.08381	86.67	0.3582
54.478	243.62	1.08646	121.9	0.4879
54.541	253.55	1.08996	194.9	0.7484
54.582	262.65	1.09316	264.8	0.9805
54.625	279.38	1.09904	592.3	2.058
54.652	303.58	1.10754	1288.	4.105
54.663	316.82	1.11218	1003.	3.058
54.673	325.28	1.11515	727.8	2.159
54.716	344.05	1.12172	271.5	0.7598
54.764	354.01	1.12520	163.9	0.4451
54.836	363.39	1.12848	105.5	0.2788
54.982	375.00	1.13253	61.5	0.1574
55.177	384.66	1.13591	40.8	0.1015
209.450°K Isotherm:				
53.893	214.50	1.07620	41.31	0.1884
54.112	225.35	1.08003	60.74	0.2633
54.255	236.03	1.08379	94.26	0.3896
54.332	244.79	1.08688	139.0	0.5536
54.400	257.26	1.09127	254.2	0.9617
54.426	265.41	1.09413	391.7	1.435
54.4487	277.40	1.09835	737.4	2.581
54.4610	289.90	1.10274	1487.	4.972
54.4697	309.40	1.10958	2596.	8.114
54.480	326.31	1.11551	1035.	3.060
54.494	336.75	1.11916	559.6	1.601
54.516	346.11	1.12244	331.9	0.9229
54.540	352.54	1.12469	215.2	0.5869
54.625	364.93	1.12902	109.3	0.2877
54.736	374.59	1.13239	69.72	0.1785
54.980	387.08	1.13675	39.10	0.09670
209.380°K Isotherm: Run I:				
53.8260	214.53	1.07621	43.3	0.1974
54.0056	223.54	1.07939	59.0	0.2578
54.2464	244.58	1.08680	144.0	0.5737
54.3232	261.04	1.09260	353.0	1.316
54.3568	288.80	1.10235	3301.	11.08
54.3661	323.76	1.11461	2300.	6.858

TABLE V (continued)

Pressure (atm)	Angle D (minute of arc)	Refractive Index	Derivative $(dD/dP)_T$ (min./atm)	Isothermal Compressibility (atm^{-1})
209.380°K Isotherm: Run I (continued) :				
54.3894	344.20	1.12177	428.9	1.200
54.4775	363.09	1.12837	128.6	0.3401
54.5973	374.40	1.13232	72.0	0.1844
54.8146	386.23	1.13645	42.8	0.1060
Run II:				
54.0074	223.91	1.07952	60.2	0.2629
54.1669	235.81	1.08371	95.4	0.3949
54.3018	255.68	1.09071	259.8	0.9893
54.3411	271.89	1.09641	732.6	2.618
54.3583	303.93	1.10766	3940.	12.54
54.3624	316.68	1.11213	2834.	8.647
54.3780	338.54	1.11979	692.4	1.970
54.4328	356.43	1.12605	185.2	0.4994
54.6016	374.66	1.13242	72.1	0.1846
209.338°K Isotherm: Run I:				
53.7721	214.56	1.07622	43.19	0.1969
53.9761	225.08	1.07993	62.90	0.2730
54.1929	245.38	1.08708	154.7	0.6144
54.2750	267.86	1.09499	631.0	2.290
54.2845	275.88	1.09781	1168.	4.113
54.2927	295.55	1.10472	5896.	19.32
54.2957	316.58	1.11210	6750.	20.60
54.3020	333.97	1.11819	1317.	3.802
54.3741	359.47	1.12711	163.6	0.4372
54.5443	376.49	1.13305	67.73	0.1724
54.7465	387.30	1.13683	43.48	0.1075
Run II:				
53.7744	214.61	1.07624	44.22	0.2015
54.0790	232.76	1.08264	85.88	0.3601
54.2381	254.48	1.09029	249.9	0.9559
54.2907	290.77	1.10304	4319.	14.40
54.2935	302.87	1.10729	5203.	16.63
54.2961	320.94	1.11363	6088.	18.32
54.3269	348.51	1.12328	346.4	0.9562
54.4486	368.84	1.13038	97.31	0.2532
54.7474	387.26	1.13681	43.21	0.1068

TABLE V (continued)

Pressure (atm)	Angle D (minute of arc)	Refractive Index	Derivative $(dD/dP)_T$ (min./atm)	Isothermal Compressibility (atm^{-1})
209.315°K Isotherm: Run I:				
53.7715	215.46	1.07654	48.82	0.2080
53.9316	223.91	1.07952	61.61	0.2689
54.1432	242.53	1.08608	137.6	0.5530
54.2288	261.22	1.09266	394.1	1.468
54.2442	269.08	1.09542	719.4	2.598
54.2528	279.42	1.09906	2211.	7.682
54.2565	299.13	1.10598	24102.	78.02
54.2581	319.97	1.11329	5651.	17.05
54.2622	331.95	1.11748	1730.	5.027
54.3097	355.07	1.12557	226.4	0.6129
54.4942	376.17	1.13294	69.29	0.1766
54.6628	385.61	1.13624	46.38	0.1152
Run II:				
53.7710	215.49	1.07655	45.50	0.2065
54.0854	235.77	1.08370	100.3	0.4150
54.1912	250.63	1.08893	209.4	0.8138
54.2546	285.19	1.10108	4481.	15.24
54.2573	312.58	1.11070	13776.	42.60
54.2581	319.97	1.11329	6250.	18.86
54.2688	339.39	1.12009	866.0	2.458
54.3981	368.18	1.13015	100.5	0.2619
54.6631	385.51	1.13620	46.73	0.1161
209.302°K Isotherm: Run I:				
53.6718	211.86	1.07527	40.65	0.1878
54.0633	235.07	1.08345	96.85	0.4021
54.1597	247.41	1.08780	177.5	0.6990
54.2217	265.30	1.09409	556.1	2.038
54.2345	275.78	1.09778	1333.	4.693
54.2397	287.20	1.10179	3798.	12.82
54.2422	302.67	1.10722	12643.	40.43
54.2439	326.64	1.11562	6547.	19.34
54.3250	361.33	1.12776	154.8	0.4116
54.4958	377.80	1.13351	65.29	0.1656
54.7128	388.78	1.13734	40.53	0.0998

TABLE V (continued)

Pressure (atm)	Angle D (minute of arc)	Refractive Index	Derivative $(dD/dP)_T$ (min./atm)	Isothermal Compressibility (atm^{-1})
209.302°K Isotherm: Run II:				
53.6694	211.64	1.07519	40.04	0.1851
53.8674	220.86	1.07844	54.98	0.2433
54.0608	234.60	1.08329	95.82	0.3986
54.1815	251.52	1.08925	225.9	0.8746
54.2330	273.88	1.09711	1187.	4.209
54.2392	285.75	1.10128	3277.	11.12
54.2414	295.63	1.10475	6554.	21.47
54.2422	302.67	1.10722	13014.	41.61
54.2439	326.64	1.11562	5648.	16.68
54.3141	359.43	1.12710	173.3	0.4633
54.4466	374.21	1.13226	77.11	0.1976
54.5905	383.11	1.13536	50.83	0.1271
54.7113	388.57	1.13727	40.50	0.0998
209.294°K Isotherm: Run I:				
53.7447	215.35	1.07650	44.82	0.2035
53.9179	224.43	1.07970	62.35	0.2714
54.1207	242.59	1.08610	140.9	0.5661
54.2079	263.67	1.09352	498.8	1.840
54.2257	278.53	1.09875	1996.	6.956
54.2279	287.06	1.10174	9223.	31.15
54.2293	319.65	1.11317	7967.	24.07
54.2308	327.12	1.11579	3350.	9.880
54.2388	339.81	1.12023	917.3	2.600
54.3253	363.78	1.12862	132.7	0.3503
54.5681	382.91	1.13529	53.35	0.1334
Run II:				
53.7446	215.33	1.07649	45.20	0.2053
54.0587	235.44	1.08358	99.52	0.4124
54.1746	252.52	1.08960	238.2	0.9187
54.2279	287.11	1.10176	9687.	32.72
54.2308	327.72	1.11600	3780.	11.13
54.2629	351.52	1.12433	305.6	0.8362
54.4129	372.84	1.13178	82.72	0.2128
54.5675	382.90	1.13529	52.81	0.1321

TABLE VI

REFRACTIVE INDEX AND ISOTHERMAL COMPRESSIBILITY OF KRYPTON ALONG ISOTHERMS BELOW THE CRITICAL TEMPERATURE

Pressure (atm)	Angle D (minute of arc)	Refractive Index	Derivative $(dD/dP)_T$ (min./atm)		Isothermal Compressibility** (atm^{-1})
			Graphical	Numerical*	
199.302°K Isotherm:					
Gas side:					
27.797	60.54	1.02161	3.20	3.01	0.0495
30.464	69.26	1.02471	3.86	3.52	0.0505
33.048	78.97	1.02817	4.16	3.99	0.0501
35.361	88.79	1.03166	4.88	4.63	0.0517
37.708	100.97	1.03599	5.86	5.71	0.0560
38.522	105.79	1.03771	6.17	6.21	0.0581
39.671	113.56	1.04047	7.39	7.32	0.0638
40.792	122.60	1.04368	8.75	9.21	0.0742
Liquid side:					
40.792	516.29	1.18162	2.85	2.98	0.00543
42.976	522.33	1.18370	2.77	2.65	0.00476
46.159	530.39	1.18649	2.45	2.39	0.00422
49.845	538.45	1.18927	2.02	1.99	0.00347
53.678	545.56	1.19172	1.87	1.76	0.00302
57.342	551.72	1.19385	1.86	1.58	0.00268
61.361	557.70	1.19591	1.24	1.41	0.00237
66.957	565.27	1.19852	-	1.31	0.00216
201.300°K Isotherm:					
Gas side:					
28.086	60.05	1.02143	-	3.04	0.0504
30.812	68.74	1.02453	3.41	3.35	0.0484
33.893	79.82	1.02847	3.91	3.88	0.0483
36.472	90.66	1.03233	4.60	4.56	0.0498
38.315	99.67	1.03553	5.24	5.28	0.0525
40.128	110.17	1.03926	6.39	6.34	0.0570
40.872	115.08	1.04101	6.93	6.87	0.0591
41.573	120.15	1.04281	7.70	7.69	0.0633
42.219	125.46	1.04469	8.65	8.70	0.0685
42.878	131.58	1.04686	10.12	10.09	0.0757
43.239	135.34	1.04820	10.94	11.78	0.0859

---

* Calculated by the numerical cubic spline fit.

**Calculated from the numerical values of the derivative.

TABLE VI (continued)

Pressure (atm)	Angle D (minute of arc)	Refractive Index	Derivative $(dD/dP)_T$ (min./atm) Graphical	Numerical	Isothermal Compressibility (atm^{-1})
201.300°K Isotherm: Liquid side:					
43.239	498.45	1.17545	4.02	3.95	0.00747
45.603	507.08	1.17843	3.42	3.33	0.00618
47.602	513.39	1.18061	2.91	2.98	0.00546
50.413	521.12	1.18329	2.61	2.53	0.00457
53.412	528.19	1.18573	2.26	2.21	0.00392
56.501	534.61	1.18794	2.07	1.95	0.00343
60.135	541.29	1.19025	1.82	1.74	0.00302
63.846	547.46	1.19238	1.36	1.58	0.00271
68.890	554.93	1.19495	-	1.38	0.00233
203.300°K Isotherm: Gas side:					
31.296	68.70	1.02451	-	3.23	0.0467
34.451	79.62	1.02840	3.61	3.72	0.0464
37.146	90.45	1.03225	4.42	4.36	0.0478
39.240	100.28	1.03575	5.02	5.04	0.0498
41.175	110.83	1.03950	5.97	5.95	0.0531
42.619	120.18	1.04282	7.02	7.06	0.0581
43.939	130.47	1.04647	8.70	8.70	0.0658
44.801	138.71	1.04939	10.5	10.6	0.0752
45.352	144.93	1.05160	12.4	11.9	0.0809
45.796	150.65	1.05362	14.0	14.2	0.0929
Liquid side:					
45.796	477.79	1.16829	5.19	5.63	0.01114
46.895	483.65	1.17032	5.14	5.12	0.01001
48.457	491.00	1.17287	4.27	4.27	0.00820
50.063	497.31	1.17505	3.70	3.68	0.00697
52.093	504.28	1.17746	3.22	3.19	0.00596
54.475	511.31	1.17990	2.80	2.74	0.00503
57.368	518.67	1.18244	2.54	2.39	0.00432
60.398	525.49	1.18480	1.96	2.12	0.00379
63.531	531.75	1.18696	-	1.88	0.00332
206.120°K Isotherm: Gas side:					
32.768	70.80	1.02526	-	3.21	0.0450
36.499	83.71	1.02986	3.81	3.75	0.0444
40.519	100.52	1.03583	4.72	4.71	0.0464

TABLE VI (continued)

Pressure (atm)	Angle D (minute of arc)	Refractive Index	Derivative $(dD/dP)_T$ (min./atm)		Isothermal Compressibility (atm^{-1})
			Graphical	Numerical	
206.120°K Isotherm: Gas side (continued) :					
43.507	116.33	1.04145	6.14	5.98	0.0508
45.581	130.20	1.04637	7.46	7.56	0.0574
47.435	146.58	1.05218	10.7	10.5	0.0705
48.582	160.65	1.05716	14.4	14.7	0.0898
49.409	175.48	1.06241	22.7	22.5	0.1261
49.600	180.07	1.06404	25.8	25.7	0.1401
Liquid side:					
49.600	440.21	1.15525	12.3	12.4	0.02677
50.628	451.26	1.15909	9.50	9.34	0.01963
52.179	463.23	1.16324	6.72	6.58	0.01345
54.633	476.82	1.16795	4.87	4.71	0.00935
57.206	487.54	1.17167	3.64	3.72	0.00721
59.544	495.55	1.17444	3.21	3.16	0.00602
62.337	503.71	1.17727	2.77	2.72	0.00508
65.037	510.61	1.17965	2.47	2.40	0.00442
67.755	516.76	1.18178	-	2.13	0.00388
207.620°K Isotherm: Gas side:					
36.700	82.61	1.02947	-	3.60	0.0432
40.694	98.50	1.03512	4.70	4.42	0.0445
43.857	114.07	1.04065	5.39	5.52	0.0478
46.365	129.61	1.04616	7.29	7.02	0.0535
48.336	145.45	1.05178	9.21	9.38	0.0636
49.638	159.57	1.05678	13.0	12.6	0.0778
50.798	177.35	1.06307	18.6	19.3	0.1070
51.330	189.78	1.06747	30.4	29.5	0.1525
51.734	204.64	1.07272	43.1	44.5	0.2129
Liquid side:					
51.734	411.23	1.14517	31.2	27.2	0.06311
51.949	416.82	1.14711	23.1	24.0	0.05490
52.888	432.52	1.15257	13.0	12.7	0.02803
54.421	447.99	1.15795	8.31	8.24	0.01746
57.157	465.85	1.16415	5.27	5.29	0.01075
60.624	481.28	1.16950	3.96	3.83	0.00752
64.396	494.05	1.17392	2.95	3.01	0.00574

TABLE VI (continued)

Pressure (atm)	Angle D (minute of arc)	Refractive Index	Derivative $(dD/dP)_T$ (min./atm) Graphical	Derivative $(dD/dP)_T$ (min./atm) Numerical	Isothermal Compressibility (atm^{-1})
207.620°K Isotherm: Liquid side (continued):					
67.489	502.61	1.17689	-	2.55	0.00479
70.987	510.87	1.17974	-	2.19	0.00403
208.400°K Isotherm: Gas side:					
35.749	78.41	1.02797	-	3.39	0.0430
41.027	98.57	1.03514	4.45	4.34	0.0436
44.179	113.71	1.04052	5.21	5.35	0.0466
46.661	128.55	1.04579	7.00	6.73	0.0517
48.771	144.77	1.05154	9.10	8.87	0.0604
50.288	160.29	1.05704	12.0	12.0	0.0738
51.357	175.46	1.06241	17.1	17.0	0.0951
52.058	189.61	1.06741	25.4	24.7	0.1276
52.508	203.21	1.07221	39.3	37.7	0.1818
52.875	223.77	1.07947	77.	93.	0.4061
Liquid side:					
52.875	389.58	1.13762	49.9	54.7	0.13437
53.218	403.74	1.14256	32.1	31.6	0.07471
54.076	421.81	1.14885	15.4	15.5	0.03507
55.034	434.13	1.15313	11.1	10.8	0.02377
56.629	448.36	1.15808	7.37	7.46	0.01579
59.112	463.69	1.16340	5.22	5.21	0.01065
62.000	476.77	1.16794	3.97	3.98	0.00789
65.083	487.77	1.17175	3.29	3.22	0.00623
68.719	498.37	1.17542	-	2.65	0.00502
208.886°K Isotherm: Gas side:					
38.808	88.79	1.03166	-	3.78	0.0423
43.363	108.34	1.03861	5.40	4.91	0.0449
46.267	124.30	1.04428	5.80	6.19	0.0492
48.448	139.46	1.04966	8.40	7.90	0.0559
50.189	155.26	1.05526	10.2	10.5	0.0668
51.435	170.46	1.06064	15.4	14.4	0.0828
52.319	185.49	1.06595	19.6	20.5	0.1085
52.914	200.27	1.07117	33.6	30.9	0.1514
53.278	214.32	1.07614	52.0	49.8	0.2274

TABLE VI (continued)

Pressure (atm)	Angle D (minute of arc)	Refractive Index	Derivative $(dD/dP)_T$ (min./atm) Graphical	Numerical	Isothermal Compressibility (atm^{-1})
208.886°K Isotherm: Gas side (continued):					
53.529	232.08	1.08240	111.	112.	0.4731
53.601	242.82	1.08618	199.	202.	0.8110
Liquid side:					
53.601	368.42	1.13024	118.	134.	0.34905
53.650	373.58	1.13204	98.2	103.	0.26504
53.843	387.62	1.13694	53.7	52.4	0.12946
54.117	398.50	1.14073	31.8	31.5	0.07561
54.676	412.10	1.14547	19.6	19.5	0.04526
55.490	425.01	1.14996	13.2	13.0	0.02923
57.070	441.22	1.15560	8.32	8.35	0.01798
59.012	454.94	1.16036	6.22	6.07	0.01265
62.181	471.03	1.16595	4.57	4.31	0.00865
65.798	484.61	1.17065	-	3.31	0.00645
69.653	496.11	1.17464	-	2.71	0.00514
209.126°K Isotherm: Gas side:					
41.475	99.14	1.03534	-	4.31	0.043
45.387	118.31	1.04215	-	5.63	0.047
48.689	140.16	1.04991	7.6	7.91	0.056
50.303	154.58	1.05502	10.6	10.2	0.065
51.546	169.21	1.06019	13.2	13.7	0.080
52.498	184.62	1.06565	20.1	19.5	0.104
53.112	198.94	1.07071	27.4	28.4	0.140
53.590	216.31	1.07684	51.1	49.2	0.222
53.835	232.80	1.08265	100.	98.2	0.412
53.945	249.11	1.08840	247.	270.	1.057
53.972	259.46	1.09204	609.	558.	2.092
Liquid side:					
53.972	350.26	1.12389	546.	440.	1.2084
54.010	361.20	1.12771	181.	195.	0.5190
54.144	376.78	1.13316	85.2	77.7	0.1956
54.380	389.92	1.13774	40.4	41.9	0.1029
54.997	407.72	1.14394	21.5	21.2	0.0496
55.881	422.42	1.14906	13.3	13.5	0.0304
56.951	434.58	1.15329	9.70	9.68	0.0212
59.021	450.81	1.15893	6.56	6.51	0.0137

TABLE VI (continued)

Pressure (atm)	Angle D (minute of arc)	Refractive Index	Derivative $(dD/dP)_T$ (min./atm) Graphical	Derivative $(dD/dP)_T$ (min./atm) Numerical	Isothermal Compressibility (atm^{-1})
209.126°K Isotherm: Liquid side (continued):					
62.292	468.32	1.16501	4.42	4.48	0.0091
66.136	483.16	1.17015	-	3.36	0.0066
69.509	493.46	1.17372	-	2.79	0.0053
209.221°K Isotherm: Gas side:					
45.379	118.11	1.04208	-	5.55	0.046
47.960	134.31	1.04783	-	7.16	0.053
49.890	150.03	1.05340	9.1	9.36	0.061
51.298	165.14	1.05875	12.5	12.5	0.074
52.359	180.70	1.06426	16.8	17.5	0.095
53.087	195.91	1.06964	24.9	25.4	0.127
53.544	210.01	1.07461	37.6	38.7	0.180
53.833	224.27	1.07965	62.8	64.8	0.282
53.998	238.46	1.08465	121.	123.	0.504
54.026	242.28	1.08599	147.	151.	0.606
54.098	259.17	1.09194	407.	457.	1.715
54.114	271.90	1.09642	2015.	1630.	5.824
Liquid side:					
54.114	337.75	1.11951	1164.	1370.	3.9083
54.137	352.17	1.12456	333.	361.	0.9873
54.203	365.66	1.12927	129.	133.	0.3503
54.369	380.08	1.13431	63.0	61.5	0.1551
54.842	398.97	1.14090	27.6	28.2	0.0676
55.923	419.97	1.14821	14.0	14.2	0.0323
57.982	441.52	1.15570	7.90	8.05	0.0173
61.248	462.09	1.16285	5.15	5.07	0.0104
64.754	477.26	1.16811	-	3.74	0.0074
68.575	489.93	1.17250	-	2.96	0.0057
209.259°K Isotherm: Gas side:					
45.940	121.09	1.04314	-	5.84	0.048
48.280	136.40	1.04857	-	7.40	0.053
50.474	155.40	1.05531	10.4	10.3	0.065
52.003	174.29	1.06199	14.7	15.1	0.085
52.877	190.07	1.06757	21.9	21.8	0.112
53.482	206.21	1.07327	33.2	34.0	0.162

TABLE VI (continued)

Pressure (atm)	Angle D (minute of arc)	Refractive Index	Derivative $(dD/dP)_T$ (min./atm) Graphical	Derivative $(dD/dP)_T$ (min./atm) Numerical	Isothermal Compressibility (atm^{-1})
209.259°K Isotherm: Gas side (continued):					
53.811	220.33	1.07826	54.4	55.6	0.247
54.019	235.65	1.08366	92.4	103.	0.428
54.1308	252.91	1.08974	256.	259.	0.996
54.1600	263.83	1.09358	561.	640.	2.358
54.1736	281.99	1.09996	2348.	3260.	11.217
Liquid side:					
54.1736	327.96	1.11609	3510.	3750.	11.341
54.1768	336.33	1.11902	1489.	1512.	4.3321
54.1950	349.50	1.12362	394.	406.	1.1186
54.2563	362.92	1.12832	133.	144.	0.3812
54.508	383.17	1.13539	47.8	51.5	0.1287
54.850	396.41	1.14000	30.7	30.2	0.0728
55.562	412.47	1.14560	16.5	17.6	0.0406
57.118	432.59	1.15260	10.2	9.92	0.0218
60.046	454.53	1.16022	-	5.89	0.0123
62.571	467.49	1.16472	-	4.52	0.0092
209.274°K Isotherm: Gas side:					
47.642	131.76	1.04693	-	6.95	0.052
49.395	145.23	1.05170	-	8.57	0.058
50.769	158.43	1.05638	-	10.9	0.068
52.041	174.71	1.06214	15.5	15.3	0.086
52.862	189.44	1.06735	20.7	21.4	0.111
53.486	205.84	1.07314	33.3	33.7	0.160
53.823	220.13	1.07818	51.5	54.8	0.243
54.0425	236.18	1.08384	100.	104.	0.429
54.1507	252.84	1.08971	253.	255.	0.981
54.1887	269.53	1.09558	877.	998.	3.600
54.1985	290.04	1.10279	5650.	5375.	17.964
Liquid side:					
54.1985	319.87	1.11325	5283.	7400.	22.341
54.2208	348.07	1.12312	396.	431.	1.1928
54.2593	358.39	1.12673	186.	189.	0.5082
54.4102	375.26	1.13262	68.6	73.8	0.1887
54.722	391.03	1.13813	36.9	36.9	0.0904

TABLE VI (continued)

Pressure (atm)	Angle D (minute of arc)	Refractive Index	Derivative (dD/dP)$_T$ (min./atm) Graphical	Numerical	Isothermal Compressibility (atm^{-1})
209.274°K Isotherm:					
Liquid side (continued):					
55.374	408.32	1.14415	18.8	20.1	0.0469
56.574	426.36	1.15043	12.6	11.7	0.0260
58.743	445.81	1.15719	-	7.17	0.0153
62.095	465.11	1.16389	-	4.72	0.0096
66.075	481.04	1.16942	-	3.44	0.0068

TABLE VII

RECTILINEAR DIAMETER ANALYSIS

$$LL_L + LL_G = 2LL_C + 2B_2|t|$$

Temperature (°K)	LL_L	LL_G	(LL_L+LL_G) Value	Error $\times 10^5$	Residual $\times 10^5$
195.002	0.12357	0.02386	0.14743	3.6	- 1.5
197.400	0.11985	0.02655	0.14640	3.6	1.0
199.302	0.11666	0.02889	0.14556	3.6	0.3
199.800	0.11571	0.02958	0.14530	3.6	- 4.2
201.300	0.11287	0.03186	0.14472	3.6	4.4
203.099	0.10888	0.03501	0.14389	3.6	- 0.1
203.300	0.10844	0.03541	0.14385	3.6	5.0
204.001	0.10668	0.03681	0.14349	3.6	- 0.6
205.299	0.10300	0.03990	0.14290	3.6	- 2.9
206.120	0.10034	0.04220	0.14254	3.6	- 2.4
206.201	0.10003	0.04246	0.14248	3.6	- 4.7
206.800	0.09776	0.04453	0.14229	3.6	2.4
207.401	0.09525	0.04684	0.14209	3.6	8.6
207.620	0.09404	0.04784	0.14188	3.6	- 2.7
207.800	0.09308	0.04877	0.14185	3.6	2.1
208.154	0.09098	0.05069	0.14167	3.7	0.3
208.400	0.08930	0.05221	0.14151	6.4	- 5.1
208.502	0.08851	0.05305	0.14156	6.4	4.2
208.799	0.08573	0.05572	0.14145	6.4	5.9

TABLE VII (continued)

Temperature (°K)	LL_L	LL_G	(LL_L+LL_G) Value	Error $\times 10^5$	Residual $\times 10^5$
208.886	0.08465	0.05654	0.14119	6.4	-15.8
209.003	0.08297	0.05830	0.14127	6.5	- 2.6
209.050	0.08219	0.05915	0.14134	6.5	6.4
209.103	0.08119	0.06006	0.14125	6.6	- 0.5
209.126	0.08064	0.06031	0.14095	6.7	-29.5
209.146	0.08034	0.06101	0.14135	6.8	11.3
209.200	0.07869	0.06251	0.14121	7.1	- 0.6
209.207	0.07852	0.06287	0.14139	7.2	18.2
209.221	0.07786	0.06312	0.14099	7.4	-21.8
209.224	0.07782	0.06341	0.14123	7.5	2.9
209.231	0.07750	0.06382	0.14132	7.7	11.6
209.249	0.07655	0.06474	0.14129	8.4	9.8
209.256	0.07604	0.06521	0.14125	8.9	5.8
209.259	0.07569	0.06540	0.14108	9.2	-10.6
209.271	0.07477	0.06627	0.14104	19.0	-14.5
209.274	0.07388	0.06721	0.14109	18.9	- 9.2

For T_c=209.286°K $2LL_C = 0.141175 \pm 0.000012$

Slope $a = 0.0918 \pm 0.0004$

$a^* = a/2LL_C = 0.65$

Standard deviation of the fit=6.75×10^{-5}

TABLE VIII

DEPENDENCE OF LL_C ON T_C

T_C (°K)	$2LL_C$* ± Error	$2LL_C$** ± Error
209.280	0.141178 ± 0.000017	0.141178 ± 0.000012
209.281	0.141178 ± 0.000017	0.141177 ± 0.000012
209.282	0.141177 ± 0.000017	0.141177 ± 0.000012
209.283	0.141177 ± 0.000017	0.141176 ± 0.000012
209.284	0.141176 ± 0.000017	0.141176 ± 0.000012
209.285	0.141176 ± 0.000017	0.141175 ± 0.000012
209.286	0.141175 ± 0.000017	0.141175 ± 0.000012
209.287	0.141175 ± 0.000017	0.141174 ± 0.000012
209.288	0.141175 ± 0.000017	0.141174 ± 0.000012
	s. d. of fit = 7.15×10^{-5}	s. d. of fit = 6.75×10^{-5}

---

* From the least-squares fitting routine of Ref. 48

** From the least-squares fitting routine of Ref. 47

TABLE IX

SHAPE OF THE COEXISTENCE CURVE

$$\ln \left[(LL_L - LL_G)/LL_C \right] = \ln 2B_1 + \beta_1 \ln|t|$$

	$(LL_L-LL_G)/LL_C$		
Temperature (°K)	Value	Error×10^4	Residual×10^4
195.002	1.4125	5.1	8.9
197.400	1.3218	5.1	- 2.1
199.302	1.2434	5.1	12.1
199.800	1.2202	5.1	4.4
201.300	1.1476	5.1	5.9
203.099	1.0465	5.1	- 6.3
203.300	1.0347	5.1	- 1.7
204.001	0.9898	5.1	- 0.5
205.299	0.8939	5.1	-11.9
206.120	0.8237	5.2	- 6.9
206.201	0.8156	5.2	-12.3
206.800	0.7542	5.2	-19.9
207.401	0.6859	5.2	8.6
207.620	0.6545	5.2	- 9.8
207.800	0.6277	5.2	-16.0
208.154	0.5708	5.3	- 2.5
208.400	0.5255	9.1	23.0
208.502	0.5024	9.1	15.2
208.799	0.4252	9.2	26.0
208.886	0.3982	9.3	43.0

TABLE IX (continued)

	$(LL_L-LL_G)/LL_C$		
Temperature (°K)	Value	Error×10^4	Residual×10^4
209.003	0.3495	9.5	14.0
209.050	0.3264	9.6	1.7
209.103	0.2994	9.8	14.7
209.126	0.2879	10.0	39.3
209.146	0.2738	10.2	30.1
209.200	0.2293	11.1	17.3
209.207	0.2217	11.3	9.9
209.221	0.2088	12.0	29.1
209.224	0.2041	12.1	16.7
209.231	0.1938	12.5	- 2.3
209.249	0.1673	14.3	-10.4
209.256	0.1534	15.5	-28.4
209.259	0.1458	16.1	-47.0
209.271	0.1204	30.4	-15.8
209.274	0.0946	30.2	-180.5

For T_C=209.286°K ; LL_C=0.070588

$\ln 2B_1 = 1.3031 \pm 0.0006$

$B_1 = 1.840$

$\beta_1 = 0.3571 \pm 0.0008$

Standard deviation of the fit = 1.76×10^{-3}

TABLE X

RESULTS OF VARYING RANGE OF $|t|_{max}$ FOR THE FIT TO THE RECTILINEAR DIAMETER

$\|t\|_{max}$ (%)	s.d.×10^5	$2LL_C$	Slope
6.82	7.15	0.141175 ±17	0.0918 ±6
5.68	7.32	0.141174 ±18	0.0919 ±7
4.77	7.51	0.141174 ±19	0.0919 ±9
4.53	7.72	0.141174 ±20	0.0919 ±10
3.82	7.83	0.141169 ±21	0.0926 ±12
2.96	8.04	0.141172 ±22	0.0922 ±15
2.86	8.30	0.141171 ±23	0.0923 ±18
2.53	8.47	0.141177 ±24	0.0913 ±21
1.91	8.79	0.141178 ±26	0.0910 ±28
1.51	9.12	0.141176 ±27	0.0916 ±34
1.47	9.49	0.141173 ±29	0.0924 ±40
1.19	9.69	0.141164 ±30	0.0956 ±50
0.901	10.2	0.141162 ±32	0.0964 ±64
0.796	10.5	0.141169 ±32	0.0917 ±75
0.710	11.1	0.141166 ±34	0.0943 ±96
0.541	11.9	0.141169 ±36	0.0916 ±140
0.423	12.9	0.141173 ±40	0.0864 ±245

TABLE XI

RESULTS OF VARYING RANGE OF $|t|_{max}$ FOR THE FIT TO THE COEXISTENCE CURVE

$\lvert t\rvert_{max}$ (%)	s.d.$\times 10^3$	$\ln 2B_1$	β_1
6.82	1.63	1.3033 ±12	0.3571 ±3
5.68	1.73	1.3027 ±14	0.3569 ±4
4.77	1.85	1.3027 ±16	0.3569 ±4
4.53	1.91	1.3016 ±18	0.3567 ±4
3.82	2.02	1.3004 ±20	0.3564 ±5
2.96	2.08	1.2986 ±22	0.3560 ±5
2.86	2.23	1.2979 ±25	0.3559 ±6
2.53	2.36	1.2960 ±28	0.3555 ±6
1.91	2.40	1.2925 ±31	0.3548 ±7
1.51	2.61	1.2912 ±36	0.3546 ±7
1.47	2.83	1.2896 ±40	0.3543 ±8
1.19	3.15	1.2880 ±47	0.3540 ±9
0.901	3.55	1.2898 ±55	0.3543 ±11
0.796	3.80	1.2855 ±59	0.3536 ±11
0.710	4.47	1.2859 ±69	0.3537 ±12
0.541	5.21	1.2935 ±84	0.3548 ±14
0.423	6.11	1.3091 ±108	0.3571 ±17

TABLE XII

ASYMPTOTIC RANGE OF (LL_C-LL_G)

$\lvert t\rvert_{max}$ (%)	s.d.×10^3	ln B_1^-	s.d.	β_1^-	s.d.
6.82	4.43	0.5183	± 0.0038	0.3418	± 0.0008
5.68	4.10	0.5207	± 0.0036	0.3423	± 0.0008
4.77	3.80	0.5232	± 0.0035	0.3428	± 0.0008
4.53	3.66	0.5252	± 0.0036	0.3432	± 0.0008
3.82	3.50	0.5274	± 0.0036	0.3436	± 0.0008
2.96	3.38	0.5298	± 0.0037	0.3441	± 0.0008
2.86	3.37	0.5316	± 0.0040	0.3444	± 0.0008
2.52	3.32	0.5341	± 0.0042	0.3449	± 0.0009
1.91	3.37	0.5360	± 0.0046	0.3453	± 0.0010
1.51	3.49	0.5374	± 0.0051	0.3455	± 0.0010
1.47	3.71	0.5374	± 0.0058	0.3455	± 0.0011
1.19	3.96	0.5376	± 0.0067	0.3456	± 0.0013
0.901	4.19	0.5419	± 0.0076	0.3464	± 0.0015
0.796	4.66	0.5416	± 0.0087	0.3463	± 0.0016
0.710	5.34	0.5422	± 0.0103	0.3464	± 0.0019
0.541	5.93	0.5555	± 0.0123	0.3485	± 0.0021
0.423	6.78	0.5750	± 0.0152	0.3515	± 0.0025
0.375	7.98	0.5728	± 0.0188	0.3512	± 0.0030
0.233	9.14	0.6094	± 0.0272	0.3567	± 0.0042
0.191	9.88	0.6508	± 0.0320	0.3623	± 0.0047
0.135	11.52	0.6076	± 0.0439	0.3564	± 0.0062

TABLE XIII

ASYMPTOTIC RANGE OF $(LL_L - LL_C)$

$\|t\|_{max}$ (%)	s.d.×10^3	ln B_1^+	s.d.	β_1^+	s.d.
6.82	5.85	0.6850 ±	0.0053	0.3687 ±	0.0012
5.68	5.58	0.6828 ±	0.0053	0.3683 ±	0.0012
4.77	5.32	0.6802 ±	0.0052	0.3678 ±	0.0011
4.53	5.01	0.6771 ±	0.0052	0.3671 ±	0.0011
3.82	4.69	0.6736 ±	0.0051	0.3664 ±	0.0011
2.96	4.28	0.6694 ±	0.0049	0.3656 ±	0.0010
2.86	4.10	0.6660 ±	0.0050	0.3649 ±	0.0011
2.52	3.65	0.6607 ±	0.0047	0.3639 ±	0.0010
1.91	3.11	0.6545 ±	0.0044	0.3627 ±	0.0009
1.51	2.97	0.6505 ±	0.0045	0.3620 ±	0.0009
1.47	2.94	0.6470 ±	0.0047	0.3613 ±	0.0009
1.19	2.98	0.6431 ±	0.0051	0.3606 ±	0.0010
0.901	3.19	0.6406 ±	0.0059	0.3612 ±	0.0011
0.796	2.32	0.6303 ±	0.0044	0.3584 ±	0.0008
0.710	2.67	0.6295 ±	0.0052	0.3583 ±	0.0009
0.541	3.16	0.6324 ±	0.0067	0.3588 ±	0.0012
0.423	3.65	0.6424 ±	0.0082	0.3603 ±	0.0014
0.375	4.25	0.6465 ±	0.0101	0.3609 ±	0.0016
0.233	5.26	0.6556 ±	0.0157	0.3623 ±	0.0024
0.191	6.20	0.6425 ±	0.0201	0.3604 ±	0.0030
0.135	7.80	0.6370 ±	0.0297	0.3597 ±	0.0042

TABLE XIV

WEIGHTED LEAST SQUARES FITTING OF ISOTHERMAL COMPRESSIBILITIES ON THE CRITICAL ISOCHORE

Temperature (°K)	K_T (atm^{-1})	Fractional Error in K_T	$\ln[(T-T_c)/T_c]$	$\ln K_T$ Value	Error $\times 10^3$	Residual $\times 10^3$
219.301	0.05637	0.01	-3.0396	-2.875	10.0	3.8
217.301	0.07274	0.01	-3.2624	-2.621	10.0	- 4.6
215.301	0.1027	0.01	-3.5494	-2.276	10.0	0.9
213.300	0.1647	0.02	-3.9539	-1.804	20.0	- 4.8
212.200	0.2371	0.02	-4.2742	-1.439	20.0	- 19.1
211.300	0.3701	0.02	-4.6436	-0.9940	20.0	- 10.4
210.310	0.8555	0.02	-5.3200	-0.1561	20.0	27.9
210.200	0.9232	0.03	-5.4336	-0.0799	30.0	- 30.2
209.800	1.726	0.03	-6.0092	0.5458	30.1	- 85.0
209.570	4.131	0.03	-6.6025	1.418	30.3	86.4
209.450	8.729	0.03	-7.1516	2.167	30.9	185.
209.380	13.34	0.05	-7.7082	2.591	51.6	- 48.4
209.338	21.22	0.05	-8.3002	3.055	55.1	-284.
209.315	67.93	0.05	-8.8842	4.218	64.9	189.

TABLE XIV (continued)

Temperature (°K)	K_T (atm^{-1})	Fractional Error in K_T	$\ln[(T-T_c)/T_c]$	$\ln K_T$ Value	Error $\times 10^3$	Residual $\times 10^3$
209.302	53.83	0.05	-9.4789	3.986	90.1	-746.
209.294	387.1	0.10	-10.172	5.959	180.	407

For T_c=209.286°K

$\gamma = 1.182 \pm 0.008$

$\Gamma = 0.00154 \pm 0.00002\ \text{atm}^{-1}$

Minimum $\sigma_{fit} = 0.00647$

TABLE XV

RESULTS OF VARYING THE RANGE OF $(T-T_c)$ IN THE FIT TO

$$\ln K_T = \ln \Gamma - \gamma \ln t$$

$(T-T_c)_{max}$ (°K)	γ	$\Gamma(\text{atm}^{-1})$	σ_{fit}
10.015	1.182 ± 0.004	0.00154	0.0647
8.015	1.183 ± 0.004	0.00154	0.0736
6.015	1.182 ± 0.005	0.00155	0.0873
4.014	1.182 ± 0.006	0.00154	0.113
2.914	1.182 ± 0.007	0.00155	0.124
2.014	1.176 ± 0.008	0.00161	0.139
1.024	1.166 ± 0.010	0.00173	0.159

TABLE XVI

LOCUS OF MAXIMUM ISOTHERMAL COMPRESSIBILITY

Temperature (°K)	Pressure (atm)	Angle D (min. of arc)	Refractive Index	LL	Max. K_T (atm^{-1})
219.301	67.315	260.28	1.09233	0.06050	0.06496
217.301	65.411	275.71	1.09775	0.06398	0.08203
215.301	62.564	273.46	1.09696	0.06347	0.1115
213.300	60.118	289.39	1.10256	0.06706	0.1751
212.200	58.470	287.08	1.10175	0.06654	0.2562
211.300	57.229	295.48	1.10470	0.06843	0.3816
210.310	55.781	302.99	1.10733	0.07011	0.8570
210.200	55.599	299.88	1.10624	0.06941	0.9377
209.800	54.988	296.45	1.10504	0.06864	1.786
209.570	54.653	305.18	1.10810	0.07060	4.131
209.450	54.468	304.82	1.10798	0.07052	8.732
209.380	54.3596	300.20	1.10635	0.06948	15.37
209.338	54.2940	310.08	1.10982	0.07170	24.06
209.315	54.2568	303.89	1.10765	0.07031	72.18
209.302	54.2424	311.10	1.11018	0.07192	79.63
209.294	54.2285	302.62	1.10720	0.07003	565.8

TABLE XVII

RESULTS OF WEIGHTED LEAST SQUARES FITTING OF COMPRESSIBILITIES ALONG THE PHASE BOUNDARY

$$\ln\,[(LL/LL_C)^2K_T] = \Gamma' - \gamma'\ln|t|$$

	Temperature		$(LL/LL_C)^2K_T$		$\ln[(LL/LL_C)^2K_T]$	
	(°K)	$K_T\,(atm^{-1})$	(atm^{-1})	$\ln\|t\|$	Experimental	Calculated
Gas side:	199.302	0.0742	0.0124	-3.043	-4.39	-4.34
	201.300	0.0859	0.0175	-3.266	-4.05	-4.08
	203.300	0.0929	0.0234	-3.554	-3.76	-3.75
	206.120	0.140	0.0501	-4.191	-2.99	-3.02
	207.620	0.213	0.0978	-4.833	-2.32	-2.28
	208.400	0.406	0.222	-5.465	-1.50	-1.55
	208.886	0.811	0.520	-6.260	-0.653	-0.636
	209.126	2.09	1.53	-7.176	0.424	0.419
	209.221	5.82	4.66	-8.077	1.54	1.46
	209.259	11.2	9.63	-8.956	2.26	2.47
	209.274	18.0	16.3	-9.767	2.79	3.40

For T_c=209.286°K

γ'_G=1.15±0.01 Γ'_G=0.00039±0.00002 (1/atm) with σ_{fit}=0.074

TABLE XVII (continued)

	Temperature (°K)	K_T (atm^{-1})	$(LL/LL_C)^2K_T$ (atm^{-1})	ln|t|	$\ln[(LL/LL_C)^2K_T$	
					Experimental	Calculated
Liquid side:	199.302	0.00543	0.0148	-3.043	-4.21	-4.21
	201.300	0.00747	0.0191	-3.266	-3.96	-3.96
	203.300	0.0111	0.0263	-3.554	-3.64	-3.64
	206.120	0.0268	0.0541	-4.191	-2.92	-2.92
	207.620	0.0631	0.112	-4.833	-2.19	-2.20
	208.400	0.134	0.215	-5.465	-1.54	-1.49
	208.886	0.349	0.502	-6.260	-0.689	-0.597
	209.126	1.21	1.58	-7.176	0.455	0.433
	209.221	3.91	4.75	-8.077	1.56	1.45
	209.259	11.0	12.7	-8.956	2.54	2.43
	209.274	22.3	24.5	-9.766	3.20	3.34

For T_C=209.286°K

$\gamma'_L=1.12\pm0.01$ $\Gamma'_L=0.00048\pm0.00001$ (1/atm) with $\sigma_{fit}=0.019$

TABLE XVIII

RESULTS OF THE FIT TO $\ln[(LL/\overline{LL})^2 K_T] = \ln\Gamma' - \gamma'\ln|t|$

	$\ln\|t\|$	$\ln[(LL/\overline{LL})^2 K_T]$ Experimental	$\ln[(LL/\overline{LL})^2 K_T]$ Calculated
Gas side:	-3.043	-4.45	-4.39
	-3.266	-4.09	-4.13
	-3.554	-3.79	-3.79
	-4.191	-3.01	-3.05
	-4.833	-2.33	-2.30
	-5.465	-1.51	-1.57
	-6.260	-0.653	-0.646
	-7.176	0.424	0.419
	-8.077	1.54	1.47
	-8.956	2.26	2.49
	-9.767	2.79	3.43
Liquid side:	-3.043	-4.27	-4.26
	-3.266	-4.01	-4.01
	-3.554	-3.68	-3.68
	-4.191	-2.94	-2.96
	-4.833	-2.20	-2.22
	-5.465	-1.54	-1.50
	-6.260	-0.689	-0.599
	-7.176	0.455	0.446
	-8.077	1.56	1.47
	-8.956	2.54	2.47
	-9.767	3.20	3.40

For T_c=209.286°K

$\gamma'_G=1.16\pm0.01$ $\Gamma'_G=0.00036\pm0.00002$ atm^{-1} with $\sigma_{fit}=0.074$

$\gamma'_L=1.14\pm0.01$ $\Gamma'_L=0.00044\pm0.00001$ atm^{-1} with $\sigma_{fit}=0.020$

TABLE XIX

$|LL-LL_c|$ AND $|P-P_c|$ DATA
USED IN DETERMINATION OF δ

	$\|LL-LL_c\|$	$\|P-P_c\|$ (atm)
$T-T_c = -0.065°K$		
$P_{coex} = 54.114$ atm.		
$LL<LL_c$	0.042740	8.735
	0.038970	6.154
	0.035324	4.224
	0.031830	2.816
	0.028244	1.755
	0.024750	1.027
	0.021521	0.570
	0.018265	0.281
	0.015036	0.116
	0.014168	0.088
	0.010340	0.016
$LL>LL_c$	0.010472	0.023
	0.013453	0.089
	0.016629	0.255
	0.020773	0.728
	0.025358	1.809
	0.030037	3.868
	0.034480	7.134
	0.037742	10.640
	0.040457	14.461
$T-T_c = -0.027°K$		
$P_{coex} = 54.1736$ atm.		
$LL<LL_c$	0.042046	8.2336
	0.038485	5.8936
	0.034081	3.6996
	0.029720	2.1706
	0.026090	1.2966
	0.022390	0.6916
	0.019164	0.3626
	0.015674	0.1546
	0.011757	0.0428
	0.009287	0.0136
$LL>LL_c$	0.006959	0.0032
	0.009617	0.0180
	0.010146	0.0244
	0.012849	0.0824

TABLE XIX (continued)

	$\lvert LL-LL_c \rvert$	$\lvert P-P_c \rvert$ (atm)
	0.017309	0.3344
	0.020213	0.6764
	0.023723	1.3884
	0.028101	2.9444
	0.032850	5.8724
	0.035643	8.3974
$T-T_c = -0.012$°K		
$P_{coex} = 54.1985$ atm.		
$LL<LL_c$	0.039563	6.5565
	0.036436	4.8035
	0.033380	3.4295
	0.029623	2.1575
	0.026235	1.3365
	0.022475	0.7125
	0.019209	0.3755
	0.015554	0.1560
	0.011773	0.0478
	0.008000	0.0098
$LL>LL_c$	0.009564	0.0223
	0.011848	0.0608
	0.015569	0.2117
	0.019034	0.5235
	0.022817	1.1755
	0.026748	2.3755
	0.030966	4.5445
	0.035131	7.8965
	0.038553	11.8765
$T-T_c = 0.008$°K		
$P(LL_c) = 54.2285$ atm.		
$LL<LL_c$	0.020305	0.4839
	0.018229	0.3106
	0.015722	0.1698
	0.014098	0.1078
	0.011846	0.0539
	0.009323	0.0206
	0.005971	0.0028
	0.004052	0.0006
$LL>LL_c$	0.003245	0.0008
	0.004910	0.0023
	0.005044	0.0023
	0.007732	0.0103
	0.010328	0.0344
	0.013038	0.0968

TABLE XIX (continued)

	$\lvert LL-LL_c \rvert$	$\lvert P-P_c \rvert$ (atm)
	0.015036	0.1844
	0.017251	0.3396
$T-T_c = 0.016°K$		
$P(LL_c) = 54.2424$ atm.		
$LL<LL_c$	0.021148	0.5730
	0.019043	0.3750
	0.015806	0.1791
	0.013004	0.0827
	0.012072	0.0609
	0.008955	0.0207
	0.007019	0.0094
	0.006591	0.0079
	0.004346	0.0032
	0.004020	0.0027
	0.002128	0.0010
	0.000550	0.0002
$LL>LL_c$	0.004803	0.0015
	0.012078	0.0717
	0.012497	0.0826
	0.015338	0.2042
	0.016128	0.2534
	0.017295	0.3481
	0.018540	0.4704
$T-T_c = 0.029°K$		
$P(LL_c) = 54.2568$ atm.		
$LL<LL_c$	0.020275	0.4853
	0.018347	0.3252
	0.015647	0.1714
	0.014111	0.1136
	0.012274	0.0656
	0.009877	0.0280
	0.008101	0.0126
	0.005771	0.0040
	0.004472	0.0022
	0.001343	0.0003
$LL>LL_c$	0.001667	0.0005
	0.003317	0.0013
	0.005985	0.0054
	0.007639	0.0120
	0.011114	0.0529
	0.014009	0.1413
	0.015769	0.2374

TABLE XIX (continued)

	$\lvert LL-LL_c \rvert$	$\lvert P-P_c \rvert$ (atm)
	0.017845	0.4060
$T-T_c= 0.052$°K		
$P(LL_c)= 54.2940$ atm.		
$LL<LL_c$	0.020481	0.5219
	0.018081	0.3179
	0.016332	0.2150
	0.013464	0.1011
	0.011402	0.0559
	0.008377	0.0190
	0.006568	0.0095
	0.003218	0.0033
	0.002146	0.0013
	0.000505	0.0005
$LL>LL_c$	0.002560	0.0017
	0.003533	0.0021
	0.006434	0.0080
	0.009661	0.0329
	0.012086	0.0801
	0.014155	0.1546
	0.015840	0.2503
	0.018216	0.4525

TABLE XX

VALUES OF δ ON ISOTHERMS CLOSE TO T_c

$T-T_c$ (°K)	$\delta(LL<LL_c)$	$\delta(LL>LL_c)$
0.052	3.86 ± 0.04	4.19 ± 0.03
0.029	3.99 ± 0.01	4.32 ± 0.02
0.016	3.99 ± 0.01	4.40 ± 0.01
0.008	4.08 ± 0.01	4.45 ± 0.02
-0.012	3.99 ± 0.03	4.44 ± 0.01
-0.027	3.97 ± 0.03	4.48 ± 0.02
-0.065	3.99 ± 0.04	4.50 ± 0.02

Best value of $\delta = 4.25 \pm 0.25$

TABLE XXI

PRESSURES TEMPERATURES AND (ΔP/ΔT) ON THE CRITICAL ISOCHORE

Temperature (°K)	Pressure (atm)	ΔP/ΔT (atm/°K)
219.301	69.788	
		1.5605
217.301	66.667	
		1.5645
215.301	63.538	
		1.5597
213.300	60.417	
		1.5536
212.200	58.708	
		1.5511
211.300	57.312	
		1.5384
210.310	55.789	
		1.5636
210.200	55.617	
		1.5325
209.800	55.004	
		1.5261
209.570	54.653	
		1.5417
209.450	54.468	
		1.5486
209.380	54.3596	
		1.5619
209.338	54.2940	
		1.6174
209.315	54.2568	
		1.1077
209.302	54.2424	
		1.7375
209.294	54.2285	

TABLE XXII
ANTISYMMETRIC RANGE ABOVE T_c
THE Δμ, ΔLL DATA

FOR LL_c=0.070588 P_c=54.213 atm

Pressure (atm)	LL	ΔLL	$\Delta\mu\times10^3$
T=219.301°K			
64.599	0.051185	-0.27488	-113.02
66.221	0.056393	-0.20110	- 73.64
67.931	0.062956	-0.10812	- 36.26
68.799	0.066498	-0.05794	- 18.79
69.165	0.068023	-0.03634	- 11.70
69.634	0.069969	-0.00877	- 2.85
70.288	0.072512	0.02726	9.10
70.694	0.073994	0.04825	16.31
71.386	0.076451	0.08306	28.29
72.199	0.079139	0.12114	41.90
73.613	0.083039	0.17639	64.59
74.012	0.084024	0.19034	70.81
75.453	0.087176	0.23499	92.71
75.745	0.087747	0.24309	97.06
T=217.301°K			
62.361	0.050726	-0.28138	- 94.46
63.592	0.055368	-0.28138	- 64.18
63.931	0.056815	-0.19512	- 56.31
64.452	0.059197	-0.16137	- 44.61
65.009	0.061913	-0.12289	- 32.63
65.422	0.064040	-0.09276	- 24.09
65.778	0.065927	-0.06603	- 16.96
66.335	0.068866	-0.02439	- 6.20
66.769	0.071110	0.00740	1.88
67.207	0.073298	0.03839	9.78
67.365	0.074065	0.04926	12.57
67.896	0.076502	0.08378	21.75
68.357	0.078422	0.11098	29.50
68.478	0.078917	0.11799	31.50
69.372	0.082128	0.16349	45.95
70.624	0.085831	0.21595	65.35
72.428	0.089944	0.27421	92.05
T=215.301°K			
60.862	0.053391	-0.24362	- 57.20
61.311	0.055652	-0.21159	- 46.47
61.759	0.058158	-0.17610	- 36.21

TABLE XXII (continued)

Pressure (atm)	LL	ΔLL	$\Delta\mu\times10^3$
62.196	0.060935	-0.13675	- 26.65
62.691	0.064378	-0.08797	- 16.36
63.099	0.067347	-0.04591	- 8.29
63.514	0.070412	-0.00249	- 0.447
63.690	0.071681	0.01548	2.78
63.898	0.073144	0.03621	6.52
64.067	0.074264	0.05207	9.50
64.369	0.076159	0.07893	14.73
64.769	0.078455	0.11145	21.45
65.219	0.080779	0.14437	28.82
65.714	0.082933	0.17489	36.69
66.257	0.084996	0.20412	45.11
66.816	0.086879	0.23079	53.58

T=213.300°K

Pressure (atm)	LL	ΔLL	$\Delta\mu\times10^3$
58.371	0.052033	-0.26286	- 44.70
58.721	0.054147	-0.23291	- 36.11
59.103	0.056922	-0.19361	- 27.15
59.432	0.059704	-0.15418	- 19.80
59.616	0.061522	-0.12843	- 15.84
60.056	0.066336	-0.06024	- 6.87
60.304	0.069261	-0.01880	- 2.11
60.478	0.071291	0.00997	1.12
60.681	0.073555	0.04203	4.77
60.949	0.076293	0.08082	9.42
61.277	0.079154	0.12136	14.92
61.624	0.081640	0.15657	20.53
61.990	0.083816	0.18740	26.29
62.482	0.086221	0.22147	33.82
62.985	0.088257	0.25031	41.33

T=212.200°K

Pressure (atm)	LL	ΔLL	$\Delta\mu\times10^3$
56.657	0.049124	-0.30407	- 46.94
57.202	0.052391	-0.25779	- 32.93
57.542	0.055023	-0.22051	- 24.68
57.786	0.057269	-0.18869	- 19.01
57.977	0.059455	-0.15771	- 14.75
58.146	0.061599	-0.12734	- 11.11
58.262	0.063211	-0.10451	- 8.69
58.455	0.066293	-0.06084	- 4.81
58.574	0.068330	-0.03199	- 2.51
58.695	0.070374	-0.00303	- 0.236
58.841	0.072773	0.03096	2.42
58.985	0.074977	0.06218	4.96

TABLE XXII (continued)

Pressure (atm)	LL	ΔLL	$\Delta\mu\times10^3$
59.138	0.077100	0.09226	7.58
59.347	0.079496	0.12619	11.05
59.565	0.081602	0.15603	14.57
59.856	0.083865	0.18809	19.15
60.243	0.086256	0.22197	25.07
60.654	0.088299	0.25090	31.20
T=211.300°K			
56.157	0.052127	-0.26154	- 25.54
56.456	0.054836	-0.22315	- 18.25
56.637	0.056919	-0.19364	- 14.03
56.822	0.059609	-0.15553	- 9.89
56.913	0.061145	-0.13378	- 7.93
57.026	0.063450	-0.10113	- 5.57
57.136	0.066050	-0.06428	- 3.35
57.202	0.067715	-0.04070	- 2.07
57.274	0.069597	-0.01404	- 0.703
57.390	0.072599	0.02849	1.42
57.558	0.076384	0.08211	4.35
57.687	0.078648	0.11419	6.52
57.873	0.081345	0.15240	9.55
58.043	0.083187	0.17849	12.24
58.244	0.084934	0.20324	15.35
58.454	0.086478	0.22511	18.54
58.795	0.088496	0.25370	23.61
T=210.310°K			
54.820	0.050054	-0.29089	- 22.48
55.090	0.052494	-0.25634	- 15.61
55.274	0.054777	-0.22399	- 11.14
55.420	0.057019	-0.19223	- 7.14
55.537	0.059652	-0.15492	- 5.12
55.589	0.061163	-0.13352	- 3.99
55.645	0.063134	-0.10560	- 2.82
55.714	0.066300	-0.06075	- 1.43
55.780	0.070038	-0.00779	- 0.169
55.824	0.072684	0.02969	0.633
55.901	0.076531	0.08419	1.97
55.986	0.079261	0.12286	3.39
56.111	0.082020	0.16196	5.41
56.254	0.084216	0.19306	7.65
56.423	0.086100	0.21975	10.23
56.710	0.088426	0.25271	14.51

TABLE XXII (continued)

Pressure (atm)	LL	ΔLL	$\Delta\mu\times10^3$
T=210.200°K			
54.866	0.051511	-0.27026	-17.06
55.055	0.053580	-0.24094	-12.37
55.326	0.058056	-0.17754	- 6.02
55.392	0.059756	-0.15345	- 4.56
55.453	0.061784	-0.12472	- 3.26
55.539	0.065742	-0.06865	- 1.50
55.602	0.069592	-0.01410	- 0.283
55.647	0.072476	0.02675	0.542
55.708	0.075750	0.07313	1.61
55.810	0.079560	0.12711	3.32
55.894	0.081711	0.15757	4.67
56.040	0.084130	0.19184	6.97
56.300	0.086965	0.23200	10.92
56.552	0.088896	0.25936	14.65
T=209.800°K			
54.471	0.052070	-0.26234	-12.15
54.653	0.054525	-0.22756	- 7.69
54.724	0.055873	-0.20847	- 6.02
54.793	0.057466	-0.18589	- 4.43
54.846	0.059032	-0.16371	- 3.25
54.908	0.061538	-0.12821	- 1.91
54.941	0.063671	-0.09800	- 1.22
54.970	0.066522	-0.05759	- 0.638
55.015	0.071947	0.01925	0.209
55.033	0.073934	0.04740	0.530
55.056	0.076053	0.07742	0.929
55.084	0.077940	0.10416	1.40
55.144	0.080573	0.14145	2.39
55.210	0.082405	0.16741	3.45
55.336	0.084811	0.20149	5.40
55.520	0.087086	0.23372	8.19
55.709	0.088736	0.25709	10.98
T=209.570°K			
54.008	0.049910	-0.29293	-15.37
54.268	0.052778	-0.25230	- 8.76
54.403	0.055011	-0.22067	- 5.50
54.478	0.056724	-0.19641	- 3.75
54.541	0.058975	-0.16451	- 2.33
54.582	0.061034	-0.13534	- 1.44

TABLE XXII (continued)

Pressure (atm)	LL	ΔLL	$\Delta\mu\times 10^3$
54.625	0.064808	-0.08188	- 0.546
54.652	0.070242	-0.00490	- 0.022
54.663	0.073202	0.03703	0.178
54.673	0.075088	0.06376	0.353
54.716	0.079261	0.12286	1.07
54.764	0.081467	0.15412	1.85
54.836	0.083540	0.18349	2.99
54.982	0.086100	0.21975	5.23
55.177	0.088224	0.24984	8.14
T=209.450°K			
53.893	0.050093	-0.29034	-13.75
54.112	0.052569	-0.25527	- 8.19
54.255	0.055000	-0.22083	- 4.72
54.332	0.056990	-0.19264	- 2.93
54.400	0.059815	-0.15261	- 1.41
54.426	0.061658	-0.12651	- 0.849
54.449	0.064362	-0.08820	- 0.379
54.461	0.067174	-0.04836	- 0.134
54.470	0.071544	0.01355	0.029
54.480	0.075318	0.06701	0.211
54.494	0.077640	0.09991	0.449
54.516	0.079718	0.12934	0.813
54.540	0.081142	0.14951	1.20
54.625	0.083880	0.18831	2.54
54.736	0.086010	0.21847	4.24
54.980	0.088755	0.25737	7.87
T=209.380°K			
53.826	0.050100	-0.29025	-12.85
54.006	0.052156	-0.26112	- 8.27
54.007	0.052241	-0.25992	- 8.16
54.167	0.054950	-0.22154	- 4.28
54.246	0.056942	-0.19332	- 2.48
54.302	0.059458	-0.15768	- 1.19
54.323	0.060670	-0.14050	- 0.772
54.341	0.063120	-0.10579	- 0.348
54.357	0.066927	-0.05186	- 0.075
54.358	0.070320	-0.00379	- 0.0064
54.362	0.073171	0.03659	0.068
54.366	0.074750	0.05896	0.096
54.378	0.078038	0.10554	0.335
54.389	0.079294	0.12334	0.486

TABLE XXII (continued)

Pressure (atm)	LL	ΔLL	$\Delta\mu\times10^3$
54.494	0.086357	0.22340	3.71
54.663	0.088411	0.25249	6.22
T=209.302°K			
53.669	0.049440	-0.29960	-13.96
53.867	0.051545	-0.26977	- 8.84
54.061	0.054675	-0.22544	- 4.09
54.063	0.054782	-0.22392	- 4.03
54.160	0.057584	-0.18422	- 1.79
54.182	0.058516	-0.17103	- 1.30
54.222	0.061633	-0.12686	- 0.423
54.233	0.063569	-0.09943	- 0.187
54.235	0.063997	-0.09337	- 0.157
54.239	0.066241	-0.06157	- 0.062
54.240	0.066567	-0.05696	- 0.053
54.241	0.068460	-0.03014	- 0.019
54.242	0.070038	-0.00779	- 0.0043
54.244	0.075391	0.06805	0.026
54.314	0.082666	0.17110	1.16
54.325	0.083085	0.17705	1.33
54.447	0.085926	0.21729	3.20
54.496	0.086716	0.22848	3.94
54.591	0.087883	0.24502	5.35
54.711	0.089082	0.26200	7.13
T=209.294°K			
53.745	0.050287	-0.28759	-11.65
53.918	0.052359	-0.25824	- 7.25
54.059	0.054866	-0.22273	- 3.83
54.121	0.056490	-0.19972	- 2.37
54.175	0.058742	-0.16782	- 1.16
54.208	0.061265	-0.13208	- 0.426
54.226	0.064617	-0.08459	- 0.055
54.228	0.066547	-0.05724	- 0.018
54.229	0.073833	0.04598	0.014
54.231	0.075498	0.06956	0.041
54.239	0.078320	0.10954	0.176
54.263	0.080916	0.14631	0.562
54.325	0.083626	0.18471	1.55
54.413	0.085624	0.21301	2.89
54.568	0.087839	0.24440	5.23

TABLE XXII (continued)

Pressure (atm)	LL	ΔLL	$\Delta\mu\times10^3$
54.433	0.082002	0.16171	1.22
54.478	0.083474	0.18255	1.89
54.597	0.085968	0.21788	3.73
54.602	0.086025	0.21869	3.83
54.815	0.088569	0.25473	6.97
T=209.338°K			
53.774	0.050118	-0.28999	-12.49
53.976	0.052507	-0.25614	- 7.38
54.079	0.054256	-0.23137	- 4.85
54.193	0.057123	-0.19075	- 2.19
54.238	0.059186	-0.16153	- 1.17
54.275	0.062211	-0.11867	- 0.385
54.285	0.064020	-0.09305	- 0.189
54.291	0.067369	-0.04559	- 0.070
54.293	0.068442	-0.03040	- 0.026
54.294	0.070083	-0.00715	- 0.0070
54.296	0.073148	0.03627	0.029
54.296	0.074121	0.05005	0.040
54.302	0.077022	0.09115	0.137
54.327	0.080249	0.13687	0.552
54.374	0.082674	0.17123	1.30
54.449	0.084743	0.20053	2.46
54.544	0.086428	0.22440	3.91
54.747	0.088795	0.25793	6.93
T=209.315°K			
53.771	0.050319	-0.28714	-11.68
53.932	0.052241	-0.25992	- 7.59
54.085	0.054941	-0.22167	- 3.85
54.143	0.056477	-0.19991	- 2.49
54.191	0.058314	-0.17388	- 1.41
54.229	0.060711	-0.13992	- 0.579
54.244	0.062486	-0.11477	- 0.253
54.253	0.064817	-0.08175	- 0.076
54.255	0.066116	-0.06336	- 0.047
54.257	0.069245	-0.01902	- 0.0037
54.257	0.072255	0.02362	0.0049
54.258	0.073905	0.04699	0.025
54.262	0.076573	0.08479	0.096
54.269	0.078227	0.10821	0.201
54.310	0.081702	0.15744	0.870
54.398	0.084597	0.19846	2.24

TABLE XXIII

THE $\Delta\mu$, ΔLL DATA IN THE ANTISYMMETRIC RANGE FOR $T<T_c$

Pressure (atm)	LL	ΔLL	$\Delta\mu\times10^3$
T=208.886°K			
53.278	0.050052	-0.29100	- 8.01
53.529	0.054101	-0.23364	- 1.70
53.650	0.085787	0.21520	0.749
53.843	0.088874	0.25893	3.62
54.117	0.091259	0.29271	7.58
T=209.126°K			
53.590	0.050507	-0.28449	- 9.28
53.835	0.054265	-0.23124	- 3.16
53.945	0.057969	-0.17876	- 0.596
54.010	0.083057	0.17664	0.603
54.144	0.086492	0.22530	2.65
54.380	0.089378	0.26620	6.14
T=209.221°K			
53.544	0.049067	-0.30488	-14.05
53.833	0.052323	-0.25876	- 6.60
53.998	0.055552	-0.21301	- 2.61
54.026	0.056420	-0.20071	- 1.96
54.098	0.060247	-0.14649	- 0.339
54.137	0.081060	0.14835	0.375
54.203	0.084041	0.19059	1.41
54.369	0.087217	0.23558	3.93
54.842	0.091361	0.29429	10.81
T=209.259°K			
53.482	0.048198	-0.31719	-17.23
53.811	0.051424	-0.27149	- 8.60
54.019	0.054913	-0.22206	- 3.49
54.131	0.058830	-0.16656	- 0.917
54.160	0.061301	-0.13157	- 0.282
54.177	0.077547	0.09859	0.054
54.195	0.080469	0.13998	0.353
54.256	0.083437	0.18202	1.32
54.508	0.087897	0.24521	5.13
54.850	0.090801	0.28635	10.11

TABLE XXIII (continued)

Pressure (atm)	LL	ΔLL	$\Delta\mu \times 10^3$
T=209.274°K			
53.486	0.048113	-0.31839	-17.75
53.823	0.051379	-0.27213	- 8.90
54.043	0.055034	-0.22035	- 3.51
54.151	0.058815	-0.16679	- 1.02
54.189	0.062588	-0.11333	- 0.198
54.221	0.080152	0.13549	0.371
54.259	0.082436	0.16784	0.987
54.410	0.086157	0.22056	3.31
54.722	0.089622	0.26965	7.92
55.374	0.093405	0.32325	17.18

TABLE XXIV

COMPARISON OF CRITICAL COEFFICIENTS[†]

Substance		Γ	Γ'	Δ
Ar	[Ref. (36)]	0.072	0.019	2.48
Kr	[this study]	0.084	0.021	2.34
	[this study][*]	0.083±0.001	0.021±0.001(gas) 0.025±0.001(liq.)	
Xe	[Ref. (29)]	0.059	0.0143	3.3
He^4	[Ref. (29)]	0.0130	0.0359	3.2
CO_2	[Ref. (29)]	0.0526	0.0119	2.6
O_2	[Ref. (55)]	0.053	0.0109	4.0

[†] Determined from the $\Delta\mu$, $\Delta\rho$ data analysis.

[*] Determined from the isothermal compressibilities.

TABLE XXV

COMPARISON OF THE CRITICAL EXPONENTS

Substance	β	γ	δ	Reference
Ar	0.3643±0.0066			Teague and Pings(6)
	0.3574±0.0027	1.17±0.013	4.35±0.10	Wu(36)
	0.362 ±0.001			Sengers(52)
Kr	0.3571±0.0008	1.18±0.01	4.25±0.25	This study
			4.3 ±0.1	" "
Xe	0.350 ±0.015			Weinberger & Schneider(57)
			4.6 ±0.1	Vicentini-Missoni *et al*(29)
		1.21±0.03		Zollweg *et al*(61)
He^4	0.352 ±0.003			Roach and Douglas(58)
			4.45±0.10	Vicentini-Missoni *et al*(29)
	0.3554±0.0028	1.1743±0.0005		Kierstead(54)
		1.2223±0.0017		Kierstead(54)
CO_2	0.347 ±0.003		4.60±0.10	Vicentini-Missoni *et al*(29)
	0.3450±0.0006			Sengers *et al*(46)
	0.3475±0.0006			Sengers *et al*(46)
		1.219±0.010		Lunacek & Conell(60)
H_2	0.375 ±0.015			Roder *et al*(59)

TABLE XXV (continued)

Substance	β	γ	δ	Reference
N_2O	0.3482±0.0007			Sengers *et al*(46)
$CClF_3$	0.3540±0.0018			Sengers *et al*(46)
O_2	0.353	1.25±0.02	4.59±0.010	Weber(55)
H_2O	0.347 ±0.005	1.20±0.05		Sengers & Greer(56)
$CrBr_3$	0.368 ±0.005	1.215±0.015		Ho & Litster(31)
SF_6		1.225±0.02		Puglielli & Ford(62)

APPENDIX A

A REVIEW OF THE DERIVATION(1) OF LL-FORMULA AND THE UNDERLYING ASSUMPTIONS(2)

The simplest theory that takes electrostatic interactions into account is that of Lorentz(1) and the method of derivation is as follows:

A particular molecule on which the local electric field intensity $\bar{E}^*$ is to be calculated is selected. A sphere of radius R that is large compared to the distance between molecules but small compared to macroscopic distances is drawn about this molecule. Then the field intensities in the dielectric $\bar{E}_1^*$ outside the sphere and $\bar{E}_2^*$ inside the sphere are computed.

To compute $\bar{E}_1^*$, the following procedure can be used: The effect of the relative displacement of positive and negative charges in the molecules of a dielectric can be described by assigning a dipole moment $\bar{P}dv$ to each volume element dv, where $\bar{P}$ is the polarization. The potential at a point outside the dielectric is given by,

$$V = (1/4\pi)\int \frac{\bar{P}\cdot\bar{r}^\circ}{r^2}\, dv \tag{A-1}$$

and $r\bar{r}^\circ = \bar{r}$ is the vector from the volume element to the point where the potential is calculated.

Since $\bar{P}\cdot(\bar{r}^\circ/r^2) = \bar{P}\cdot\nabla(\frac{1}{r}) = \nabla\cdot\frac{\bar{P}}{r} - \frac{\nabla\cdot\bar{P}}{r}$ (A-2)

Then, through the use of the divergence theorem, Eq. (A-1) can be expressed as,

$$V = (1/4\pi)\left\{ \int(\sigma_p/r)dS+\int(\rho_p/r)dv\right\} \qquad \text{(A-3)}$$

where the surface charge density $\sigma_p=\bar{n}\cdot\bar{P}$, with $\bar{n}$ being the outward unit normal to the surface element dS and the volume charge density $\rho_p=-\nabla\cdot\bar{P}$.

The field intensity $\bar{E}$ can then be obtained from Eq. (A-3) by differentiation.

$$\bar{E} = (1/4\pi)\{\int(\sigma_p\bar{r}^\circ/r^2)dS+\int(\rho_p\bar{r}^\circ/r^2)dv \qquad \text{(A-4)}$$

The extension of these formulas to points inside the dielectric can be done by excluding from the region of integration v a small volume v' with surface S' about the point where V and $\bar{E}$ are calculated. Then Eqs. (A-3) and (A-4) are valid if the surface integral is taken over S as well as S' and the volume integral over v-v' and v' is shrunk to vanishing volume. From the original integral, the result of this process must be independent of the shape of v' but this condition is not satisfied in Eq. (A-4) and the integral over S' depends on v'. It is $(4\pi/3)\bar{P}$ when v' is a sphere. Hence $\bar{E}_1^*$ is given by

$$\bar{E}_1^* = \bar{E} + (4\pi/3)\bar{P} \qquad \text{(A-5)}$$

where $\bar{E}$ is the external field.

To compute $\bar{E}_2^*$ is more involved and assumptions about the distribution of molecules have to be made in order to obtain a simple result. Lorentz has treated the case of a cubic lattice of molecules, each having the same dipole moment $\overline{m}$, and has shown $\overline{E}_2^*=0$.

In general, therefore

$$\overline{E}^* = \overline{E}_1^* + \overline{E}_2^* = \overline{E} + (4\pi/3)\overline{P} + \overline{E}_2^* \qquad \text{(A-6)}$$

Setting $\overline{E}_2^*=0$, the Lorentz local field formula is obtained.

$$\overline{E}^* = \overline{E} + (4\pi/3)\overline{P} \qquad \text{(A-7)}$$

If the dielectric displacement vector $\overline{D}$ is defined by

$$\overline{D} = \overline{E} + 4\pi\overline{P} \qquad \text{(A-8)}$$

and

$$\overline{P} = \chi\overline{E} \qquad \text{(A-9)}$$

with the susceptibility χ being independent of $\overline{E}$ but a function of density and temperature, it then follows that

$$\overline{D} = \varepsilon\overline{E} \qquad \text{(A-10)}$$

with the dielectric constant $\varepsilon=1+4\pi\chi$ (A-11)

On the molecular scale, $\overline{P} = N\langle\overline{m}\rangle_{av}$ (A-12)

where N is the number of molecules per unit volume and $\langle\overline{m}\rangle_{av}$ is the mean moment of a representative molecule computed by methods of statistical mechanics.

On the macroscopic scale, for non-polar isotropic molecules with only induced moments,

$$\overline{m} = \alpha_m\overline{E}^* \qquad \text{(A-13)}$$

where α_m is the molecular polarizability and is a scalar.

Therefore from Eq. (A-11) and (A-13), $\overline{P} = N\alpha_m\overline{E}$ (A-14)

and combining Eqs. (A-7), (A-9), (A-11) and (A-14),

$$\overline{P}/\overline{E}^* = N\alpha_m = \frac{3\chi}{3+4\pi\chi} = (1/4\pi)\,\frac{3(\varepsilon-1)}{(\varepsilon+2)} \qquad \text{(A-15)}$$

If N is replaced by ρ/M, where ρ is the density and M is the molecular mass, Eq. (A-15) becomes

$$\frac{\varepsilon-1}{\varepsilon+2} = (4\pi/3M)\alpha_m\rho = \text{constant}\times\rho \qquad \text{(A-16)}$$

Eq. (A-16) is known as the Claussius-Mossotti formula.

The optical analog of the CM-formula is the Lorentz-Lorenz formula which can be obtained by replacing ε with n^2, n being the refractive index.

$$\frac{n^2-1}{n^2+2} = (4\pi/3M)\alpha_m\rho \qquad \text{(A-17)}$$

This transformation is valid at optical frequencies for the case of non-polar molecules with negligible atomic polarizabilities. It is even justified for polar molecules because at optical frequencies the oscillations of the field are so fast that there is no appreciable orientation effect and the material behaves as though it is non-polar.

APPENDIX B

RELATIONS AMONG THE CRITICAL-POINT EXPONENTS AS PREDICTED BY THE SCALING LAW

Using magnetic variables Stanley(10) has shown the relations among the critical-point exponents as predicted by the scaling hypothesis. Here, these relations will be translated into the fluid systems by appropriate choice of thermodynamic potentials and variables.

Griffiths and Wheeler(28) have shown that it is advantageous to discuss critical phenomena in terms of intensive variables. A choice of the chemical potential $\Delta\mu$ and the reduced temperature difference from the critical temperature t as independent variables leads to a thermodynamic potential $P^*(\Delta\mu, t)$ such that,

$$dP^* = \Delta\rho \, d(\Delta\mu) + \Delta s \, dt \qquad \text{(B-1)}$$

where $\Delta\rho$ is the density and Δs is the entropy with Δ indicating a linear transformation of the form $\Delta\rho = \rho - \rho_c$.

The homogeneous function assumption of the scaling hypothesis applied to P^* implies that for the two parameters a_t and a_μ,

$$P^*(\lambda^{a_t} t, \lambda^{a_\mu} \Delta\mu) = \lambda P^*(t, \Delta\mu) \qquad \text{(B-2)}$$

for any value of λ. If both sides of Eq. (B-2) are differentiated with respect to $\Delta\mu$, the resulting equation is

$$\lambda^{a_\mu} \, \partial\{P^*(\lambda^{a_t} t, \lambda^{a_\mu} \Delta\mu)\} / \partial(\lambda^{a_\mu} \Delta\mu) = \lambda \partial P^*(t, \Delta\mu)/\partial\Delta\mu \qquad \text{(B-3)}$$

From the choice of P^*, the first $\Delta\mu$ derivative of P^* is proportional to $\Delta\rho$. Therefore Eq. (B-3) is equivalent to,

$$\lambda^{a_\mu}\, \Delta\rho(\lambda^{a_t}t, \lambda^{a_\mu}\Delta\mu) = \lambda\, \Delta\rho(t,\Delta\mu) \qquad \text{(B-4)}$$

Near the critical point when $\Delta\mu=0$ and $t\to 0$, β is associated with the behaviour of $\Delta\rho$. Hence,

$$\Delta\rho(t,0) = \lambda^{a_\mu - 1}\, \Delta\rho(\lambda^{a_t}t,0) \qquad \text{(B-5)}$$

Since Eq. (B-5) is valid for all values of λ, it must hold for $\lambda=(-1/t)^{1/a_t}$, thus

$$\Delta\rho(t,0) = (-t)^{(1-a_\mu)/a_t}\, \Delta\rho(-1,0) \qquad \text{(B-6)}$$

But from Eq. (11), $\Delta\rho \simeq B(-t)^{\beta}$, so that

$$\beta = (1-a_\mu)/a_t \qquad \text{(B-7)}$$

When $t=0$ and $\Delta\mu\to 0$, the exponent $1/\delta$ is associated with the behaviour of $\Delta\rho$. Hence,

$$\Delta\rho(0,\Delta\mu) = \lambda^{a_\mu - 1}\, \Delta\rho(0,\lambda^{a_\mu}\Delta\mu) \qquad \text{(B-8)}$$

If $\lambda=\Delta\mu^{-1/a_\mu}$,

$$\Delta\rho(0,\Delta\mu) = \Delta\mu^{(1-a_\mu)/a_\mu}\Delta\rho(0,1) \qquad \text{(B-9)}$$

But from Eq. (12), $\Delta\rho \simeq |\Delta\mu|^{1/\delta}$, so that

$$\delta = a_\mu/(1-a_\mu) \qquad \text{(B-10)}$$

Eqs. (B-7) and (B-10) can be solved simultaneously for a_t and a_μ in terms of the exponents, yielding

$$a_t = 1/\beta(\delta+1) \qquad \text{(B-11)}$$

$$a_\mu = \delta/(\delta+1) \qquad \text{(B-12)}$$

Additional exponent relations can be obtained by taking higher order partial derivatives of the potential P*. For example, when P* is differentiated twice with respect to $\Delta\mu$, a quantity proportional to the product of the isothermal compressibility and the density squared ρ^2K_T is obtained.

$$\lambda^{2a_\mu}\ \rho^2K_T(\lambda^{a_t}t,\lambda^{a_\mu}\Delta\mu) = \lambda\ \rho^2K_T(t,\Delta\mu) \qquad \text{(B-13)}$$

Along the coexistence curve where $\Delta\mu=0$ and $t\rightarrow 0$, γ' refers to the behaviour of the isothermal compressibility. For $\lambda=(-t)^{-1/a_t}$,

$$\rho^2K_T(t,0) = (-t)^{-(2a_\mu-1)/a_t}\ \rho^2K_T(-1,0) \qquad \text{(B-14)}$$

But from Eq. (14), $\rho^2K_T \approx \Gamma'(-t)^{-\gamma'}$. Hence,

$$\gamma' = (2a_\mu-1)/a_t \qquad \text{(B-15)}$$

If a_μ and a_t from Eqs. (B-11) and (B-12) are substituted into Eq. (B-15), the relation

$$\gamma' = \beta(\delta-1) \qquad \text{(B-16)}$$

which is called the Widom equality is obtained.

The scaling hypothesis also predicts that the primed and the unprimed critical-point exponents are equal. This can be illustrated by letting $\lambda=t^{-1/a_t}$ in Eq. (B-13) and obtaining,

$$\gamma = (2a\ -1)/a_t \qquad \text{(B-17)}$$

Combining Eqs. (B-15) and (B-17),

$$\gamma = \gamma' \qquad \text{(B-18)}$$

P* can also be differentiated with respect to temperature for further exponent relations. In particular the second temperature derivative of P* can be related to the specific heat at constant volume.

$$\lambda^{2a_t}\rho C_v(\lambda^{a_t}t,\lambda^{a_\mu}\Delta\mu) = \lambda\ \rho C_v(t,\Delta\mu) \qquad \text{(B-19)}$$

On setting $\Delta\mu=0$, $\lambda=(-t)^{-1/a_t}$ and using $\rho C_v \approx (-t)^{-\alpha'}$, one obtains

$$\alpha' = 2-1/a_t \qquad \text{(B-20)}$$

When a_t from Eq. (B-11) is substituted into Eq. (B-20), the result is the Griffith's inequality satisfied as an equality.

$$\alpha'+\beta(\delta+1) = 2 \qquad \text{(B-21)}$$

If Eqs. (B-16) and (B-21) are combined the Rushbrooke inequality in the form of an equality is obtained.

$$\alpha'+2\beta+\gamma' = 2 \qquad \text{(B-22)}$$

APPENDIX C

AUTOMATIC PRESSURE CONTROL UNIT

The components and the electrical circuit for the automatic pressure control unit are shown in Fig. C. The principle of the operation of this device was the variable supply of radiant heat to a portion of the sample line so that very small pressure corrections could be made by heating and cooling of the gas in this segment by radiation. The pressure of the hydraulic oil and the pressure of the sample inside the cryostat were very stable but the pressure in the sample lines at room temperature varied. Thus, the main function of the pressure control unit was to compensate for such pressure changes.

The operation of this unit was as follows: The signal from the Pace network which was proportional to the pressure difference across the diaphragm was converted into a light signal by the use of a Leeds and Northrup 2435D galvanometer. The sensitivity of the galvanometer was 0.01 μa/mm and it was further adjusted by a 150 KΩ resistor. An oil-filled 10 mfd condensor connected across this resistor produced rate control. The signal from the Pace network for a steady position of the indicator of the microammeter was proportional to the magnitude of the deflection from the null point and produced a proportional current. The insertion of the condensor produced an additional current proportional to the rate of this deflection. Thus, the current to correct an abrupt pressure decrease was greater than the current to correct a gradual pressure decrease of the same magnitude. The torsional pendulum motion of the galvanometer was dampened by a shunt resistor of 10 KΩ connected in parallel with the galvanometer coil. The deflection of the galvanometer was sensed by a photo-conductive type, Clairex-603AL photocell. The photocell was connected directly to a model D600P Lutron light dimmer for resistive loads. The load in this case was a pair of 30 Watts, reflector type heat lamps in parallel with each other. The components inside the light dimmer are shown in Fig. C and their explanation can be found in any commercial manual such as Ref. 40. The purpose of using the light dimmer was to regulate the intensity of the heat lamps by setting the variable resistance of the dimmer at its maximum so that the varying resistance of the photocell determined the current for the charging of the capacitors inside the light dimmer. When the pressure was controlling, the light dimmer could be set such that the heat lamps operated at a medium intensity. This permitted some range for increasing or decreasing the intensity of the lamps to correct the pressure variations. The portion of the sample line on which the heat lamps were shining was painted black to ensure efficient heating by radiation.

The pressure could be controlled automatically within ±0.001 atm. with this unit.

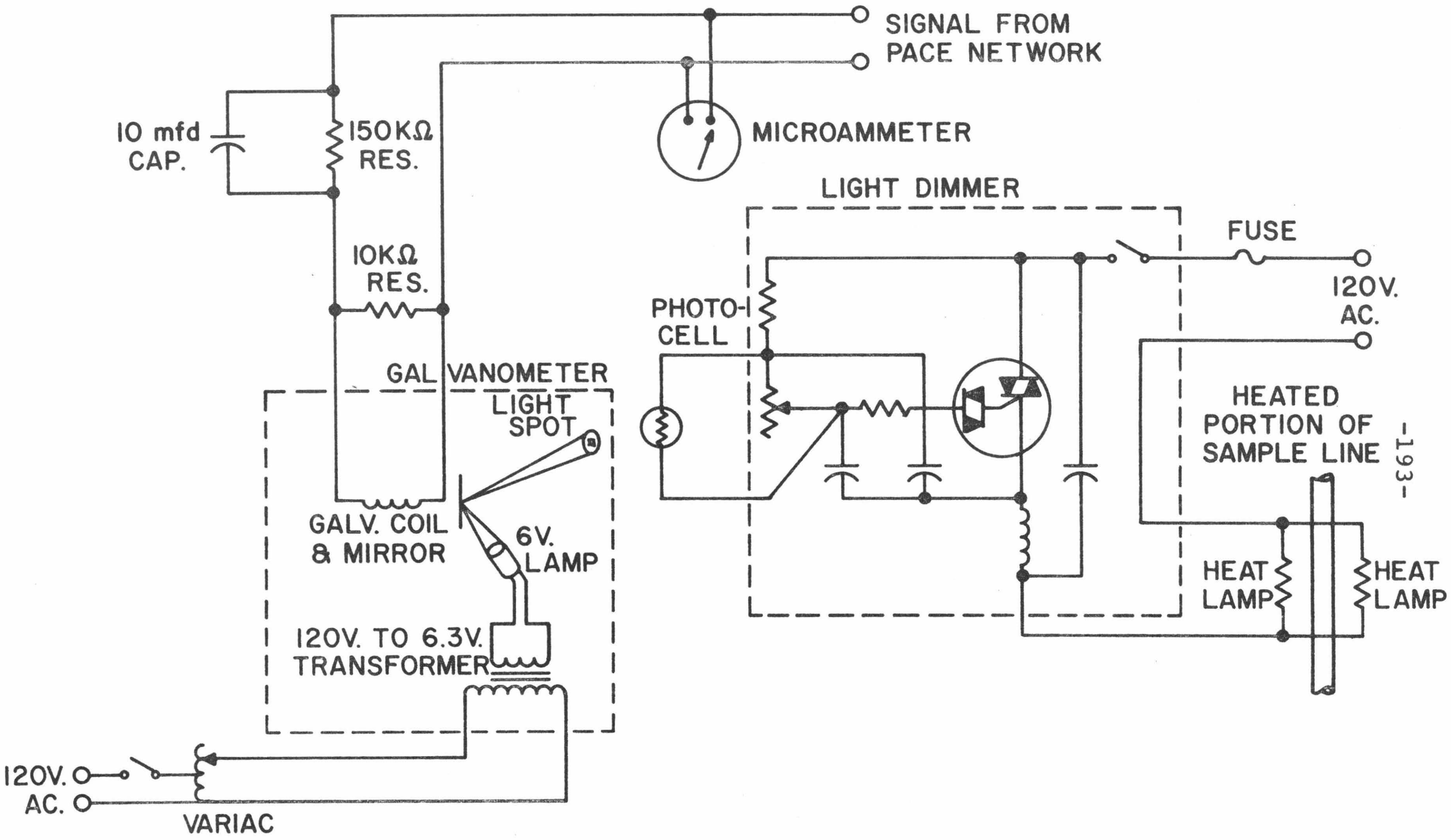

Figure C. Automatic Pressure Control Unit

APPENDIX D

AN ATTEMPT TO CHECK THE DENSITY DEPENDENCE OF LL-FUNCTION FOR KRYPTON

F. Theeuwes and R. J. Bearman(44) have studied the P,V,T behaviour of liquid and dense gaseous krypton. An attempt to compare the present data with those of Ref. 44 showed that there were overlapping ranges of temperature and pressure but no two states matched exactly. Therefore an interpolation technique had to be employed.

After careful scanning of the data reported in Ref. 44 four states were chosen such that their temperatures were wihtin the range of this study and their pressures were included in the pressure range of the present investigation at least along three isotherms. Then fitting a cubic spline (See Appendix E) and interpolating for the Lorentz-Lorenz function, LL-function, corresponding to each pressure along several isotherms, temperature versus LL-function values at a known constant pressure were generated as tabulated in Table D. These values were then plotted as shown in Figures D1-D4, and the LL-function values corresponding to the temperatures of each of the chosen states form Ref. 44, were read from these plots.

The conventional treatment of the density dependence of the LL-function is simple and only a constant of proportionality is involved such that

$$\rho = A \times LL \qquad \text{(D-1)}$$

where ρ is the density, LL is the LL-function and A is the constant of proportionality.

The purpose here was to investigate the changes in the value of A for differing densities, pressures and temperatures. The values of A obtained from the comparison of the two sets of data are summarized below:

	Temperature (°K)	Pressure (atm)	Density (g/cm^3)	LL-function	A (g/cm^3)
State 1	217.001	66.766	0.9586	0.0733	13.078
State 2	209.004	54.391	1.1890	0.09142	13.006
State 3	205.000	53.766	1.4454	0.11085	13.039
State 4	201.000	54.832	1.5727	0.12035	13.068

States 1,2 and 4 were in the dense gas region with their temperatures being 7.71°K above, 0.28°K below and 8.29°K below the critical temperature respectively. State 3 was in the liquid region at 4.27°K below the critical temperature.

The value of A did not show a striking dependence on density. Its maximum variation for these four states covering two different states of matter was $\pm$0.28%. This value incorporated errors introduced by the interpolation technique and the experimental uncertainties associated with both sets of data.

Consequently, for the purposes of this study, LL-function will be treated as density within a constant of proportionality.

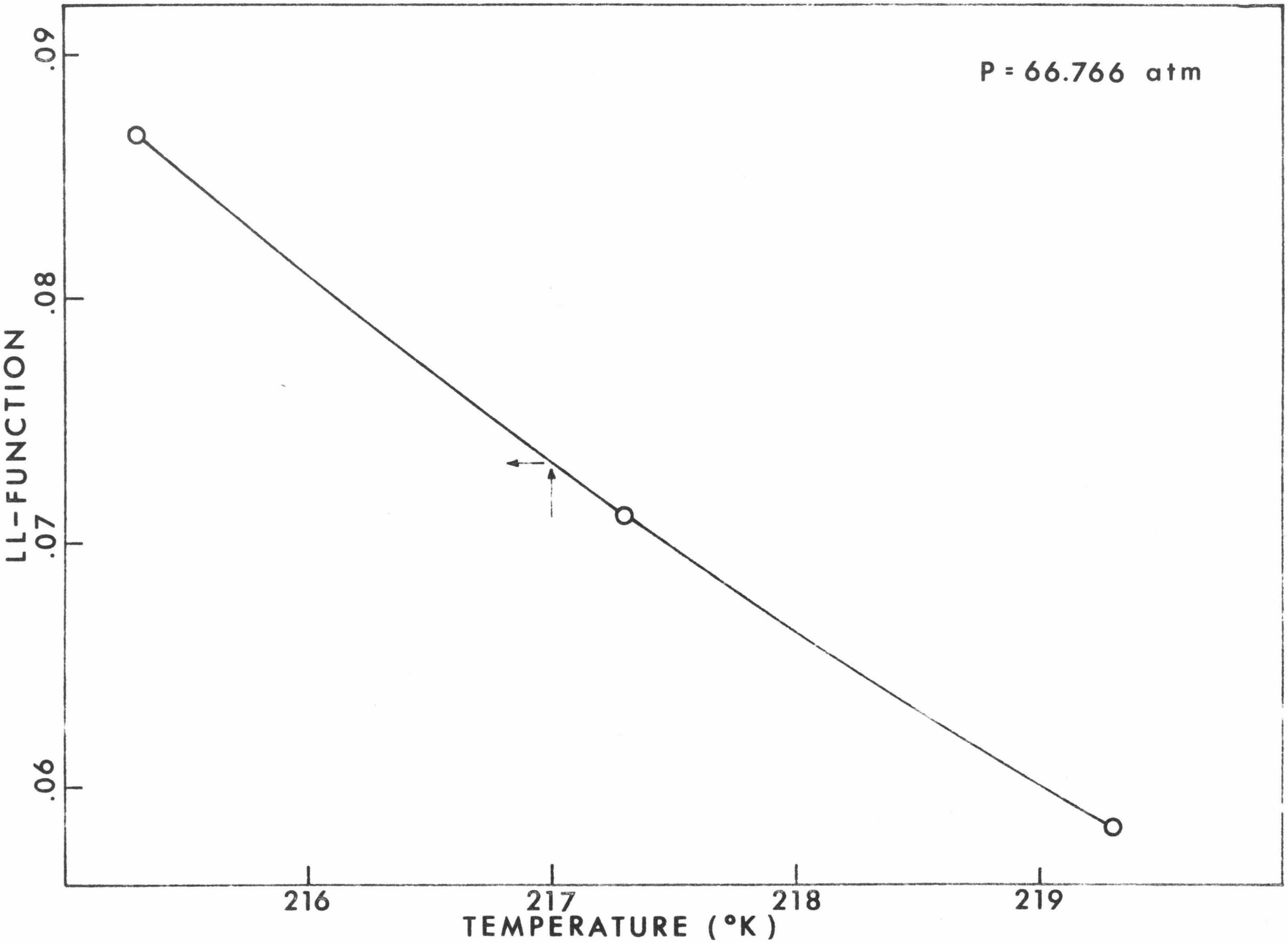

Figure D-1. LL(207.001°K) = 0.0733

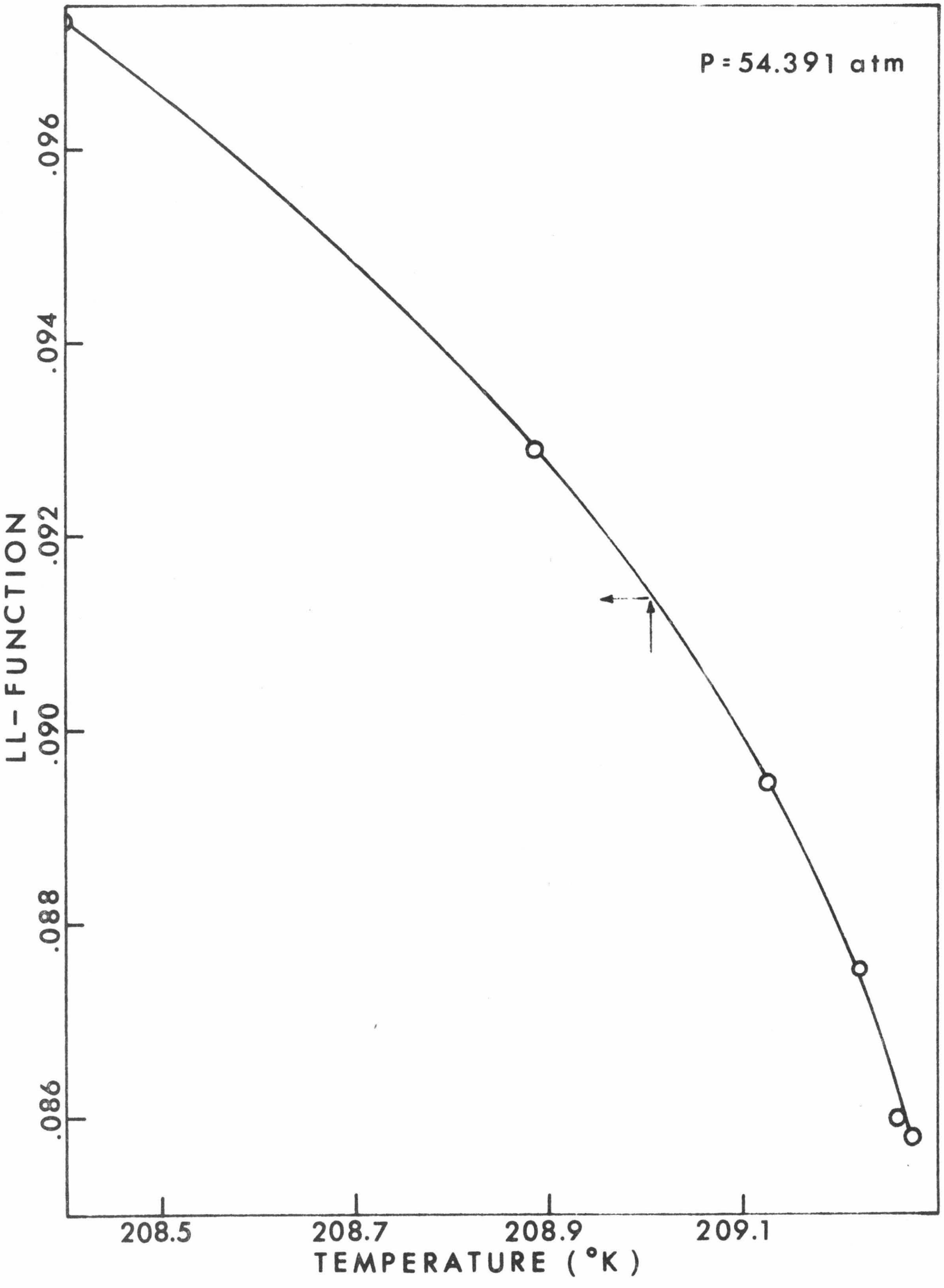

Figure D-2. LL(209.004°K) = 0.09142

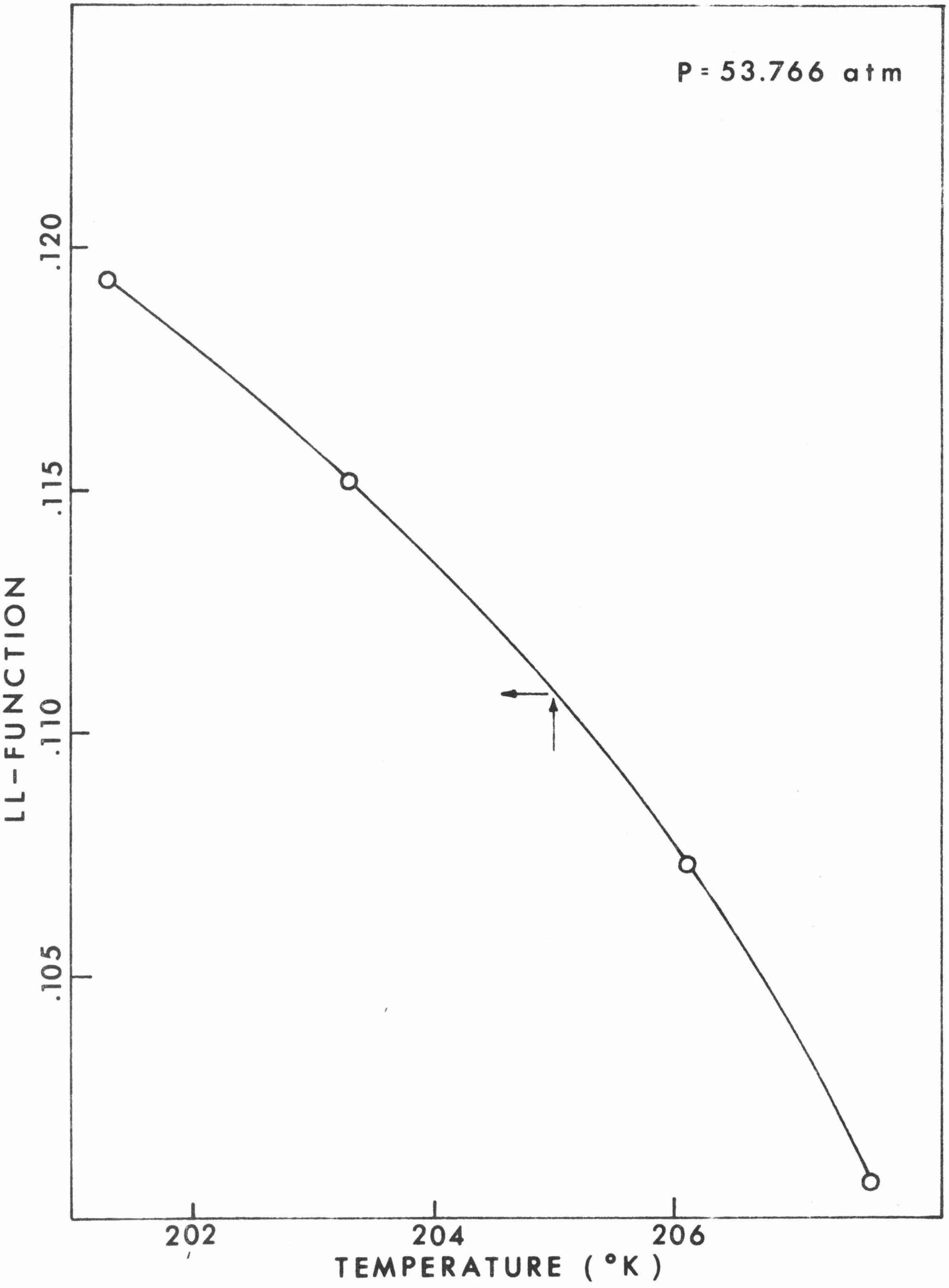

Figure D-3. LL(205.000°K) = 0.11085

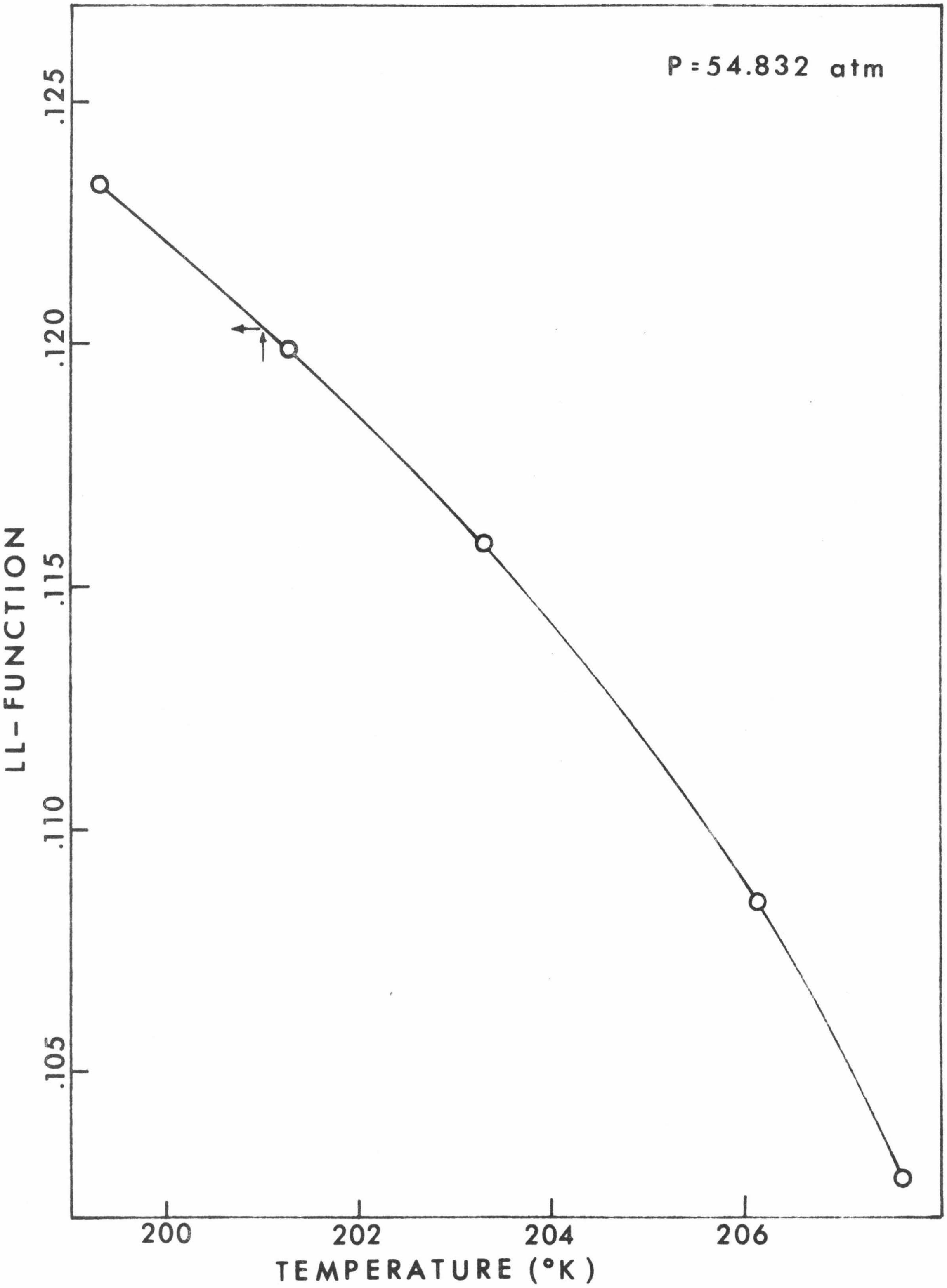

Figure D-4. LL(201.000°K) = 0.12035

TABLE D

GENERATED TEMPERATURE VERSUS LL-FUNCTION VALUES AT CONSTANT PRESSURE

	Temperature (°K)	Refractive Index	LL-Function
State 1:			
At P=66.766 atm.			
	219.301	1.08906	0.05840
	217.301	1.10888	0.07109
	215.301	1.13352	0.08672
State 2:			
At P=54.391 atm.			
	208.400	1.15039	0.09731
	208.886	1.14333	0.09289
	209.126	1.13791	0.08948
	209.221	1.13481	0.08753
	209.259	1.13239	0.08601
	209.274	1.13209	0.08582
State 3:			
At P=53.766 atm.			
	201.300	1.18600	0.11935
	203.300	1.17921	0.11518
	206.120	1.16646	0.10731
	207.620	1.15590	0.10075
State 4:			
At P=54.832 atm.			
	199.302	1.19241	0.12328
	201.300	1.18678	0.11983
	203.300	1.18023	0.11581
	206.120	1.16828	0.10844
	207.620	1.15910	0.10274

APPENDIX E

CUBIC SPLINE FIT(45)

The task of the numerical spline fit is to determine a smooth approximating function through a set of data points (x_1,y_1), $(x_2,y_2),\ldots.(x_n,y_n)$. In the cubic spline fit, this approximating function consists of cubics assigned to each interval requiring the slopes to be continuous at the junction points.

The procedure to determine these cubics is as follows: If the values of the second derivative of the approximating function $F(x)$ at each point are $M_1,M_2,\ldots.M_n$, and if a linear relationship of the second derivative between the points (x_{k-1},y_{k-1}) and (x_k,y_k) is assumed, then

$$F''= M_{k-1}\frac{x_k-x}{d_k} + M_k\frac{x-x_{k-1}}{d_k}, \quad x_k\geq x\geq x_{k-1} \qquad \text{(E-1)}$$

where $d_k=x_k-x_{k-1}$.

After integrating F'' twice, the resulting function is a third degree polynomial in x,

$$F = \frac{M_{k-1}}{6d_k}(x_k-x)^3+\frac{M_k}{6d_k}(x-x_{k-1})^3+C_1x+C_2 \qquad \text{(E-2)}$$

The two constants of integration C_1 and C_2 can be evaluated by passing the cubic through the end ponts (x_k,y_k) and (x_{k-1},y_{k-1}). Hence the equation of the cubic rearranges into,

$$F = C_{1,k}(x_k-x)^3+C_{2,k}(x-x_{k-1})^3+C_{3,k}(x_k-x)+C_{4,k}(x-x_{k-1})$$

where $C_{1,k}=\dfrac{M_{k-1}}{6d_k}$, $C_{2,k}=\dfrac{M_k}{6d_k}$, $C_{3,k}=\dfrac{y_{k-1}}{d_k}-\dfrac{M_{k-1}d_k}{6}$

and $C_{4,k}=\dfrac{y_k}{d_k}-\dfrac{M_kd_k}{6}$ (E-3)

Eq. (E-3) contains two unknowns namely M_k and M_{k-1}. For n points there are n-1 intervals each being assigned a cubic of the form of Eq. (E-3). Further there are n unknowns and n conditions are needed. All points except the first and the last points are junctions and the requirement of the first derivative to be continuous at the junction points, i.e. $F'(x_k^+) = F'(x_k^-)$, creates (n-2) conditions of the form,

$$\frac{d_k}{6}M_{k-1}+\frac{d_k+d_{k+1}}{3}M_k+\frac{d_{k+1}}{6}M_{k+1}=\frac{y_{k+1}-y_k}{d_{k+1}}-\frac{y_k-y_{k-1}}{d_k} \qquad \text{(E-4)}$$

To determine all M_k, two more arbitrary end conditions are needed. One choice which leads to a simple relation is to match the third derivatives at (x_2,y_2) and (x_{n-1},y_{n-1}). Thus, at (x_2,y_2) and at (x_{n-1},y_{n-1}) respectively,

$$-\frac{M_1}{d_1}+M_2\left(\frac{1}{d_1}+\frac{1}{d_2}\right)-\frac{M_3}{d_2}=0 \qquad \text{(E-5)}$$

$$-\frac{M_{n-2}}{d_{n-2}}+M_{n-1}\left(\frac{1}{d_{n-2}}+\frac{1}{d_{n-1}}\right)-\frac{M_n}{d_{n-1}}=0 \qquad \text{(E-6)}$$

All M_k can then be determined explicitly by solving n equations for n unknowns simultaneously. These n equations in matrix form are

$$a\,M = b \qquad \text{(E-7)}$$

where

$$a=\begin{bmatrix} \frac{-1}{d_1}, & \frac{1}{d_1}+\frac{1}{d_2}, & \frac{-1}{d_2} & , 0 & , \dots\dots, & 0 & , 0 \\ \frac{d_1}{6}, & \frac{d_1+d_2}{3}, & \frac{d_2}{6} & , 0 & , \dots\dots, & 0 & , 0 \\ 0, & \frac{d_2}{6}, & \frac{d_2+d_3}{3}, & \frac{d_3}{6} & , \dots\dots, & 0 & , 0 \\ \cdot\cdot\cdot & \cdot\cdot\cdot & \cdot\cdot\cdot & \cdot\cdot\cdot & \cdot\cdot\cdot & \cdot\cdot\cdot & \cdot\cdot\cdot \\ 0, & 0 & , \dots\dots, & \dots, & \frac{d_{n-2}}{6}, & \frac{d_{n-2}+d_{n-1}}{3}, & \frac{d_{n-1}}{6} \\ 0, & 0 & , \dots\dots, & \dots, & \frac{-1}{d_{n-2}}, & \frac{1}{d_{n-2}}+\frac{1}{d_{n-1}}, & \frac{-1}{d_{n-1}} \end{bmatrix}$$

and

$$b=\begin{bmatrix} 0 \\ \frac{y_3-y_2}{d_2}-\frac{y_2-y_1}{d_1} \\ \cdot \\ \cdot \\ \cdot \\ \frac{y_n-y_{n-1}}{d_{n-1}}-\frac{y_{n-1}-y_{n-2}}{d_{n-2}} \\ 0 \end{bmatrix}$$

A series of cubics of the form of Eq. (E-3), whose four constants are calculated as above, provides the smooth approximating function which can be used for the interpolation, differentiation or integration of the data.

The specific choice of the two arbitrary end conditions affects the fits of the end intervals. In the present study one of the uses of the cubic spline fit was for differentiation of the data in calculating the isothermal compressibilities. In order to calculate the isothermal compressibilities along the phase boundary, the values of the first derivative at the ends of the isotherms were needed. It was observed that the spline fit stayed smooth if the data was smooth irrespective of the size of the intervals. Hence, one logical improvement in determining the derivatives at the end points was to create smaller intervals and then extrapolate graphically. Large graphs of angle of minimum deviation D versus pressure P were plotted and a smooth curve was drawn through all the points. Then D and P values corresponding to several points in the last interval were read from such a graph and inserted into the cubic spline fit. The values of the first derivative computed at these points were plotted versus D as shown in Figs. E-1 and E-2 for the isotherm closest to the critical point. Assuming that the derivative changed smoothly, the value of the derivative corresponding to the value of D on the coexistence curve was read. This procedure was repeated for every isotherm below the critical temperature.

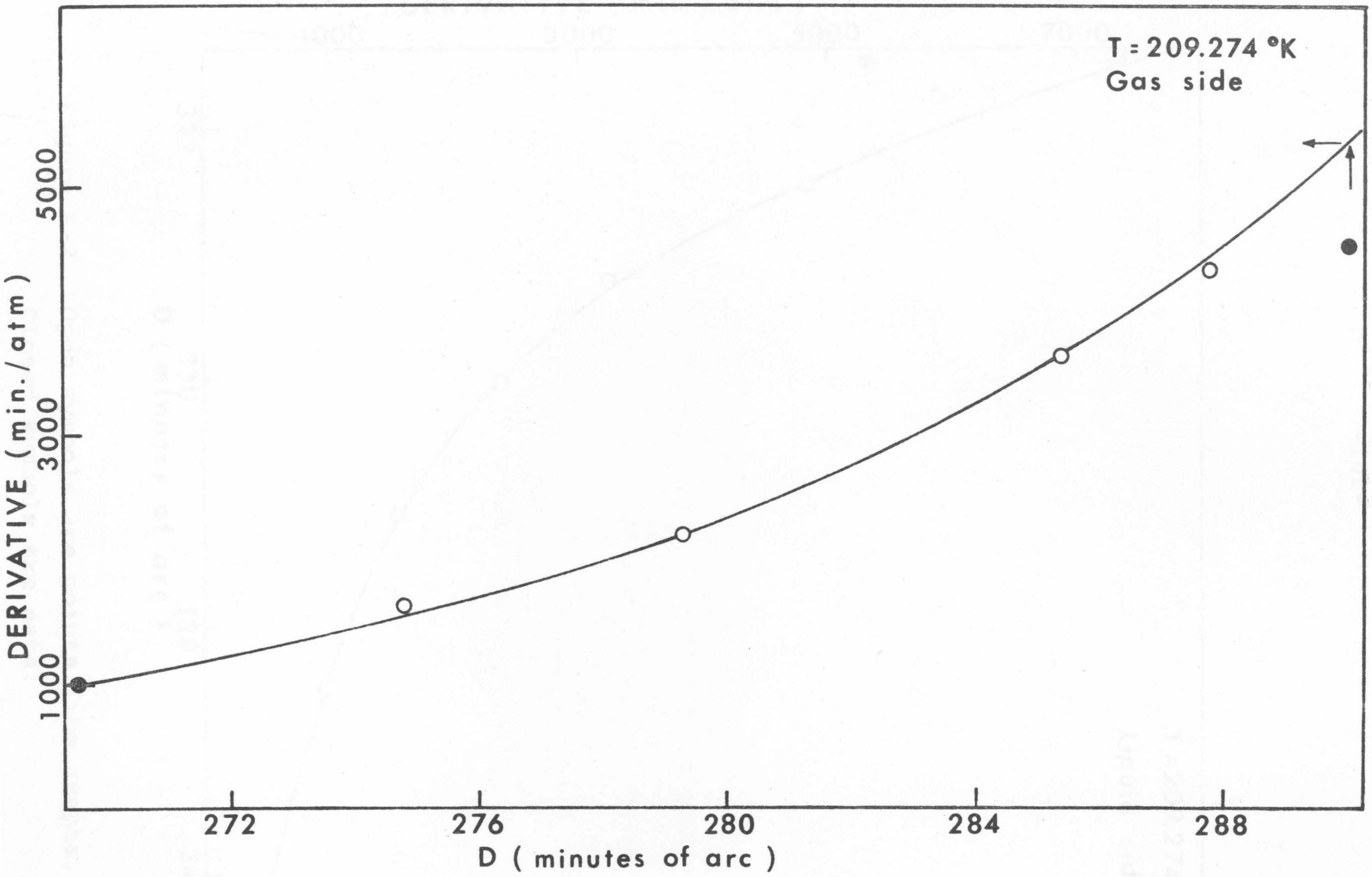

Figure E-1. Open symbols are points from graphs, closed symbols are data.

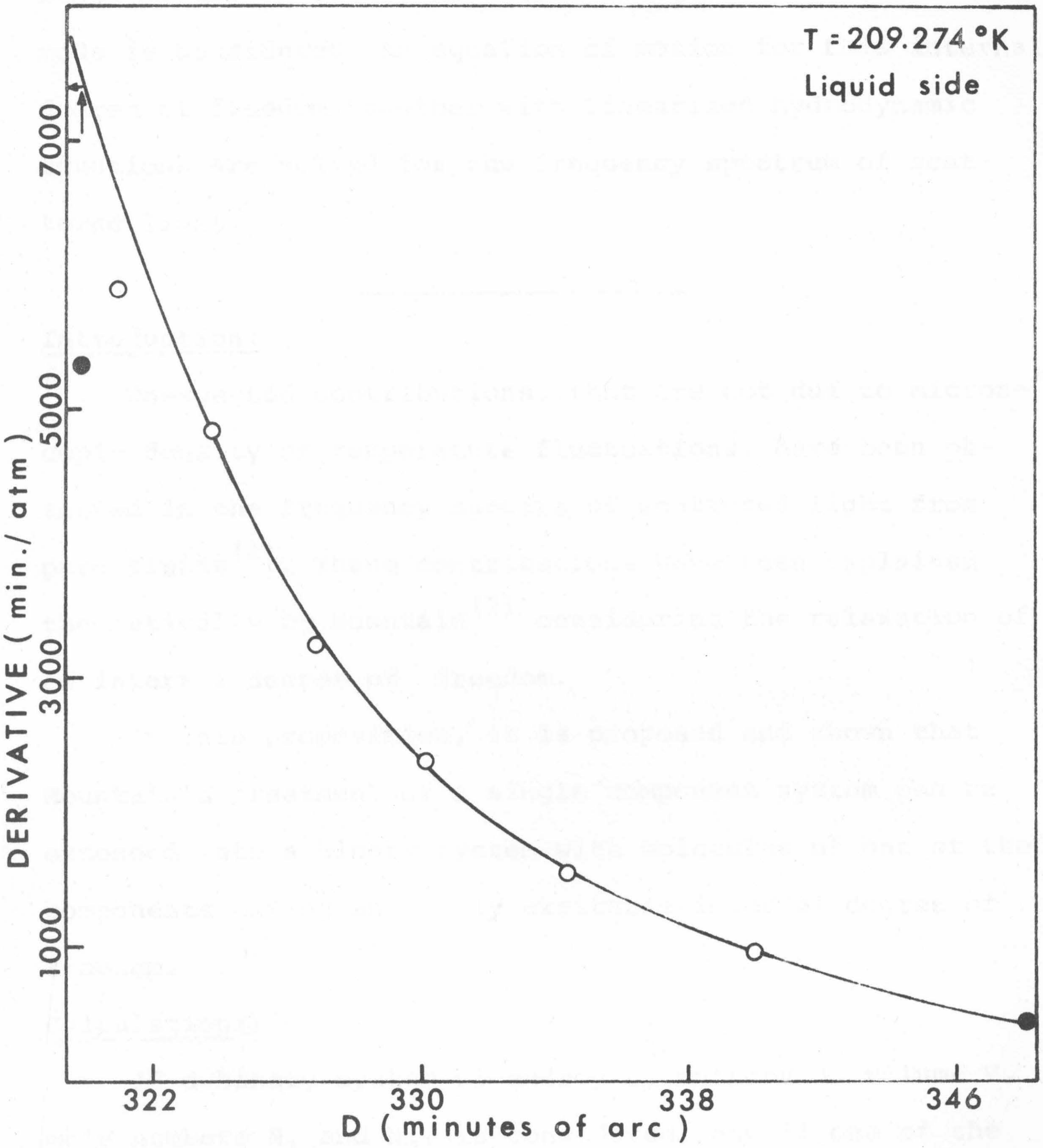

Figure E-2. Open symbols are points from graphs, Closed symbols are data.

PROPOSITION I

A binary system with molecules of one of the components having an easily excitable rotational or vibrational mode is considered. An equation of motion for this internal degree of freedom together with linearized hydrodynamic equations are solved for the frequency spectrum of scattered light.

Introduction:

Unexpected contributions, that are not due to microscopic density or temperature fluctuations, have been observed in the frequency spectra of scattered light from pure fluids(1). These contributions have been explained theoretically by Mountain(2) considering the relaxation of an internal degree of freedom.

In this proposition, it is proposed and shown that Mountain's treatment of a single component system can be extended into a binary system with molecules of one of the components having an easily excitable internal degree of freedom.

Calculation:

If a binary system of energy E, entropy S, volume V, mole numbers N_1 and N_2, is considered, and if one of the components has an internal degree of freedom ξ, a change in the internal energy of the system is given by,

$$dE = TdS - PdV + \mu_1 dN_1 + \mu_2 dN_2 + A_\xi d\xi \qquad (1)$$

where T is temperature, P is pressure, μ_1 and μ_2 are chemical potentials, and A_ξ is the partial derivative of the Helmoltz free energy with respect to ξ.

$$A_\xi = (\partial A/\partial \xi)_{V,T,N_i} \qquad (2)$$

If one gram of solution is considered with m_1 and m_2 mass fractions,

$$m_1 N_1 + m_2 N_2 = 1 \qquad (3)$$

$$dN_1 = -(m_2/m_1)\ dN_2 \qquad (4)$$

Letting $\mu = (\mu_1 - \mu_2 m_1/m_2)$ and $dN_1 = dN$ (5)

and changing from volume to density ρ, Eq. (1) becomes

$$dE = TdS + (P/\rho_o^2)d\rho + \mu dN + A_\xi d\xi \qquad (6)$$

where subscript zero refers to equilibrium quantities. It will be required that

$$A_\xi(\rho,T,N,\overline{\xi}) = 0 \qquad (7)$$

where $\overline{\xi} = \xi(\rho,T,N)$ is the local equilibrium value of ξ. Eq. (7) describes the condition when ξ is in local equilibrium with density, temperature and concentration whether or not the density, temperature and concentration have their equilibrium values.

It will be assumed that ξ relaxes with time according to

$$(\partial\xi/\partial t) = -LA_\xi \qquad (8)$$

with L>0.

Since only small deviations from equilibrium are considered

A_ξ can be expanded so that,

$$(\partial\xi/\partial t) = -L\{A_{\xi T}(T-T_o)+A_{\xi\rho}(\rho-\rho_o)+A_{\xi\phi}(\phi-\phi_o)+A_{\xi\xi}(\xi-\xi_o)\} \quad (9)$$

T, ρ, and φ are the set of statistically independent variables determined in Appendix A for a binary system with $\phi=N+b\rho$ where b is a constant given by Eq. (15) of Appendix A.

Also expanding $A_\xi(\rho,T,\phi,\bar{\xi})=0$ one obtains

$$A_{\xi\xi}(\xi_o-\bar{\xi}) = A_{\xi T}(T-T_o)+A_{\xi\rho}(\rho-\rho_o)+A_{\xi\phi}(\phi-\phi_o) \quad (10)$$

Combining Eqs. (9) and (10)

$$(\partial\xi/\partial t) = -LA_{\xi\xi}(\xi-\bar{\xi}) \quad (11)$$

The fluctuations in the pressure, entropy and chemical potential can be written in terms of the statistically independent variables.

$$dP = \left(\frac{\partial P}{\partial\rho}\right)_{T,\phi,\xi} d\rho + \left(\frac{\partial P}{\partial T}\right)_{\rho,\phi,\xi} dT + \left(\frac{\partial P}{\partial\phi}\right)_{T,\rho,\xi} d\phi + \left(\frac{\partial P}{\partial\xi}\right)_{T,\rho,\phi} d\xi \quad (12)$$

$$dS = \left(\frac{\partial S}{\partial\rho}\right)_{T,\phi,\xi} d\rho + \left(\frac{\partial S}{\partial T}\right)_{\rho,\phi,\xi} dT + \left(\frac{\partial S}{\partial\phi}\right)_{T,\rho,\xi} d\phi + \left(\frac{\partial S}{\partial\xi}\right)_{T,\rho,\phi} d\xi \quad (13)$$

$$d\mu = \left(\frac{\partial \mu}{\partial\rho}\right)_{T,\phi,\xi} d\rho + \left(\frac{\partial \mu}{\partial T}\right)_{\rho,\phi,\xi} dT + \left(\frac{\partial \mu}{\partial\phi}\right)_{T,\rho,\xi} d\phi + \left(\frac{\partial \mu}{\partial\xi}\right)_{T,\rho,\phi} d\xi \quad (14)$$

The internal degree of freedom ξ can be eliminated from Eqs. (12), (13) and (14) by taking the total derivative of Eq. (9),

$$\partial(d\xi)/\partial t = -L[A_{\xi T}dT+A_{\xi\rho}d\rho+A_{\xi\phi}d\phi+A_{\xi\xi}d\xi] \quad (15)$$

solving Eqs. (12), (13) and (14) for $d\xi$ and substituting these values into Eq. (15). The results of these manipulations are:

$$dP+\tau\ \frac{\partial(dP)}{\partial t} = \left(\frac{\partial P}{\partial\rho}\right)_{T,\phi,\xi}\left[d\rho+\tau\ \frac{\partial(d\rho)}{\partial t}\right]+\left(\frac{\partial P}{\partial T}\right)_{\rho,\phi,\xi}\left[dT+\tau\ \frac{\partial(dT)}{\partial t}\right]$$

$$+\left(\frac{\partial P}{\partial\phi}\right)_{T,\rho,\xi}\left[d\phi+\tau\ \frac{\partial(d\phi)}{\partial t}\right]$$

$$+\left(\frac{\partial P}{\partial\xi}\right)_{\rho,T,\phi}\left[-\frac{A_{\xi T}}{A_{\xi\xi}}dT-\frac{A_{\xi\rho}}{A_{\xi\xi}}d\rho-\frac{A_{\xi\phi}}{A_{\xi\xi}}d\phi\right] \tag{16}$$

$$dS+\tau\ \frac{\partial(dS)}{\partial t} = \left(\frac{\partial S}{\partial\rho}\right)_{T,\phi,\xi}\left[d\rho+\tau\ \frac{\partial(d\rho)}{\partial t}\right]+\left(\frac{\partial S}{\partial T}\right)_{\rho,\phi,\xi}\left[dT+\tau\ \frac{\partial(dT)}{\partial t}\right]$$

$$+\left(\frac{\partial S}{\partial\phi}\right)_{T,\rho,\xi}\left[d\phi+\tau\ \frac{\partial(d\phi)}{\partial t}\right]$$

$$+\left(\frac{\partial S}{\partial\xi}\right)_{\rho,T,\phi}\left[-\frac{A_{\xi T}}{A_{\xi\xi}}dT-\frac{A_{\xi\rho}}{A_{\xi\xi}}d\rho-\frac{A_{\xi\phi}}{A_{\xi\xi}}d\phi\right] \tag{17}$$

$$d\mu+\tau\ \frac{\partial(d\mu)}{\partial t} = \left(\frac{\partial\mu}{\partial\rho}\right)_{T,\phi,\xi}\left[d\rho+\tau\ \frac{\partial(d\rho)}{\partial t}\right]+\left(\frac{\partial\mu}{\partial T}\right)_{\rho,\phi,\xi}\left[dT+\tau\ \frac{\partial(dT)}{\partial t}\right]$$

$$+\left(\frac{\partial\mu}{\partial\phi}\right)_{T,\rho,\xi}\left[d\phi+\tau\ \frac{\partial(d\phi)}{\partial t}\right]$$

$$+\left(\frac{\partial\mu}{\partial\phi}\right)_{\rho,T,\phi}\left[-\frac{A_{\xi T}}{A_{\xi\xi}}dT-\frac{A_{\xi\rho}}{A_{\xi\xi}}d\rho-\frac{A_{\xi\phi}}{A_{\xi\xi}}d\phi\right] \tag{18}$$

Linearized equations of change(3) for a dilute binary system are:

$$(\partial\rho/\partial t) + \rho_o\psi = 0 \tag{19}$$

$$\rho_o(\partial\psi/\partial t) = -\nabla^2 P + (4\eta_s/3+\eta_v)\nabla^2\psi \tag{20}$$

$$\rho_o T_o(\partial S/\partial t) = \lambda\nabla^2 T \tag{21}$$

$$\partial(\phi-b\rho)/\partial t = D'\nabla^2(\phi-b\rho) \tag{22}$$

where $\psi = \text{div}\,\bar{v}$, η_s is shear viscosity, η_v is volume viscosity, λ is thermal conductivity and D' is the diffusion coefficient.

The next step is to take Fourier-Laplace (space-time) transforms of the equations of change, i.e. $\rho(r,t)\to\rho_k(z)$. The results are:

$$z\rho_k(z) - \rho_k + \rho_o\psi_k(z) = 0 \tag{23}$$

$$\rho_o[z\psi_k(z)-\psi_k] = k^2P_k(z) - k^2(4\eta_s/3+\eta_v)\psi_k(z) \tag{24}$$

$$\rho_oT_o[zS_k(z)-S_k] = -\lambda k^2T_k(z) \tag{25}$$

$$z\phi_k(z) - \phi_k-b[z\rho_k(z)-\rho_k] = -k^2D'[\phi_k(z)-b\rho_k(z)] \tag{26}$$

In these transformed equations $P_k(z)$ and $S_k(z)$ appear. These quantities can be eliminated by taking the space-time transforms of Eqs. (16) and (17) and solving these transformed equations for $P_k(z)$ and $S_k(z)$ with the proper values of the coefficients inserted from Appendix B.

Then Eqs. (24) and (25) become

$$\begin{aligned}(z+b_ok^2)\ \psi_k(z) &- \left[\ \frac{C_o^2k^2}{\rho_o\gamma} + \frac{k^2\Delta}{\rho_o}\left(\frac{\tau z}{1+\tau z}\right) - \frac{k^2b}{\rho_o}\left(\frac{\partial P}{\partial N}\right)_{\rho,T}\right]\ \rho_k(z)\\ &- \left[\ \frac{C_o^2k^2\beta_T}{\gamma} + \rho_oA_{\xi\xi}\xi_\rho\xi_Tk^2\left(\frac{\tau z}{1+\tau z}\right)\right]\ T_k(z)\\ &- \left[\ \frac{k^2}{C_o}\left(\frac{\partial P}{\partial N}\right)_{\rho,T} + \rho_oA_{\xi\xi}\xi_\rho\xi_Nk^2\left(\frac{\tau z}{1+\tau z}\right)\right]\ \phi_k(z) =\end{aligned}$$

$$\psi_k + \frac{\tau k^2}{1+\tau z}\{\frac{P_k}{\rho_o} - [\frac{C_o^2}{\gamma\rho_o} - \frac{b}{\rho_o}\left(\frac{\partial P}{\partial N}\right)_{\rho,T} + \frac{\Delta}{\rho_o}]\rho_k - (\frac{\beta_TC_o^2}{\gamma} + \rho_oA_{\xi\xi}\xi_\rho\xi_T)T_k -$$

$$[(1/\rho_o)(\frac{\partial P}{\partial N})_{\rho,T} + \rho_o A_{\xi\xi}\xi_\rho\xi_N]\phi_k\} \qquad (27)$$

and

$$-[\frac{z(\gamma-1)}{\rho_o\beta_T} + \frac{T_o bz}{C_v}(\frac{\partial S}{\partial N})_{\rho,T} + \frac{z^2\tau T_o A_{\xi\xi}\xi_T\xi_\rho}{C_v(\tau z+1)}]\ \rho_k(z)$$

$$+[z+ ak^2- \frac{\tau z^2 C_1/C_v}{1+\tau z}]\ T_k(z) + [\frac{T_o z}{C_v}(\frac{\partial S}{\partial N})_{\rho,T} - \frac{z^2\tau T_o A_{\xi\xi}\xi_T\xi_N}{C_v(\tau z+1)}]\ \phi_k(z)$$

$$= \frac{T_o}{C_v}\ S_k - \frac{\tau z}{1+\tau z}\{\frac{T_o S_k}{C_v} + [\frac{\gamma-1}{\rho_o\beta_T} + \frac{T_o A_{\xi\xi}\xi_T\xi_\rho}{C_v} + \frac{T_o b}{C_v}(\frac{\partial S}{\partial N})_{\rho,T}]\rho_k -$$

$$[\frac{T_o}{C_v}(\frac{\partial S}{\partial N})_{\rho,T} - \frac{T_o A_{\xi\xi}\xi_T\xi_N}{C_v}]\phi_k - (1- \frac{C_1}{C_v})T_k\} \qquad (28)$$

where $b_o = (4\eta_s/3+\eta_v)/\rho_o$

$\Delta = \rho_o^2 A_{\xi\xi}\xi_\rho^2$

C_o = speed of sound

γ = ratio of specific heats

β_T = coefficient of thermal expansion

$C_1 = T_o A_{\xi\xi}\xi_T^2$

$a = \lambda/\rho_o C_v$

Eqs. (23), (26), (27) and (28) constitute a set of four independent equations in the four unknowns $\rho_k(z)$, $T_k(z)$, $\phi_k(z)$ and $\psi_k(z)$.

The purpose is to obtain the correlation function $<\rho_k\rho_{-k}(z)>$ in terms of the equilibrium correlation function $<|\rho_k|^2>$. This necessitates the simultaneous solution of these equations in terms of the initial values of ρ_k, T_k, ϕ_k and ψ_k.

The right hand sides of Eqs. (27) and (28) can be simplified by considering that in equilibrium,

$$\frac{1}{\rho_o} dP = [\frac{C_o^2}{\rho_o \gamma} - \frac{b}{\rho_o} (\frac{\partial P}{\partial N})_{\rho,T}] d\rho + \frac{\beta_T C_o^2}{\gamma} dT + \frac{1}{\rho_o} (\frac{\partial P}{\partial N})_{\rho,T} d\phi \tag{29}$$

$$\frac{T_o}{C_v} dS = [\frac{-(\gamma-1)}{\rho_o \beta_T} - \frac{T_o b}{C_v} (\frac{\partial S}{\partial N})_{\rho,T}] d\rho + dT + \frac{T_o}{C_v} (\frac{\partial S}{\partial N})_{\rho,\, T} d\phi \tag{30}$$

Consequently the final forms of the transformed hydrodynamic equations are:

Continuity equation:

$$z\rho_k(z) + \rho_o \psi_k(z) = \rho_k \tag{31}$$

Momentum equation:

$$[z+b_o k^2] \psi_k(z) - [(C_o^2 k^2)/(\rho_o \gamma) + \frac{k^2 \Delta \tau z}{\rho_o (1+\tau z)} - (k^2 b/\rho_o) (\frac{\partial P}{\partial N})_{\rho,T}] \rho_k(z)$$

$$-[(C_o^2 k^2 \beta_T/\gamma) + \rho_o A_{\xi\xi} \xi_\rho \xi_T k^2 \frac{\tau z}{1+\tau z}] T_k(z)$$

$$-[(k^2/\rho_o)(\frac{\partial P}{\partial N})_{\rho,T} + \rho_o A_{\xi\xi} \xi_\rho \xi_N k^2 \frac{\tau z}{1+\tau z}] \phi_k(z) =$$

$$\psi_k + \frac{\tau k^2}{1+\tau z} [\frac{\Delta}{\rho_o} \rho_k - \rho_o A_{\xi\xi} \xi_\rho \xi_T T_k - \rho_o A_{\xi\xi} \xi_\rho \xi_N \phi_k] \tag{32}$$

Heat equation:

$$-[\frac{z(\gamma-1)}{\rho_o \beta_T} + (T_o bz/C_v)(\frac{\partial S}{\partial N})_{\rho,T} + \frac{z^2 \tau T_o A_{\xi\xi} \xi_T \xi_\rho}{C_v (\tau z+1)}] \rho_k(z)$$

$$+[z+ak^2 - (C_1/C_v) \frac{\tau z^2}{1+\tau z}] T_k(z) + [\frac{T_o z}{C_v} (\frac{\partial S}{\partial N})_{\rho,T} - \frac{z^2 \tau T_o A_{\xi\xi} \xi_T \xi_N}{C_v (\tau z+1)}] \phi_k(z)$$

$$= \frac{T_o}{C_v} S_k - \frac{\tau z}{1+\tau z} [(T_o A_{\xi\xi} \xi_T \xi_\rho / C_v) \rho_k + \frac{C_1}{C_v} T_k + (T_o A_{\xi\xi} \xi_T \xi_N / C_v) \phi_k] \tag{33}$$

Diffusion equation:

$$(bz+bk^2 D') \rho_k(z) - (z+k^2 D') \phi_k(z) = b\rho_k - \phi_k \tag{34}$$

These four equations can be solved simultaneously to obtain $\rho_k(z)$, $T_k(z)$, $\phi_k(z)$ and $\psi_k(z)$ in terms of the initial values ρ_k, T_k, ϕ_k and ψ_k. These solutions are then inverse Laplace transformed to determine the time dependence of the fluctuations which in turn are related to the fluctuations in the local dielectric constant through a Taylor series expansion in the statistically independent thermodynamic variables of the system.

Then the frequency spectrum defined by the generalized structure factor$^{(3)}$ $S(k,\omega)$ is given by,

$$S(k,\omega) = 2\,\mathrm{Re}\int_0^\infty dt \int dr\,dr' \times \langle \delta\varepsilon(r+r',t)\,\delta\varepsilon(r',0)\rangle \times \exp[i(k\cdot r-\omega t)] \qquad (35)$$

where $\delta\varepsilon(r,t)$ is the fluctuation in the local dielectric constant at the point r at time t.

References:

1. R. D. Mountain, J. Res. Natl. Bur. Std. (U.S.) A70, 207(1966).
2. R. D. Mountain, J. Res. Natl. Bur. Std. (U.S.) A72, 95(1967).
3. R. D. Mountain and J. M. Deutch, J. Chem. Phys. 50, 1103(1969).

Appendix A: Determination of Statistically Independent Variables.

Consider a binary system of energy E', entropy S', volume V' and mole numbers N_1' and N_2'. Let this system be composed of a subsystem with properties E, S, V, N_1 and N_2 and a complementary subsystem with properties E_o, S_o, V_o, N_{1_o}, and N_{2_o}. Assume that the subsystem is very small compared to the total system, hence also compared to the complimentary system.

$$dE' = dE + dE_o \tag{1}$$

$$dE_o = T_o dS_o - P_o dV_o + \mu_{1_o} dN_{1_o} + \mu_{2_o} dN_{2_o} \tag{2}$$

But $dV = -dV_o$, $dN_i = -dN_{i_o}$, and $dS = -dS_o$. (3)

Let $m_1 N_1 + m_2 N_2 = 1$, $= [\mu_1 - \mu_2 (m_1/m_2)]$, $dN_1 = dN$ (4)

Then from Eqs. (2), (3) and (4)

$$dE_o = -T_o dS + P_o dV - \mu_o dN \tag{5}$$

If dE is expanded in Taylor series,

$$dE = \left(\frac{\partial E}{\partial S}\right)_{V,N} dS + \left(\frac{\partial E}{\partial V}\right)_{S,N} dV + \left(\frac{\partial E}{\partial N}\right)_{S,V} dN +$$

$$\frac{1}{2}\left[\frac{\partial^2 E}{\partial S^2}(dS)^2 + \frac{\partial^2 E}{\partial V^2}(dV)^2 + \frac{\partial^2 E}{\partial N^2}(dN)^2 + 2\frac{\partial^2 E}{\partial S \partial V} dS dV + \right.$$

$$\left. 2\frac{\partial^2 E}{\partial S \partial N} dS dN + 2\frac{\partial^2 E}{\partial V \partial N} dV dN \right] + \cdots\cdots\cdot \tag{6}$$

From $dT = (\partial T/\partial S)\ dS$ and similar relations for dP and dμ, and combining Eqs. (1), (5) and (6),

$$\begin{aligned} dE' &= \frac{1}{2}(dT dS - dP dV + d\mu dN) \\ &= \frac{1}{2}[dT dS + (1/\rho^2) dP d\rho + d\mu dN] \end{aligned} \tag{7}$$

Let T, ρ, and $\phi = N+b\rho$ be a set of statistically independent variables with b a constant. Using these variables,

$$dS = \left(\frac{\partial S}{\partial T}\right)_{\rho,\phi} dT + \left(\frac{\partial S}{\partial \rho}\right)_{T,\phi} d\rho + \left(\frac{\partial S}{\partial \phi}\right)_{T,\rho} d\phi \tag{8}$$

$$dP = \left(\frac{\partial P}{\partial T}\right)_{\rho,\phi} dT + \left(\frac{\partial P}{\partial \rho}\right)_{T,\phi} d\rho + \left(\frac{\partial P}{\partial \phi}\right)_{T,\rho} d\phi \tag{9}$$

$$d\mu = \left(\frac{\partial \mu}{\partial T}\right)_{\rho,\phi} dT + \left(\frac{\partial \mu}{\partial \rho}\right)_{T,\phi} d\rho + \left(\frac{\partial \mu}{\partial \phi}\right)_{T,\rho} d\phi \tag{10}$$

Substituting Eqs. (8), (9) and (10) into Eq. (7),

$$\begin{aligned} dE' = \frac{1}{2}\{ &\left(\frac{\partial S}{\partial T}\right)_{\rho,\phi} (dT)^2 + [(1/\rho^2)\left(\frac{\partial P}{\partial \rho}\right)_{T,\phi} - b\left(\frac{\partial \mu}{\partial \rho}\right)_{T,\phi}](d\rho)^2 + \\ &\left(\frac{\partial \mu}{\partial \phi}\right)_{T,\rho}(d\phi)^2 + [\left(\frac{\partial S}{\partial \rho}\right)_{T,\phi} d\rho dT + (1/\rho^2)\left(\frac{\partial P}{\partial T}\right)_{\rho,\phi} dT d\rho - \\ &b\left(\frac{\partial \mu}{\partial T}\right)_{\rho,\phi} dT d\rho] + [\left(\frac{\partial S}{\partial \phi}\right)_{T,\rho} d\phi dT + \left(\frac{\partial \mu}{\partial T}\right)_{\rho,\phi} d\phi dT] + \\ &[(1/\rho^2)\left(\frac{\partial P}{\partial \phi}\right)_{T,\rho} d\phi d\rho + \left(\frac{\partial \mu}{\partial \rho}\right)_{T,\phi} d\phi d\rho - b\left(\frac{\partial \mu}{\partial \phi}\right)_{T,\rho} d\phi d\rho]\} \end{aligned} \tag{11}$$

For T, ρ, and ϕ to be independent the terms containing cross derivatives must be zero.

From the definition of ϕ,

$$\left(\frac{\partial \mu}{\partial T}\right)_{\rho,\phi} = \left(\frac{\partial \mu}{\partial T}\right)_{\rho,N} \quad \text{and} \quad \left(\frac{\partial S}{\partial \phi}\right)_{T,\rho} = \left(\frac{\partial S}{\partial N}\right)_{T,\rho} \tag{12}$$

Maxwell relation: $\left(\frac{\partial S}{\partial N}\right)_{T,\rho} = -\left(\frac{\partial \mu}{\partial T}\right)_{N,\rho}$

Therefore, terms containing dϕdT vanish. For terms containing dϕdρ to vanish,

$$b = \frac{\left(\frac{\partial \mu}{\partial \rho}\right)_{T,\phi} + (1/\rho^2)\left(\frac{\partial P}{\partial \phi}\right)_{T,\rho}}{\left(\frac{\partial \mu}{\partial \phi}\right)_{T,\rho}} \tag{13}$$

But $$\left(\frac{\partial\mu}{\partial\rho}\right)_{\phi} = \frac{\partial(\mu,\phi)}{\partial(\rho,\phi)} = \frac{\partial(\mu,\phi)/\partial(\rho,N)}{\partial(\rho,\phi)/\partial(\rho,N)}$$

$$= \left(\frac{\partial\mu}{\partial\rho}\right)_{N} - b\left(\frac{\partial\mu}{\partial N}\right)_{\rho} \tag{14}$$

and from definition of ϕ,

$$\left(\frac{\partial P}{\partial\phi}\right)_{\rho,T} = \left(\frac{\partial P}{\partial N}\right)_{\rho,T} \quad \text{and} \quad \left(\frac{\partial\mu}{\partial\phi}\right)_{\rho,T} + \left(\frac{\partial\mu}{\partial N}\right)_{\rho,T}$$

Therefore

$$b = \frac{1}{2}\left\{-\left(\frac{\partial N}{\partial\rho}\right)_{\mu,T} + (1/\rho^2)\left(\frac{\partial P}{\partial\mu}\right)_{T,N}\right\} \tag{15}$$

T, ρ, and ϕ are a set of statistically independent variables with $\phi = N + b\rho$ and b given by Eq. (15).

Appendix B: Determination of the Coefficients in the Pressure and Entropy Expressions.

$$(\partial P/\partial \rho)_{T,\xi,\phi} = (\partial P/\partial \rho)_{T,\phi} - (\partial P/\partial \xi)_{T,\rho,\phi}\xi_\rho$$

$$(\partial P/\partial T)_{\rho,\phi,\xi} = (\partial P/\partial T)_{\rho,\phi} - (\partial P/\partial \xi)_{T,\rho,\phi}\xi_T$$

$$(\partial P/\partial \phi)_{\rho,\xi,T} = (\partial P/\partial \phi)_{\rho,T} - (\partial P/\partial \xi)_{T,\rho,\phi}\xi_\phi$$

$$(\partial S/\partial \rho)_{T,\xi,\phi} = (\partial S/\partial \rho)_{T,\phi} - (\partial S/\partial \xi)_{T,\rho,\phi}\xi_\rho$$

$$(\partial S/\partial T)_{\rho,\phi,\xi} = (\partial S/\partial T)_{\rho,\phi} - (\partial S/\partial \xi)_{T,\rho,\phi}\xi_T$$

$$(\partial S/\partial \phi)_{\rho,\xi,T} = (\partial S/\partial \phi)_{\rho,T} - (\partial S/\partial \xi)_{T,\rho,\phi}\xi_\phi$$

where $\xi_\rho = (\partial \xi/\partial \rho)_{T,\phi}$; $\xi_T = (\partial \xi/\partial T)_{\rho,\phi}$;
$\xi_\phi = (\partial \xi/\partial \phi)_{\rho,T} = (\partial \xi/\partial N)_{\rho,T} = \xi_N$

Maxwell relations:

$$(\partial P/\partial \xi)_{\rho,T,\phi} = \rho_o^2 A_{\xi\rho}$$

$$(\partial S/\partial \xi)_{\rho,T,\phi} = -A_{\xi T}$$

with $A_{\xi\rho} = (\partial A_\xi/\partial \rho)_{T,\phi,\xi}$; $A_{\xi T} = (\partial A_\xi/\partial T)_{\rho,\phi,\xi}$

Also, $dA_\xi = A_{\xi\rho}d\rho + A_{\xi T}dT + A_{\xi\phi}d\phi + A_{\xi\xi}d\xi = 0$

$$A_{\xi\rho} = -A_{\xi\xi}\xi_\rho$$

$$A_{\xi T} = -A_{\xi\xi}\xi_T$$

$$A_{\xi\phi} = -A_{\xi\xi}\xi_\phi$$

Therefore,

$$(\partial P/\partial \rho)_{T,\xi,\phi} = (\partial P/\partial \rho)_{T,\phi} + \rho_o^2 A_{\xi\xi}\xi_\rho^2$$

$$(\partial P/\partial T)_{\rho,\phi,\xi} = (\partial P/\partial T)_{\rho,\phi} + \rho_o^2 A_{\xi\xi}\xi_\rho\xi_T$$

$$(\partial P/\partial \phi)_{\rho,\xi,T} = (\partial P/\partial \phi)_{\rho,T} + \rho_o^2 A_{\xi\xi}\xi_\rho\xi_N$$

$$(\partial S/\partial \rho)_{T,\xi,\phi} = (\partial S/\partial \rho)_{T,\phi} - A_{\xi\xi}\xi_T\xi_\rho$$

$$(\partial S/\partial T)_{\rho,\phi,\xi} = (\partial S/\partial T)_{\rho,\phi} - A_{\xi\xi}\xi_T^2$$

$$(\partial S/\partial \phi)_{\rho,\xi,T} = (\partial S/\partial \phi)_{\rho,T} - A_{\xi\xi}\xi_T\xi_N$$

We also note that,

$$(\partial P/\partial \rho)_{T,\phi} = (\partial P/\partial \rho)_{T,N} - b(\partial P/\partial N)_{T,\rho}$$

$$(\partial S/\partial \rho)_{T,\phi} = (\partial S/\partial \rho)_{T,N} - b(\partial S/\partial N)_{T,\rho}$$

and $(\partial P/\partial \rho)_{T,N} = C_o^2/\gamma$

$$(\partial S/\partial \rho)_{T,N} = -[C_v(\gamma-1)/(\rho_o T_o \beta_T)]$$

also

$$(\partial P/\partial T)_{\rho,\phi} = (\partial P/\partial T)_{\rho,N} = [\rho_o \beta_T C_o^2/\gamma]$$

$$(\partial S/\partial T)_{\rho,\phi} = (\partial S/\partial T)_{\rho,N} = C_v/T_o$$

$$(\partial P/\partial \phi)_{\rho,T} = (\partial P/\partial N)_{\rho,T}$$

$$(\partial S/\partial \phi)_{\rho,T} = (\partial S/\partial N)_{\rho,T}$$

where C_o = speed of sound

γ = ratio of specific heats

β_T = coefficient of thermal expansion

C_v = specific heat at constant volume

PROPOSITION II

It is proposed that accurate viscosity measurements free of gravity effects can be made using a vibrating multiple-wire viscometer.

Introduction:

There are basically three methods of measuring viscosity. One involves measuring the flow rate through a capillary tube and another measuring the torque transmitted by the fluid. A third method requires measurement of viscous damping due to the fluid.

Viscosity measurements are hardest to make near the critical point. Due to the highly compressible nature of such a system, small pressure differences lead to large density gradients and hence all viscometers that require or result in pressure changes are undesirable. A successfully(1) applied method of measuring the viscosity near the critical point is the torsional crystal technique(2). The possible limitation of this method is the finite height of the crystal which leads to density gradients in the gravitational field. Moreover, in this method the density-viscosity product is measured and therefore a knowledge of the fluid density is necessary.

Using a modified "vibrating wire viscometer"(3) described below, the kinematic viscosity and the density can be measured simultaneously. Also, accurate viscosity measurements of coexisting phases or determining the height dependence of viscosity are possible with this arrangement.

Theory of Vibrating Wire Viscometer:

This viscometer is based on the damping of the transverse oscillations of a taut wire in a fluid. The kinematic viscosity is obtained from measurements of the frequency and the decay time of these oscillations.

The equation of motion of a taut wire of length L, weight μL, under a tension T, immersed in a fluid of density ρ and viscosity η , is

$$\mu \frac{\partial^2 y}{\partial t^2} = T \frac{\partial^2 y}{\partial x^2} + F \tag{1}$$

where $y(x,t)$ is the displacement of the wire from its equilibrium position and F is the force exerted by the fluid. If D is the drag effective mass and μ' is the hydrodynamic effective mass of the fluid with ω the frequence of vibration of the wire, F can be written as

$$F = -(D \frac{\partial y}{\partial t} + \mu' \frac{\partial^2 y}{\partial t^2}) = -(D + i\omega\mu') \frac{\partial y}{\partial t} \tag{2}$$

For the case in which only the first mode is excited and the decay time τ is much greater than the period of the oscillations, Eq. (1) with F given by Eq. (2) has the solution

$$y = A \sin(\pi x/L)\, e^{-t/\tau}\, e^{i\omega t} \tag{3}$$

$$1/\tau = \frac{D}{2}\,(\mu+\mu') \tag{4}$$

$$\omega^2 = T(\pi/L)^2/(\mu+\mu') \tag{5}$$

For $[y(x,t)]_{max} << L$, the solution obtained by Stokes$^{(4)}$ for an infinite cylinder oscillating perpendicular to its axis can be used.

$$F = -\pi\rho a^2\omega(k'+ik)\,\frac{\partial y}{\partial t} \tag{6}$$

where k and k' are functions of m and

$$m = a/(2\lambda) \qquad \lambda = (\eta/\omega\rho)^{1/2} \tag{7}$$

with a the radius and λ the penetration depth of the vibrations. This solution is obtained keeping only terms linear in velocity in the Navier-Stokes equation and is therefore limited to

$$m \geq 0.5 \tag{8}$$

From Eqs. (7) and (2) D and μ' can be expressed in terms of k and k' as

$$D = \pi\rho a^2\omega k'(m) \tag{9}$$

$$\mu' = \pi\rho a^2 k(m) \tag{10}$$

Finally, the viscosity can be evaluated combining Eqs. (7), (9) and (10)

$$\eta = \frac{a^2\omega\rho}{4[m(k')]^2} \tag{11}$$

with $$k' = \frac{2\mu}{\pi\rho a^2\omega\tau} + \frac{2k(m)}{\omega\tau} \tag{12}$$

If τ, ω and ρ are measured, k' and correspoding m can be calculated by iteration using Stokes' tables(4). The viscosity can then be computed from Eq. (11).

The Proposed Viscometer:

The viscometer consists of the sample cell assembly, the temperature measuring and controlling accessories, the spectrometer for measuring the refractive index and the electronics for signal detection.

The cell assembly is shown schematically in Fig. 1. The proposed design improvements compared to those described in Refs. (3) and (5) are the inclusion of four vibrating wires to study the viscosity as a function of height and a triangular end section with two flat windows to measure the refractive index also as a function of height simultaneously. The cell is used in a magnetic field and must be built out of 300 series stainless steel. The vibrating wires made from tungsten for its high density and tensile strength can be 2 cm. long, 0.02 mm. in diameter and separated from each other by about 3 mm.

The temperature can be controlled by immersing the cell assembly in a water bath(1) and the temperature can be measured by a platinum resistance thermometer. With this arrangement, the temperature can be controlled better than 0.001°C.

The spectrometer can be an adaptation of the one described in Ref. (6). A small laser mounted on a vertically adjustable platform can be used as the light source.

The components of the signal detection system are shown in the block diagram of Fig. 2. A lead acid battery supplies the dc current to displace the wires from their equilibrium positions. The electronic chopper turns the dc current on and off for set periods of time and sends a trigger pulse to the signal averager each time the dc current is cut off. The signal from each wire is amplified before it is fed into the signal averager. The output of the signal averager can be obtained in digital form on paper tape or in analog form on an X-Y-recorder. A scope can also be used to get a visual display of the output. This detection system is expected to produce a more accurate data accumulation than those of Refs. (3) and (5) due to the fact that each output will be an average of many determinations.

The Proposed Procedure of Operation:

The operation will consist of the following steps:

1) Evacuate the cell assembly.

2) Load the cell and the weighing bomb at a supercritical temperature.

3) Determine the average density by disconnecting and weighing the weighing bomb.

4) Set the first operating temperature and measure it

after allowing sufficient time to reach equilibrium.

5) Start measurements using one wire at a time and continue signal averaging until a well-defined decay curve is developed.

6) Measure the refractive index at the height of the wire used in step 5.

7) Repeat steps 5 and 6 for the remaining wires.

8) Change to a new temperature and repeat steps 4 to 7.

Data Analysis:

The output of the signal averager contains information about the damped oscillations in the form of amplitude versus time. The frequency ω can be deduced immediately from this information and the decay time τ can be obtained from the slope of a semilogarithmic plot of peak amplitude versus time.

If the refractive index n does not change as a function of height, the average density determined from the weighing bomb can be used. If the refractive index changes with height, using

$$\frac{n^2-1}{n^2+2} = \text{constant} \times \rho \qquad (13)$$

and the average density, density can be corrected for gravity effects.

After ω, τ and ρ are determined, a guess at m can be made and using Stokes' tables for k(m) and k'(m), k' can be calculated from Eq. (12). If the assumed m does not check with m corresponding to the calculated k', an iteration can be performed until agreement between the assumed and the calculated values of m is reached. Once m is determined, the viscosity η can be computed from Eq. (11).

Discussion:

Due to the thinness of the wire this method provides the means of making viscosity measurements that are free of gravitational error. It also does not introduce any macroscopic disturbances because the penetration depth of the vibrations is much smaller than the diameter of the wire. Another advantage is the availability of highly accurate density data through the refractive index measurements for converting the kinematic viscosity to shear viscosity. This method also provides height dependent viscosity and density data which can be analyzed to determine the gravity effects. Finally, this technique promises to be extremely versatile in that it can be used for a variety of systems such as simple fluids and binary mixtures near their critical points or systems containing coexisting phases.

References:

1. H. J. Strumf, doctoral thesis, California Institute of Technology, Pasadena, California, 1972.
2. W. P. Mason, Trans. ASME 69, 359(1947); P. E. Rouse, E. D. Bailey and J. A. Minkin, API Symposium Anal. Res. (1950).
3. J. T. Tough, W. D. McCormick and J. G. Dash, Rev. Sci. Instr. 35, 1345(1964).
4. G. G. Stokes, Mathematical and Physical Papers (Cambridge University Press, London, 1922), Vol.III, p. 38.
5. S. Ballaro', G. Maisano, P. Migliardo and F. Wanderlingh, Phys. Rev. A6, 1633(1972).
6. B. L. Smith, Rev. Sci. Instr. 34, 19(1963).

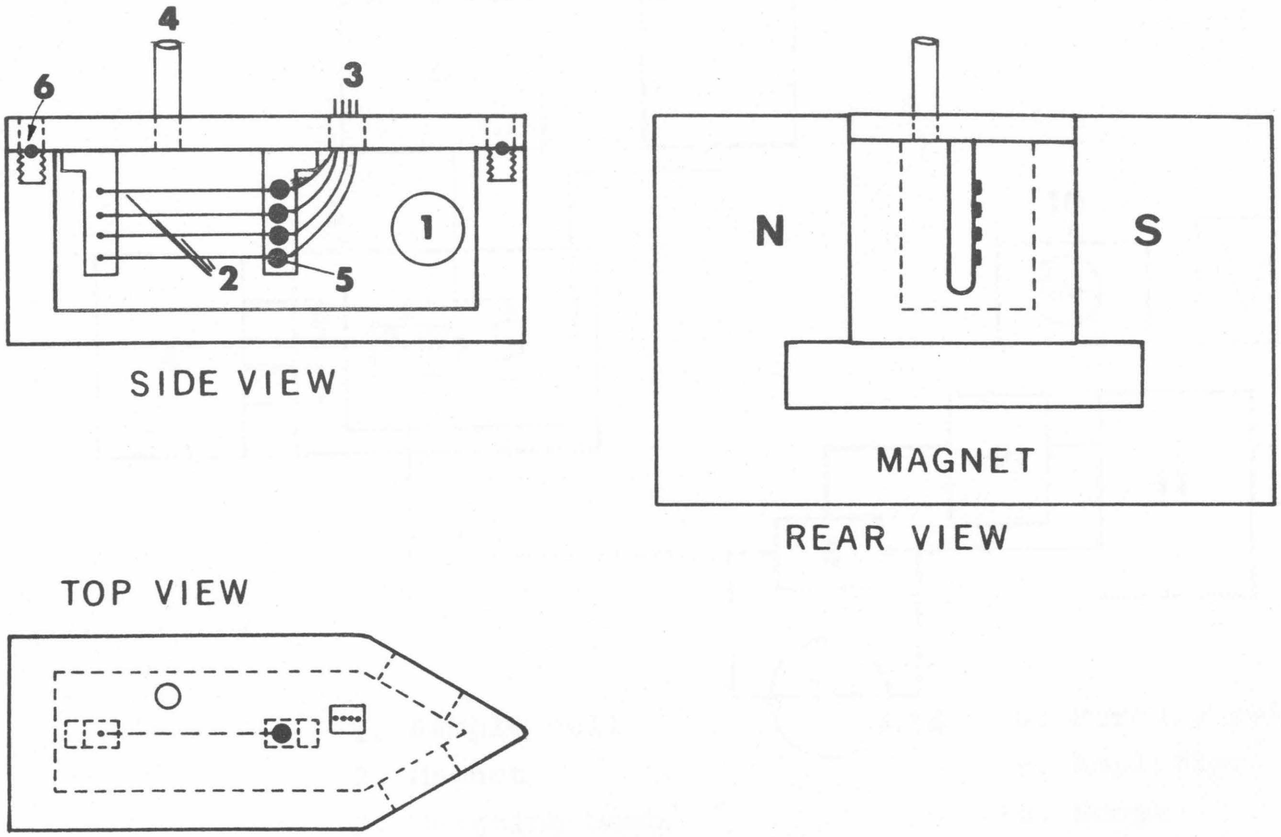

1. Window
2. Vibrating Wires
3. Feed-through
4. Filling Line
5. Teflon Insulators
6. O-ring

Figure 1. The Cell Assembly.

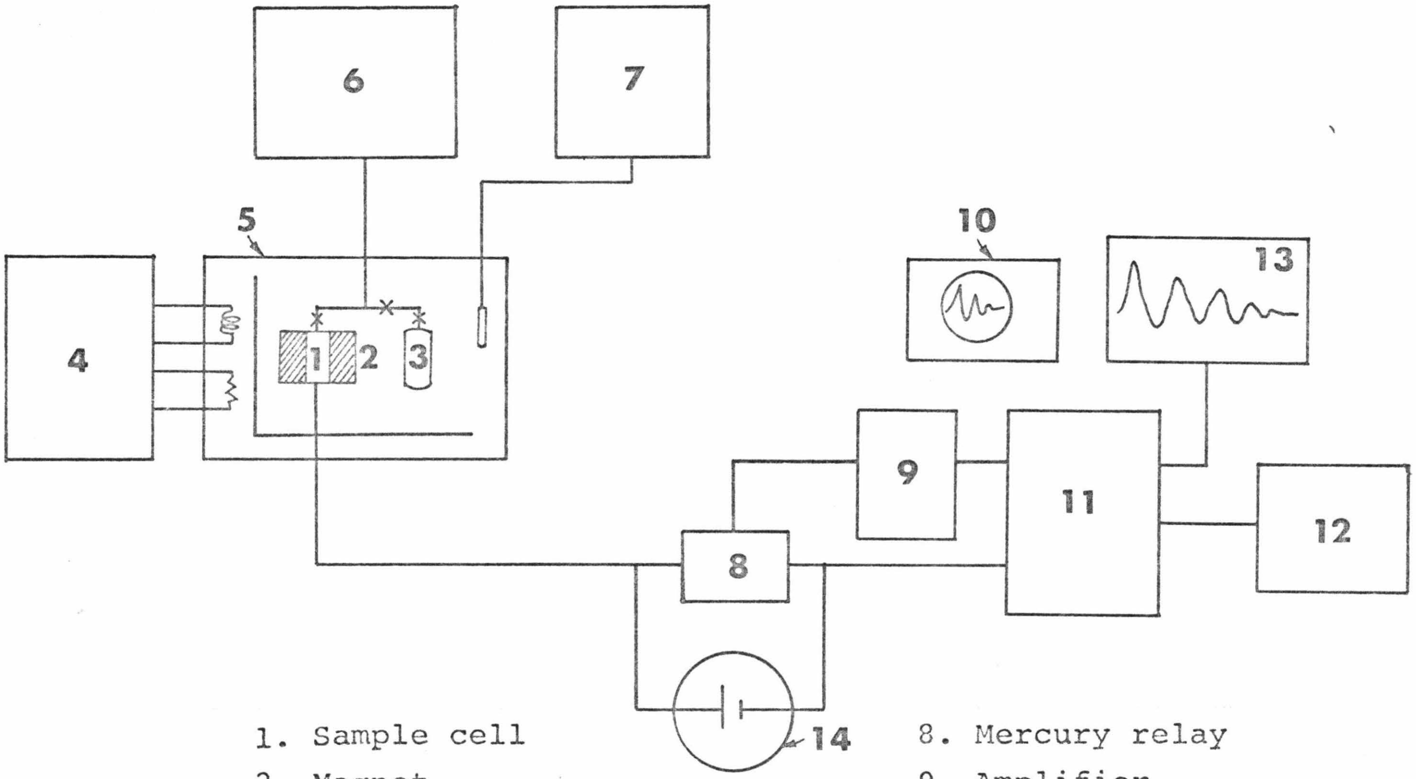

1. Sample cell
2. Magnet
3. Weighing bomb
4. Water bath controls
5. Water bath
6. Loading and vacuum system
7. Temperature measuring system
8. Mercury relay
9. Amplifier
10. Scope
11. Signal averager
12. Paper tape punch
13. X-Y-recorder
14. D. C. Supply

Figure 2. Block Diagram of the Proposed Viscometer.

PROPOSITION III

A sudden increase in the diffusion coefficient in the binary systems composed of primary alcohols (ethanol, propanol and butanol) in carbon disulfide has been observed experimentally(1,2). A mechanism is proposed to explain this phenomenon.

Recent measurements of the diffusion coefficient as a function of concentration in the binary systems of ethanol-carbon disulfide(2), n-propanol-carbon disulfide(2) and n-butanol-carbon disulfide(2) are illustrated in Fig 1. It is observed that the diffusion coefficient in all of the three systems varies very little with concentration up to 50% volume of alcohol. Then at a concentration of alcohol slightly above 50% by volume, the diffusion coefficient starts to increase. The magnitude of this change is especially pronounced for the ethanol-carbon disulfide system.

It is proposed that this phenomenon can be explained by assuming that the alcohol molecules form aggregates uniform in size in the solvent carbon disulfide. As the concentration of the alcohol increases, the number of these aggregates rather than their size increases. As more and more aggregates form, the mean distance between them becomes smaller and smaller until at a certain concentration they no longer exist as aggregates but form a matrix of alcohol solvent. At this point the diffusion coefficient starts to increase because from there on the diffusion depends mainly on the motion of smaller CS_2 molecules within the alcohol matrix.

A crude test of this proposed mechanism can be made. If it is assumed that the alcohol aggregates are spherical and they form the solvent matrix when they start touching each other, then the volume percent at which the diffusion coefficient will start to increase can be predicted.

$$\text{Volume fraction occupied by alcohol} = \frac{(4/3)\pi r^3}{(2r)^3} = 0.52$$

where r is the radius of the spherical aggregate. This value of 52% by volume obtained by a simple approximation agrees quite well with the experimental observations presented in Fig. 1.

Assuming the existence of many alcohol molecules as an aggregate is reasonable because the formation of multimers due to hydrogen bonding of normal alcohols has been observed and their structures have been studied by many investigators(3-9). It has been found that the structure of normal alcohols in pure state is dominated by large multimers(4) with a high dipole moment while they exist in smaller multimers(5-9) (ranging from dimers to hendecamers and even to cyclic multimers) when dissolved in a solvent.

From the knowledge of the diffusion coefficient, an approximate value for the number of alcohol molecules composing an aggregate can be calculated. The mean diameter of an aggregate can be estimated using the Stokes-Einstein relationship for the diffusion coefficient of a spherical molecule of radius r diffusing in a solvent of viscosity η.

$$D = \frac{k_B T}{6\pi\eta r} \tag{1}$$

where D is the diffusion coefficient, k_B is Boltzmann's constant and T is the temperature in °K.
Using $D=0.5\times10^{-5}$ cm^2/sec for ethanol, $D=0.6\times10^{-5}$ cm^2/sec for propanol and $D=1.0\times10^{-5}$ cm^2/sec for butanol in CS_2, the diameters of the aggregates calculated from Eq. (1) are 23.6 Å, 19.6 Å and 11.2 Å for ethanol, propanol and butanol respectively. From the density and the molecular weight of each alcohol, these diameters correspond to 70 molecules in an ethanol aggregate, 32 molecules in a propanol aggregate and 6 molecules in a butanol aggregate. It is hard to attach any meaning to these estimates of the number of molecules because the structures of alcohols in CS_2 have not been studied. But, by all means, multimers composed of many hydrogen bonded monomers are expected$^{(4)}$ according to studies on the structures of alcohols.

Consequently, to study the structure of alcohols in CS_2 together with accurate measurements of the diffusion coefficient as a function of concentration in such systems promises to furnish information to explain the behaviour of the diffusion coefficient.

References:

1. A. M. Jamieson and A. G. Walton, J. Chem. Phys. 58, 1054(1973)
2. Erdoğan Gülari, doctoral thesis, California Institute of Technology, Pasadena, California, 1973.
3. S. N. Vinogradov and R. H. Linell, Hydrogen Bonding (Van Nostrand-Reinhold, New York, N. Y., 1971)
4. P. Bordewijk, F. Gransch and C. J. F. Böttcher, J. Phys. Chem. 73, 3255(1969)
5. E. Tucker, S. B. Farnham and S. D. Christian, J. Phys. Chem. 73, 3820(1969)
6. W. Dannhauser and A. F. Flueckinger, Phys. Chem. Liquids 2, 37(1970)
7. J. Crossley, L. Glasser and C. P. Smyth, J. Chem. Phys. 55, 2197(1971)
8. A. N. Fletcher, J. Phys. Chem. 75, 1808(1971)
9. P. Bordewijk, M. Kunst and A. Rip, J. Phys. Chem. 77, 548(1973)

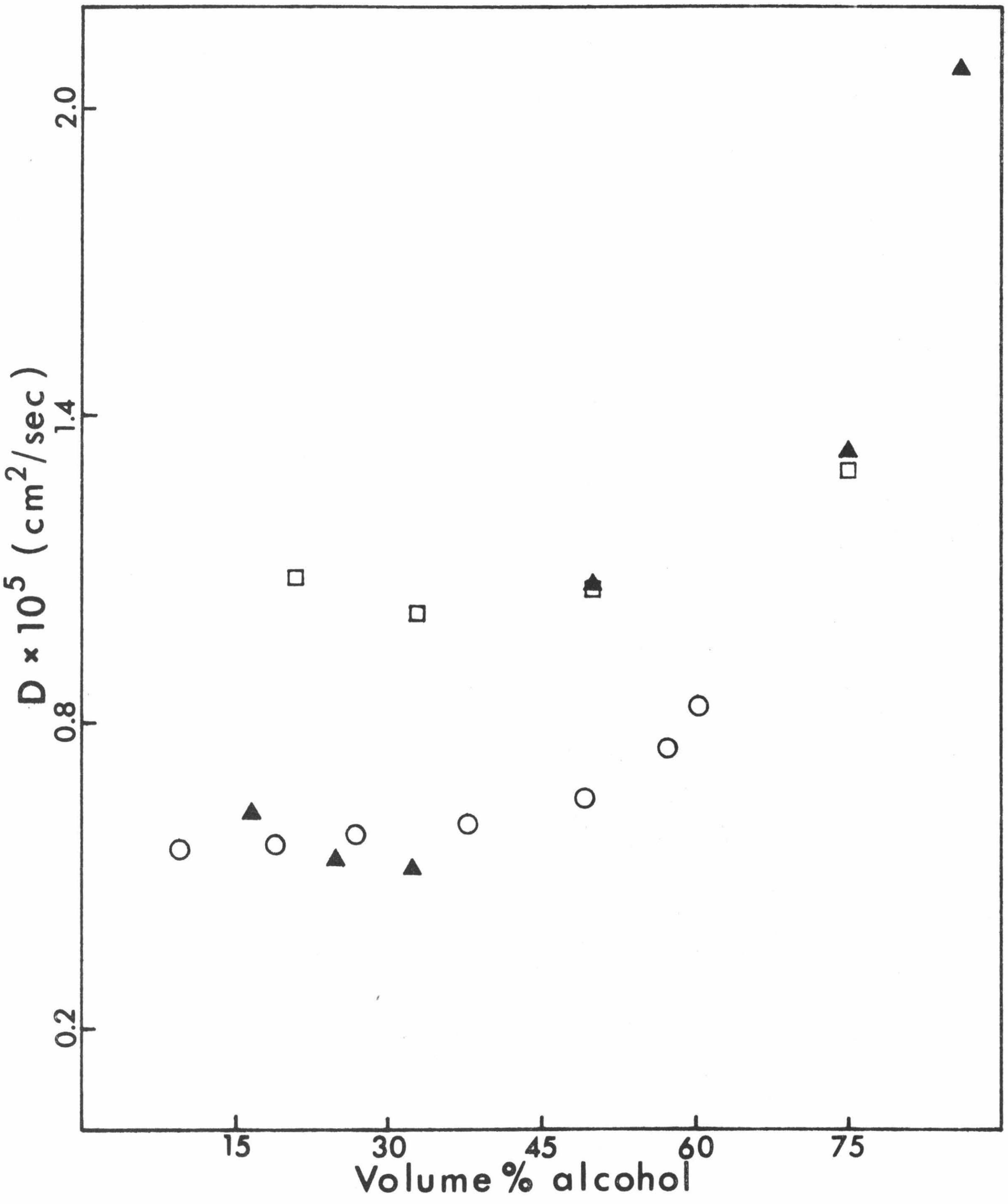

Figure 1.

▲ - Ethanol-carbon disulfide[(2)]

○ - n-Propanol-carbon disulfide[(1)]

□ - n-Butanol-carbon disulfide[(2)]